frontiers | Research Topics

Processes, mechanisms and solutions in coastal wetland to adapt to changing environment

Edited by
Qing Wang, Dongdong Shao, Yu Zhang and Qin Zhu

Published in
Frontiers in Marine Science

ISSN 1664-8714
ISBN 978-2-8325-6423-3
DOI 10.3389/978-2-8325-6423-3

About Frontiers

Frontiers is more than just an open access publisher of scholarly articles: it is a pioneering approach to the world of academia, radically improving the way scholarly research is managed. The grand vision of Frontiers is a world where all people have an equal opportunity to seek, share and generate knowledge. Frontiers provides immediate and permanent online open access to all its publications, but this alone is not enough to realize our grand goals.

Frontiers journal series

The Frontiers journal series is a multi-tier and interdisciplinary set of open-access, online journals, promising a paradigm shift from the current review, selection and dissemination processes in academic publishing. All Frontiers journals are driven by researchers for researchers; therefore, they constitute a service to the scholarly community. At the same time, the *Frontiers journal series* operates on a revolutionary invention, the tiered publishing system, initially addressing specific communities of scholars, and gradually climbing up to broader public understanding, thus serving the interests of the lay society, too.

Dedication to quality

Each Frontiers article is a landmark of the highest quality, thanks to genuinely collaborative interactions between authors and review editors, who include some of the world's best academicians. Research must be certified by peers before entering a stream of knowledge that may eventually reach the public - and shape society; therefore, Frontiers only applies the most rigorous and unbiased reviews. Frontiers revolutionizes research publishing by freely delivering the most outstanding research, evaluated with no bias from both the academic and social point of view. By applying the most advanced information technologies, Frontiers is catapulting scholarly publishing into a new generation.

What are Frontiers Research Topics?

Frontiers Research Topics are very popular trademarks of the *Frontiers journals series*: they are collections of at least ten articles, all centered on a particular subject. With their unique mix of varied contributions from Original Research to Review Articles, Frontiers Research Topics unify the most influential researchers, the latest key findings and historical advances in a hot research area.

Find out more on how to host your own Frontiers Research Topic or contribute to one as an author by contacting the Frontiers editorial office: frontiersin.org/about/contact

Processes, mechanisms and solutions in coastal wetland to adapt to changing environment

Topic editors

Qing Wang — Beijing Normal University, Zhuhai, China
Dongdong Shao — Beijing Normal University, China
Yu Zhang — Los Alamos National Laboratory (DOE), United States
Qin Zhu — Southern Marine Science and Engineering Guangdong Laboratory (Guangzhou), China

Citation

Wang, Q., Shao, D., Zhang, Y., Zhu, Q., eds. (2025). *Processes, mechanisms and solutions in coastal wetland to adapt to changing environment*. Lausanne: Frontiers Media SA. doi: 10.3389/978-2-8325-6423-3

Table of contents

04 Editorial: Processes, mechanisms and solutions in coastal wetland to adapt to changing environment
Qing Wang, Qin Zhu and Dongdong Shao

06 The role of tidal creeks in shaping carbon and nitrogen patterns in a Chinese salt marsh
Ziwen Ma, Yanan Wu, Siqi Zhao, Yueyan Pan, Jiakai Liu, Mingxiang Zhang and Zhenming Zhang

17 Sediment resuspension and transport in the offshore subaqueous Yangtze Delta during winter storms
Min Tian, Haifei Yang, Wenxiang Zhang, Kehui Xu, Benwei Shi, Yaping Wang and Shilun Yang

33 Crab bioturbation reduces carbon storage in salt marshes under more robust mechanisms than plant invasiveness
Yujie Hua, Huayu Chen, Linjing Ren, Jianwu Tang and Xiuzhen Li

48 Divergence in spatial patterns of leaf stoichiometry between native and non-native plants across coastal wetlands
Youzheng Zhang, Yaolin Guo, Hui Wang, Niu Li, Hengtao Xu, Dongrong Zhang, Jian Qian and Yukun Hu

57 Mechanism and threshold of environmental stressors on seagrass in high-turbidity estuary: case of *Zostera japonica* in Yellow River Estuary, China
Yujun Yi, Fanxuan Zhao, Chuanying Hou, Chengxiang Zhang and Caihong Tang

71 Assessment of the community status of seagrass bed and its relationship with environmental characteristics in Wenchang, Hainan Island, China
Miao Fu, Junyi Jiang, Dacheng Wang, Guowei Fu, Yanwei Song, Hongbing Wang and Daheng Zhang

82 The effect of *Sesuvium portulacastrum* for reducing inorganic nitrogen pollution in coastal mariculture wetland
Kai Liu, Wei Gao, Zhenzhen Yu, Yongchao Hu, Ming Zuo, Chen Sun, Xiaotao Zou and Lizhi Wang

94 Coastal exotic plant serves as a habitat for a notorious wetland pest in unfavorable seasons: A case study of exotic *Spartina alterniflora* in China
Tianping Xu, Xu Ma, Yunjing Li, Hao Xue, Shilin Zhao and Zezheng Liu

104 Study on the three-dimensional numerical simulation of concentrated brine dispersal processes in estuarine bays
Huaiyuan Xue, Hongyuan Shi, Chao Zhan, Qing Wang, Yan Li and Zaijin You

118 Variations in the archaeal community in wetlands soils under various hydrologic conditions in the Yellow River Estuary
Qingqing Zhao, Jia Jia, Fanyong Song, Tianyuan Li, Wen Zhang and Yujie Huang

frontiers | Frontiers in Marine Science

TYPE Editorial
PUBLISHED 22 May 2025
DOI 10.3389/fmars.2025.1614900

OPEN ACCESS

EDITED AND REVIEWED BY
Marta Marcos,
University of the Balearic Islands, Spain

*CORRESPONDENCE
Qing Wang
wq@bnu.edu.cn

RECEIVED 20 April 2025
ACCEPTED 07 May 2025
PUBLISHED 22 May 2025

CITATION
Wang Q, Zhu Q and Shao D (2025) Editorial: Processes, mechanisms and solutions in coastal wetland to adapt to changing environment. *Front. Mar. Sci.* 12:1614900. doi: 10.3389/fmars.2025.1614900

Editorial: Processes, mechanisms and solutions in coastal wetland to adapt to changing environment

Qing Wang[1,2,3]*, Qin Zhu[4] and Dongdong Shao[1,3]

[1]State Key Laboratory of Wetland Conservation and Restoration, Beijing Normal University, Beijing, China, [2]Research and Development Center for Watershed Environmental Eco-Engineering, Advanced Institute of Natural Sciences, Beijing Normal University, Zhuhai, China, [3]Yellow River Estuary Wetland Ecosystem Observation and Research StationMinistry of Education, Dongying, China, [4]Southern Marine Science and Engineering Guangdong Laboratory (Guangzhou), Guangzhou, China

KEYWORDS

coastal wetlands, climate change, ecological process, adaptive solutions, conservation

Editorial on the Research Topic

Processes, mechanisms and solutions in coastal wetland to adapt to changing environment

Coastal wetlands provide valuable ecological services, such as coastal protection, carbon storage, flood mitigation, and food production (Kirwan and Megonigal, 2013; He and Silliman, 2019; Newton et al., 2020). Each type of coastal wetland (i.e., salt marshes, mangroves, sea grasses) has its adaptive strategies to face the changing environment. In the context of climate change and anthropogenic activities, external disturbances are more complicated and changeable, causing the responses of species and ecological processes to be more secluded and unpredictable (Kirwan and Megonigal, 2013; Schuerch et al., 2018; FitzGerald and Hughes, 2019). Elucidating how these coastal ecosystems adapt to the changing environment, especially the key processes, mechanisms and solutions are quite important and urgent. We aim to advance discussions on various processes, mechanisms, and solutions to multiple challenges in coastal wetlands all over the world. This Research Topic collects 10 research papers, which include hydrological, biological, and chemical processes, together with their relationships and influence mechanisms in salt marshes, seagrass, estuarine waters, and mariculture ponds.

Two papers have studied the physical processes of brine dispersal (Xue et al.) and winter storms (Tian et al.). Xue et al. conducted a numerical simulation to reveal the effects of brine dispersal under the combined influence of river flow and tides. They found that releasing brine in areas with strong currents helps it mix and spread better. Tian et al. did a field study in the Yangtze Delta. They measured waves, currents, water depth, and water clarity. They found that storms, especially in winter, play a big role in moving sediments along the coast. This is important because storms are expected to get stronger with global warming.

Three studies have focused on the relationship between environmental factors and biocenosis, such as archaeal communities (Zhao et al.) and seagrasses (Yi et al.; Fu et al.). Zhao et al. analyzed the diversity and community structure of archaeal in the 0–20 cm soils under different hydrological conditions in the Yellow River Delta. They confirmed that the

variation in soil salinity caused by hydrological conditions is a major driver of the variation of archaeal community structure. Yi et al. focused on a laboratory experiments of the response of sea grass to environmental pressures at different life stages. They mainly considered salinity and turbidity. The results provide a molecular mechanism for the adaptation of seagrass to environmental stress. These findings will help developing coping strategies to mitigate the adverse effects of environmental stress and enhance resilience. Fu et al. also conducted seagrass research using an investigation method in Wenchang, Hainan province. The results show the negative effects of human activities on seagrass. To reverse these degradation trends, controlling multiple human activities and planning rational marine engineering are essential.

Biogenic elements and their cycling are essential processes in wetlands, which are closely linked to carbon storage, vegetation growth, and pollution. Ma et al. studied how tidal flooding through creeks affects carbon and nitrogen in the soil of a Chinese salt marsh. They found that tidal creeks play a key role in how these elements are spread in the marsh. Hua et al. looked at how plant invasiveness and crab activity affect carbon storage. They discovered that crabs have a bigger impact on carbon storage than plant invasion. Zhang et al. did a detailed study on leaf nutrient patterns in coastal wetlands. They found differences in leaf nutrients between native and non-native plants, which should be considered in future studies on nutrient cycles and plant-animal interactions. Liu et al. used the plant *Sesuvium Portulacastrum* to study how it controls dissolved inorganic nitrogen in fish farming ponds. They suggest that coastal plants can help remove nitrogen pollutants from these ponds.

Coastal biological invasions are a big threat to ecosystems. Xu et al. studied how the invasive plant *Spartina alterniflora* affects the native moth *Laelia coenosa*. This moth is known to harm native *Phragmites australis* marshes in China's coastal wetlands. They used field surveys and feeding tests for their study. They discovered a new indirect way that coastal invasions can impact ecosystems. They also stressed the need to consider seasonal changes in plant and herbivore interactions.

We anticipate that the compilation of papers we have assembled will offer clear and valuable insights into the crucial ecological processes occurring in coastal wetlands, presenting management implications and specific strategies to address the challenges posed by environmental changes.

Author contributions

QW: Writing – review & editing, Writing – original draft. QZ: Writing – review & editing. DS: Writing – review & editing.

Funding

The author(s) declare that financial support was received for the research and/or publication of this article. The study was supported financially by the Natural Science Foundation of Guangdong Province (2025A1515011055) and the Natural Science Foundation of China (42107057).

Acknowledgments

The editors are grateful to be contributions made by the many authors involved in this project.

Conflict of interest

The authors declare that the research was conducted in the absence of any commercial or financial relationships that could be construed as a potential conflict of interest.

Generative AI statement

The author(s) declare that no Generative AI was used in the creation of this manuscript.

Publisher's note

References

FitzGerald, D. M., and Hughes, Z. (2019). Marsh processes and their response to climate change and sea-level rise. *Annu. Rev. Earth Pl Sc* 47, 481–517. doi: 10.1146/annurev-earth-082517-010255

He, Q., and Silliman, B. R. (2019). Climate change, human impacts, and coastal ecosystems in the anthropocene. *Curr. Biol.* 29, R1021–R1035. doi: 10.1016/j.cub.2019.08.042

Kirwan, M., and Megonigal, J. (2013). Tidal wetland stability in the face of human impacts and sea-level rise. *Nature* 504, 53–60. doi: 10.1038/nature12856

Newton, A., Icely, J., Cristina, S., Perillo, G. M. E., Turner, R. E., Ashan, D. W., et al. (2020). Anthropogenic, direct pressures on coastal wetlands. *Front. Ecol. Evol.* 8, 144. doi: 10.3389/fevo.2020.00144

Schuerch, M., Spencer, T., Temmerman, S., Kirwan, M., Wolff, C., Lincke, D., et al. (2018). Future response of global coastal wetlands to sea-level rise. *Nature* 561, 231–234. doi: 10.1038/s41586-018-0476-5

frontiers | Frontiers in Marine Science

TYPE Original Research
PUBLISHED 11 April 2024
DOI 10.3389/fmars.2024.1361474

OPEN ACCESS

EDITED BY
Yu Zhang,
Los Alamos National Laboratory (DOE), United States

REVIEWED BY
Rong Xiao,
Fuzhou University, China
Tian Xie,
Beijing Normal University, China
John Gallagher,
University of Tasmania, Australia

*CORRESPONDENCE
Mingxiang Zhang
zhangmingxiang@bjfu.edu.cn
Zhenming Zhang
zhenmingzhang@bjfu.edu.cn

RECEIVED 26 December 2023
ACCEPTED 28 March 2024
PUBLISHED 11 April 2024

CITATION
Ma Z, Wu Y, Zhao S, Pan Y, Liu J, Zhang M and Zhang Z (2024) The role of tidal creeks in shaping carbon and nitrogen patterns in a Chinese salt marsh.
Front. Mar. Sci. 11:1361474.
doi: 10.3389/fmars.2024.1361474

The role of tidal creeks in shaping carbon and nitrogen patterns in a Chinese salt marsh

Ziwen Ma, Yanan Wu, Siqi Zhao, Yueyan Pan, Jiakai Liu, Mingxiang Zhang* and Zhenming Zhang*

College of Ecology and Nature Conservation, Beijing Forestry University, Beijing, China

Tidal creeks play a crucial role in lateral transport of carbon and nutrients from tidal salt marshes. However, the specific impact of tidal creek development on carbon and nutrient distribution within the marsh remains poorly understood. The objective of this study is to assess the influence of lateral tidal flooding through the tidal creeks on the spatial distribution of carbon and nitrogen fractions in the soils of a Chinese temperate salt marsh. We conducted a comprehensive analysis of the relative variations in different carbon and nitrogen fractions, along with soil physicochemical and microbial indicators, between the bank soil of the tidal creek and its lateral inland soils across high, middle, and low flats. Our findings highlight that tidal creek development significantly affects the middle flat, leading to substantial variations in organic carbon and total nitrogen. The low flat mainly experiences changes in dissolved inorganic carbon levels. Furthermore, a lateral increase in microbial biomass is observed in the middle flat, indicating that the significantly lower SOC in the middle flat might be ascribed to enhanced microbial decomposition. The lateral enrichment of dissolved inorganic carbon in the low flat is possibly related to the nearshore location and/or abiotic adsorption in inorganic carbon sequestration. Overall, this study demonstrates the critical role of tidal creek development in shaping the distribution patterns of carbon and nitrogen fractions in tidal salt marshes.

KEYWORDS

blue carbon, nitrogen, tidal creek, salt marsh, Yellow River Delta

1 Introduction

Tidal wetlands, occurring in geomorphic settings with constant exchange of water and matter (dissolved and particulate) with adjacent estuaries, play a critical role in hydrological and biogeochemical cycling at the land-sea interface on local to global scales (Mcleod et al., 2011; Duarte et al., 2013; Santos et al., 2019; Webb et al., 2019). Salt marshes, widely thriving in tidal wetlands, are regarded as blue carbon ecosystems together with mangroves and seagrass beds, and are the most efficient soil carbon sinks on Earth on an areal basis

(Mcleod et al., 2011; van Ardenne et al., 2018). With the increasing global recognition of the significant role of blue carbon ecosystems in sequestrating carbon and mitigating climate change (Atwood et al., 2017), numerous studies have been conducted to quantify soil carbon stocks and explore the specific processes of carbon cycling in these ecosystems (Sanders et al., 2016; Asanopoulos et al., 2021; Santos et al., 2021).

Tidal creeks, cutting through low permeable salt marsh mud, are crucial in the transportation of carbon and nutrients, where they can export these materials through the flushing of plant and sediment materials or import marine organic matter over a full tidal period (Krest et al., 2000; Odum, 2002; Call et al., 2019; Tan et al., 2020). The sediment found on the banks and the suspended matter in the water can originate from tidal-driven erosion or resuspension occurring in adjacent tidal creeks (Fagherazzi et al., 2013). Additionally, tidal creeks serve as a link between surface marsh soils and tidal creek waters, which eventually connect to the ocean and/or the atmosphere through porewater exchange (Santos et al., 2019). Furthermore, tidal creeks function in directly connecting surface waters with underlying aquifers, where submarine groundwater discharge has been recognized as a significant exchange mechanism between land and sea (Taniguchi et al., 2019; Glaser et al., 2021).

Areas within the coastal ocean carbon cycle that remain uncertain have been subjected to decades of research (Windham-Myers et al., 2018). The question of whether salt marshes act as sinks or sources to adjacent estuaries has long been debated. Previous studies have suggested that this may be influenced by factors such as vegetation type (e.g., Tan et al., 2020), and/or tidal extent and magnitude (e.g., Regier et al., 2021). Furthermore, different carbon pools demonstrate distinct variation patterns in tidal creek-mediated lateral carbon fluxes. For example, research conducted on Taskinas Creek, a temperate tidal marsh creek system in the York River Estuary, revealed that the salt marsh acted as a sink for particulate organic carbon (POC) and a source of dissolved inorganic carbon (DIC) (Knobloch et al., 2021). In contrast, dissolved organic carbon (DOC) levels showed little variation across tidal stages (Knobloch et al., 2021). In another study conducted on Chongming Dongtan wetland, a temperate tidal salt marsh in the Yangtze estuary, it was found that the Poaceae creek served as a source of DOC and DIC throughout the year and as a sink of POC and particulate inorganic carbon (PIC) seasonally (Tan et al., 2020). Additionally, the Cyperaceae creek acted as a source of all investigated carbon components consistently throughout the year (Tan et al., 2020).

Great efforts have been made to quantify lateral outwelling carbon fluxes through spatial and temporal investigations in creek waters. However, little is known about the impact of tidal creek development on the spatial distribution of carbon and nutrient within the marsh itself. This lack of information also means that the relationship between carbon sequestration and environmental or geomorphic characteristics has not been well established. The changing climate, with its shifts in tidal extent and coastal geomorphology due to sea level rise, increased storm activity, and altered precipitation patterns, will have a significant impact on the role of tidal marsh systems in the coastal carbon cycle (Gabler et al., 2017; Ensign and Noe, 2018). Therefore, it is essential to have reliable estimates of the effect of tidal creek development on carbon and nutrient distribution and the potential drivers under current hydrological conditions. Such information would greatly enhance our understanding of the biogeochemical processes that influence carbon in the coastal zone (Knobloch et al., 2021).

Our previous investigations found that soil inorganic carbon (SIC) distribution was significantly influenced by sedimentary processes from land to sea, demonstrating a clear seaward decreasing trend (Ma et al., 2024). Conversely, soil organic carbon (SOC) did not exhibit consistent variation patterns from land to sea, which is thus hypothesized to be related to the development of tidal creeks in the tidal flat. This hypothesis is based on previous findings that biological activities, such as the growth of vegetation (Wu et al., 2021), seed fluxes and germination (Wu et al., 2023a, 2023b) in tidal flats can be influenced by tidal creek development. Additionally, substantial variations in tidal creek distribution patterns were observed among high, middle, and low flats, resulting in significant effects on soil moisture and salinity gradients (Wu et al., 2020). Therefore, we propose that the spatial distribution of different carbon and nitrogen fractions in tidal salt marshes would also respond differently to varying tidal creek development. However, SOC distribution could also be impacted by the sedimentary process from land to sea, so it was hard to further verify the role of tidal creeks in impacting carbon and nutrient distribution without excluding the influence of the original sedimentation in affecting SOC variation. Therefore, we investigated the relative variations of different carbon and nitrogen fractions between the bank soil and its perpendicularly flooding inland soils along the creek-perpendicular sampling transect at high, middle, and low flats. The bank soil of tidal creek underwent the highest hydrodynamical energy and constant scouring of seawater, which significantly limited biological activities, such as seed settling and plant growth (Bouma et al., 2009; Lai et al., 2018). As seawater floods into the marsh through the creek, the hydrodynamic forces weakened and gradually created suitable soil environments for salt-tolerated plants to thrive (Wang et al., 2021). The barren bank soil was accordingly regarded as the starting point of the impact of the development of tidal creeks for saltmarshes. The calculation of the relative variation of different carbon and nitrogen fractions between the bank soil and lateral inland soil in each creek-perpendicular transect can eliminate the originally vertical sedimentary effects on their distribution from land to sea. Comparison of the relative variations of different carbon and nitrogen fractions among high, middle and low flats were intended to demonstrate the potentially different role of lateral tidal flooding through the tidal creeks in shaping the distribution patterns of carbon and nitrogen in tidal salt marshes.

2 Materials and methods

2.1 Site description

The study was conducted in the Yellow River Delta (YRD), which is the youngest and largest coastal wetland in temperate

China with a high biodiversity level. This region is featured by a continental monsoon climate as the annual mean temperature of 12-13°C and average annual precipitation of 560-590 mm (Ning et al., 2023). The soil type along the coastline, identified as Calcaric Fluvisols and Gleyic Solonchaks, is mainly derived from the Loess Plateau in the middle and upper reaches of the Yellow River. The tides in this region are irregular and semi-diurnal, with the average tidal amplitude ranging from 1.1 to 1.5 m (Chang et al., 2022). The salt marsh plants were distributed in the intertidal zone. Among them, the *Suaeda salsa* is the dominant therophyte and pioneer species in the tidal native salt marsh of the YRD, distributing from middle to high marshes. The *S. salsa* tidal salt marsh is formed due to the development of numerous tidal creeks, which bring enough seeds and sustain suitable hydrologic and saline environments for the growth of *S. salsa* (Wang et al., 2021). In turn, the *S. salsa* tidal salt marshes provide pivotal stopover habitats for millions of migratory shorebirds of the East Asian-Australasian Flyway (Studds et al., 2017). These marshes, also known as the iconic "Red Beach," not only support a vast number of migratory shorebirds but also have substantial economic and tourism potential (Ren et al., 2021). To study the relationship between the spatial distribution of carbon and nitrogen fractions and the development of tidal creeks, the study area (119°9′~119°11′ E, 37°46′ ~37°49′ N) chosen was a region with a relatively complete and undisturbed tidal creek network (Figure 1).

2.2 Soil collection and analysis

Before the field sampling, the tidal creek in the high, middle, and low flat of the YRD was identified using aerial images. Two sample transects were then established in the high, middle, and low flats of the study area, respectively, following the direction of the vertical tidal creek. A total of six transects were set up from the seaward to the landward (Figure 1). In each sampling transect, five plots were designated at 0, 10, 20, 30, and 40 m. Due to the great hydrodynamical energy and constant scouring of seawater it underwent, the bank soil of tidal creek barely supported plant growth. Therefore, the bank soil at the 0 m plot served as the reference soil, while the soils at the rest plots of the same transect were considered inland soils. Soil samples were collected separately from each plot, including a five-multi-point mixed surface soil sample (0-10 cm) and a cutting ring surface soil sample. Vegetation information of the high, middle, and low flat has been recorded based on both unmanned aerial vehicle (UAV) aerial photography and field surveys in another study (Wu et al., 2020). It is worth mentioning that the sampling focused on shallow soil depths (0-10 cm) to ensure the recent influence of the tidal marsh creek system was captured, rather than historical influences from greater depth within the soil profile (Kelleway et al., 2017; Asanopoulos et al., 2021). During the sampling process, all wetland soil samples were collected during low tide to eliminate any additional effects of tides. A total of 30 soil samples and 30 cutting ring samples were collected in March 2021, which marked the beginning of the growing season with the least precipitation throughout the year. This timing was chosen to minimize the impact of other hydrological processes on the distribution of carbon and nitrogen fractions driven by the local climate. Within a week, all collected soil samples were transported to the laboratory. Prior to analysis, visible roots and debris were manually removed, and each sample was divided into three parts. One part was utilized for physical and chemical analysis, another part was stored at 4°C for the measurement of microbial biomass within a week, and the third part was freeze-dried and preserved in a refrigerator at -80°C to determine the phospholipid fatty acids (PLFAs) content in the soils.

The bulk density (BD) and moisture were measured by drying cutting ring samples at 105°C for 24 h, and further salt correction was calculated for BD measurement (Lavelle et al., 1985). The soil pH was determined using a HANNA pH meter (Hanna Instruments, Woonsocket, RI, USA) with a soil to water ratio of 1:5. Electric conductivity (EC) was measured in the supernatant of 1:5 soil-water mixtures using an EC meter (VWR Scientific, West Chester, PA, USA). The soil texture was characterized by analyzing the soil particle size distribution with a laser particle size analyzer (SEDIMAT 4–12, Germany), after the removal of organic matter by digestion in a heated hydrogen peroxide solution with sodium hexametaphosphate as a dispersing agent (Peng et al., 2014). The total carbon (TC) and total nitrogen (TN) contents were quantified using an elemental analyzer (Heraeus Elementar Vario EL, Hanau, Germany). SOC was measured using the dichromate oxidation method (Anderson and Domsch, 1989), on dried and sieved soils with a particle size of 0.149 mm. SIC was calculated as the difference

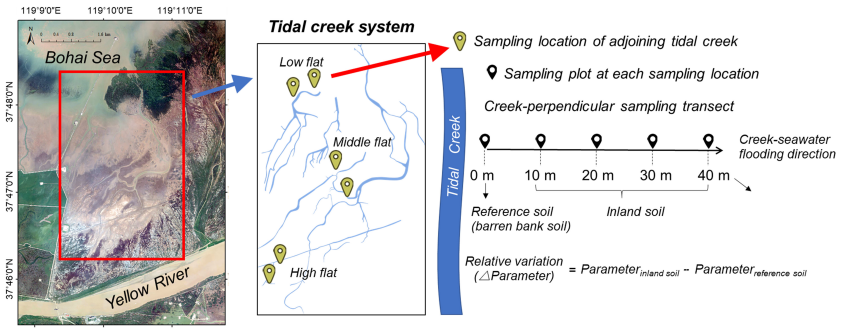

FIGURE 1
Location map of sampling sites in the Yellow River Delta, China.

between TC and SOC. The microbial biomass carbon (MBC) and microbial biomass nitrogen (MBN) were measured using the chloroform fumigation-extraction (CFE) method (Vance et al., 1987), as described by Ma et al. (2017). The DOC and DIC were measured using a total organic carbon analyzer (TOC-V, Shimadzu, Kyoto, Japan), with soil extracts obtained by shaking a mass ratio of soil to water of 1:10 for 24 h in the dark and passing through 0.45 μm filter membranes.

Soil PLFAs were identified based on a modified single-phase extraction according to Bossio et al. (1998), as described by Ma et al. (2017). Total PLFAs (TotPLFA), which were calculated as the sum of PLFAs with more than 1% of the total relative abundance, served as an overall indicator of microbial biomass. Bacterial PLFAs (BacPLFA) were calculated as the sum of 14:0, i15:0, a15:0, 15:0, i16:0, 16:1ω9c, 16:1ω7c, 16:0, 16:1ω7cDMA, i17:0, a17:0, 17:1ω8c, 17:1ω6c, cy17:0, 17:0, 18:1ω7c, 18:1ω5c, 18:0, cy19:0 (García-Orenes et al., 2013). Branched phospholipids i15:0, a15:0, i16:0, i17:0, a17:0 were used as gram-positive bacterial biomarkers (GpPLFA), and gram-negative bacterial biomass (GnPLFA) were assessed by 16:1ω9c, 16:1ω7c, 17:1ω8c, 17:1ω6c, cy17:0, 18:1ω7c, 18:1ω5c, cy19:0 (Olsson et al., 1995; García-Orenes et al., 2013). Fungal PLFAs (FungalPLFA) were quantified by summing 18:2ω6c and 18:1ω9c (Frostegård and Bååth, 1996; Olsson, 1999). Actinomycetes PLFAs (ActinoPLFA) were calculated as the sum of 10Me fatty acids (Zelles et al., 1995). The fatty acid 16:1ω5c was employed as an indicator of arbuscular mycorrhizal fungi (AMFungalPLFA) (Olsson et al., 1995), and the presence of protozoa was determined by the abundance of 20:4ω6c (ProtozoaPLFA) (Doran et al., 2007).

2.3 Statistical analysis

Soil carbon/nitrogen fraction stocks (g/m^2) in total soils were calculated as:

$$\text{Soilcarbon/nitrogenfractionstocks} = D \times BD \times C \times 10$$

where D was the thickness (cm) of the soil layer, BD was the bulk density (g/cm^3) and C was the contents (g/kg) of corresponding carbon/nitrogen fraction (including TC, SOC, DOC, MBC, SIC, DIC, TN, MBN) at the 0-10 cm soil depth.

Relative variations of soil physicochemical properties/microbial PLFAs/carbon and nitrogen fraction concentrations and stocks were calculated as:

$$\text{Relative variations of single parameter } (\Delta\,\text{Parameter}) = \text{Parameter}_{\text{inland soil}} - \text{Parameter}_{\text{reference soil}}$$

Data analysis and figure creation were carried out using R v.4.1.1 (R Development Core Team, 2021). Prior to statistical analysis, tests for normality on the raw data were performed. One-way analyses of variance with a Tukey's honestly significant difference *post hoc* test were used to assess differences among high, middle and low flats ($P < 0.05$). Principle component analysis (PCA) was conducted to identify the spatial differences of sampling sites and explore potential relationship among relative variations of soil physicochemical properties, microbial parameters and carbon and nitrogen fraction concentrations and stocks.

3 Results

Two simplified effects, including vertical sedimentation effect and lateral tidal effect through the development of tidal creeks, on the distribution patterns of carbon and nitrogen fractions were illustrated in Figure 2. Accordingly, the absolute values of soil metrics in different locations relative to the seashore primarily reflected the effect of sedimentary processes on the soil from land to sea. While the relative variations calculated in this study were aimed to eliminate the vertical sedimentation effect and demonstrate the lateral tidal effect on the soil metrics.

3.1 Lateral tidal effect on soil physicochemical properties

The comparison of absolute values of soil physicochemical properties across high, middle and low flats showed relatively obvious vertical sedimentary characteristics from land to sea as indicated by soil texture, BD, moisture and EC (Supplementary Figure S1). Specifically, soil texture tended to be coarser and BD tended to be greater in the seaward side of tidal flats. This is largely due to the vertical influence of tidal seawater on the transportation and deposition of soil particles, as finer soils were more easily transported by water flow compared to coarser ones (Nguyen et al., 2013). These vertical sedimentary characteristics played a dominant role in creating a water-salt gradient from land to sea, as well (Rabot et al., 2018). When eliminating the vertical sedimentary effect by calculating the relative variation of inland soils relative to the reference soil, it could be observed that the locations of tidal flats relative to the seashore also exert distinct effects on soil texture and salinity in relation to the development of tidal creeks. In the middle

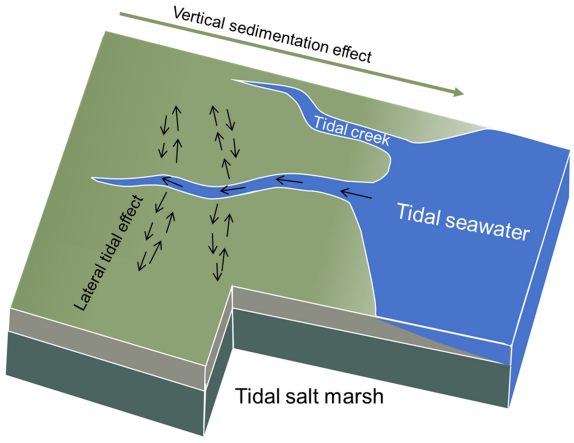

FIGURE 2
A simplified conceptual diagram of the role of tidal creeks in exerting lateral effect on the distribution patterns of carbon and nitrogen fractions in salt marsh.

flat, the lateral inland soils showed lower clay contents compared to the reference soil, and their relative variations were all below 0 (Figure 3E). However, the relative variations of clay content in high and low flats were roughly all above 0, and significantly higher than those in the middle flat (Figure 3E). Conversely, the middle flat exhibited significantly higher relative variations of sand content compared to high and low flats (Figure 3G). This suggests that the lateral deposition of large-sized soil particles in tides through the development of tidal creeks tends to occur more in the middle flat than in high and low flats. Moreover, the high flat exhibited significantly higher relative variations of soil EC compared to the middle and low flats (Figure 3D). This indicates that the development of tidal creeks in the high flat leads to the accumulation of soil salinity in their lateral flooding inland soils. However, no statistically significant difference was found in the relative variations of soil moisture, pH, and silt content across high, middle, and low flats.

3.2 Lateral tidal effect on soil PLFAs

Both the vertical sedimentation processes and lateral tidal flooding exert similar effects on the distribution of soil PLFAs indicative of most taxonomic soil microbes, as significantly higher absolute contents and relative variations of TotPLFA, BacPLFA, GpPLFA, GnPLFA, FungalPLFA, ActinoPLFA, and AMFungalPLFA were detected in the middle flat compared to high and low flats (Supplementary Figures S2, 4), indicating a enrichment of biomass of most microbial communities induced by both vertical sedimentation and lateral tidal effect. However, ProtozoaPLFA showed relatively different varied patterns from other PLFAs, as its absolute content was increased from land to sea, while there was no significant difference in the relative variation of ProtozoaPLFA across high, middle and low flats. This suggests that protozoa is likely to be affected by vertical sedimentary processes instead of lateral tidal flooding through the tidal creeks.

3.3 Lateral tidal effect on soil carbon and nitrogen contents and stocks

There was an increasing trend for SOC contents and stocks and decreasing trend for SIC contents and stocks along the vertical sedimentation gradient from land to sea, leading to overall insignificant changes in TC levels (Supplementary Figures S3–S5). However, there was no significant change in MBC, DOC, DIC, TN and MBN contents and stocks regarding the vertical sedimentation effect (Supplementary Figures S3–S5). Comparatively, when eliminating vertical sedimentation effect by calculating relative variations to the reference soil, it was shown that the development of tidal creeks showed a similar lateral impact on the contents and stocks of TC and SOC. The middle flat had

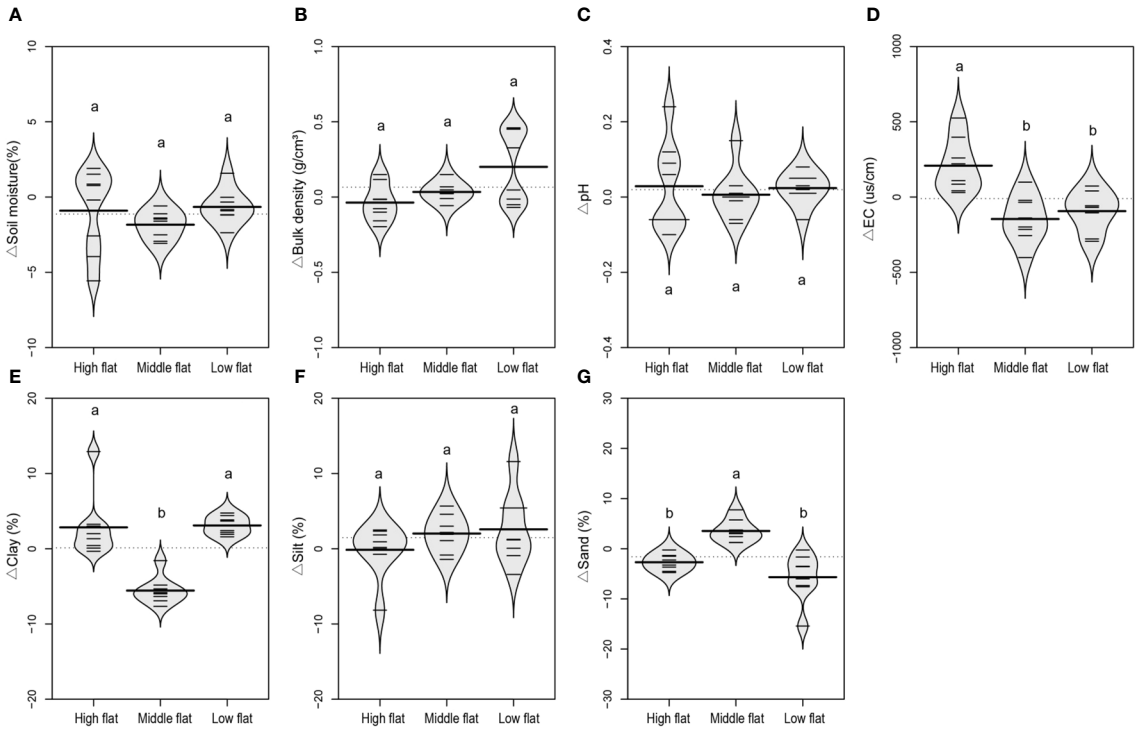

FIGURE 3
A beanplot of relative variation of inland surface (0-10 cm) soils (sampled at 10, 20, 30 and 40 m vertical distance from the tidal channel) to the reference soil (sampled at 0 m vertical distance from the tidal channel) in soil moisture **(A)**, bulk density **(B)**, pH **(C)**, electrical conductivity **(D)**, clay content **(E)**, silt content **(F)**, and sand content **(G)**. Individual observations are shown as small black lines and the median value with a longer black line. The grey area shows the distribution of concentrations (N = 8). Different lowercase letters (a, b) in the same graph indicate significant differences ($P < 0.05$).

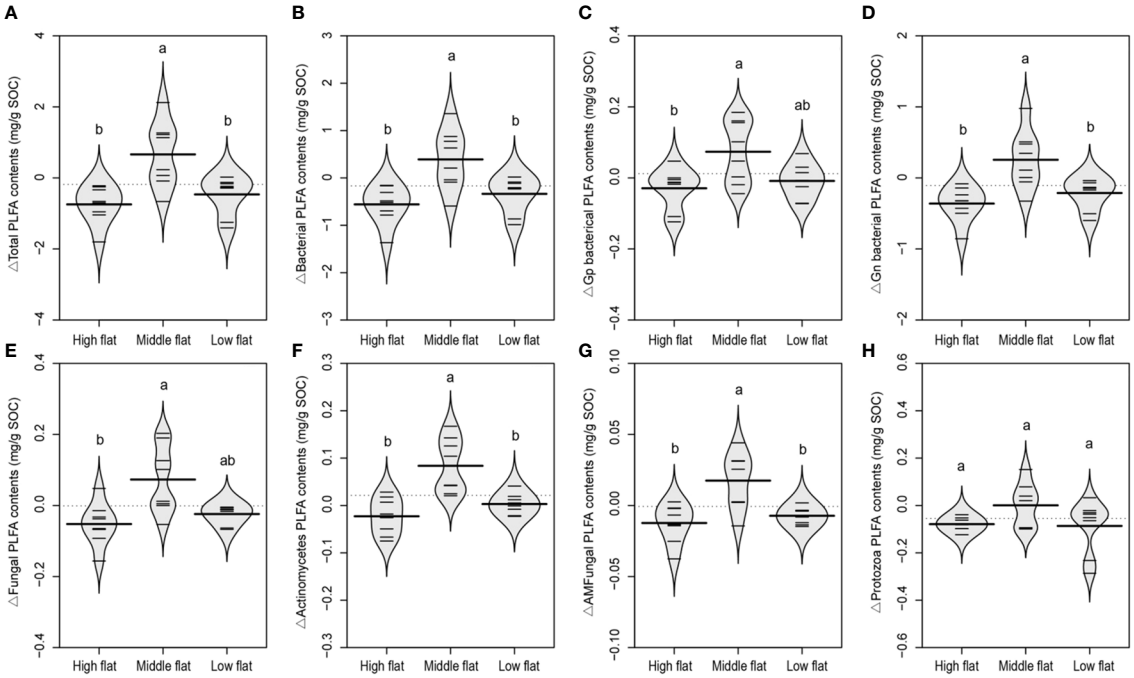

FIGURE 4
A beanplot of relative variation of inland surface (0-10 cm) soils (sampled at 10, 20, 30 and 40 m vertical distance from the tidal channel) to the reference soil (sampled at 0 m vertical distance from the tidal channel) in contents of total PLFA **(A)**, bacterial PLFA **(B)**, gram-positive bacterial PLFA **(C)**, gram-negative bacterial PLFA **(D)**, fungal PLFA **(E)**, actinomycete PLFA **(F)**, arbuscular mycorrhizal fungal PLFA **(G)**, and protozoa PLFA **(H)**. Individual observations are shown as small black lines and the median value with a longer black line. The grey area shows the distribution of concentrations (N = 8). Different lowercase letters (a, b) in the same graph indicate significant differences (P< 0.05).

significantly lower relative variations of TC and SOC compared to the high and low flats (Figures 5A, B, 6A, B). The same spatially divergent response to tidal creek development was observed for TN and MBN contents and stocks, with significantly lower relative variations in the middle flat than in the high and low flats (Figures 5E, F, 6E, F). This suggests that the middle flat accumulated less organic carbon and nitrogen induced by the lateral tidal effect within the zone. However, this divergence was not observed for DOC, MBC and SIC, as their relative variations of contents and stocks did not differ significantly among different flats (Figures 5–7). Interestingly, levels of DIC tended to be higher near the seashore with the effect of lateral tidal flooding, as relative variations of DIC contents and stocks were significantly higher in the low flat compared to the high and middle flats (Figure 7).

3.4 PCA of soil carbon and nitrogen fractions and soil physicochemical and microbiological properties

The spatial divergence in soil physicochemical, microbiological, and carbon and nitrogen parameters across the three tidal flats was illustrated using multivariate PCA (Figure 8). The PCA analysis revealed that PC1 and PC2 accounted for 44.12% and 16.70% of the variability in carbon and nitrogen contents, respectively (Figure 8A), and 44.35% and 12.41% of the variability in carbon and nitrogen stocks, respectively (Figure 8B). The location of the sampling tidal flats relative to the seashore had a significant impact on the variability. Specifically, the PCA loading scores showed that the middle flat exhibited a distinct cluster along PC1, separate from the high and low flats, primarily due to significantly higher soil microbial PLFAs and lower SOC and clay content.

4 Discussion

4.1 The middle flat was a potential hotspot of carbon and nitrogen variation induced by lateral tidal effect

Based on the results of our investigations, the middle flat in tidal *S. salsa* salt marsh of the YRD exhibited significantly lower organic carbon and nitrogen levels under the influence of lateral tidal flooding compared to the high and low flats. Given the bank soil barely supported plant growth, the direct measurements of vegetation parameters could be equal to the relative variation calculated in this study. Therefore, variations of SOC and TN induced by lateral tidal effect tended to contradict that of vegetation, as previous studies showed that the middle flat had a denser growth of *S. salsa* and greater seed germination rates (Wu et al., 2021; Wu et al., 2023a, b). Typically, aboveground vegetation should have a positive influence on the accumulation of SOC through the input of plant detritus, root exudates, and particle trapping (Santini et al., 2019; Santos et al., 2019). However, in this

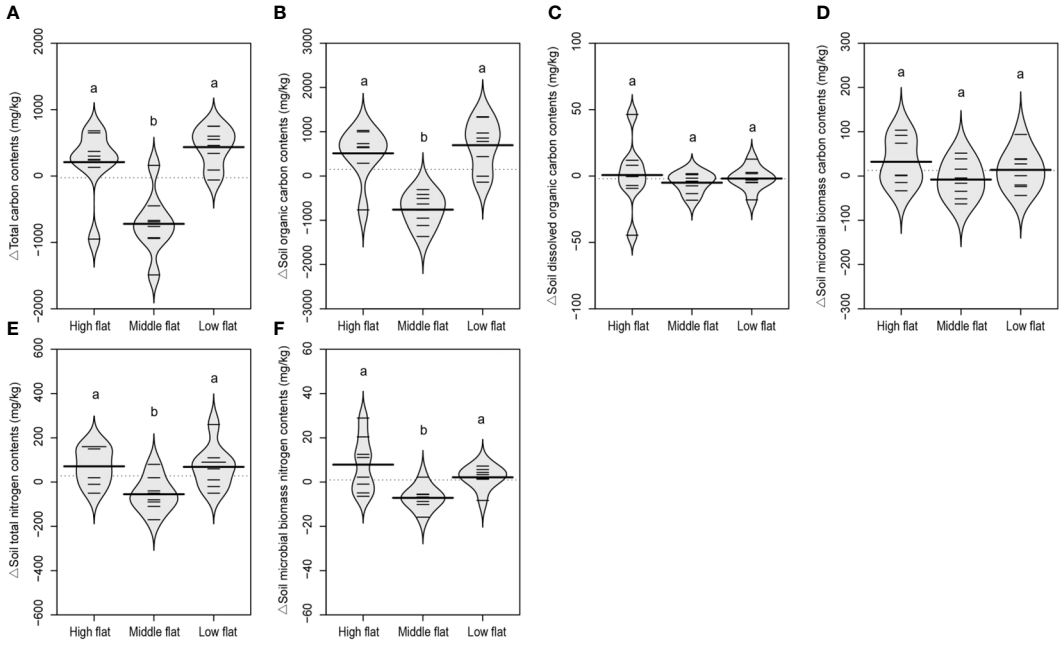

FIGURE 5
A beanplot of relative variation of inland surface (0-10 cm) soils (sampled at 5, 10, 20, 30 and 40 m vertical distance from the tidal channel) to the reference soil (sampled at 0 m vertical distance from the tidal channel) in soil total carbon contents **(A)**, organic carbon contents **(B)**, dissolved organic carbon contents **(C)**, microbial biomass carbon contents **(D)**, total nitrogen contents **(E)**, and microbial biomass nitrogen contents **(F)**. Individual observations are shown as small black lines and the median value with a longer black line. The grey area shows the distribution of concentrations (N = 8). Different lowercase letters (a, b) in the same graph indicate significant differences (P< 0.05).

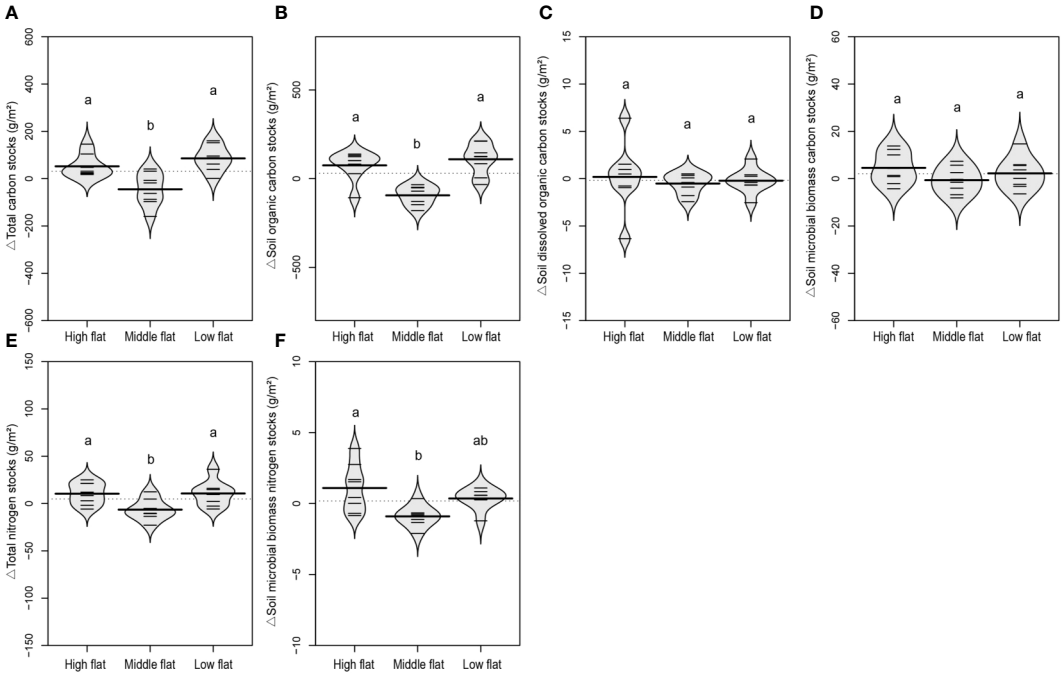

FIGURE 6
A beanplot of relative variation of inland surface (0-10 cm) soils (sampled at 10, 20, 30 and 40 m vertical distance from the tidal channel) to the reference soil (sampled at 0 m vertical distance from the tidal channel) in soil total carbon stocks **(A)**, organic carbon stocks **(B)**, dissolved organic carbon stocks **(C)**, microbial biomass carbon stocks **(D)**, total nitrogen stocks **(E)**, and microbial biomass nitrogen stocks **(F)**. Individual observations are shown as small black lines and the median value with a longer black line. The grey area shows the distribution of concentrations (N = 8). Different lowercase letters (a, b) in the same graph indicate significant differences (P< 0.05).

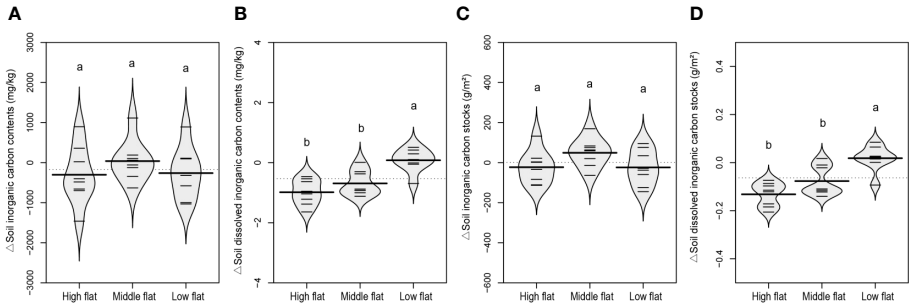

FIGURE 7
A beanplot of relative variation of inland surface (0-10 cm) soils (sampled at 10, 20, 30 and 40 m vertical distance from the tidal channel) to the reference soil (sampled at 0 m vertical distance from the tidal channel) in soil inorganic carbon contents **(A)**, dissolved inorganic carbon contents **(B)**, inorganic carbon stocks **(C)**, and dissolved inorganic carbon stocks **(D)**. Individual observations are shown as small black lines and the median value with a longer black line. The grey area shows the distribution of concentrations (N = 8). Different lowercase letters (a, b) in the same graph indicate significant differences (P< 0.05).

study, no such positive association was observed. Several potential explanations for this inverse pattern can be considered. Firstly, the higher germination rates and better connectivity of plant patches in the middle flat indicated potentially higher nutrient uptake, resulting in a significant reduction of SOC and TN concentrations and stocks. Secondly, the middle flat had a denser distribution of tidal creeks. Our previous investigations have found that the average branching rate and density of tidal creeks in the middle flat was 6.23 pcs/km^2 (pieces of bifurcation point per unit area) and 2.22 km/km^2 (lengths of tidal creeks per unit area), respectively, higher than the high flat (3.79 pcs/km^2, 1.44 km/km^2) and low flat (2.61 pcs/km^2, 2.21 km/km^2) (Wu et al., 2020). These morphological differences of tidal creeks potentially led to intensified hydrodynamic energy resulting from superimposed effect of multiple tidal creeks in the middle flat that weakened the trapping and sedimentation abilities of this area, thereby reducing the burial of SOC. This distinct pattern of sedimentation was further reflected in the composition of soil texture, with the middle flat exhibiting significantly more sand and less clay content compared to the high and low flats (Figure 3). This reduction in clay content induced by lateral tidal effect could also contribute to the decreased SOC levels in the middle flat, as larger-sized soil particles bind less SOC due to their smaller surface areas (Pedersen et al., 2011).

Furthermore, higher relative variations of microbial biomass as indicated by soil PLFAs (Figure 4) and lower SOC levels were concomitant in the middle flat, suggesting enhanced microbial decomposition that could contribute to the decrease in sequestered SOC impacted by the lateral tidal flooding. Both the vertical and lateral enrichment of microbial biomass in the middle flat partly aligns with the intermediate disturbance hypothesis, which postulates that disturbances of an intermediate frequency or intensity maximize community biodiversity/richness (Odum, 1963). The distribution pattern and germination rates of *S. salsa* in tidal flats of the YRD have been previously demonstrated to respond in a curvilinear mode with the hydrologic connectivity (Wang et al., 2021; Wu et al., 2021). Coastal areas with intermediate disturbances have been reported to support more biodiversity albeit

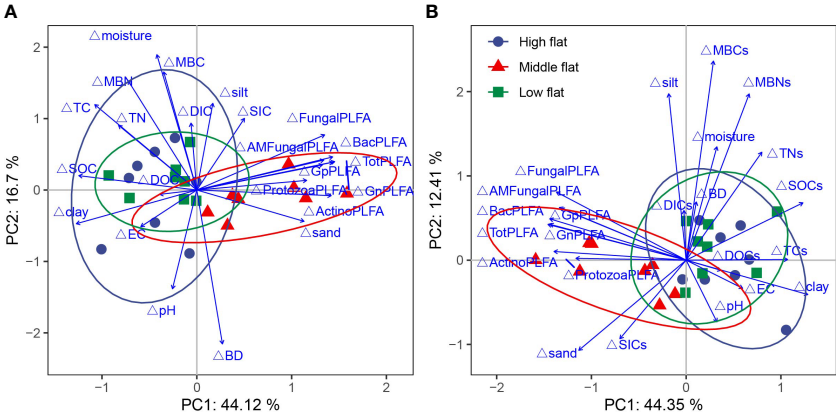

FIGURE 8
Principal component analysis (PCA) of relative variation of soil physicochemical properties, microbial parameters and carbon contents **(A)** and stocks **(B)** in tidal *S. salsa* saltmarsh in the YRD. Blue solid circles represent soils sampled in high flat, red solid triangles represent soils sampled in middle flat, and green solid squares represent soils sampled in low flat. Solid arrows are soil physicochemical properties and microbial parameters.

with disputes (England et al., 2008; Gerwing et al., 2017). This trend was partially followed by soil microbes, suggesting a potential interconnected network linking all biodiversity, from flora and fauna to soil microbes, which leads them to respond similarly to external disturbances. However, the regulating mechanisms of the enrichment of soil microorganisms in the middle flat and their connections to the ecological functions of salt marshes, such as carbon sequestration, require further verification and exploration.

4.2 Different carbon and nitrogen fractions exhibited varied responding patterns to the lateral tidal effect

In this study, there were no consistent patterns observed for the investigated carbon and nitrogen fractions in response to the lateral tidal effect. Specifically, although lateral tidal flooding through tidal creeks in the middle flat tended to reduce SOC, no significant difference was found for SIC levels. The relatively contrasting distribution pattern between SIC and SOC along the vertical sedimentation gradient from land to sea showed a negative interaction between SOC and SIC variations, which partly resulted from the limited packing density of the sedimentation process of organic matter fraction and mineral fraction of the soil (Breithaupt et al., 2017; Asanopoulos et al., 2021). However, no such contrasting variation pattern between SOC and SIC induced by the lateral tidal flooding through the tidal creeks was indicative of their distinct responding patterns to the development of tidal creeks. Furthermore, the insignificant difference in SIC variation may also be ascribed to its more complicated formation and transformation mechanisms that counteract with each other (Lal, 2008; Han et al., 2018). On the whole, our previous study conducted in the YRD has shown that SIC contents and stocks significantly decreased from land to sea, while SOC exhibited inconsistently varied pattern along the vertical sedimentation gradient (Ma et al., 2024). Taking the findings of this study and the previous study into consideration, it appears that SOC is likely to be more impacted by the lateral tidal flooding through the tidal creeks, whereas SIC is more influenced by the vertical sedimentary processes from land to sea.

Likewise, neither lateral tidal flooding nor vertical sedimentary processes exerted significant effects on DOC variation in tidal *S. salsa* salt marshes of the YRD. Previous studies exploring the contributions of marsh creek systems to the lateral export of carbon components reported that DOC did not show an obvious gradient across tidal stages, possibly due to the high processing of DOC within tidal creeks, which homogenized the signals from the estuary and marsh system (Santos et al., 2019; Knobloch et al., 2021). Accordingly, the homogenizing effect of tidal seawater entering the salt marsh with high residence time may also occur in soils, resulting in insignificant changes of DOC levels in tidal salt marshes. Additionally, despite the insignificant changes in DOC contents and stocks, the sources of DOC can be distinct, which can be indicated by CDOM and/or other analysis methods (Knobloch et al., 2021). Consequently, it is essential to incorporate other indicators of DOC dynamics in further studies to provide more information on its variation.

DIC exhibited a distinct distribution pattern with lateral enrichment in the low flat (Figure 7), which was different from other carbon and nitrogen fractions in this study. As an important component of outwelling carbon, DIC plays a crucial role in coastal carbon cycling, as its outwelling and subsequent oceanic storage is a potential mechanism for long-term carbon sequestration (Santos et al., 2021). Previous studies have reported that the flux of DIC exceeds that of DOC in tidal ecosystems, although this finding is still debated (Call et al., 2019; Santos et al., 2019). DIC typically exhibits non-conservative behavior in estuary ecosystems, with its fate regulated by various factors (e.g., salinity and vegetation) (Tzortziou et al., 2011; Tan et al., 2020). The significant lateral enrichment of DIC in the low flat was likely to result from the case that the nearshore sites principally received more tidal seawater containing a greater amount of dissolved components per unit volume of the sediment column down to 10 cm, thereby elevating the DIC levels in the soil. On the other hand, it could also be attributable to the enhanced abiotic absorption of CO_2 induced by the lateral tidal flooding in the low flat, which is widely existed in inorganic carbon sequestration for high saline-alkali coastal soils (Wang et al., 2019). However, this needs further research to provide more direct evidence on the lateral tidal effect on the abiotic absorption of CO_2.

In addition to lateral outwelling, respiration was an important process for the export of fixed carbon in salt marshes. Although direct measurements of export gasses were not conducted in this study, soil microbial decomposition can be partially indicated by MBC and soil PLFAs. However, MBC exhibited no significant difference in tidal flats at different locations, while soil PLFAs tended to be abundant in the middle flat. This difference may be due to the different approaches used to measure microbial biomass. MBC was measured based on extracts and elements from lysed cells, representing the living part of soil organic matter (Kaur et al., 2005). On the other hand, PLFA is a constituent of living cell membranes (Kaur et al., 2005). Similar inconsistencies have been reported in previous studies (Leckie et al., 2004; Liu et al., 2018). Therefore, it is recommended to incorporate both indicators of microbial biomass for comprehensive results (Liu et al., 2018). Notably, PLFA analysis provides not only information on biomass but also taxonomic identity (Bossio and Scow, 1998). While most taxonomic PLFAs showed lateral enrichment in the middle flat, ProtozoaPLFA was found to be irresponsive to the lateral tidal effect, but varied along the vertical sedimentary gradient from land to sea. This also reflects divergent microbial inhabitation characteristics in response to the distinct vertical sedimentation and lateral tidal flooding in tidal flats.

5 Conclusions

This study demonstrates that the lateral tidal flooding through the tidal creeks in salt marsh exerts a marked effect on the distribution of carbon and nitrogen fractions. The divergent variation patterns of these carbon and nitrogen fractions ascross high, middle, and low flats demonstrate that the lateral tidal flooding has a strong impact on the sequestration of carbon in tidal salt marsh. Overall, the middle flat tended to be a hotpot of SOC, TN, and MBN variation, while DIC tended to be affected in the low flat under the influence of lateral tidal flooding. Significantly

lower relative variations of SOC in the middle flat induced by the lateral tidal effect may be ascribed to the enhanced microbial decomposition in the middle flat, suggested by concomitantly higher relative variations of microbial biomass as indicated by soil PLFAs and lower SOC levels. Additionally, better plant growth and denser creek distribution in the middle flat may also result in the reduction of SOC and TN levels due to increased nutrient uptake and superimposed scouring effects of multiple tidal creeks. However, the lateral enrichment of DIC in the low flat was possibly related to the greater amount of dissolved components contained in the seawater and/or abiotic adsorption, which needs further research. These findings underscore the critical role of lateral tidal effect in shaping the distribution patterns of carbon and nitrogen fractions in the soils of tidal salt marshes.

Data availability statement

The raw data supporting the conclusions of this article will be made available by the authors, without undue reservation.

Author contributions

ZM: Conceptualization, Writing – original draft, Writing – review & editing. YW: Data curation, Investigation, Writing – original draft. SZ: Formal analysis, Writing – original draft. YP: Visualization, Writing – original draft. JL: Methodology, Software, Writing – original draft. MZ: Funding acquisition, Supervision, Writing – review & editing. ZZ: Data curation, Supervision, Writing – review & editing.

Funding

The author(s) declare financial support was received for the research, authorship, and/or publication of this article. We acknowledge the financial support from the National Key R&D Program of China (2022YFF1301004) and the Fundamental Research Funds for the Central Universities (PTYX202346).

Conflict of interest

The authors declare that the research was conducted in the absence of any commercial or financial relationships that could be construed as a potential conflict of interest.

Publisher's note

Supplementary material

The Supplementary Material for this article can be found online at: https://www.frontiersin.org/articles/10.3389/fmars.2024.1361474/full#supplementary-material

References

Anderson, T. H., and Domsch, K. H. (1989). Ratios of microbial biomass carbon to total organic carbon in arable soils. *Soil Biol. Biochem.* 21, 471–479. doi: 10.1016/0038-0717(89)90117-X

Asanopoulos, C. H., Baldock, J. A., Macdonald, L. M., and Cavagnaro, T. R. (2021). Quantifying blue carbon and nitrogen stocks in surface soils of temperate coastal wetlands. *Soil Res.* 59, 619–629. doi: 10.1071/SR20040

Atwood, T. B., Connolly, R. M., Almahasheer, H., Carnell, P. E., Duarte, C. M., Ewers Lewis, C. J., et al. (2017). Global patterns in mangrove soil carbon stocks and losses. *Nat. Climate Change* 7, 523–528. doi: 10.1038/nclimate3326

Bossio, D. A., and Scow, K. M. (1998). Impacts of carbon and flooding on soil microbial communities: phospholipid fatty acid profiles and substrate utilization patterns. *Microbial. Ecol.* 35, 265–278. doi: 10.1007/s002489900082

Bossio, D. A., Scow, K. M., Gunapala, N., and Graham, K. J. (1998). Determinants of soil microbial communities: effects of agricultural management, season, and soil type on phospholipid fatty acid profiles. *Microbial. Ecol.* 36, 1–12. doi: 10.1007/s002489900087

Bouma, T. J., Friedrichs, M., Van Wesenbeeck, B. K., Temmerman, S., Graf, G., and Herman, P. M. J. (2009). Density-dependent linkage of scale-dependent feedbacks: A flume study on the intertidal macrophyte spartina anglica. *Oikos* 118 (2), 260–268.

Breithaupt, J. L., Smoak, J. M., Rivera-Monroy, V. H., Castañeda-Moya, E., Moyer, R. P., Simard, M., et al. (2017). Partitioning the relative contributions of organic matter and mineral sediment to accretion rates in carbonate platform mangrove soils. *Mar. Geology* 390, 170–180.

Call, M., Sanders, C. J., Macklin, P. A., Santos, I. R., and Maher, D. T. (2019). Carbon outwelling and emissions from two contrasting mangrove creeks during the monsoon storm season in palau, micronesia. *Estuarine Coast. Shelf Sci.* 218, 340–348.

Chang, D., Wang, Z., Ning, X., Li, Z., Zhang, L., and Liu, X. (2022). Vegetation changes in Yellow River Delta wetlands from 2018 to 2020 using PIE-Engine and short time series Sentinel-2 images. *Front. Mar. Sci.* 9, 977050. doi: 10.3389/fmars.2022.977050

Doran, J. W., Paul, E. A., and Clark, F. E. (2007). Soil microbiology and biochemistry. *J. Range Manage* 51 (2), 254. doi: 10.2307/4003217

Duarte, C. M., Losada, I. J., Hendriks, I. E., Mazarrasa, I., and Marbà, N. (2013). The role of coastal plant communities for climate change mitigation and adaptation. *Nat. Climate Change* 3, 961–968. doi: 10.1038/nclimate1970

England, P. R., Phillips, J., Waring, J. R., Symonds, G., and Babcock, R. (2008). Modelling wave-induced disturbance in highly biodiverse marine macroalgal communities: support for the intermediate disturbance hypothesis. *Mar. Freshw. Res.* 59, 515–520. doi: 10.1071/MF07224

Ensign, S. H., and Noe, G. B. (2018). Tidal extension and sea-level rise: recommendations for a research agenda. *Front. Ecol. Environ.* 16 (1), 37–43.

Fagherazzi, S., Wiberg, P. L., Temmerman, S., Struyf, E., Zhao, Y., and Raymond, P. A. (2013). Fluxes of water, sediments, and biogeochemical compounds in salt marshes. *Ecol. Processes* 2, 1–16. doi: 10.1186/2192-1709-2-3

Frostegård, A., and Bååth, E. (1996). The use of phospholipid fatty acid analysis to estimate bacterial and fungal biomass in soil. *Biol. Fertility soils* 22, 59–65. doi: 10.1007/BF00384433

Gabler, C. A., Osland, M. J., Grace, J. B., Stagg, C. L., Day, R. H., Hartley, S. B., et al. (2017). Macroclimatic change expected to transform coastal wetland ecosystems this century. *Nat. Climate Change* 7, 142–147. doi: 10.1038/nclimate3203

García-Orenes, F., Morugán-Coronado, A., Zornoza, R., and Scow, K. (2013). Changes in soil microbial community structure influenced by agricultural

management practices in a Mediterranean agro-ecosystem. *PloS One* 8, e80522. doi: 10.1371/journal.pone.0080522

Gerwing, T. G., Gerwing, A. M. A., Macdonald, T., Cox, K., Juanes, F., and Dudas, S. E. (2017). Intertidal soft-sediment community does not respond to disturbance as postulated by the intermediate disturbance hypothesis. *J. Sea Res.* 129, 22–28. doi: 10.1016/j.seares.2017.09.001

Glaser, C., Frei, S., Massmann, G., and Gilfedder, B. S. (2021). Tidal creeks as hot-spots for hydrological exchange in a coastal landscape. *J. Hydrol.* 597, 126158. doi: 10.1016/j.jhydrol.2021.126158

Han, X., Gao, G., Chang, R., Li, Z., Ma, Y., Wang, S., et al. (2018). Changes in soil organic and inorganic carbon stocks in deep profiles following cropland abandonment along a precipitation gradient across the Loess Plateau of China. *Agric. Ecosyst. Environ.* 258, 1–13. doi: 10.1016/j.agee.2018.02.006

Kaur, A., Chaudhary, A., Kaur, A., Choudhary, R., and Kaushik, R. (2005). Phospholipid fatty acid–a bioindicator of environment monitoring and assessment in soil ecosystem. *Curr. Sci.* 89 (7), 1103–1112.

Kelleway, J. J., Saintilan, N., Macreadie, P. I., Baldock, J. A., Heijnis, H., Zawadzki, A., et al. (2017). Geochemical analyses reveal the importance of environmental history for blue carbon sequestration. *J. Geophysical Research: Biogeosciences* 122, 1789–1805. doi: 10.1002/2017JG003775

Knobloch, A. L., Reay, W. G., and Canuel, E. A. (2021). Carbon pools differ in source and temporal patterns in a tidal marsh creek system of the York River, VA Estuary. *Estuaries Coasts* 44, 1848–1865. doi: 10.1007/s12237-020-00878-y

Krest, J. M., Moore, W. S., Gardner, L. R., and Morris, J. T. (2000). Marsh nutrient export supplied by groundwater discharge: Evidence from radium measurements. *Global Biogeochemical Cycles* 14, 167–176. doi: 10.1029/1999GB001197

Lai, S., Yaakub, S. M., Poh, T. S., Bouma, T. J., and Todd, P. A. (2018). Unlikely nomads: settlement, establishment, and dislodgement processes of vegetative seagrass fragments. *Front. Plant Sci.* 9, 328860.

Lal, R. (2008). Carbon sequestration. *Philos. Trans. R. Soc. B: Biol. Sci.* 363, 815–830. doi: 10.1098/rstb.2007.2185

Lavelle, J. W., Massoth, G. J., and Crecelius, E. A. (1985). *Sedimentation rates in Puget Sound from ^{210}PB measurements. NOAA Technical Memorandum ERL PMEL-61.* Seattle, Washington: Contribution (Pacific Marine Environmental Laboratory (U.S.)), 732. https://repository.library.noaa.gov/view/noaa/9479.

Leckie, S. E., Prescott, C. E., Grayston, S. J., Neufeld, J. D., and Mohn, W. W. (2004). Comparison of chloroform fumigation-extraction, phospholipid fatty acid, and DNA methods to determine microbial biomass in forest humus. *Soil Biol. Biochem.* 36, 529–532. doi: 10.1016/j.soilbio.2003.10.014

Liu, D., Huang, Y., Sun, H., and An, S. (2018). The restoration age of Robinia pseudoacacia plantation impacts soil microbial biomass and microbial community structure in the Loess Plateau. *Catena* 165, 192–200. doi: 10.1016/j.catena.2018.02.001

Ma, Z., Wu, Y., Cui, Y., Pan, Y., Zhao, S., Liu, J., et al. (2024). Coastal distribution and driving factors for blue carbon fractions in the surface soil of a warm-temperate salt marsh in China. *Chemosphere* 350, 141044. doi: 10.1016/j.chemosphere.2023.141044

Ma, Z., Zhang, M., Xiao, R., Cui, Y., and Yu, F. (2017). Changes in soil microbial biomass and community composition in coastal wetlands affected by restoration projects in a Chinese delta. *Geoderma* 289, 124–134. doi: 10.1016/j.geoderma.2016.11.037

Mcleod, E., Chmura, G. L., Bouillon, S., Salm, R., Björk, M., Duarte, C. M., et al. (2011). A blueprint for blue carbon: toward an improved understanding of the role of vegetated coastal habitats in sequestering CO2. *Front. Ecol. Environ.* 9, 552–560. doi: 10.1890/110004

Nguyen, H. Y. T., Cao, D. M., and Schmitt, K. (2013). Soil particle-size composition and coastal erosion and accretion study in Soc Trang mangrove forests. *J. Coast. Conserv.* 17, 93–104. doi: 10.1007/s11852-012-0221-4

Ning, Z., Li, D., Chen, C., Xie, C., Chen, G., Xie, T., et al. (2023). The importance of structural and functional characteristics of tidal channels to smooth cordgrass invasion in the Yellow River Delta, China: Implications for coastal wetland management. *J. Environ. Manage.* 342, 118297. doi: 10.1016/j.jenvman.2023.118297

Odum, E. P. (1963). *Ecology*. Modern Biology Series. Eds. H. Rinehart and W. New York (New York (NY, USA): Holt, Rinehart and Winston).

Odum, E. (2002). "Tidal Marshes as Outwelling/Pulsing Systems," in *Concepts and Controversies in Tidal Marsh Ecology* (Kluwer Academic Publishers, New York), 3–7.

Olsson, P. A. (1999). Signature fatty acids provide tools for determination of the distribution and interactions of mycorrhizal fungi in soil. *FEMS Microbiol. Ecol.* 29, 303–310. doi: 10.1111/fem.1999.29.issue-4

Olsson, P. A., Bååth, E., Jakobsen, I., and Söderström, B. (1995). The use of phospholipid and neutral lipid fatty acids to estimate biomass of arbuscular mycorrhizal fungi in soil. *Mycological Res.* 99 (5), 623–629.

Pedersen, M.Ø., Serrano, O., Mateo, M. A., and Holmer, M. (2011). Decomposition of Posidonia oceanica matte in a climate change setting. *Aquat. Microb. Ecol.* 65, 169–182. doi: 10.3354/ame01543

Peng, G., Xiang, N., Lv, S. Q., and Zhang, G. C. (2014). Fractal characterization of soil particle-size distribution under different land-use patterns in the Yellow River Delta Wetland in China. *J. Soils Sediments* 14, 1116–1122. doi: 10.1007/s11368-014-0876-6

R Core Team (2021). *R: A language and environment for statistical computing* (Vienna, Austria: R Foundation for Statistical Computing). Available at: http://www.R-project.org/.

Rabot, E., Wiesmeier, M., Schlüter, S., and Vogel, H. J. (2018). Soil structure as an indicator of soil functions: A review. *Geoderma* 314, 122–137.

Regier, P., Ward, N. D., Indivero, J., Wiese Moore, C., Norwood, M., and Myers-Pigg, A. (2021). Biogeochemical control points of connectivity between a tidal creek and its floodplain. *Limnol. Oceanogr. Lett.* 6, 134–142. doi: 10.1002/lol2.10183

Ren, J., Chen, J., Xu, C., van de Koppel, J., Thomsen, M. S., Qiu, S., et al. (2021). An invasive species erodes the performance of coastal wetland protected areas. *Sci. Adv.* 7, eabi8943. doi: 10.1126/sciadv.abi8943

Sanders, C. J., Maher, D. T., Tait, D. R., Williams, D., Holloway, C., Sippo, J. Z., et al. (2016). Are global mangrove carbon stocks driven by rainfall? *J. Geophysical Research: Biogeosciences* 121, 2600–2609. doi: 10.1002/2016JG003510

Santini, N. S., Lovelock, C. E., Hua, Q., Zawadzki, A., Mazumder, D., Mercer, T. R., et al. (2019). Natural and regenerated saltmarshes exhibit similar soil and belowground organic carbon stocks, root production and soil respiration. *Ecosystems* 22, 1803–1822. doi: 10.1007/s10021-019-00373-x

Santos, I. R., Burdige, D. J., Jennerjahn, T. C., Bouillon, S., Cabral, A., Serrano, O., et al. (2021). The renaissance of Odum's outwelling hypothesis in'Blue Carbon'science. *Estuarine Coast. Shelf Sci.* 255, 107361. doi: 10.1016/j.ecss.2021.107361

Santos, I. R., Maher, D. T., Larkin, R., Webb, J. R., and Sanders, C. J. (2019). Carbon outwelling and outgassing vs. burial in an estuarine tidal creek surrounded by mangrove and saltmarsh wetlands. *Limnol. Oceanogr.* 64, 996–1013. doi: 10.1002/lno.11090

Studds, C. E., Kendall, B. E., Murray, N. J., Wilson, H. B., Rogers, D. I., Clemens, R. S., et al. (2017). Rapid population decline in migratory shorebirds relying on Yellow Sea tidal mudflats as stopover sites. *Nat. Commun.* 8, 14895. doi: 10.1038/ncomms14895

Tan, L., Ge, Z., Fei, B., Xie, L., Li, Y., Li, S., et al. (2020). The roles of vegetation, tide and sediment in the variability of carbon in the salt marsh dominated tidal creeks. *Estuarine Coast. Shelf Sci.* 239, 106752. doi: 10.1016/j.ecss.2020.106752

Taniguchi, M., Dulai, H., Burnett, K. M., Santos, I. R., Sugimoto, R., Stieglitz, T., et al. (2019). Submarine groundwater discharge: updates on its measurement techniques, geophysical drivers, magnitudes, and effects. *Front. Environ. Sci.* 7, 141.

Tzortziou, M., Neale, P. J., Megonigal, J. P., Pow, C. L., and Butterworth, M. (2011). Spatial gradients in dissolved carbon due to tidal marsh outwelling into a Chesapeake Bay estuary. *Mar. Ecol. Prog. Ser.* 426, 41–56. doi: 10.3354/meps09017

van Ardenne, L. B., Jolicouer, S., Bérubé, D., Burdick, D., and Chmura, G. L. (2018). The importance of geomorphic context for estimating the carbon stock of salt marshes. *Geoderma* 330, 264–275. doi: 10.1016/j.geoderma.2018.06.003

Vance, E. D., Brookes, P. C., and Jenkinson, D. S. (1987). An extraction method for measuring soil microbial biomass C. *Soil Biol. Biochem.* 19, 703–707. doi: 10.1016/0038-0717(87)90052-6

Wang, X., Jiang, Z., Li, Y., Kong, F., and Xi, M. (2019). Inorganic carbon sequestration and its mechanism of coastal saline-alkali wetlands in Jiaozhou Bay, China. *Geoderma* 351, 221–234. doi: 10.1016/j.geoderma.2019.05.027

Wang, Q., Xie, T., Luo, M., Bai, J., Chen, C., Ning, Z., et al. (2021). How hydrological connectivity regulates the plant recovery process in salt marshes. *J. Appl. Ecol.* 58, 1314–1324. doi: 10.1111/1365-2664.13879

Webb, J. R., Santos, I. R., Maher, D. T., Tait, D. R., Cyronak, T., Sadat-Noori, M., et al. (2019). Groundwater as a source of dissolved organic matter to coastal waters: Insights from radon and CDOM observations in 12 shallow coastal systems. *Limnol. Oceanogr.* 64, 182–196. doi: 10.1002/lno.11028

Windham-Myers, L., Cai, W.-J., Alin, S. R., Andersson, A., Crosswell, J., Dunton, K. H., et al. (2018). "Chapter 15: Tidal wetlands and estuaries," in *Second state of the carbon cycle report (SOCCR2): a sustained assessment report*. Eds. N. Cavallaro, G. Shrestha, R. Birdsey, M. A. Mayes, R. G. Najjar, S. C. Reed, P. Romero-Lankao and Z. Zhu (U.S. Global Change Research Program, Washington), 596–648. doi: 10.7930/SOCCR2.2018.Ch15

Wu, Y., Liu, J., Yan, G., Zhai, J., Cong, L., Dai, L., et al. (2020). The size and distribution of tidal creeks affects salt marsh restoration. *J. Environ. Manage.* 259, 110070. doi: 10.1016/j.jenvman.2020.110070

Wu, Y., Zhang, Z., Hipsey, M., and Zhang, M. (2023a). Tides as a key factor driving effective seed dispersal in coastal wetlands. *Ecol. Indic.* 148, 110110. doi: 10.1016/j.ecolind.2023.110110

Wu, Y., Zhang, Z., Hipsey, M. R., and Zhang, M. (2023b). Tidal action enhances coastal wetland plant connectivity. *Chemosphere* 331, 138784. doi: 10.1016/j.chemosphere.2023.138784

Wu, Y., Zhao, S., Dai, L., Liu, Y., Xie, L., Zhang, Z., et al. (2021). Tides affect plant connectivity in coastal wetlands on a small-patch scale. *Chemosphere* 262, 127977. doi: 10.1016/j.chemosphere.2020.127977

Zelles, L., Bai, Q. Y., Rackwitz, R., Chadwick, D., and Beese, F. (1995). Determination of phospholipid-and lipopolysaccharide-derived fatty acids as an estimate of microbial biomass and community structures in soils. *Biol. Fertility Soils* 19, 115–123.

frontiers | Frontiers in Marine Science

TYPE Original Research
PUBLISHED 05 June 2024
DOI 10.3389/fmars.2024.1420559

OPEN ACCESS

EDITED BY
Qing Wang,
Beijing Normal University, Zhuhai, China

REVIEWED BY
Shaohua Zhao,
Third Institute of Oceanography, MNR, China
Wei Huang,
Florida International University, United States

*CORRESPONDENCE
Haifei Yang
hfyang@sklec.ecnu.edu.cn
Shilun Yang
slyang@sklec.ecnu.edu.cn

RECEIVED 20 April 2024
ACCEPTED 22 May 2024
PUBLISHED 05 June 2024

CITATION
Tian M, Yang H, Zhang W, Xu K, Shi B, Wang Y and Yang S (2024) Sediment resuspension and transport in the offshore subaqueous Yangtze Delta during winter storms. *Front. Mar. Sci.* 11:1420559. doi: 10.3389/fmars.2024.1420559

Sediment resuspension and transport in the offshore subaqueous Yangtze Delta during winter storms

Min Tian[1], Haifei Yang[1*], Wenxiang Zhang[1], Kehui Xu[2,3], Benwei Shi[1], Yaping Wang[1] and Shilun Yang[1*]

[1]State Key Laboratory of Estuarine and Coastal Research, East China Normal University, Shanghai, China, [2]Department of Oceanography and Coastal Sciences, Louisiana State University, Baton Rouge, LA, United States, [3]Coastal Studies Institute, Louisiana State University, Baton Rouge, LA, United States

Storm-induced episodic sediment redistribution in coastal systems can reshape geomorphic bodies, disrupt ecosystems, and cause economic damage. However, cold-wave-storm-induced hydrodynamic changes and residual sediment transport in large, exposed subaqueous deltas, such as the Yangtze Delta, are poorly understood because it is typically expensive and difficult to obtain systematic field data in open coast settings during storm events. We conducted a successful field survey of waves, currents, changes in water depth, and turbidity at a station (time-averaged water depth of 20 m) in the offshore subaqueous Yangtze Delta over 10 days during winter, covering two storms and two fair-weather periods. During the storm events, strong northerly winds drove southward longshore currents (~0.2 m/s) and resulted in increased wave height and sediment resuspension, thereby leading to massive southward sediment transport. In contrast, both southward and northward transports were limited during the fair-weather periods. A better understanding of the storm-induced sediment transport can be obtained by using an approximately half-day lag in sediment transport behind wind force, given the time needed to form waves and longshore drift, the inertia of water motion, and the slow settling velocity of fine-grained sediment. Our results directly support previous findings of southward sediment transport from the Yangtze Delta during winter, which is deposited in the Zhejiang–Fujian mud belt in the inner shelf of the East China Sea. In addition, the southward sediment transport from the Yangtze Delta occurs mainly during episodic storm events, rather than during the winter monsoon, and winter storms dominate over typhoons in driving southward sediment transport from the delta. This study highlights the importance of storms, especially during winter storms, in coastal sediment redistribution, which is of particular significance when considering the projected increase in storm intensity with global warming.

KEYWORDS

sediment resuspension, longshore current, sediment transport, winter storm, Yangtze Delta

Introduction

Coastal environments and ecosystems are particularly vulnerable to the impacts of storms (e.g., typhoons, hurricanes, and cold-air outbreaks). Storm waves in coastal waters (i.e., local storm waves combined with swells propagating from the open ocean where larger waves are generated owing to storm winds) increase bed shear stress, and sediment resuspension occurs once the bed shear stress exceeds the critical limit for erosion (Partheniades, 1965; Winterwerp et al., 2012; Shi et al., 2021). Storm waves may also fluidize the seabed, making sediments more susceptible to erosion (Green & Coco, 2014). Storm-induced resuspension and redistribution of sediments in coastal seas have important implications for habitat stability, subsea pipeline/cable security, port and waterway maintenance, and morphological evolution. These impacts are being amplified under increasing trends in storm activity (i.e., integration of their frequency, lifetime, and intensity) and their destructiveness in response to global warming (Emanuel, 2013; Cheal et al., 2017; Bhatia et al., 2019; Zhou & Qian, 2021).

Winter storms derived from cold-air outbreaks, and typhoons and hurricanes as tropical cyclones can all bring strong wind events. Sediment redistribution induced by typhoons and hurricanes in coastal systems has been widely studied especially on rapid erosion/deposition in beach, coastal dune, and wetland environment (Turner et al., 2006; Leonardi et al., 2016; Williams & Liu, 2019; McKee et al., 2020), offshore sediment transport (Li et al., 2015; Lin et al., 2024), and sediment gravity flows across continental shelves (Puig et al., 2004; Wright & Friedrichs, 2006; Kudrass et al., 2018; Sequeiros et al., 2019). Compared to tremendous studies on typhoons- and hurricanes-induced sediment transport and hydrology changes, studies on winter storms and their impacts on sediment resuspension and longshore sediment transport in large subaqueous deltas seem relatively rare (Yang et al., 2007; Mo et al., 2021). Data on sediment transport across large subaqueous deltas are necessary because of the large magnitude of sediment transport and its potential influence on large ecosystems and socioeconomic megacenters. Therefore, it is vital to investigate the winter storm-induced redistribution of sediments in large deltas.

The Yangtze Delta is one of the world's largest deltas in terms of area (60,000 km^2), wetland ecosystem, population (110 million people), and economy (15% of China's gross domestic product) (Xu et al., 2014; Wang et al., 2018a; Yang et al., 2020a). Shanghai is the largest harbor city in the world and lies at the mouth of the Yangtze River. The magnitude and direction of sediment transport in the subaqueous Yangtze Delta under fair weather conditions are controlled mainly by tidal currents (Milliman et al., 1985; Yang et al., 2017a). Located on the northwestern Pacific coast (Figure 1A), the Yangtze Delta is frequently affected by typhoons and cold fronts (Fan et al., 2006; Yang et al., 2019). Previous studies on the delta have focused mainly on storm-induced erosion and deposition in mudflat and wetland systems (Yang et al., 2003; Fan et al., 2006; Shi et al., 2017), and waterway siltation in mouth-bar areas (Kuang et al., 2014; Kong et al., 2015; Lu et al., 2018). In contrast, winter storm-induced changes in hydrodynamics and sediment transport in the offshore subaqueous Yangtze Delta are poorly understood. This lack of knowledge is mainly due to the difficulty in collecting high-resolution data for currents, waves, water-depth changes, and suspended sediment concentrations (SSCs) in the exposed offshore waters of the delta where waves are large. Ship-based field studies are dangerous and bottom-observation racks are often covered by sediment during storm events (Yang et al., 2007).

Since the mid-Holocene, a vast longshore mud belt (~1,000 km long, 100 km wide, and 40 m thick) has formed in the inner shelf of the East China Sea along the macrotidal coasts of Zhejiang and Fujian provinces in southeastern China (Figure 1A), mainly owing to southward transport of sediment from the Yangtze Delta (e.g., Fang et al., 2018; Xu et al., 2023). This mud belt is larger than the Yangtze Delta in terms of area and volume (Xu et al., 2012; Wang et al., 2018a), suggesting that more than half of the sediments from the Yangtze River have been transported southward to form the mud belt. The mud belt extends into coastal embayments, where it leads to the formation of tidal wetlands (Xie et al., 2017a). Historical reclamation of tidal wetlands in these embayments has yielded

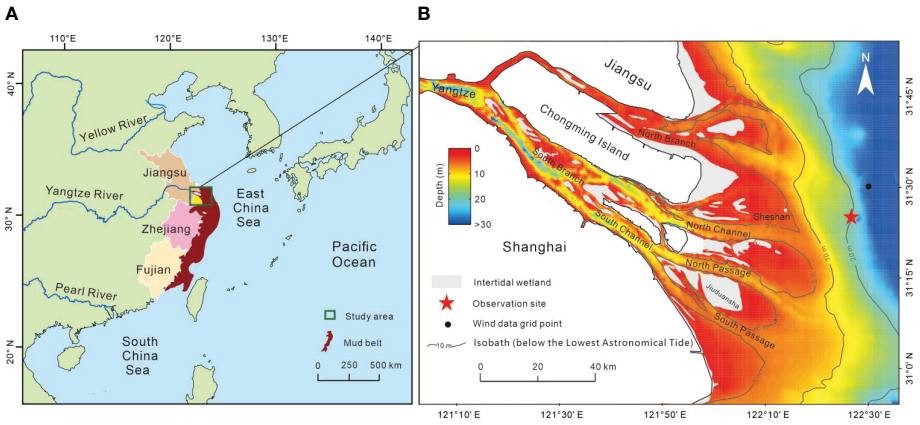

FIGURE 1
Maps of the study area. **(A)** Locations of the Yangtze Delta and the Zhejiang–Fujian mud belt. The mud belt is modified after Xu et al., 2012. **(B)** Location of the observation station in the offshore subaqueous Yangtze Delta. The topography data of river estuary is modified after Yang et al., 2023.

abundant new land and promoted socioeconomic development (Liao et al., 2016). Previous studies have attributed the southward transport of sediment from the Yangtze Delta to longshore currents (Shepard, 1932; Liu et al., 2007; Xu et al., 2023); however, it is controversial whether the southward longshore currents are driven mainly by monsoon winds or storms (Milliman et al., 1985; Deng et al., 2017; Tian et al., 2019; Yang et al., 2023), and whether the southward sediment transport occurs only in winter or also in other seasons (Xiao et al., 2006; Xu et al., 2023; Yang et al., 2023), and it is unclear whether winter storms or typhoons are more important in driving the southward sediment transport from the delta. Field observations during winter storm events, which would provide explanatory data, are particularly lacking.

In this study, we investigate the role of winter storms in southward sediment transport from the Yangtze Delta using high-resolution *in situ* observations in combination with systematic wind data. Our major objectives are to (1) identify the temporal variations in wave height, current velocity, and SSC; (2) estimate the residual currents and longshore sediment transport rates during tidal cycles; (3) compare the hydrodynamics and sediment transport between storm events and periods of fair weather; and (4) assess the relative importance of winter storms in driving southward sediment transport from the delta. Fulfilling these objectives will help us to determine whether massive southward longshore sediment transport from the offshore subaqueous Yangtze Delta occurs during winter, and whether it is continuous or episodic. We also consider the dominant factor driving southward sediment transport and whether southward sediment transport from the Yangtze Delta occur in seasons other than winter, as well as the season in which the greatest magnitude of sediment transport occurs.

Study area

The 6,300-km long Yangtze River is one of the world's longest rivers and has a drainage area of 1.8 million km^2, a water discharge rate of 900 km^3/yr, and a sediment discharge rate of 500 Mt/yr (Mt: million tons) prior to the closure of the Danjiangkou Dam in the end of the 1960s (Milliman & Farnsworth, 2011; Wang et al., 2011). Because of numerous dams constructed in the past decades (in particular the Three Gorges Dam in 2003), the Yangtze sediment discharge rate has decreased to ~120 Mt/yr (Yang et al., 2018, 2023). The Yangtze River Basin is currently home to 450 million people (Yang et al., 2015).

The offshore subaqueous Yangtze Delta has an area of ~10,000 km^2 (Figure 1B; Yang et al., 2023). Unconsolidated sediment in the delta is composed mainly of silt, clay, and very fine sand (Luo et al., 2017; Xue et al., 2020; Yan et al., 2022) that are readily resuspended by waves and currents (Yang et al., 2017a). The suspended sediment is composed mainly of silt and clay, with median grain sizes of 3–16 μm depending on the tidal stages and seasons (Liu et al., 2014; Xie et al., 2017b). Tides in the Yangtze Delta are semidiurnal with a diurnal inequality. The tidal range is 2.7 m on average, but can exceed 4.0 m during spring tides (Yang et al., 2020a). More than ten major storms impact the Yangtze Delta every year accompanied with interannual variations. On average, winter storms and typhoons respectively occupy ~67% and ~33%, based on the wind data during the last 40 years obtained from the European Centre for Medium-Range Weather Forecasts (https://www.ecmwf.int/). The significant wave height at Sheshan Station, a fixed gauging station at the 5-m isobath on the landward side of our observation site (Figure 1B) is < 1.0 m during fair weather, but can increase to several meters during storm events (Fan et al., 2006). The SSC in the offshore subaqueous delta ranges from < 0.1 to > 2.0 kg/m^3, increasing from neap to spring tides, from fair to stormy weather, and from surface to near-bed water layers (Liu et al., 2014; Deng et al., 2017; Yang et al., 2020b). The offshore subaqueous Yangtze Delta is characterized by a long-term southward longshore current (Yang et al., 2023) that is believed to be driven mainly by the East Asian winter monsoon (Milliman et al., 1985; Deng et al., 2017). In response to the dam-induced decline in fluvial sediment supply, the subaqueous Yangtze Delta have converted from net accumulation to net erosion in recent years (Yang et al., 2011; Yang et al., 2017b; Guo et al., 2021; Luan et al., 2021). Sediments in the Zhejiang–Fujian longshore mud belt are dominated by silts and clays, with a gradual fining trend from north to south (Gao et al., 2019).

Methods

Field observations

Field observations were conducted at an offshore station in the subaqueous Yangtze Delta at a mean water depth of ~20 m (122.44° E, 31.40°N; Figure 1B) during a winter period covering both storm events and fair weather (28 January to 7 February 2018). An acoustic Doppler current profiler (Teledyne RD Instruments, San Diego, USA) sensor was mounted 0.5 m above the seabed on a tripod and facing upward (with a blind spot of 0.7 m and a layer interval of 0.5 m) to measure current profiles at 20-min intervals. The currents in the first 32 layers between 1.2 and 17.2 m above the seabed (each with a thickness of 0.5 m) were effectively measured, and flow velocity and direction data were later used to calculate the residual currents. Layers located > 17.2 m above the seabed were only partly submerged because of water-level changes during tidal cycles; therefore, current data were incomplete and thus not used. A SBE 26plus Seagauge Wave and Tide Recorder (Sea-Bird Electronics, Bellevue, USA) was mounted 0.6 m above the seabed on the tripod to measure wave parameters and water-depth changes at 10-min intervals. An optical backscatter sensor (OBS_{637}; Campbell Scientific, Salt Lake City, USA) was mounted 0.5 m above the seabed on the tripod to measure near-bed turbidities at 2.5-min intervals. An optical backscatter sensor (OBS_{344}; Campbell Scientific, Salt Lake City, USA) tied to a windlass mounted on a boat was employed to measure turbidity profiles at 1-s intervals once an hour during a tidal cycle under fair weather (30–31 January 2018). During these measurements, the OBS was gradually moved from water surface to seabed and back again. Each measurement of the turbidity profile took ~3 min. During free periods between turbidity profile measurements, the OBS_{344} was used to measure near-surface (1.5 m below the water surface) turbidity at 1-s intervals.

Data mining

Wind speed and direction data with a time resolution of 1 h and spatial resolution of 0.25° × 0.25° were obtained from the European Centre for Medium-Range Weather Forecasts (https://www.ecmwf.int/), and wind data collected at the grid point (122.5°E, 31.5°N) closest to the observation station were used to elucidate changes in wind speed and direction. Data on typhoon tracks were obtained from the National Meteorological Center of China (http://www.nmc.cn/).

Data processing

In laboratory, the OBS_{637} was calibrated using water and sediment samples collected from the study area to establish correlation between turbidity and SSC. Firstly, the sediment was mixed thoroughly with water in a barrel (0.6-m diameter) to generate turbidity. Turbidity was measured using the OBS_{637}, and the turbid water was sampled. Secondly, the volumes of water or sediment in the barrel were increased to produce new turbidities. The new turbidities were measured using the OBS_{637}, and the new turbid water was sampled. Thirdly, the water samples were filtered, rinsed, dried, and weighed, and an SSC value was calculated as the ratio of dry sediment weight to water volume for each sample. By doing so, a series of SSC and turbidity data from low to high levels was obtained, and close correlations between SSC and turbidity (R^2 =0.99, $p < 0.001$) were established (Figure 2A). The *in situ* turbidity data obtained from the OBS_{637} were then converted into SSC data using the regression equations shown in Figure 2A. To convert the turbidity data measured by OBS_{344} into SSC data, we identified a close correlation between the OBS_{344} and OBS_{637} turbidity data (R^2 =0.95, $p < 0.001$) and used the resulting regression equation (Figure 2B).

Residual wind speed and direction, current velocity and direction, and sediment transport rate and direction were calculated by the method of vector composition. To effectively filter out the influence of the tidal signal on the residual current, we used a low-pass Butterworth filter (Thompson, 1983; Matte et al., 2014; Wan et al., 2015; Chen et al., 2016) with a filtering period of 34 h to process the raw flow data and obtained the residual currents. We define a tide cycle as the duration between two mean waters during the successive flood tides. Here, we identified 20 tidal cycles with durations of 12–13 h (average 12.5 h). In quantifying the influence of wind speed on wave height, to filter out the effect of tide-induced water-depth changes on wave height, we used tide-averaged data in constructing cross-correlations between wave height and wind speed. To find the optimal estimate for the time lag of wave height behind wind speed, we first constructed cross-correlations with different time lags of wave height behind wind speed, and then plotted the coefficient of determination (R^2) against time lag.

Definitions

In this study, we use the term "storm" to refer to an extreme weather event during which wind speed is markedly higher than that during fair weather (Leonardi et al., 2016). Upon consideration of the wind speed in the study area, and for the purpose of examining the impact of storms on residual sediment transport in tidal cycles, we define a storm event as a period during which 1) the wind speed exceeds 9.5 m/s for >20 h without interruption (i.e., markedly longer than a semidiurnal tidal cycle), 2) the maximum wind speed is >10.8 m/s (i.e., ≥ 6 on the Beaufort scale; Singleton, 2008), and 3) the mean wind speed is >10 m/s. To compare hydrodynamics and sediment transport between storm and fair weather periods, we define weak wind as a wind speed of < 5.0 m/s, moderate wind as a wind speed of 5.0–9.4 m/s, and storm wind as a wind speed of ≥ 9.5 m/s. We used the eight-orientation calculation method to describe wind directions, in which each orientation encompasses a direction scope of 45°. For example, northerly winds are winds that concentrated at 0°/360° and varied between 337.5° and 22.5°. The net wind component during a given period is

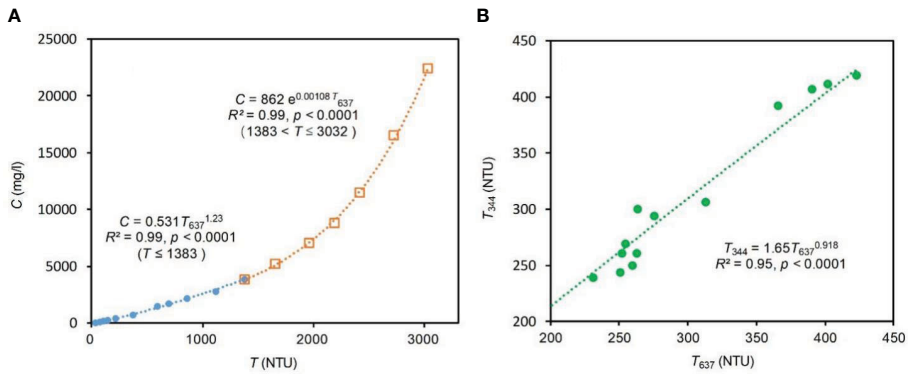

FIGURE 2
(A) Power-law correlations between the OBS_{637} turbidity (T_{637}) and SSC (C) measurements based on calibration using *in situ* sediment samples (for maximum fit effect, two formulas were established in segments), and **(B)** power-law correlation between the OBS_{344} turbidity (T_{344}) and OBS_{637} turbidity (T_{637}) measurements. NTU: nephelometric turbidity unit. The OBS_{637} was used to measure near-bed turbidities, whereas the OBS_{344} was used to measure turbidity profiles.

10.3389/fmars.2024.1420559

defined as the algebraic sum of the wind components. The cumulative force of a wind component is defined as the sum of the products of the wind component and its duration.

Results

Wind speed and direction

During the field observation period, wind directions were generally northerly (i.e., southward), northwesterly, or northeasterly. The residual wind speed and direction were 6.7 m/s and 341°. There were two winter storm events, each followed by a fair-weather period. The durations of the first and second storm events were 21 and 42 hours, respectively. The storm winds were more stable in direction and had a greater southward component than the non-storm winds. Although the storm winds accounted for only 25% of the observation period, they contributed more than 40% of the total southward component of wind force (Figure 3A). The residual wind speed and direction were 10.1 m/s and 344°for the 6 tidal cycles with storm winds, 7.1 m/s and 338°for the 10 cycles with moderate winds, and 2.0 m/s and 7°for the 4 cycles with weak winds, respectively (Table 1). The time-averaged southward components of wind speed during the first and second storm events were 10.2 and 9.8 m/s, and the cumulative southward components of wind speed during the first and second storm events were 771,120 m (or 771,120 m/21 hours) and 1,446,480 m (or 1,446,480 m/42 hours), respectively.

Based on our definition, 21 storm events occurred in 2018. These events accounted for 9.2% of the annual total wind duration. Twelve storm events (57%) occurred in the winter half-year (mid-October to mid-April) and nine (43%) in the summer half-year. Eight storm events (38%) were associated with typhoons that occurred in July to early October, suggesting that most of the storm events were derived from cold-air outbreaks (Figure 4A). 14 of the 21 storm events (67%) had a dominant southward component. These storm events accounted for 6.4% of the annual total wind duration; however, they contributed 86% of the annual residual southward wind component. Three of the eight typhoon storm events (38%) had a dominant southward component. These events contributed 19% of the annual residual southward wind component. Overall, cold-wave-derived storm events contributed

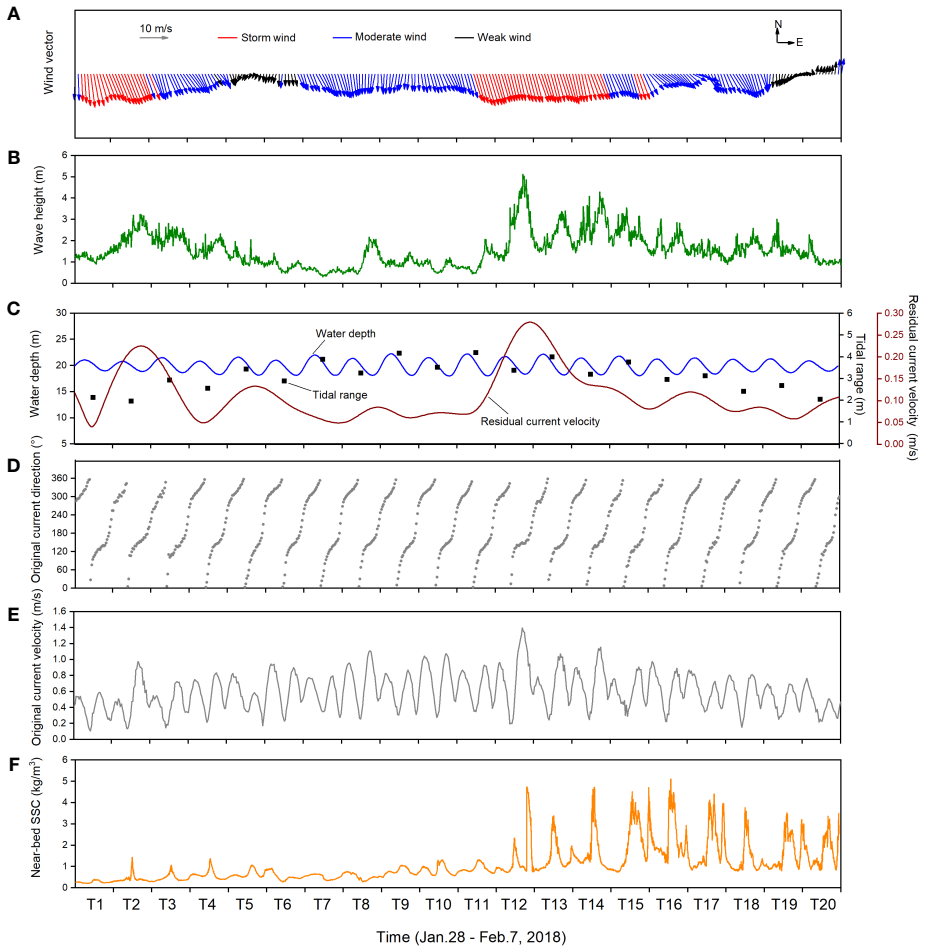

FIGURE 3
Time series of **(A)** wind speed and direction, **(B)** significant wave height, **(C)** water depth, depth-averaged residual current velocity and tidal range, **(D)** depth-averaged current direction, **(E)** depth-averaged original current velocity and **(F)** near-bed SSC during the observation period.

TABLE 1 Residual suspended sediment transport and influencing factors in tidal cycles.

Tide cycles	Tide type	Start and end time	*t* (s)	Wind strength	*Sw* (m/s)	*Dw* (°)	H_s (m)	*H* (m)	R_t (m)	V_a (m/s)	Ca (kg/m^3)	*Vr* (m/s)	*Dr* (°)	*Aw-c* (°)	S_r (t/m)	S_r (cross-shore) (t/m)	S_r (longshore) (t/m)
Tide 1	Neap	04:27–17:05 28 Jan	45600	Storm	10.4	347	1.28	20.4	2.12	0.39	0.189	0.05	220	50	8	-5	-7
Tide 2	Neap	17:06 28 Jan to 05:20 29 Jan	44400	Storm	10.5	338	2.33	20.1	1.95	0.52	0.288	0.21	173	15	53	6	-53
Tide 3	Mean	05:21–18:25 29 Jan	46800	Moderate	8.3	334	2.08	20.3	2.93	0.46	0.326	0.14	186	32	43	-5	-43
Tide 4	Mean	18:26 29 Jan to 06:25 30 Jan	43200	Moderate	5.8	332	1.63	19.8	2.55	0.58	0.418	0.06	277	128	20	-20	3
Tide 5	Mean	06:26–19:18 30 Jan	46800	Weak	2.8	15	1.13	20.1	3.43	0.55	0.465	0.12	319	124	54	-36	41
Tide 6	Mean	19:19 30 Jan to 07:10 31 Jan	43200	Weak	4.6	352	0.80	19.9	2.89	0.67	0.354	0.09	304	131	28	-23	15
Tide 7	Spring	07:11–19:57 31 Jan	45600	Moderate	7.9	340	0.55	20.3	3.88	0.58	0.364	0.05	275	113	18	-18	1
Tide 8	Spring	19:58 31 Jan to 07:55 1 Feb	43200	Moderate	7.1	360	1.15	20.0	3.25	0.73	0.361	0.07	220	40	22	-14	-17
Tide 9	Spring	07:56–20:32 1 Feb	45600	Moderate	6.3	3	0.99	20.4	4.16	0.62	0.535	0.06	239	58	32	-28	-16
Tide 10	Spring	20:33 1 Feb to 08:42 2 Feb	43200	Moderate	6.7	341	0.81	20.0	3.52	0.76	0.586	0.07	280	118	35	-35	6
Tide 11	Spring	08:43–17:30 2 Feb	45600	Storm	10.2	344	1.03	20.3	4.19	0.66	0.626	0.09	215	49	50	-27	-43
Tide 12	Spring	17:31 2 Feb to 09:20 3 Feb	43200	Storm	9.9	346	2.81	20.3	3.37	0.82	0.979	0.24	177	11	208	13	-207
Tide 13	Spring	09:21–22:02 3 Feb	45600	Storm	10.3	344	2.19	20.4	4.00	0.66	0.970	0.22	176	12	197	12	-196
Tide 14	Spring	22:03 3 Feb to 10:05 4 Feb	43200	Storm	9.5	341	2.71	20.1	3.20	0.73	1.135	0.14	187	26	133	-17	-132
Tide 15	Spring	10:06–22:45 4 Feb	45600	Moderate	8.7	336	2.32	20.2	3.76	0.60	1.383	0.10	200	45	124	-44	-116
Tide 16	Mean	22:46 4 Feb to 10:45 5 Feb	43200	Moderate	7.0	311	1.88	20.0	2.95	0.66	1.611	0.10	268	138	133	-133	-3
Tide 17	Mean	10:46–23:15 5 Feb	45600	Moderate	6.7	323	1.49	20.1	3.12	0.60	1.323	0.10	282	139	124	-122	24
Tide 18	Mean	23:16 5 Feb to 11:12 6 Feb	43200	Moderate	8.2	336	1.65	20.2	2.40	0.59	0.931	0.08	232	74	62	-48	-40
Tide 19	Mean	11:13 6 Feb to 00:02 7 Feb	45600	Weak	3.5	18	1.62	20.2	2.67	0.52	1.070	0.06	232	36	61	-49	-36
Tide 20	Neap	00:03–12:11 7 Feb	44400	Weak	3.0	183	1.17	20.1	2.04	0.45	1.188	0.09	308	55	92	-72	57

t: Duration. S_w: Time-averaged residual wind speed. D_w: Time-averaged residual wind direction. H_s: Significant wave height. h: Mean water depth within the corresponding interval. R_t: Tidal range. V_a: Depth-time-averaged current velocity. C_a: Depth-averaged SSC. V_r: Tide depth-averaged residual current velocity. D_r: Tide depth-averaged residual flow and sediment transport direction. $A_{w\text{-}c}$: Angle between residual wind and residual current. S_r: Tidal cycle residual sediment transport per meter width of the water column. $S_r = V_r \times C_a \times h \times t$. $S_{r\ (cross\text{-}shore)}$: Cross-shore (east–west) component of S_r. Positive values represent offshore transport, and negative values represent onshore transport. $S_{r\ (longshore)}$: Longshore (north–south) component of S_r. Positive values represent northward transport, and negative values represent southward transport.

10.3389/fmars.2024.1420559

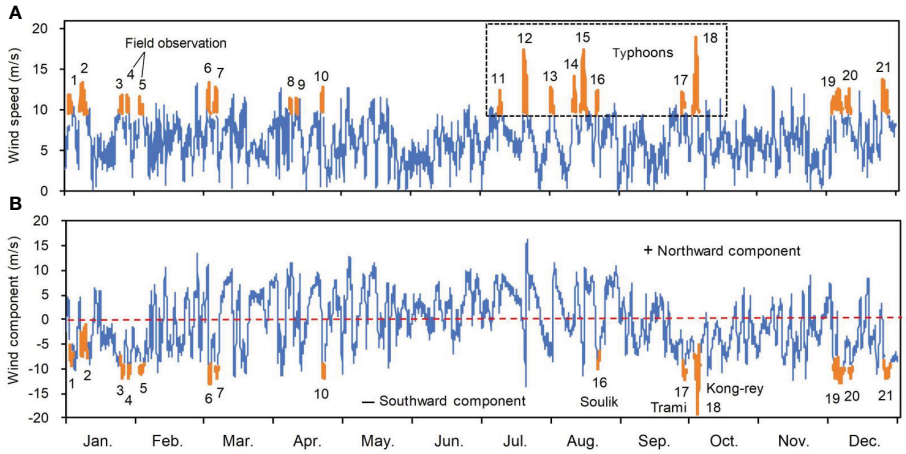

FIGURE 4
Time series of hourly wind speed and the longshore component in 2018. **(A)** Wind speed and storm events. **(B)** Wind component and storm events dominated by a southward component. The orange peaks in **(A)** represents storm events, as defined in the present study (see the Methods section). Numbers 1–21 represent storm events. Numbers 11–18 represent typhoons Maria, Ampil, Jangdari, Yagi, Rumbia, Soulik, Trami, and Kong-rey, respectively. Positive and negative values in **(B)** represent northward and southward components, respectively. The orange troughs in **(B)** represent storm events dominated by a southward component; numbers indicate storm events corresponding to those in **(A)**.

much more of the southward wind component compared with the typhoon storm events (Figure 4B). This dominance of winter storms over typhoons in contributing southward wind component is also true in the past four decades, based on analysis of wind data during the period 1979–2018 (Yang et al., 2023).

Wave height

The temporal pattern of wave height is similar to that of wind speed, allowing for a time lag of wave height behind wind speed. A peak wave height of 3.2 m occurred ~17 h after the maximum wind speed of the first storm event, and a peak wave height of 5.1 m occurred ~12 h after the maximum wind speed of the second storm event (Figure 3B). In order to identify the contributions of wind waves and swells, the analysis on power spectral density of water depth was conducted for the two periods of waves peaks (Figures 5A, B). The results showed that the energy of swells was weak and was barely detected in the former peak (Figures 5A, B). Therefore, the variations of wave height primarily reflected the domination of local winds, and the unsynchronization between wave height and wind speed was probably due to the time lag effect. Subsequently, changes in the coefficient of determination (R^2) with time lag were analyzed (Figure 5C). The R^2 is 0.24 for the in-phase wave height and wind speed. The value of R^2 increases to a maximum of 0.75 in the case of a 12.5-hour lag of wave height behind wind speed. However, R^2 decreases to 0.38 in the case of a 25-hour lag of wave height behind wind speed, and to ~0.01 in the case of a 50-hour lag (Figure 5C). On average, the significant wave height was 2.06 m for the 6 tidal cycles with storm winds, 1.46 m for the 10 cycles with moderate winds, and 1.18 m for the 4 cycles with weak winds. Allowing for a one-tide lag of wave height behind wind speed, the significant wave height was 2.41 m for the tidal cycles with storm winds, 1.33 m for the cycles with moderate winds, and 0.84 m for the cycles with weak winds. Allowing for a two-tide lag of wave height behind wind speed, the significant wave height was 2.14 m for the tidal cycles with storm winds, 1.43 m for the cycles with moderate winds, and 0.85 m for the cycles with weak winds (Table 2). Thus, the effect of storm wind on wave height is best reflected by a one-tide lag of wave height behind wind speed, and in this case the storm-increased wave height was nearly three folds high than that under calm weathers.

Tidal range and current velocity

The temporal change in tidal range was fluctuant (Figure 3C), reflecting the occurrence of irregular, semi-diurnal tides. The mean tidal range of the 6 storm-wind tides was 3.14 m, and the mean tidal range of the 14 non-storm-wind tides was 3.11 m (3.25 m for the 10 moderate-wind tides and 2.76 m for the 4 weak-wind tides; Table 1). The current directions were mainly back and forth. The dominant directions during the flood phases were northwesterly (towards the inner Yangtze Estuary), whist the dominant directions during the ebb phases were southeasterly. These dominant directions normally corresponded to peak velocities during the flood and ebb phases, respectively (Figures 3C-E). Despite the intra-tidal cyclicity, the current velocity showed a temporal pattern of increase from neap to spring tides and decrease from spring to neap tides (Figure 3E; Table 1).

Residual current

On average, the residual current velocity was 0.16 m/s under winter storm conditions and 0.08–0.09 m/s during fair weather. The

10.3389/fmars.2024.1420559

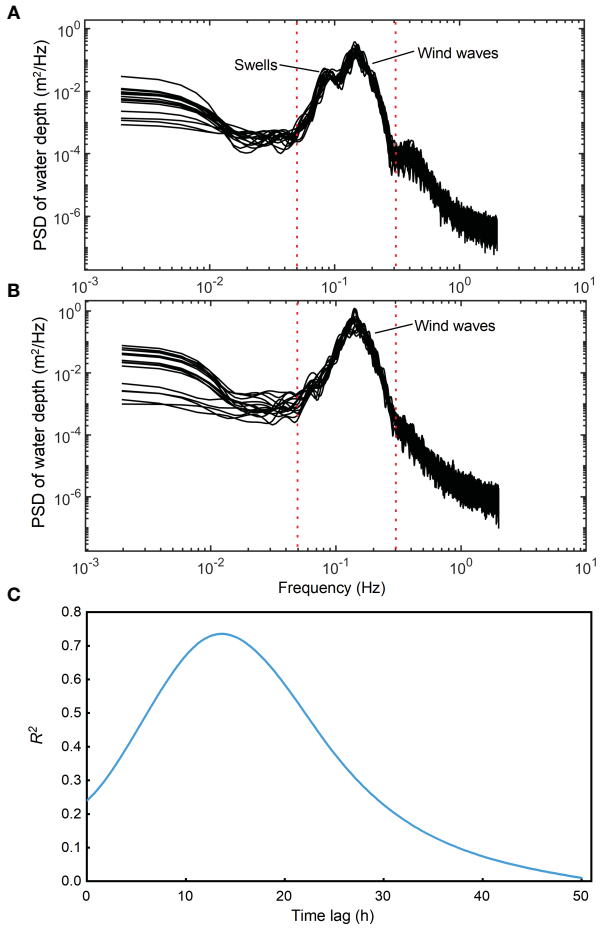

FIGURE 5
(A) The power spectral density of water depth during the first winter storm event. **(B)** The power spectral density of water depth during the second winter storm event. **(C)** Changes in the coefficient of determination (R^2) with time lag of wave height behind wind speed, suggesting a maximum cross-correlation at a 12.5-hours lag. This plot is based on correlations using the wind speed and wave height data shown in Table 1.

tidal-cycle residual current directions varied between 173° and 220° under winter storm conditions and between 186° and 319° in fair weather. The residual current direction was southward during four of the six tidal cycles with winter storm winds and southwestward during the other two. The residual current direction during periods of moderate wind was southward during two tides, southwestward during three tides, and westward during five tides. The residual current direction during periods of weak wind was southwestward during one tide and northwestward during three tides. The angle between the residual current and wind ranged from 11° to 139°; the greater the wind speed, the smaller the angle between the residual current and wind. There was a significant negative correlation between this angle and wind speed (R^2 = 0.27, p = 0.023). Assuming a one-tide lag of residual current behind the wind event, the coefficient of determination increased (R^2 = 0.31, p = 0.017). However, the coefficient of determination decreased markedly for a two-tide lag, and the negative correlation between the angle and wind speed became insignificant (R^2 =0.02, $p > 0.05$; Table 1). Similar patterns between residual current velocity and wind speeds were also revealed. The coefficient of determination were 0.21, 0.35 and 0.12 under the in phase, one-tide lag and two-tide lag, respectively. Therefore, to better understand the effect of wind on the residual current, a one-tide lag of residual current behind the wind event must be considered. Using this time lag, the average residual current velocity was 0.18 m/s under storm-wind conditions compared with 0.08 m/s under fair weather, and all the residual current directions under storm conditions were southward (173°–200°; Figures 6A, B; Tables 1, 2).

All the vertical profiles of residual current velocity show marked decreasing trends. Overall, the residual current velocity decreased from 0.11 m/s at the near-surface layer to 0.04 m/s at the near-bed layer. However, the profiles under storm conditions show greater regularity than those obtained under fair-weather conditions. For example, the R^2 value between the residual current velocity and the height above the seabed ranged from 0.91 to 0.97 (average 0.94) for tidal cycles under storm conditions and from 0.20 to 0.96 (average

TABLE 2 Comparison of residual suspended sediment transport and key factors between storm and non-storm scenarios.

Weather condition	Sw (m/s)	In phase					1-tide lag behind wind					2-tide lag behind wind				
		H_s (m)	Vr (m/s)	Ca (kg/m³)	F_{E-W} (kg/s)	F_{N-S} (kg/s)	H_s (m)	Vr (m/s)	Ca (kg/m³)	F_{E-W} (kg/s)	F_{N-S} (kg/s)	H_s (m)	Vr (m/s)	Ca (kg/m³)	F_{E-W} (kg/s)	F_{N-S} (kg/s)
Storm wind	10.1	2.06	0.16	0.70	-0.07	-2.40	2.41	0.18	0.85	-0.13	-2.80	2.14	0.13	0.97	-0.79	-1.80
Moderate wind	7.3	1.46	0.08	0.78	-1.05	-0.44	1.33	0.08	0.74	-1.06	-0.18	1.43	0.11	0.71	-0.79	-0.49
Weak wind	3.5	1.18	0.09	0.77	-1.00	0.43	0.84	0.08	0.64	-0.86	0.56	0.85	0.06	0.36	-0.36	-0.18

S_w: Time-averaged residual wind speed. H_s: Significant wave height. V_r: Depth-time-averaged residual current velocity. C_a: Depth-averaged SSC. F_{E-W}: East–west component of sediment transport rate (negative values represent the west component). F_{N-S}: North–south component of sediment transport rate (negative values represent the south component). Data are provided in Table S1.

10.3389/fmars.2024.1420559

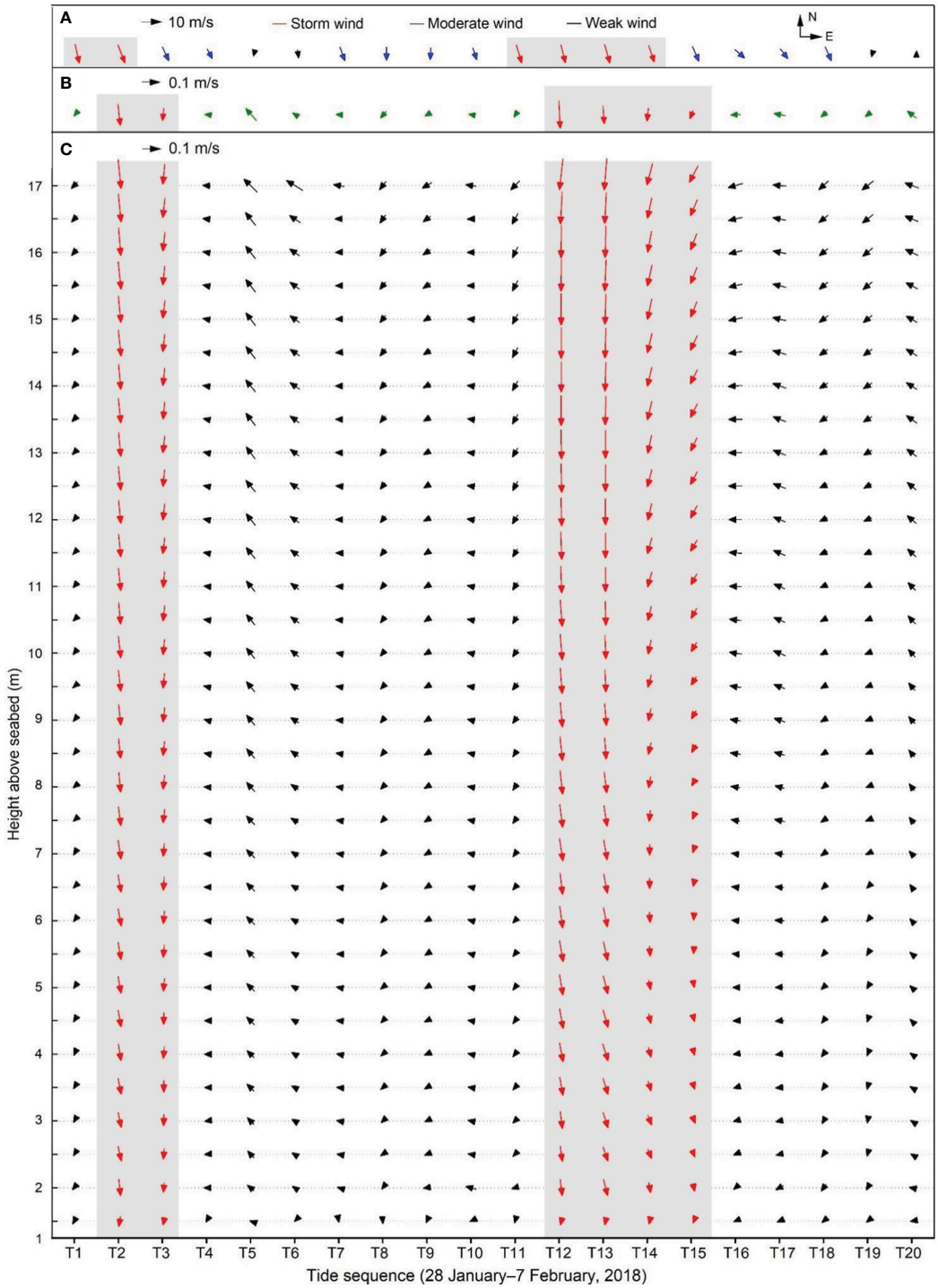

FIGURE 6
(A) Tidal-cycle residual wind vectors, **(B)** depth-averaged current, and (*C*) current profile during the study period. Gray shading in **(A)** represents storm winds, and in **(B,C)** represents residual currents under storm impacts that are best reflected with a one-tide lag behind storm winds. T1–T20 represent tides 1–20, respectively.

0.79) for tidal cycles under fair-weather conditions. The maximum difference in residual current direction in the profiles ranges from 9° to 54° (average 30°) for tidal cycles under storm conditions and from 24° to 122° (average 57°) for those under fair-weather conditions (Figure 6C; Supplementary Table S2).

Suspended sediment concentration

In addition to exhibiting tidal cyclicity, SSCs increased from 28 January to 5 February (tides 1–16) and decreased from 5 to 7 February (tides 16–20). The SSC increased gradually during the

10.3389/fmars.2024.1420559

period prior to 3 February, on which date there was an abrupt increase. The gradual increasing trend in SSC corresponds to the increasing trends in tidal range and current velocity, and the abrupt increase on 3 February corresponds to the highest significant wave height during the major storm event (Figure 3F; Table 1). A high SSC (0.7–5.6 kg/m^3) was maintained until 5 February, despite reductions in wave height and tidal current velocity after 3 February, suggesting a time lag of SSC behind tidal hydrodynamics (Figure 3). Near-surface SSCs were consistently lower than near-bed SSCs, with difference varying during the tidal cycle. The SSC profiles show significant downward trends (Figure 7; Supplementary Figure S1). The regression trends indicate that the ratios of surface to near-bed SSC were 0.09–0.70 (average 0.34), and the ratios of depth-averaged to near-bed SSC were 0.49–0.90

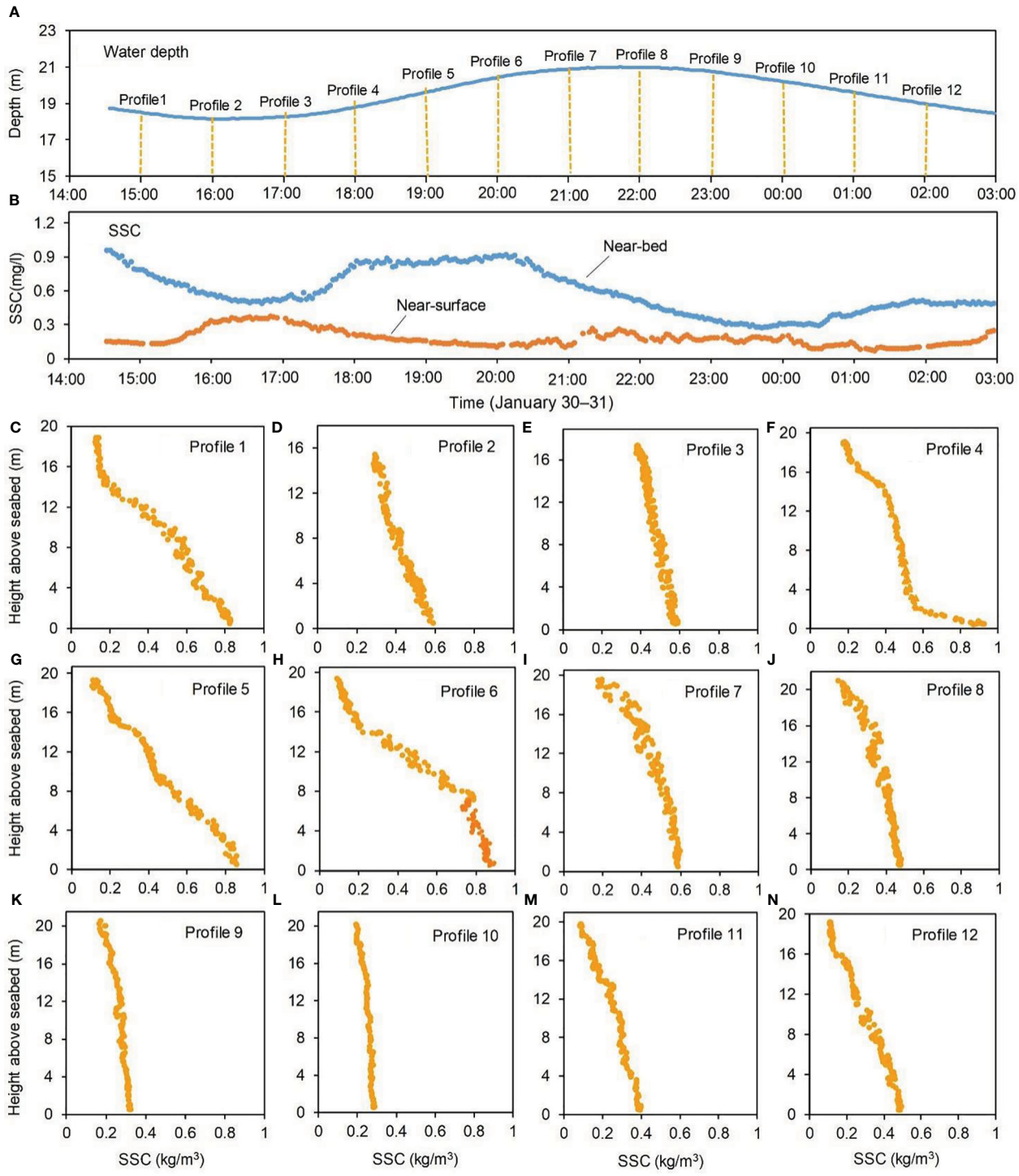

FIGURE 7
Intra-tidal variations in **(A)** water depth, **(B)** SSC, and **(C–N)** hourly vertical profiles of SSC, based on measurements obtained during tide 6.

TABLE 3 Ratios of near-surface SSC (C_s) and depth-averaged SSC (C_a) to near-bed SSC (C_b) in vertical profiles of SSC during tidal cycles, based on measurements obtained during tide 6.

Names of profiles	C_s (kg/m^3)	C_b (kg/m^3)	C_a (kg/m^3)	Ratio of C_s to C_b	Ratio of C_a to C_b
Profile 1 (1 hour prior to low tide)	0.114	0.826	0.457	0.138	0.553
Profile 2 (at low tide)	0.287	0.588	0.42	0.489	0.715
Profile 3 (1 hour after low tide)	0.388	0.575	0.482	0.675	0.838
Profile 4 (2 hours after low tide)	0.17	0.914	0.444	0.186	0.486
Profile 5 (3 hours after low tide)	0.076	0.868	0.472	0.088	0.544
Profile 6 (2 hours prior to high tide)	0.085	0.88	0.518	0.097	0.589
Profile 7 (1 hour prior to high tide)	0.214	0.583	0.457	0.367	0.784
Profile 8 (at high tide)	0.173	0.461	0.357	0.375	0.774
Profile 9 (1 hour after high tide)	0.179	0.313	0.265	0.572	0.847
Profile 10 (2 hours after high tide)	0.195	0.252	0.280	0.696	0.900
Profile11 (3 hours after high tide)	0.082	0.387	0.258	0.212	0.667
Profile 12 (4 hours after high tide)	0.099	0.508	0.303	0.195	0.596
Profiles 1–12 (Tidal average)	0.172	0.589	0.401	0.341	0.691

Values are based on regression trends in SSC profiles (see Supplementary Tables S1.1–S1.12 for details).

(average 0.69; Table 3). The mean ratio of depth-averaged to near-bed SSC (0.69) and the tide-averaged near-bed SSCs (0.27–2.33 kg/m^3) indicate that the tide-depth-averaged SSCs during the twenty observed tidal cycles ranged from 0.19 to 1.61 kg/m^3 (average 0.76 kg/m^3; Table 1).

Residual and longshore sediment transport

The cross-shore residual sediment transport component was onshore (westward) during 17 tidal cycles and offshore (eastward) during the other 3 (tides 2, 12, and 13) that occurred during storm events with northwesterly winds (338°–346°). The longshore residual sediment transport component was southward during 13 tidal cycles and northward during the other 7. The residual sediment transport direction was southward during the six tidal cycles under storm conditions, and the rates of sediment transport per unit width of cross-section ranged from 43 to 207 t/m (ton/meter) (average 125 t/m), considering a one-tide lag of sediment transport behind wind force (Table 1). During the tidal cycles under moderate-wind conditions, the residual sediment transport direction was either southward or northward, with the rates of the southward sediment transport ranging from 3 to 43 t/m (average 26 t/m) and those of northward sediment transport ranging from 3 to 41 t/m (average 19 t/m) (Table 1). During the tidal cycles under weak-wind conditions, the residual sediment transport direction was northward, and the rates of sediment transport ranged from 1 to 57 t/m (average 24 t/m) (Table 1). The highest northward residual transport rate (57 t/m) occurred at tide 20. Considering a one-tide lag of sediment transport behind wind force, the cumulative southward sediment transport at the six tidal cycles under storm impact (tides 2–3 and 12–15) (747 t/m) accounts for 82% of the total southward sediment transport during the thirteen tidal cycles (tides 1, 2–3, 8–9, 11–16 and 18–19) (909 t/m), and contributes 98% of the overall net southward sediment transport in the observation period (tides 1–20) (762 t/m) (Figure 8; Table 1).

Discussion

Our results suggest that massive southward longshore sediment transport from the offshore subaqueous Yangtze Delta occurred during the winter storm study period, and this was most likely the case during other winter storm periods over the course of the year. This southward sediment transport occurred mainly during storm events because storms result in enhanced wave power and sediment resuspension, and because most winter storms are dominated by a northerly wind component and thereby drive strong southward residual currents (Yang et al., 2023; Zhu et al., 2024). Minimal

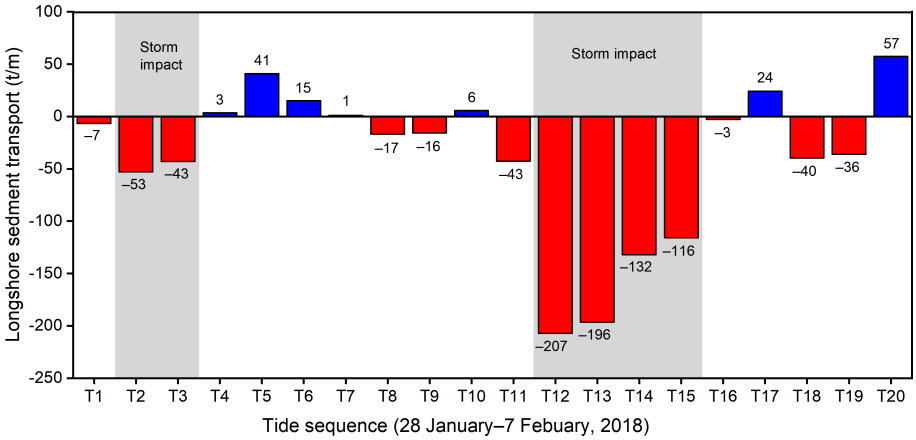

FIGURE 8
Residual longshore sediment transport per meter width of the water column during the tidal cycles in the study period. Negative values denote southward transport. Gray shading represents sediment transport under storm-weather conditions that are best reflected with a one-tide lag behind storm wind.

southward sediment transport occurs during fair-weather conditions, even if the winds are dominated by a southward component. Therefore, the southward sediment transport is episodic and discontinuous, even during the winter monsoon season. There is a nonlinear relation between longshore sediment rate and wind force. To better understand the impact of winter storms on longshore sediment transport, a certain time-lag effect should be considered.

Winter storms dominate over typhoons in driving longshore sediment transport from the Yangtze Delta

It is expected that all winter storms in the Northern Hemisphere contribute a strong southward wind component. However, only some of the typhoons influencing the Yangtze Delta contribute a strong southward wind component. In the case of 2018, only three of the eight typhoons (i.e., Soulik, Trami, and Kong-rey) led to southward storm winds in the Yangtze Delta region. The tracks of Soulik, Trami, and Kong-rey indicate that they migrated from south to north over the Western Pacific and crossed the 31° latitude line to the east of the Yangtze Delta. The other five typhoons made landfall either at or south of the Yangtze Delta. This finding is consistent with the results of a previous study that demonstrated that the migration path of a typhoon dictates whether it would lead to the development of southward storm winds in the Yangtze Delta (Yang et al., 2023). In contrast, all storm events during winter were dominated by a southward wind component (Figure 4). During our observation period, winter storm events accounted for 30% of the wind duration and 40% of the net southward wind component (Figure 3A), and likely contributed 82% of the total southward sediment transport and 98% of the net southward sediment transport (Figure 8). During the winter season of 2018 (December–February), winter storm events accounted for 19% of the wind duration and 60% of the net southward wind component. During 2018, storm events accounted for 9% of the wind duration and 70% of the net southward wind component; but the winter storms contributed much more of the southward wind component than the typhoons (Figure 4). Therefore, storm events assumedly dominated the annual net southward sediment transport from the Yangtze Delta to the Zhejiang–Fujian coasts, but winter storms most likely dominated over typhoons in driving this transport. This dominance is the result of winter storms being the key driver of southward longshore currents (Figure 6) and because the storm-induced waves give rise to increased sediment resuspension (Figure 3). The dominance of winter storms over typhoons in driving southward delivery of sediment from the Yangtze Delta may be also true in decadal scale, considering that, as shown above, winter storms dominated over typhoons in contributing southward wind component during the period 1979–2018 (Yang et al., 2023). A recent study also emphasized the importance of winter storms. By utilizing long-term field observations, bathymetric data, and simulation modeling, they analyzed 108 deltas around the world and found that winter storms caused subaqueous deltas to degrade (Zhu et al. 2024).

Despite the general dominance of winter storms over typhoons in annual or long-term longshore sediment transport from the Yangtze Delta, individual typhoons may lead to greater sediment redistribution than individual winter storm, because the maximum wind speeds of typhoons tend to be higher than the maximum wind speeds of winter storms (e.g., Figure 4A), and the increased wave height and sediment resuspension during individual typhoons are usually greater than those during individual winter storms (Yang et al., 2023; Wu et al., 2024). Larger increased waves during typhoon events also mean greater area of sediment resuspension, because larger waves can disturb deeper seabed (Yang et al., 2023). In short, winter storm is a different extreme weather pattern from typhoon and hurricane. While both extreme weather patterns can cause massive coastal sediment redistribution, winter storm impact is higher in frequency and more consistent in southward sediment transport than typhoon and hurricane impacts. On the other hand,

individual typhoons and hurricanes can lead to greater sediment redistribution than individual winter storms, even though the direction of sediment transport during typhoon and hurricane events is variable, depending on their tracks.

Time-lag effect of winter storm events on longshore sediment transport

The time series of wind, wave, SSC, residual current, and longshore sediment transport data (Figures 3, 6; Table 1), and the coefficient of determination between wave height and wind speed as a function of time (Figure 5C) suggest an approximate one-tide lag in longshore sediment transport rate behind wind force. This time lag is due to the following factors. 1) The formation of waves and drifts requires a certain period of wind blowing. 2) Because of the inertia of water motion, wave propagation and tidal drift will continue for some time after the storm ends. 3) It takes time for sediment particles to be re-suspended and deposited, especially in deep water. 4) Immediately after the storm abates, wave power may be maintained at a level much higher than the critical water energy between sediment resuspension and deposition, which would lead to net resuspension and a continued increase in SSC (Liu et al., 2014; Yang et al., 2019). The settling velocities of the Yangtze Estuary sediments are 0.016–0.39 mm/s (Chen, 2013). Therefore, a period of 14–350 h would be required for storm-resuspended sediments to settle out from the water to the seafloor at our observation site (~20 m water depth). The coarser the sediment particle and the smaller the distance from the particle to the seabed, the shorter the time for the particle to settle out. Strictly speaking, the time lag in wave power behind a winter storm and the time lag in SSC behind tidal hydrodynamics should be variable. Different storm intensities may result in varying time delays. In this study, a one-tide lag is an optimal estimation but is not the only option. A one-tide lag may be partly relevant to the statistical unit (i.e., one tide); e.g., if the statistical unit is a day, the optimal estimation would be a one-day lag. An optimal estimation of a one-day lag in SSC behind tidal range has been suggested for the offshore subaqueous Yangtze Delta (Yang et al., 2023). In the present study, the high SSC maintained in the first few tidal cycles after the end of the second storm was likely caused by a lag in the effects of wind waves and tides on the SSC (Figure 3; Table 1). A similar time lag in SSC behind storm winds (i.e., where the maximum SSC occurred after the storm had abated) has also been determined for the mud belt area south of the Yangtze Delta (Yang et al., 2007).

Other factors influencing longshore sediment transport during winter storms

In addition to wind speed and direction, which control wave-induced sediment resuspension and drift-induced residual sediment transport, other factors (e.g., sediment properties, tidal conditions, and wave power under fair weather) may also influence the rate of longshore sediment transport under storm-weather conditions. As noted above, the sediments of the offshore subaqueous Yangtze Delta are composed mainly of silt and clay (Luo et al., 2017). The water content of these sediments is relatively high (suggesting low compaction) because of the rapid deposition since the late Holocene. Macrotidal (spring tidal range > 4 m; Davies, 1964) and semidiurnal tidal conditions in the offshore subaqueous Yangtze Delta result in a high current velocity (Figure 3E). The Yangtze Delta is exposed to the East China Sea (Figure 1A), leading to the development of large waves even during periods of fair weather. Therefore, background SSCs are usually high, even under fair-weather and neap-tide conditions (Figure 3F; Yang et al., 2007; Yang et al., 2020b, 2023). Storm waves increase SSCs, but they are not the sole cause of the high SSCs in the Yangtze Delta. The massive southward sediment transport from the Yangtze Delta during the study period should be attributed not only to a direct contribution from storm winds but also an indirect contribution from other factors such as easily erodible loose sediments, macrotidal conditions and moderate background wave heights. Without the storm winds, southward longshore currents and sediment transport would be minimal. Without the other factors, the rate of the southward sediment transport would be greatly decreased, even during individual storm events, although it is difficult for us to quantify this decrease in sediment transport. Specifically, if neap tides had occurred during the second storm event in the study period, the SSCs would have been much lower than those observed, and the southward sediment transport from the Yangtze Delta would have been greatly reduced.

The Mississippi and Yangtze rivers have a comparable sediment discharge (~500 Mt/yr prior to dam construction in the last century and ~120 Mt/yr in the recent decade), and both deltas are among the world's largest deltas (Yang et al., 2021). However, in contrast to the Yangtze Delta, the subaqueous Mississippi Delta is microtidal (tidal range < 0.5 m) and has a diurnal tidal cycle (Arndorfer, 1973), leading to much weaker tidal currents (tidal-depth-averaged velocities of < 0.2 m/s) than in the Yangtze Delta (tide-depth-averaged velocities of 0.4–0.8 m/s, Table 1) (Wang et al., 2018b). And the significant wave height in the subaqueous Mississippi Delta is typically < 0.4 m, which is also lower than that in the Yangtze Delta (Figure 3B; Fan et al., 2006; Wang et al., 2018b). As a result, SSCs in the subaqueous Mississippi Delta are an order of magnitude lower than those in the subaqueous Yangtze Delta (Yang et al., 2021). Under these low-SSC conditions, residual sediment transport would be limited, even under storm-weather conditions, which is most likely why the Mississippi Delta forms a bird-foot delta. Like the Mississippi Delta, the Nile Delta is microtidal (tidal range ≤ 0.5 m), and the progradation of the Nile Delta formed promontories prior to river damming. After the construction of the Aswan High Dam, rapid retreat of the promontories was observed (Milliman & Farnsworth, 2011). If the subaqueous Yangtze Delta was microtidal, the delta would be substantially larger and the Zhejiang–Fujian mud belt would be much smaller. There are many other deltas such as the Ebro, Mackenzie, Rhone, Rio Grande, Vistula, Yenisei and Yesil deltas whose tidal range is very small (≤ 0.5 m). On the other hand, some deltas (e.g., Amazon, Irrawaddy, Gange, Namada, and Han deltas) have tidal ranges greater than or equal to the tidal range of the Yangtze Delta (Yang et al., 2020a). In short, the rate of longshore sediment transport during a storm event is controlled not only by the storm itself but also by local tides, waves, and sediment properties.

Limitations

This study has several limitations. First, we conducted field observations at only one station, and the observations lasted for only ten days; therefore, it is difficult to estimate the total sediment transport over the cross-shore section during winter or over the entire year. Second, we defined storms and storm events based on the characteristics of local winds to evaluate the effects of the low-frequency but strongest winds on longshore sediment transport. This definition might not apply to winds in regions elsewhere. Third, our identification of a one-tide lag in sediment transport behind wind force may be partly related to the time unit (one tide) needed to calculate the residual current; i.e., the one-tide lag is an estimation and is not precise. These limitations need to be addressed in future work.

Conclusions

Our results suggest the occurrence of massive southward longshore residual sediment transport from the offshore subaqueous Yangtze Delta during winter storm events. The mechanisms controlling this transport include intense resuspension of fine-grained sediments in the delta and strong southward longshore residual currents during storm events. There is a half-day lag in longshore sediment transport behind the winter storm winds because the development of waves and drifts requires a certain period of wind, water flow and wave propagation are subject to inertia, and the settling velocity of fine-grained sediments is slow. Under fair-weather conditions during periods between winter storms, there is minimal sediment transport from the Yangtze Delta. Although southward storms occur mainly during winter, they also occur at other times, including in the typhoon season. Despite their low frequency (~6%), the southward storm events mainly derived from winter storms may make the greatest contribution to the southward sediment transport from the Yangtze Delta and play a dominant role in the supply of sediment to the Zhejiang–Fujian mud belt. Because the sediments transported southward from the delta during storm events are derived mainly from the resuspension of delta deposits, the rate of southward sediment transport would not be markedly affected by the recent decline in fluvial sediment discharge caused by dam construction. However, erosion of the Yangtze Delta and the southward transport of sediment will most likely increase with storm activity under global warming. Although the effects of storms on longshore sediment transport are influenced by local tidal hydrodynamics and sediment properties, and may vary among different coasts, our findings may be helpful for evaluating the relative importance of low-frequency storms and high-frequency non-storm winds in terms of sediment redistribution, especially for ecosystems such as wetland and tidal flats that are highly sensitive to hydrological and climate change.

Data availability statement

The original contributions presented in the study are included in the article/Supplementary Material. Further inquiries can be directed to the corresponding authors.

Author contributions

MT: Conceptualization, Methodology, Visualization, Writing – original draft. HY: Writing – review & editing, Investigation. WZ: Data curation, Investigation, Supervision, Writing – review & editing. KX: Supervision, Writing – review & editing. BS: Writing – review & editing. YW: Writing – review & editing. SY: Funding acquisition, Supervision, Validation, Writing – review & editing.

Funding

The author(s) declare financial support was received for the research, authorship, and/or publication of this article. This work was supported by the National Natural Science Foundation of China (U2240220, 42106167, 41576092, 42076170).

Acknowledgments

We Thank S. S. Zhang, J. Q. Fan and Q.Y. Wu for their assistance in the filed observation.

Conflict of interest

The authors declare that the research was conducted in the absence of any commercial or financial relationships that could be construed as a potential conflict of interest.

Publisher's note

Supplementary material

The Supplementary Material for this article can be found online at: https://www.frontiersin.org/articles/10.3389/fmars.2024.1420559/full#supplementary-material

References

Arndorfer, D. J. (1973). Discharge patterns in two crevasses of the Mississippi River delta. *Mar. Geol.* 15, 269–287. doi: 10.1016/0025-3227(73)90074-1

Bhatia, K. T., Vecchi, G. A., Knutson, T. R., Murakami, H., Kossin, J., Dixon, K. W., et al. (2019). Recent increases in tropical cyclone intensification rates. *Nat. Commun.* 10, 635. doi: 10.1038/s41467-019-08471-z

Cheal, A. J., MacNeil, M. A., Emslie, M. J., and Sweatman, H. (2017). The threat to coral reefs from more intense cyclones under climate change. *Global Change Biol.* 23, 1511–1524. doi: 10.1111/gcb.13593

Chen, X. (2013). Experimental study on deposition in static water of fine-grained sediments of the Yangtze River Estuary. Ocean University of China, Shandong, Qingdao, 78.

Chen, Z. G., Wang, S. P., Leng, C., and Wang, Z. X. (2016). Study on synthesized filtering algorithm for ADCP velocity data (in Chinese). *Yangtze River* 47, 42–47 + 89. doi: 10.16232/j.cnki.1001–4179.2016.13.010

Davies, J. L. (1964). A morphogenic approach to world shorelines. *Z. fur. Geomorphol.* 8, 127–142. doi: 10.1127/zfg/mortensen/8/1964/127

Deng, B., Wu, H., Yang, S. L., and Zhang, J. (2017). Longshore suspended sediment transport and its implications for submarine erosion off the Yangtze River Estuary. *Estuar. Coast. Shelf Sci.* 190, 1–10. doi: 10.1016/j.ecss.2017.03.015

Emanuel, K. A. (2013). Downscaling CMIP5 climate models shows increased tropical cyclone activity over the 21st century. *Proc. Natl. Acad. Sci.* 110, 12219–12224. doi: 10.1073/pnas.1301293110

Fan, D. D., Guo, Y. X., Wang, P., and Shi, J. Z. (2006). Cross-shore variations in morphodynamic processes of an offshore-coast mudflat in the Changjiang Delta, China: With an emphasis on storm impacts. *Cont. Shelf Res.* 26, 517–538. doi: 10.1016/j.csr.2005.12.011

Fang, J. Y., Liu, Z. F., and Zhao, Y. L. (2018). High-resolution clay mineral assemblages in the inner shelf mud wedge of the East China Sea during the Holocene: Implications for the East Asian Monsoon evolution. *Sci. China: Earth Sci.* 61, 1316–1329. doi: 10.1007/s11430–017-9208–1

Gao, J. H., Shi, Y., Sheng, H., Kettneret, A. J., Yang, Y., Jia, J. J., et al. (2019). Rapid response of the Changjiang (Yangtze) River and East China Sea source-to-sink conveying system to human induced catchment perturbations. *Mar. Geol.* 414, 1–17. doi: 10.1016/j.margeo.2019.05.003

Green, M. O., and Coco, G. (2014). Review of wave-driven sediment resuspension and transport in estuaries. *Rev. Geophys.* 52, 77–117. doi: 10.1002/rog.v52.1

Guo, X. J., Fan, D. D., Zheng, S. W., Wang, H. M., Zhao, B. C., and Qin, C. J. (2021). Revisited sediment budget with latest bathymetric data in the highly altered Yangtze (Changjiang) Estuary. *Geomorphology* 391, 107873. doi: 10.1016/j.geomorph.2021.107873

Kong, L. S., Gu, F. F., Wang, W., and Shen, Q. (2015). Statistics and analysis of typhoon-induced sudden siltation for Yangtze estuary deepwater channel (in Chinese). *Port Waterway Eng.* 503, 150–152. doi: 10.16233/j.cnki.issn1002-4972.2015.05.027

Kuang, C. P., Chen, W., Gu, J., and He, L. L. (2014). Comprehensive analysis on the sediment siltation in the upper reach of the deepwater navigation channel in the Yangtze Estuary. *J. Hydrodyn.* 26, 299–308. doi: 10.1016/S1001-6058(14)60033-0

Kudrass, H. R., Machalett, B., Palamenghi, L., Meyer, I., and Zhang, W. Y. (2018). Sediment transport by tropical cyclones recorded in a submarine canyon off Bangladesh. *Geo-Mar Lett.* 38, 481–496. doi: 10.1007/s00367-018-0550-x

Leonardi, N., Ganju, N. K., and Fagherazzi, S. (2016). A linear relationship between wave power and erosion determines salt-marsh resilience to violent storms and hurricane. *PNAS* 133, 64–68. doi: 10.1073/pnas.1510095112

Li, Y. H., Xu, X. H., Yin, X. J., Fang, J. Y., Hu, W. Y., and Chen, J. (2015). Remote-sensing observations of typhoon soulik, (2013) forced upwelling and sediment transport enhancement in the northern Taiwan Strait. *Int. J. Remote Sens.* 36, 2201–2218. doi: 10.1080/01431161.2015.1035407

Liao, T., Cai, T. L., Liu, Y. F., and Xia, X. M. (2016). Continental shoreline change in Zhejiang during the last one hundred years (in Chinese). *J. Mar. Sci.* 34, 25–33. doi: 10.3969/j.issn.1001-909X.2016.03.005

Lin, Y., Li, Y., Liu, M., Wang, L., Zheng, B., Long, Z., et al. (2024). Typhoon chan-hom, (2015) induced sediment cross-shore transport in the mud depocenter of the East China Sea inner shelf. *Mar. Geol.* 469, 107443. doi: 10.1016/j.margeo.2024.107223

Liu, J. H., Yang, S. L., Zhu, Q., and Zhang, J. (2014). Controls on suspended sediment concentration profiles in the shallow and turbid Yangtze Estuary. *Cont. Shelf Res.* 90, 96–108. doi: 10.1016/j.csr.2014.01.021

Liu, J. P., Xu, K. H., Li, A. C., Millinman, J. D., Velozzi, D. M., Xiao, S. B., et al. (2007). Flux and fate of Yangtze River sediment delivered to the East China Sea. *Geomorphology* 85, 208–224. doi: 10.1016/j.geomorph.2006.03.023

Lu, C. T., Jia, X., Han, Y. F., and Bai, Y. B. (2018). Numerical simulation of sudden silting in the Yangtze Estuary deepwater channel by the wave of typhoon. *Adv. Water Sci.* 29, 696–705. doi: 10.14042/j.cnki.32.1309.2018.05.010

Luan, H. L., Ding, P. X., Yang, S. L., and Wang, Z. B. (2021). Accretion-erosion conversion in the subaqueous Yangtze Delta in response to fluvial sediment decline. *Geomorphology* 382, 107680. doi: 10.1016/j.geomorph.2021.107680

Luo, X. X., Yang, S. L., Wang, R. S., Zhang, C. Y., and Li, P. (2017). New evidence of Yangtze delta recession after closing of the Three Gorges Dam. *Sci. Rep.* 7, 41735. doi: 10.1038/srep41735

Matte, P., Secretan, Y., and Morin, J. (2014). Quantifying lateral and intratidal variability in water level and velocity in a tide-dominated river using combined RTK GPS and ADCP measurements. *Limnol. Oceanogr.: Methods* 12, 280–302. doi: 10.4319/lom.2014.12.281

McKee, K. L., Mendelssohn, I. A., and Hester, M. W. (2020). Hurricane sedimentation in a subtropical salt marsh-mangrove community is unaffected by vegetation type. *Estuarine Coast. Shelf Sci.* 239, 106733. doi: 10.1016/j.ecss.2020.106733

Milliman, J. D., and Farnsworth, K. L. (2011). *River Discharge to the Coastal Ocean: A Global Synthesis* (Cambridge: Cambridge University Press), 384. doi: 10.1017/cbo9780511781247

Milliman, J. D., Shen, H. T., Yang, Z. S., and Meade, R. H. (1985). Transport and deposition of river sediment in the Changjiang estuary and adjacent continental shelf. *Cont. Shelf Res.* 4, 37–45. doi: 10.1016/0278-4343(85)90020-2

Mo, D. X., Li, J., and Hou, Y. J. (2021). Assessing the impact of wave-wurrent interactions on storm surges and waves during cold air outbreaks in the Northern East China Sea. *J. Mar. Sci. Eng.* 9, 824. doi: 10.3390/jmse9080824

Partheniades, E. (1965). Erosion and deposition of cohesive soils. *Am. Soc Civ. Eng.* 90, 105–139. doi: 10.1061/JYCEAJ.0001165

Puig, P., Ogston, A. S., Mullenbach, B. L., Nittrouer, C. A., Parsons, J. D., and Sternberg, R. W. (2004). Storm-induced sediment gravity flows at the head of the Eel submarine canyon, northern California margin. *J. Geophys. Res.* 109, C03019. doi: 10.1029/2003JC001918

Sequeiros, O. E., Pittaluga, M. B., Frascati, A., Pirmez, C., Masson, D. G., Weaver, P., et al. (2019). How typhoons trigger turbidity currents in submarine canyons. *Sci. Rep.* 9, 9220. doi: 10.1038/s41598–019-45615-z

Shepard, F. P. (1932). Sediments of the continental shelves. *GSA Bull.* 43, 1017–1040. doi: 10.1130/GSAB-43-1017

Shi, B. W., Yang, S. L., Temmerman, S., Bouma, T., Ysebaert, T., Wang, S., et al. (2021). Effect of typhoon-induced intertidal-flat erosion on dominant macrobenthic species (Meretrix meretrix). *Limnol. Oceanogr.* 66, 4197–4209. doi: 10.1002/lno.11953

Shi, B. W., Yang, S. L., Wang, Y. P., Li, G. C., Li, M. L., Li, P., et al. (2017). Role of wind in erosion-accretion cycles on an estuarine mudflat. *J. Geophys. Res.: Oceans* 122, 193–206. doi: 10.1002/2016JC011902

Singleton, F. (2008). The Beaufort scale of winds - its relevance, and its use by sailors. *Weather* 63, 37–41. doi: 10.1002/wea.153

Thompson, R. O. R. Y. (1983). Low-pass filters to suppress iner-tial and tidal frequencies. *J. Phys. Oceanogr.* 13, 1077–1083. doi: 10.1175/1520–0485(1983)013<1077:lpftsi>2.0.co;2

Tian, Y., Fan, D. J., Zhang, X. L., Chen, B., Wang, L., Liu, M., et al. (2019). Event deposits of intense typhoons in the muddy wedge of the East China Sea over the past 150 years. *Mar. Geol.* 410, 109–121. doi: 10.1016/j.margeo.2018.12.010

Turner, R. E., Baustian, J. J., Swenson, E. M., and Spicer, J. S. (2006). Wetland sedimentation from hurricanes Katrina and Rita. *Science* 314, 449–452. doi: 10.1126/science.1129116

Wan, K., Bao, X. W., Wang, Y., Wan, X. Q., Li, H. Q., and Liu, K. (2015). Barotropic current fluctuations coupled with sea level drawdown in Yellow and Bohai Seas. *Chin. J. Oceanol. Limnol.* 33, 272–281. doi: 10.1007/s00343-015-4056-3

Wang, H. J., Saito, Y., Zhang, Y., Bi, N. S., Sun, X. X., and Yang, Z. S. (2011). Recent changes of sediment flux to the western Pacific Ocean from major rivers in East and Southeast Asia. *Earth-Sci. Rev.* 108, 80–100. doi: 10.1016/j.earscirev.2011.06.003

Wang, Z. H., Saito, Y., Zhan, Q., Nian, X. M., Pan, D. L., Wang, L., et al. (2018a). Three-dimensional evolution of the Yangtze River mouth, China during the Holocene: Impacts of sea level, climate and human activity. *Earth-Sci. Rev.* 185, 938–955. doi: 10.1016/j.earscirev.2018.08.012

Wang, J. Z., Xu, K. H., Li, C. Y., and Obelcz, J. (2018b). Forces driving the morphological evolution of a mud-capped dredge pit, Northern Gulf of Mexico. *Water* 10, 1001. doi: 10.3390/w10081001

Williams, H., and Liu, K.-b. (2019). Contrasting Hurricane Ike washover sedimentation and Hurricane Harvey flood sedimentation in a Southeastern Texas coastal marsh. *Mar. Geol.* 417, 10601. doi: 10.1016/j.margeo.2019.106011

Winterwerp, J. C., van Kesteren, W. G. M., van Prooijen, B., and Jacobs, W. (2012). A conceptual framework for shear flow–induced erosion of soft cohesive sediment beds. *J. Geophys. Res.* 117, C10020. doi: 10.1029/2012JC008072

Wright, L. D., and Friedrichs, C. T. (2006). Gravity driven sediment transport on continental shelves: a status report. *Cont. Shelf Res.* 26, 2092–2107. doi: 10.1016/j.csr.2006.07.008

Wu, X. F., He, Q., Shen, J., Peng, Z., Guo, L. C., Xie, W. M., et al. (2024). Different effects between cold front and tropical cyclone on short-term morphodynamics in the Changjiang Delta. *J. Mar. Syst.* 243, 103961. doi: 10.1016/j.jmarsys.2023.103961

Xiao, S. B., Li, A. C., Liu, J. P., Chen, M. H., Xie, Q., Jiang, F. Q., et al. (2006). Coherence between solar activity and the East Asian winter monsoon variability in the

past 8000 years from Yangtze River-derived mud in the East China Sea. *Palaeogeogr. Palaeoclimatol. Palaeoecol.* 237, 293–304. doi: 10.1016/j.palaeo.2005.12.003

Xie, D. F., Pan, C. H., Wu, X. G., Gao, S., and Wang, Z. B. (2017a). Local human activities overwhelm decreased sediment supply from the Changjiang River: Continued rapid accumulation in the Hangzhou Bay-Qiantang Estuary system. *Mar. Geol.* 392, 66–77. doi: 10.1016/j.margeo.2017.08.013

Xie, D. F., Pan, C. H., Wu, X. G., Gao, S., and Wang, Z. B. (2017b). The variations of sediment transport patterns in the outer Changjiang Estuary and Hangzhou Bay over the last 30 years. *J. Geophys. Res. Oceans* 122, 2999–3020. doi: 10.1002/2016JC012264

Xu, G., Bi, S. P., Gugliotta, M., Liu, J., and Liu, J. P. (2023). Dispersal mechanism of fine-grained sediment in the modern mud belt of the East China Sea. *Earth-Science Rev.* 240, 104388. doi: 10.1016/j.earscirev.2023.104388

Xu, K. H., Liu, A. C., Liu, J. P., Milliman, J. D., Yang, Z. S., Liu, C.-S., et al. (2012). Provenance, structure, and formation of the mud wedge along inner continental shelf of the East China Sea: a synthesis of the Yangtze dispersal system. *Mar. Geol.* 291–294, 176–191. doi: 10.1016/j.margeo.2011.06.003

Xu, X. B., Tan, Y., Chen, S., and Yang, G. S. (2014). Changing patterns and determinants of natural capital in the Yangtze River Delta of China 2000–2010. *Sci. Total Environ.* 466–467, 326–337. doi: 10.1016/j.scitotenv.2013.07.043

Xue, C. F., Sheng, H., Wei, D. Y., Yang, Y., Wang, Y. P., and Jia, J. J. (2020). Dry bulk density analysis for inner shelf sediments of the East China Sea and its sedimentary implications (in Chinese). *Oceanol. Limnol. Sin.* 51, 1093–1107. doi: 10.11693/hyhz20191000200

Yan, C. Y., Zhang, W. G., Chen, Y. L., Nian, X. M., and Hu, Z. X. (2022). Change of sediment composition in the Yangtze River subaqueous delta and its environmental implications. *Quat. Sci.* 42, 412–420. doi: 10.11928/j.issn.1001–7410.2022.02.07

Yang, S. L., Bouma, T. J., Xu, K. H., Shi, B. W., Yang, H. F., Zhang, W. X., et al. (2023). Storms dominate the erosion of the Yangtze Delta and southward sediment transport. *Sci. Bull.* 68, 553–556. doi: 10.1016/j.scib.2023.03.005

Yang, S. L., Fan, J. Q., Shi, B. W., Bouma, T. J., Xu, K. H., Yang, H. F., et al. (2019). Remote impacts of typhoons on the hydrodynamics, sediment transport and bed stability of an intertidal wetland in the Yangtze Delta. *J. Hydrol.* 575, 755–766. doi: 10.1016/j.jhydrol.2019.05.077

Yang, S. L., Friedrichs, C. T., Shi, Z., Ding, P. X., Zhu, J., and Zhao, Q. Y. (2003). Morphological response of tidal marshes, flats and channels of the deeper Yangtze River mouth to a major storm. *Estuaries* 26, 1416–1425. doi: 10.1007/BF02803650

Yang, Z. S., Lei, K., Guo, Z. G., and Wang, H. J. (2007). Effect of a winter storm on sediment transport and resuspension in the distal mud area, the East China Sea. *J. Coast. Res.* 232, 310–318. doi: 10.2112/03-0130.1

Yang, H. F., Li, B. C., Zhang, C. Y., Qiao, H. J., Liu, Y. T., Bi, J. F., et al. (2020b). Recent spatio-temporal variations of suspended sediment concentrations in the Yangtze Estuary. *Water* 12, 818. doi: 10.3390/w12030818

Yang, S. L., Luo, X. X., Temmerman, S., Kirwan, M., Bouma, T., Xu, K. H., et al. (2020a). Role of delta-front erosion in sustaining salt marshes under sea-level rise and fluvial sediment decline. *Limnol. Oceanogr.* 65, 1990–2009. doi: 10.1002/lno.11432

Yang, S. L., Milliman, J. D., Li, P., and Xu, K. H. (2011). 50,000 dams later: Erosion of the Yangtze River and its delta. *Global Planet. Change.* 75, 14–20. doi: 10.1016/j.gloplacha.2010.09.006

Yang, S. L., Xu, K. H., Milliman, J. D., Yang, H. F., and Wu, C. S. (2015). Decline of Yangtze River water and sediment discharge: Impact from natural and anthropogenic changes. *Sci. Rep.* 5, 12581. doi: 10.1038/srep12581

Yang, H. F., Yang, S. L., Li, B. C., Wang, Y. P., Wang, J. Z., Zhang, Z. L., et al. (2021). Different fates of the Yangtze and Mississippi deltaic wetlands under similar riverine sediment decline and sea-level rise. *Geomorphology* 381, 107646. doi: 10.1016/j.geomorph.2021.107646

Yang, H. F., Yang, S. L., and Xu, K. H. (2017a). River-sea transitions of sediment dynamics: A case study of the tide-impacted Yangtze River estuary. *Estuarine Coast. Shelf Sci.* 196, 207–216. doi: 10.1016/j.ecss.2017.07.005

Yang, H. F., Yang, S. L., Xu, K. H., Milliman, J. D., Wang, H., Yang, Z., et al. (2018). Human impacts on sediment in the Yangtze River: A review and new perspectives. *Glob. Planet. Change* 162, 8–17. doi: 10.1016/j.gloplacha.2018.01.001

Yang, H. F., Yang, S. L., Xu, K. H., Wu, H., Shi, B. W., Zhu, Q., et al. (2017b). Erosion potential of the Yangtze Delta under sediment starvation and climate change. *Sci. Rep.* 7, 10535. doi: 10.1038/s41598-017-10958-y

Zhou, B. T., and Qian, J. (2021). Changes of weather and climate extremes in the IPCC AR6. *ACCR* 17, 713–718. doi: 10.12006/.issn.1673–1719.2021.167

Zhu, Q. G., Xing, F., Wang, Y. P., Syvitski, J., Overeem, I., and Guo, J. (2024). Hidden delta degradation due to fluvial sediment decline and intensified marine storms. *Sci. Adv.* 10, eadk1698. doi: 10.1126/sciadv.adk169

frontiers | Frontiers in Marine Science

TYPE Original Research
PUBLISHED 11 June 2024
DOI 10.3389/fmars.2024.1413145

OPEN ACCESS

EDITED BY
Qin Zhu,
Southern Marine Science and Engineering Guangdong Laboratory (Guangzhou), China

REVIEWED BY
Xiaoguang Ouyang,
Southern Marine Science and Engineering Guangdong Laboratory (Guangzhou), China
Haobing Cao,
Hohai University, China

*CORRESPONDENCE
Xiuzhen Li
xzli@sklec.ecnu.edu.cn

RECEIVED 06 April 2024
ACCEPTED 20 May 2024
PUBLISHED 11 June 2024

CITATION
Hua Y, Chen H, Ren L, Tang J and Li X (2024) Crab bioturbation reduces carbon storage in salt marshes under more robust mechanisms than plant invasiveness. *Front. Mar. Sci.* 11:1413145. doi: 10.3389/fmars.2024.1413145

Crab bioturbation reduces carbon storage in salt marshes under more robust mechanisms than plant invasiveness

Yujie Hua[1], Huayu Chen[1], Linjing Ren[1], Jianwu Tang[1,2] and Xiuzhen Li[1,2]*

[1]State Key Laboratory of Estuarine and Coastal Research, Institute of Eco-Chongming, East China Normal University, Shanghai, China, [2]Yangtze Delta Estuarine Wetland Ecosystem Observation and Research Station, Ministry of Education and Shanghai Science and Technology Committee, Shanghai, China

Introduction: The macrobenthos are crucial for the stability of estuarine ecosystems due to their burrowing behavior in the sediment and their uptake of nutrients from plants. These activities lead to significant alterations in both the morphological and biogeochemical processes within the region.

Methods: However, there is limited investigation into carbon cycling processes specifically related to crab bioturbation. Additionally, few studies have examined enzymatic activities and carbon fractions in sediments from crab burrow walls at different crab growth stages. This study aims to explore the impact of both plant invasiveness and crab bioturbation on carbon storage.

Results: Our findings suggest that plant invasion leads to higher organic accumulation due to the reduction of recalcitrant organic carbon (ROC) (decreased by 11.6% in invasive and 62.6% in native site from April to December), faster photosynthetic rates (25.8 μmol/m^2 s in invasive and 10.7 μmol/m^2 s in native site), and an increased presence of arbuscular mycorrhizal fungi (AMF) in the soil over time. However, the increase of easy oxidized carbon (EOC) may lead to less carbon storage in soil (increase by 67.7% in invasive and 48.8% in native site from April to December). In addition to invasiveness, the bioturbation activities of macrobenthos also affect carbon storage. Sediments from crab burrows exhibit higher EOC content (33.6% more than the bulk soil) and higher levels of carbon cycling-related enzymes, including S-ACT, S-β-GC, and S-ACP activities (24.2%, 8.99%, and 135.6% higher than the bulk soil, respectively).

Discussion: These changes contribute to reduced carbon accumulation in the soil. Therefore, crab bioturbation is a more significant factor affecting carbon sink capacity than plant invasion.

KEYWORDS

carbon storage, salt marshes, crab bioturbation, plant invasion, mycorrhiza fungi, sediment organic carbon, enzymatic activity

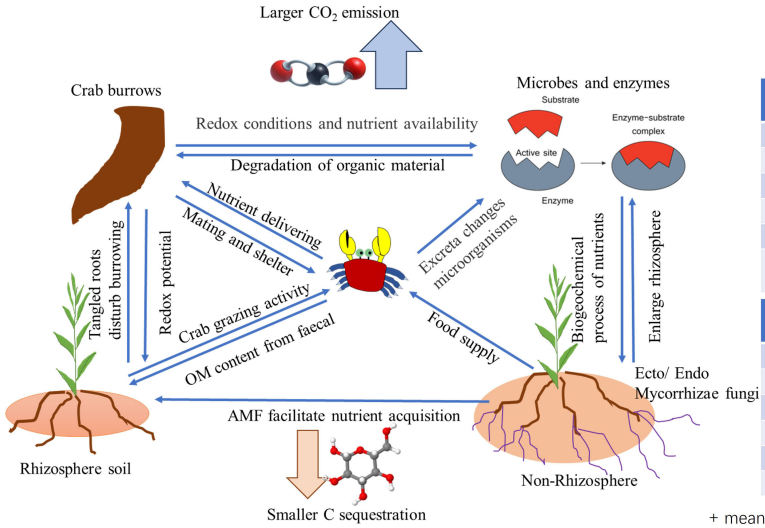

C sequestration comparison

Environmental factors	*P. australis*	*S. alterniflora*
Crab bioturbation	--	-
AMF infection	+	++
Photosynthesis	+	++
EOC	-	--
ROC	--	-
Enzymatic activity	N/A	N/A

Environmental factors	Bulk soil	Mature crab	Rhizo-sphere
TC,TN,TOC		+	
EOC		--	-
ROC		-	-
S-ACT		-	-
S-β-GC		-	
S-ACP		-	-

+ means positively affect carbon sequestration
- means negatively affect carbon sequestration

GRAPHICAL ABSTRACT

Highlights

- We analyzed the biogeochemical properties of sediments in bulk soil, rhizosphere, and crab burrow walls.
- Sediments collected from mature crab burrow walls showed increased enzymatic activities related to CO_2.
- Crab burrows and plant rhizosphere soil had more carbon transfer into easy oxidized carbon and labile forms than other soil.
- Plant invasion enhances carbon sequestration through increased photosynthesis and expansion of arbuscular mycorrhizal fungi.

1 Introduction

Global climate change poses a significant threat to human survival and development (Tang et al., 2018). The burning of fossil fuels and industrial processes have resulted in substantial carbon emissions, estimated at 7.8 Pg C yr^{-1} (IPCC, 2013), disrupting the equilibrium between the global ecosystem and the atmosphere. Coastal salt marshes play a crucial role in carbon burial, with an estimated rate of 10.2 Tg C yr^{-1} (Ouyang and Lee, 2014). This burial is equivalent to approximately 1 to 2.5% of CO_2 emissions from anthropogenic activities (Hinson et al., 2017; Grow et al., 2022). However, salt marshes are facing significant losses due to human activities such as filling, draining, and the "coastal squeeze" caused by sea level rise.

Crabs, such as fiddler crabs and Sesarmidae crabs, have significant impacts on sediment carbon cycling in coastal saltmarshes (Andreetta et al., 2014; Alberti et al., 2015) and other farmlands (Khoshnevisan et al., 2021). While recent studies have focused on the diversity, biomass, sediment topography, and nutrient cycling of benthic organisms in mangroves and salt marshes, little is known about the mechanisms and processes of carbon cycling within crab burrows in habitats dominated by native or invasive plants. They accelerate the rate of carbon cycling through biological and geochemical processes (Huhta, 2007; Agusto et al., 2022; Grow et al., 2022). Fiddler crab burrows increase oxygen penetration and create a more oxidized environment, leading to a 59% increase in effective surface area (Grow et al., 2022). The disturbance caused by fiddler crabs in saltmarshes results in a 12.7% increase in sediment CO_2 efflux and a 51.7% increase in CH_4 efflux (Agusto et al., 2022). The highest efflux rates occur immediately after burrowing activity ceases and gradually decrease over the following two hours (Grow et al., 2022). Additionally, fiddler crab-related greenhouse gas emissions decrease in the presence of oil contamination (Grow et al., 2022). This suggests that crab burrow walls harbor microbial communities with distinct functional characteristics compared to bulk soil, which may explain differences in sediment organic matter (OM) (Gillis et al., 2019). In mangrove forests, the respiration and burrowing activities of marine benthos double the CO_2 emission rate from the bare sediment surface (Ouyang et al., 2021). However, the mechanism by which burrowing activity affects sediment CO_2 emissions is still poorly understood.

Crabs also influence sediment physical properties through their burrowing activities. Sesarmidae crabs, in particular, create deep, multi-chambered burrows with large openings and substantial below-ground surface areas (Gillis et al., 2019). For example, Sesarmidae crabs are considered critical, which create deep (up to 2 m), multi-chambered burrows with large openings (maximum of 11 cm), and have sizeable below-ground surface areas up to 3.8 m^2 (Stieglitz et al., 2000). These burrows serve as important shelters during summertime, as crabs prefer temperatures below 29°C (Thongtham et al., 2008). The burrowing activities of crabs

accelerate litter decomposition and the mixing of sediment from the surface to deeper horizons (Wang et al., 2010). In Thailand, crabs remove an average of 87% of daily mangrove litter fall through ingestion or burial, with the removal rate being positively correlated with the number of crab burrows and negatively correlated with inundation time (Thongtham et al., 2008). In Japan, ocypodid crabs accelerate the removal of organic matter three times faster than weathering and mineralization processes (Koo et al., 2019). Therefore, crab bioturbation plays a crucial role in bio-geomorphological processes.

Crab bioturbation has multiple effects on the biogeochemical processes in sediments. Studies have shown significant differences in microbial diversity between wild and aquacultural macrobenthos, such as shrimps and crabs, using molecular-dependent methods (Chu et al., 2011; Liu et al., 2011; Li et al., 2012). The bacterial community plays a crucial role in various biochemical processes, including enzyme activity (Zhu et al., 2019). Sediment enzymes catalyze biochemical processes related to energy and material cycling (Bueno De Mesquita et al., 2017; Zhu et al., 2019). Extracellular enzymes target different organic carbon pools in sediments, such as cellulases and ligninase targeting polyphenolic macromolecules and simplified polysaccharides, respectively (Yang et al., 2020; Feng et al., 2023). Extracellular enzyme activity (EEA) can serve as an indicator for organic matter decomposition (Burns et al., 2013). Sediments disturbed by crabs have lower total and labile carbon contents, indicating a decrease in carbon concentration (Gutiérrez et al., 2006). However, there is limited research on the impact of crab bioturbation on EEA and organic carbon fractions, such as recalcitrant carbon and easily oxidized carbon, in sediments from active burrow walls.

Crabs have noticeable effects on plant density, height, and nutrient uptake in natural coastal salt marshes and farmlands (Bertness and Coverdale, 2013; Khoshnevisan et al., 2021). Crabs can be classified as herbivorous, omnivorous, or carnivorous based on their dietary preferences. Factors such as moisture content, resilience, and vegetation decomposition also influence crab feeding preferences (Harada and Lee, 2016). Herbivorous crabs tend to prefer leaves over fine roots and stems when consuming different plant tissues (Luo et al., 2019). This dietary variation leads to differences in CO_2 respiration rates (Ouyang et al., 2021). Crab grazing can have both positive and negative effects on plants. For example, excessive grazing by *Sesarma reticulatum* crabs in New England (USA) has caused significant die-off of *S. alterniflora* in salt marshes (Altieri et al., 2012; Coverdale et al., 2012). However, the invasion of the green crab species *Carcinus maenas* has promoted the recovery of cordgrass by consuming and displacing *Sesarma* crabs from their burrows, thus reducing herbivory pressure (Bertness and Coverdale, 2013). Similar top-down control relationship between birds, crabs and terrestrial/aquatic plants are also observed and synthesized (Ge et al., 2023). Crabs are more likely to graze on seedlings because halophytic plants have higher nitrogen and lower fiber content (Bortolus and Iribarne, 1999). However, halophytes develop defenses, such as burrs or chemical compounds, to protect themselves, which can hinder crab ingestion (Bortolus and Iribarne, 1999; Chen et al., 2021). Crabs show a preference for invasive plant species (*S. alterniflora*) over native species (*P. australis*) due to differences in crude protein content (Ji et al., 2011). Macrobenthic animals play a crucial role in accelerating the decomposition of underwater debris, regulating material exchange at interfaces, and promoting the self-purification of water bodies. They also serve as key components in the food chain, and these processes can significantly influence carbon cycling. However, these factors are often overlooked, and the impact of crab grazing on plant invasion is rarely considered.

To address this gap, we conducted a series of experiments to investigate factors influencing carbon sequestration and emission. These factors included: (1) the presence of native and invasive plant species (i.e., SA vs. PA in the Yangtze estuary); (2) sediment zones (i.e., mud flats, juvenile crab burrows, mature crab burrows, rhizosphere, and non-rhizosphere); (3) different fractions of organic carbon (i.e., total organic carbon (TOC), EOC, and ROC); (4) carbon-related extracellular enzymes activities; and (5) seasonal variations within a year.

Upon all these related factors, we hypothesize that: (1) plant invasiveness would impact carbon cycling; (2) sediments within crab burrows would have higher levels of organic carbon and enzymatic activity; and (3) there would be significant changes in the carbon pool within crab burrows throughout the year. To test these hypotheses, we conducted field and laboratory experiments over 12 months. We aim to put forward the novel notion: crab burrowing activity reduces the carbon sequestration capacity more dramatically as they grow larger in native plant dominated saltmarshes.

2 Methods

2.1 Study sites

This study was conducted in two study sites on Chongming Island, Shanghai, China. Chongming Island has a subtropical monsoon climate with ample precipitation, sunshine, and four distinct seasons. The field experiment took place from March 2021 to February 2022. Chongming Island is located at the Yangtze River, and salinity increases from northwest to southeast (see Figure 1). One of the sampling sites is a salt marsh in the Xisha Pearl Lake scenic area (see Figure 1). The dominant plant species in this area is *Phragmites australis*, a native freshwater species, and the major macrobenthic species is *Chiromantes haematocheir*. The second site is a brackish salt marsh on the north fringe of Chongming, which has been invaded by *S. alterniflora* (see Figure 1). The major benthic species in this area is *Chiromantes dehaani*, a grayish-greencrab species. Both crab species are omnivores, feeding on sediments, detritus, and plant tissues.

To account for spatial heterogeneity and internal variability, we selected five distinct sampling locations, including mud flats, juvenile crab burrows, mature crab burrows, plant rhizosphere, and non-rhizosphere (bulk sediments). We observed the crab physical appearance with their corresponding burrows, and categorized juvenile and mature crab burrows with opening diameter of less than 2 cm and 2 to 5 cm, respectively. Each type of sampling location was replicated three times at each site. For the sediments from crab burrows, we specifically chose active burrows where crabs were observed to ensure their presence.

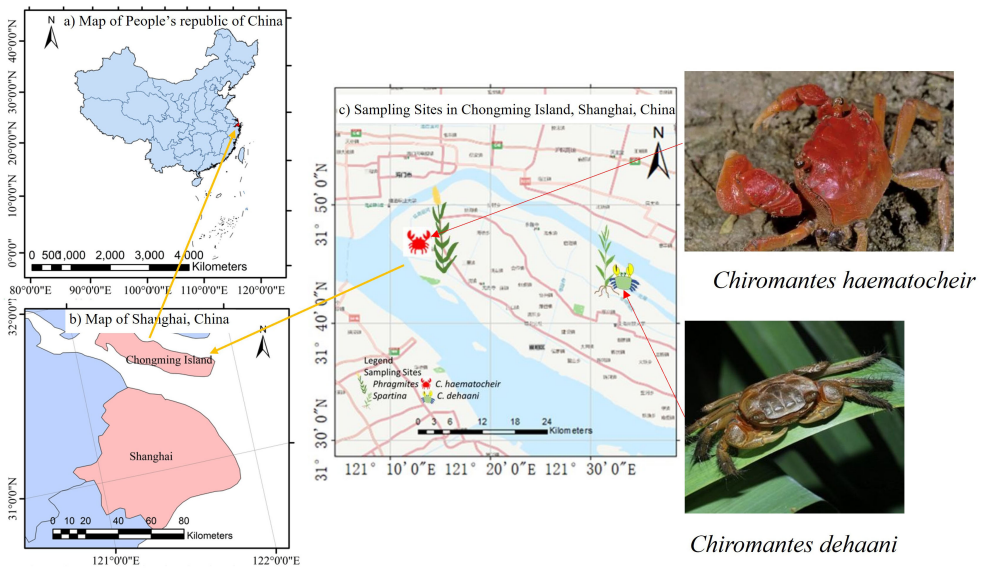

FIGURE 1
Distribution of sampling sites in the Yangtze Estuary. **(A)** map of People's Republic of China, **(B)** map of Shanghai, **(C)** map of sampling sites in Chongming Island, Shanghai, China.

2.2 Crab and sediments respiration analysis

The concentration of CO_2 was measured using a portable analyzer (UGGA, model 915–0011, Los Gatos Research Inc., Mountain View, USA). We collected 40 crabs randomly of each species for census analysis and respiration measurements in the field. The crabs were kept in a bucket with salt marsh plants to prevent injury or death from fighting. Previous research (Ouyang et al., 2021) showed that crab respiration declined rapidly after being caught, so measurements were taken on the same day using a closed-loop system to minimize bias.

We also measured the *in-situ* CO_2 fluxes from sediment, roots, and plants every month for one year. Root respiration was measured by removing above-ground vegetation and connecting the sediment and roots to a portable greenhouse gas analyzer using a closed-loop system. Plant respiration rate was measured by subtracting the CO_2 flux under dark and light environments. The system included a PVC collar with dimensions of 20 cm in diameter and 20 to 50 cm in height to create an air-concealed headspace.

2.3 AMF infection

From April to November, we collected root samples from *S. alterniflora* and *P. australis* sites to analyze the infection rate of arbuscular fungi (AMF). We used a combination of methods from McGonigle et al. (1990), Sheng et al. (2011), and Soti et al. (2021) to optimize the results. Fine roots were rinsed with water and only roots with a diameter of less than 2mm were selected and stored in a 70% alcohol solution. The roots were cut into 1.5 cm fragments and softened in 15% KOH at 60°C for 110 minutes for *P. australis* and 4 hours for *S. alterniflora*. The softening period differ mainly caused by the structural difference and permeability of plant root cell wall. After rinsing off the KOH, the roots were acidified in 5% CH_3COOH for 5 minutes. To stain the roots, a 5% CH_3COOH-ink solution (5% Quink ink and 95% CH_3COOH) was used at 60°C for 30 minutes, followed by clearing the ink in DI water for 14 hours at room temperature. The roots were then stained again with Sudan III solution (3g of Sudan III in 1000 ml of 70% alcohol) at 60°C for 60 minutes and clarified using 70% alcohol for 5 minutes. The degree of mycorrhizal colonization in roots is estimated by:

$$\text{Coloniation\%} = \frac{\text{Todal number of root segments affected by AMF}}{\text{Total number of root segments observed}} \times 100$$

2.4 Enzymatic activities

Soil extracellular enzyme activity can be useful for monitoring microbial activity linked to substrate dynamics because enzymes catalyze the rate and initiation steps in soil organic matter decomposition (Sinsabaugh et al., 2008; Burns et al., 2013). We analyzed enzymatic activities in sediments collected from *S. alterniflora* and *P. australis* sites. The sampling was done in April, August, and November, corresponding to the pre-growing, growing, and post-growing seasons respectively. Sediment samples were collected from mudflats, juvenile crab burrow walls, mature crab burrow walls, rhizosphere, and non-rhizosphere in both *S. alterniflora* and *P. australis* sites. Sampling depth are different to ensure the sample's representative for its corresponding category.

The activities of β-glucosidase, acid phosphatase, and catalase enzymes in sediments were determined using Solarbio (S-β-GC) Activity Assay Kit (Solarbio BC0160), S-ACP Activity Assay Kit (Solarbio BC0140), and (S-CAT) Activity Assay Kit (Solarbio

BC0100) respectively. The detailed methods are expressed in the manual. The enzyme plays a crucial role in the carbon cycling process.

2.5 Sediments carbon and nitrogen contents

The sediment samples were dried at 60°C, ground, and sieved. For TC and TN analysis, 40 mg of dry sediments were weighed and placed in aluminum foil, then analyzed using a Vario EL III element analyzer (Elementar, Germany). For TOC analysis, 1N HCl was added to remove carbonates from the sediments. For ROC analysis, HCl was used to remove inorganic carbon, followed by a hydrolysis reaction with 20 mL of H_2SO_4 (5 mol/L) at 105°C for 30 minutes. The samples were rinsed with DI water, dried, and then hydrolyzed again with 2 mL of 26 mol/L H_2SO_4 at room temperature for 3 hours (Rovira and Vallejo, 2002). The sediment samples were rinsed, dried, and analyzed using the Vario EL III element analyzer. EOC analysis was performed using a modified method of Hassan et al. (2016) by oxidizing the sample with $KMnO_4$ solution (333 mmol/L).

2.6 Photosynthetic rate

We measured the photosynthesis of *S. alterniflora* and *P. australis* during the pre-growing season, growing season, and post-growing season in May, August, and November respectively. This was done using a portable photosynthesis system (LI-6800) with a Multiphase Flash^{TM} Fluorometer (LI-COR, Nebraska). The parameters measured included net photosynthetic rate, transpiration rate, intercellular CO_2 concentration, and stomatal conductance. All measurements were conducted under sunny weather conditions, with a pause in measurements from 11 am to 2 pm to avoid photoinhibition of *P. australis*.

2.7 Statistical analysis

The data for gas flux were organized in Excel and calculated using MATLAB R2020b. Statistical analyses were performed using ANOVA and t-test at a significance level of 0.05 (P=0.05) in IBM statistics SPSS 23. The goal of ANOVA is to determine the amount of variability in groups of data, and test if this variation is greater within groups to between groups. Linear regression was conducted in Excel to predict the value of a variable during the sampling period. PCA analysis and graphing were conducted using GraphPad Prism 9.5.3. aiming to extract the important information from a set of summary indices.

3 Results

3.1 Sediment carbon contents at different sites and annual variation

We tested the total organic carbon content (TOC) for sediments collected from mudflat, juvenile crab burrow walls, mature crab burrow walls, rhizosphere, and non-rhizosphere at both *S. alterniflora* and *P. australis* sites. The highest TOC content value was found in the rhizosphere sediment at the *S. alterniflora* site, but not significant. In the *P. australis* site, TOC was significantly higher in mature crab burrows (0.157 ± 0.040%) compared to all other sediment types (0.048 ± 0.027%, 0.058 ± 0.019%, 0.099 ± 0.033%, and 0.059 ± 0.024% in mudflat, juvenile crab burrows, rhizosphere, and non-rhizosphere soil, respectively) (Figure 2A). Rhizosphere sediment in *P. australis* also exhibited significantly higher TOC content compared to other sediment types (P<0.05). The presence of plant litter in the rhizosphere contributes to a substantial portion of organic carbon in the sediment carbon pool. The changes in TOC content correspond well with total carbon (TC) and total nitrogen (TN) content in the five sampling locations at both sites.

The content of EOC in sediments did not show significant differences among sampling locations in the *S. alterniflora* site. However, the EOC in mature crab burrow walls (0.211 ± 0.087 mg/g) and rhizosphere (0.142 ± 0.079 mg/g) was slightly higher than that in other sediment types (0.061 ± 0.043 mg/g, 0.085 ± 0.055 mg/g, and 0.129 ± 0.054 mg/g in mudflat, juvenile crab burrows, and non-rhizosphere soil, respectively) (Figure 2B). In the *P. australis* site, EOC content was significantly higher in mature crab burrows (0.211 ± 0.087 mg/g) compared to mudflat (0.061 ± 0.042 mg/g), juvenile crab burrows (0.085 ± 0.055 mg/g), and non-rhizosphere soil (0.129 ± 0.055 mg/g) (P<0.005) (Figure 2B). This indicates a significant amount of carbon in mature crab burrows that are readily available for oxidation due to crab burrowing and metabolic activities. Meanwhile, the background EOC content was lower in the *P. australis* site (0.126 ± 0.083 mg/g) compared to the *S. alterniflora* site (0.213 ± 0.099 mg/g) (P<0.005) (Table 1).

The sediment ROC content is higher in mature crab burrows at the *P. australis* site (0.651 ± 0.169%) and the *S. alterniflora* site (0.725 ± 0.111%) compared to the other four sediment sources (average of 0.686 ± 0.112% and 0.309 ± 0.133% at *S. alterniflora* and *P. australis* site, respectively). However, there is a decrease in ROC content and an increase in EOC in mature crab burrows over the sampling period (Table 2), indicating that sediments organic carbon in crab burrows are becoming a carbon source to the atmosphere.

Overall, the TC, TN, TOC, EOC, and ROC contents are significantly higher at the *S. alterniflora* site compared to the *P. australis* site (Table 1). As shown in Figure 2, the sediment from mature crab burrow walls is the only type with higher TOC content in *P. australis* than in *S. alterniflora*. All other sediment types have higher carbon and nitrogen contents in *S. alterniflora* compared to *P. australis* throughout the sampling period (Supplementary Figure S1A, B).

We conducted monthly sampling and analysis of sediments from five sources at *S. alterniflora* and *P. australis* sites to examine the annual variation in EOC and ROC content. Our results showed that EOC content increased at sampling locations disturbed by plants and macrobenthos, such as sediments collected from crab burrows and rhizosphere. In contrast, ROC content decreased at all sampling locations throughout the year, particularly at crab-disturbed locations (Figure 2 and Table 2) (P<0.05 for all mature crab burrows, P<0.05 for juvenile crab burrows at *P. australis* site). These fluctuations of EOC and ROC among the sampling periods suggest that soil organic matter tends

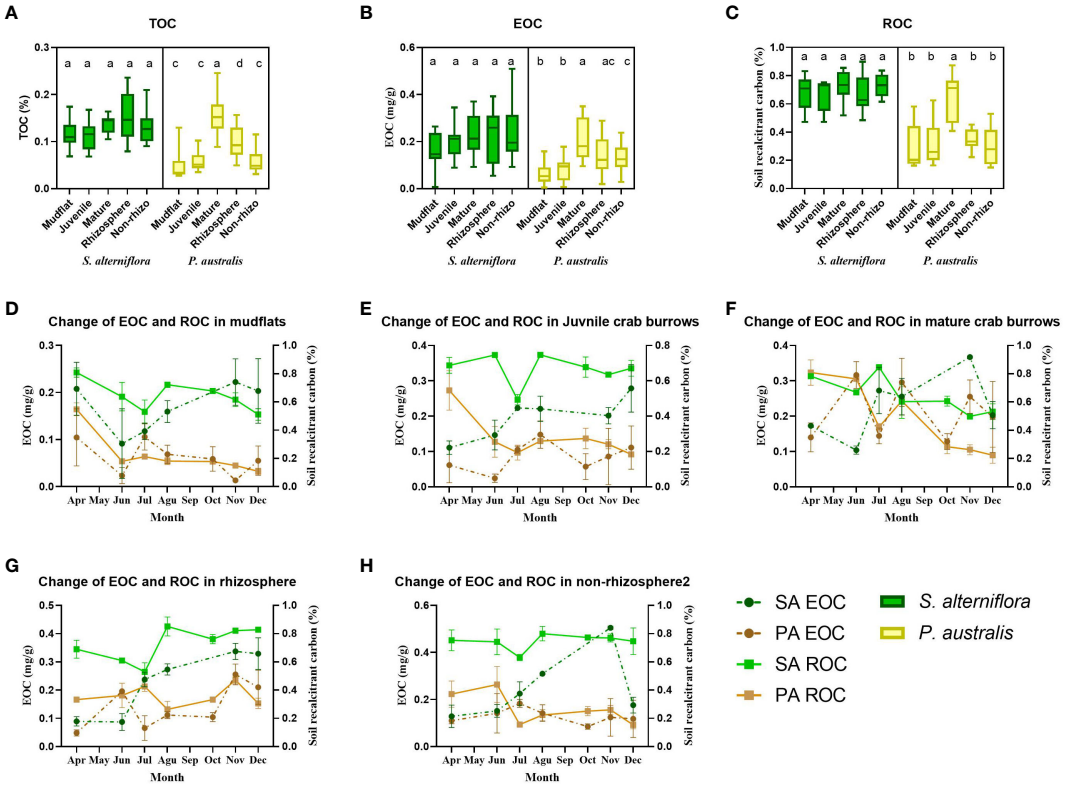

FIGURE 2
Comparion of sediment total organic carbon (TOC) **(A)**, easy oxidized carbon (EOC) **(B)** and recalcitrant orgnic carbon (ROC) **(C)** at five sampling sites, including sediments from mudflats, juvenile crab burrows, mature crab burrows, rhizosphere and non rhizosphere from *S. alterniflora* and *P. australis* dominated salt marshes. Stars connecting two boxes represent valuses of significant difference. Changes of EOC and ROC contents in sediments collected from mudflats **(D)**, juvenile crab burrows **(E)**, mature crab burrows **(F)**, rhizosphere **(G)** and non-rhizosphere **(H)** of *S. alterniflora* and *P. australis* from April to December.

to switch to labile and atmospheric carbon in the presence of crab bioturbation activities.

Figure 2 and Table 2 illustrate the seasonal changes in EOC and ROC at the invasive *S. alterniflora* and native *P. australis* sites. The increase in EOC content was more pronounced in sediments collected from crab burrows and rhizosphere regions in *S. alterniflora* compared to *P. australis*. The regression slopes between month and EOC were steeper at *S. alterniflora* (0.0165, 0.0161, and 0.034 in juvenile crab burrows, natural crab burrows, and rhizosphere, respectively) than that at *P. australis* site (0.005, 0.002, and 0.018 in juvenile crab burrows, natural crab burrows, and rhizosphere, respectively), indicating a more significant transformation of soil organic carbon into a labile form at the invasive site. In contrast, ROC content did not show the same trend at the invasive site, while it decreased in all sampling locations at the native site (with significance). This decrease in ROC content suggests a lower capability for organic matter accumulation in *P. australis*.

Overall, the comparison of ROC and EOC at invasive and native sites give rise to an assertion that invasive habitats can increase OM

TABLE 1 Two-way ANOVA analysis results of the carbon and nitrogen storage comparison at *S. alterniflora* and *P. australias* sites.

Environmental parameters	Mean of *S. alterniflora* (%)	Mean of *P. australis* (%)	Difference between means (%)	SE of Significant	P-value
TC	0.0812	0.0601	0.02116	0.0030	**<0.0001**
TN	1.501	1.421	0.07985	0.0285	**<0.0001**
TC/TN	0.0526	0.0414	0.01114	0.0013	**0.0066**
TOC	0.1291	0.0842	0.04495	0.0067	**<0.0001**
EOC	0.2137	0.1321	0.08154	0.0126	**<0.0001**
ROC	0.6939	0.3778	0.3161	0.0336	**<0.0001**

TABLE 2 Linear regression results of the changes of EOC and ROC at *S. alterniflora* and *P. australis* sites in the five types of sediments during sampling period.

Simple linear regression Tabular results	SA EOC		PA EOC		SA ROC		PA ROC	
	slope	*P*-value	slope	*P*-value	slope	*P*-value	slope	*P*-value
Mudflats	0.008	0.192	(0.006)	0.067	**(0.022)**	0.041	**(0.040)**	0.001
Juvenile crab burrows	**0.017**	0.001	0.005	0.285	(0.002)	0.787	**(0.029)**	0.014
Mature crab burrows	**0.016**	0.033	0.001	0.886	**(0.036)**	0.001	**(0.079)**	<0.0001
Rhizosphere	**0.034**	<0.0001	**0.018**	0.003	**0.027**	0.020	0.002	0.789
Non-rhizosphere	0.026	0.021	(0.003)	0.512	0.005	0.536	**(0.023)**	0.033

Numbers in bold suggest correlation with significance. Numbers in brackets have negative values.
SA, Spartina alterniflora; PA, Phragmites australis; EOC, easy oxidized carbon; ROC, recalcitrant organic carbon.

accumulation through less transformation of ROC into labile carbon; and decrease OM accumulation through higher transformation rate of carbon into EOC. Thus, plant invasiveness does not significantly affect total organic carbon in soil.

3.2 Plant photosynthesis and respiration

Our findings show that the highest photosynthetic rate for *P. australis* occurs during the growing season (Figure 3). This photosynthetic rate is negatively correlated with intercellular CO_2 concentration (Supplementary Figure S2A) and positively correlated with evapotranspiration and stomatal conductance (Supplementary Figure S2B). *S. alterniflora* exhibits a higher photosynthetic rate from spring to summer compared to other seasons, while *P. australis* has the highest photosynthetic rate during summer. Additionally, the photosynthetic rate of *S. alterniflora* is significantly higher than that of *P. australis*. Consequently, the longer growing period and higher photosynthetic rate of *S. alterniflora* result in greater carbon accumulation in *S. alterniflora* fields compared to *P. australis* fields.

Figure 3C demonstrates that the roots of *P. australis* release more CO_2 into the atmosphere than *S. alterniflora*. The highest CO_2 efflux occurs in June for *S. alterniflora* and October for *P. australis*.

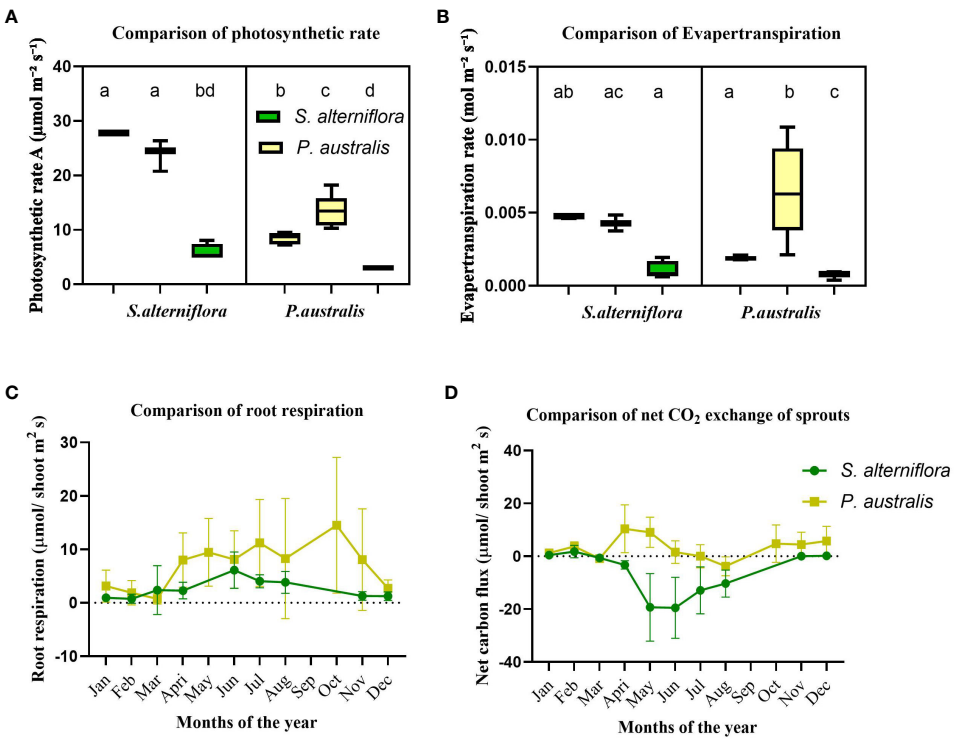

FIGURE 3
Comparison of photosynthesis (**A, B**), roots respiration of mature stands **(C)** and net exchange of CO_2 of sprouts at marsh front **(D)** in *S. alterniflora* and *P. australis* during pre-growing season, growing season and post-growing season. Parameters include photosynthetic rate **(A)**, evapertranspiration **(B)**. Root respiration of mature *S. alterniflora* and *P. australis* **(C)** and the net CO_2 exchange of whole sprouts at edge of *S. alterniflora* and *P. australis* salt marshes from January to December.

During the warm summer period, the favorable environmental conditions promote rhizosphere microbial activity and root respiration.

Both *S. alterniflora* and *P. australis* are perennial plants that produce sprouts from below-ground rhizomes during the growing season. We measured the net CO_2 exchange of these sprouts using similar method for plant respiration under light condition. Sprouts typically have a height ranging from 30 to 70 cm. As depicted in Figure 3D, *S. alterniflora* sprouts exhibit negative net CO_2 exchange from March to October, whereas *P. australis* sprouts only show negative net CO_2 exchange for 1 to 2 months during the growing season. This indicates that the carbon accumulation capacity of *S. alterniflora* sprouts is higher than that of *P. australis*.

3.3 Crab and crab respiration comparisons

C. haematocheir crabs have higher respiration rates (0.960 ± 0.506 µmol/s individual) compared to *C. dehaani* crabs (0.289 ± 0.188 µmol/s individual) (Figure 4A). There is also a significant difference in respiration rates between male and female *C. haematocheir* crabs (1.12 ± 0.627 µmol/s individual for females and 0.780 ± 0.254 µmol/s individual for males, P<0.005) (Figure 4A). Generally, crabs in *P. australis* marshes have higher respiration rates.

We observed a positive correlation between the carapace width of crabs and their respiration rate (Figure 4B). Despite being smaller in size (4.675 ± 2.442 cm), *C. haematocheir* crabs have higher respiration rates (1.789 ± 0.858 µmol/s individual) compared to *C. dehaani* crabs (8.55 ± 0.721 cm) (1.188 ± 0.574 µmol/s individual, *P*<0.005) (Figure 4B).

There is no significant difference in mature crab burrow densities between *S. alterniflora* and *P. australis* sites (9.9 ± 3.1 per m^2 on average, *P*>0.005) (Figure 4C). However, the density of juvenile crab burrows is significantly higher in the invaded *S. alterniflora* salt marsh compared to the *P. australis* marsh (106.4 ± 8.8 per m^2 and 80.6 ± 35.2 per m^2 in *S. alterniflora* and *P. australis*, respectively, *P*<0.005) (Figure 4C). Despite the smaller carapace size of *C. haematocheir* crabs in the *P. australis* site (Figure 4B), their burrow openings are significantly wider (2.96 ± 0.32 cm and 3.50 ± 0.37 cm for *C. haematocheir* and *C. dehaani*, respectively) (Figure 4D). This finding challenges the prevailing belief that bigger crabs create bigger burrows. However, it may be linked to the need to disperse higher levels of CO_2 generated by *C.*

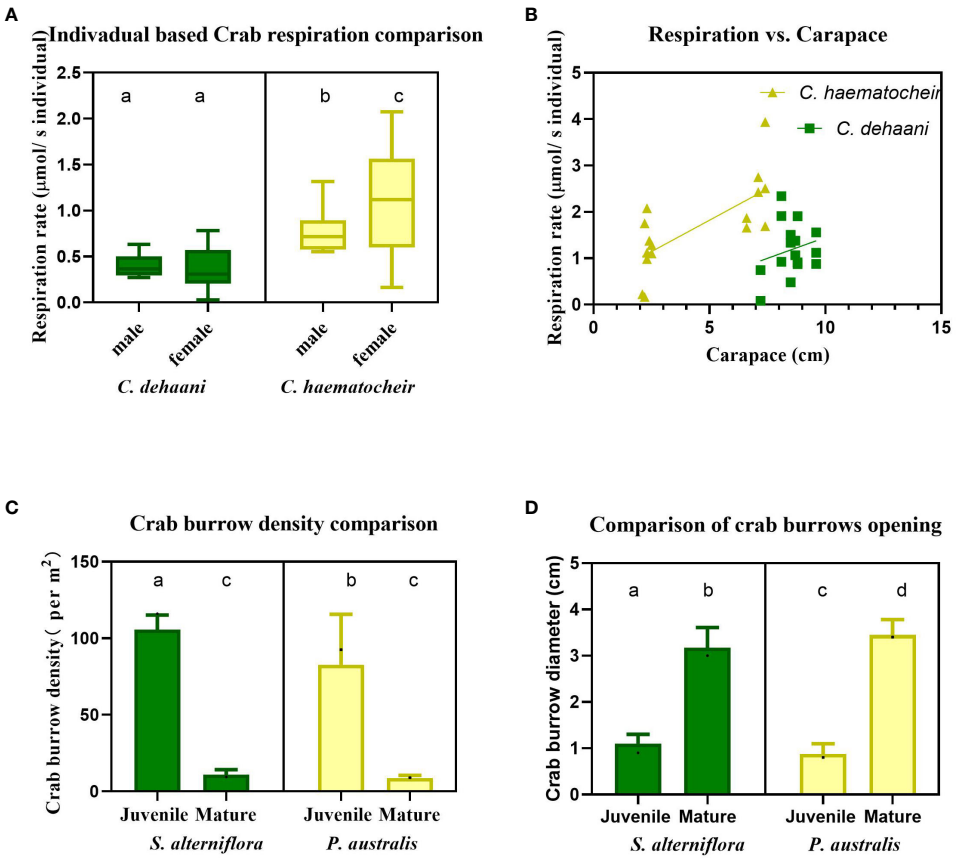

FIGURE 4
Crab related parameters, including **(A)** the respiration rate of female and male crabs from *C. dehaani* and *C. haematocheir* species; **(B)** the correlation between crab respiration rate and their carapace width; **(C)** the juvenile and mature crab burrow density in both *S. alterniflora* and *P. australis* salt marshes; **(D)** the opening area of burrows occupied by juvenile and mature crabs in *S. alterniflora* and *P. australis* salt marshes. Different lower-cased letters represent values of significant differences. All boxes and dots colored in green represent results of *C. dehaani* living in *S. alterniflora* site, colored in yellow represent results of *C. haematocheir* living in *P. australis*.

haematocheir crabs within the burrow. Additionally, the larger burrows indicate increased energy expenditure during burrowing, leading to higher metabolic and respiration rates. This corresponds with the observed higher respiration rate in *C. haematocheir* crabs (Figure 4A).

3.4 Arbuscular mycorrhiza fungi and enzymatic activities

Figure 5A displays the infection rates of roots collected from high and low tidal zones. There is no significant difference in infection rates between tidal zones. However, *P. australis* exhibits a significantly higher infection rate (67.8 ± 17.0%) compared to *S. alterniflora* (37.9 ± 22.5%). We also collected root samples from sprouts and mature stands of *S. alterniflora* and *P. australis*. There is no difference in infection rates within species (Figure 5B), but *P. australis* shows a higher infection rate. Additionally, we collected mature root samples from high tidal zones during the pre-growing season (April), growing season (August), and post-growing season (November). For *S. alterniflora*, there is no significant change in AMF infection throughout the year. However, the infection rate is higher in *P. australis* roots during the three growing seasons, with a slight increase during the growing period (Figure 5C).

The morphology of mycorrhiza in *P. australis* and *S. alterniflora* roots is distinct (Figure 5D). Most mycorrhiza found in *P. australis* are endo-mycorrhiza or vesicular-arbuscular. In contrast, the mycorrhizae in *S. alterniflora* are generally ectomycorrhiza, which spread hyphae further into the sediment matrix and significantly increase the surface area of roots and the volume of sediments that the roots can access. This facilitates the invasion of *S. alterniflora* into salt marshes initially dominated by *P. australis* by enhancing nutrient accessibility.

According to Figure 6A, S-CAT shows significantly higher activity in rhizosphere sediments compared to other locations at both *S. alterniflora* and *P. australis* sites during the pre-growing season. The activity levels were 60.8 ± 0.99 U/g dry soil and 47.6 ± 1.05 U/g dry soil at *S. alterniflora* and *P. australis* sites, respectively, while the average activity levels at other locations were 38.6 ± 2.76 U/g dry soil and 37.7 ± 4.4 U/g dry soil at *S. alterniflora* and *P. australis* sites, respectively. In the *P. australis* site, S-CAT is less active in catalyzing organic matter decomposition in the soil. In April, the S-CAT activities in crab burrow walls are as low as those in bulk sediments, which corresponds to the lower metabolism level of crabs at lower temperatures. As plants grow and crabs mature, there is an overall decrease in S-CAT activities during the growing season (Figures 6A, B). However, S-CAT activity becomes significantly higher in mature crab burrows (44.72 ± 2.82 U/g dry soil and 53.19 ± 2.36 U/g dry soil for *C. dehaani* and *C. haematocheir* burrow walls, respectively) and rhizosphere (42.76 ± 2.11 U/g dry soil and 51.96 ± 4.22 U/g dry soil for *S. alterniflora* and *P. australis* sites, respectively) compared to bulk sediments and juvenile crab burrow walls (27.99 ± 2.064 U/g dry soil and 41.86 ± 2.30 U/g dry soil for *S. alterniflora* and *P. australis* sites, respectively) (Figure 6C). The enzymatic activity is higher in *P. australis*, which enhances the carbon cycling process and increases

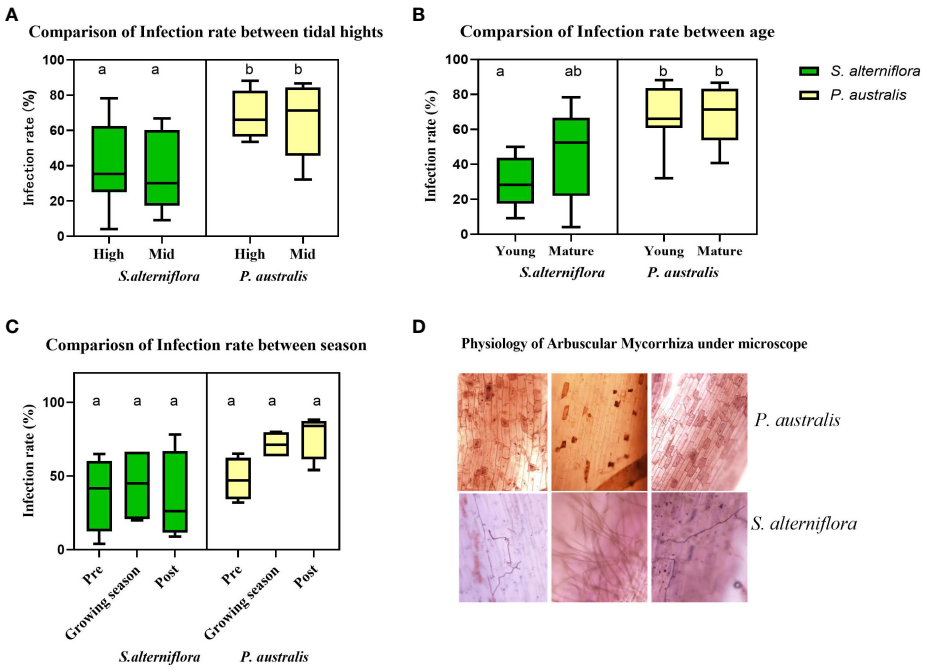

FIGURE 5
Comparison of Arbuscular-Mycorrhizal-Fungi infection rate in *S. alterniflora* and *P. australis* roots. **(A)** infection rate at samples collected from high and mid tidal heights. **(B)** infection rate at sprout and mature stage. **(C)** infection rate of mature plant roots collected at pre-growing, growing and post growing seasons. **(D)** morphological differences of AMF colonized in the two species. Different lower-cased letters represent values of significant differences.

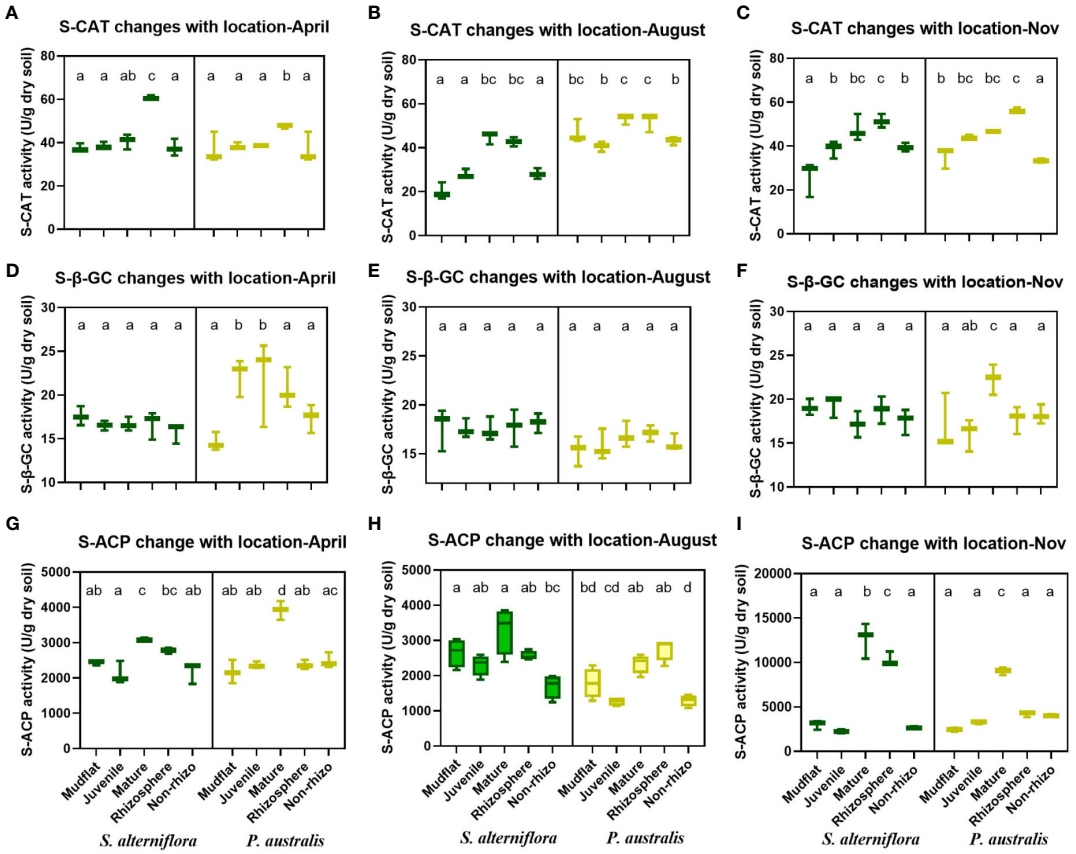

FIGURE 6
Comparison of sediments enzymatic activities at five sampling sites, including sediments from mudflats, juvenile crab burrows, mature crab burrows, rhizosphere and non-rhizosphere from *S. alterniflora* and *P. australis* dominated salt marshes. **(A, D, G)** are results from April (pre-growing season). **(B, E, H)** are results from August (growing season). **(C, F, I)** are results from November (post growing season). Different lower-cased letters represent values of significant differences.

CO_2 efflux in this native salt marsh. In November, the rhizosphere sediments showed the highest enzymatic activity, followed by sediments collected from mature crab burrow walls in both *S. alterniflora* and *P. australis* sites.

There was no significant difference in S-β-GC activity among the five sampling locations and different sampling periods at the *S. alterniflora* site (Figures 6D–F). However, at the *P. australis* site, we observed higher enzymatic activity in mature crab burrow walls (22.00 ± 4.96 U/g dry soil in April, 16.89 ± 1.36 U/g dry soil in August, and 22.31 ± 1.71 U/g dry soil in November) compared to other sampling locations (18.70 ± 3.45 U/g dry soil in April, 16.09 ± 1.26 U/g dry soil in August, and 17.25 ± 1.98 U/g dry soil in November). Although there was no significant difference in S-β-GC activity in August, the activity was slightly higher in mature crab burrows and rhizosphere sediments (Figure 6E). In November, the S-β-GC activity was significantly higher in mature crab burrows (22.31 ± 1.71 U/g dry soil) compared to juvenile crab burrows (16.08 ± 1.83 U/g dry soil), which corresponds to the larger size of crab burrows and higher respiration rate in mature crab burrows compared to juvenile crab burrows (Figures 4A, C).

The S-ACP activity in both *S. alterniflora* and *P. australis* salt marshes showed similar patterns during the three sampling periods (Figures 6G–I), indicating higher enzymatic activity in sediments collected from mature crab burrow walls (5115.56 ± 3984.73 U/g dry soil in *C. dehaani* and 4822.51 ± 2995.27 U/g dry soil in *C. haematocheir*) and plant rhizosphere (4953.52 ± 3720.62 U/g dry soil in *S. alterniflora* and 30669.14 ± 821.97 U/g dry soil in *P. australis*) compared to other sampling locations (2354.98 ± 462.70 U/g dry soil in *S. alterniflora* and 2253.32 ± 883.00 U/g dry soil in *P. australis*). In the *P. australis* site, the highest enzymatic activity in mature crab burrow walls was observed during the post-growing season (11782.5 ± 6934.52 U/g dry soil in *S. alterniflora* and 9026.84 ± 428.40 U/g dry soil in *P. australis*) compared to the growing season (3327.65 ± 818.36 U/g dry soil in *S. alterniflora* and 2472.7 ± 95.79 U/g dry soil in *P. australis*). During the growing season, both mature crab burrow walls and rhizosphere sediments showed significantly higher S-ACP activity compared to other sampling locations in both the invasive *S. alterniflora* and native *P. australis* sites. Additionally, the S-ACP activity in November was more than three times higher in November than that in April and August.

Table 3 indicates that sediment from mudflats, juvenile crab burrow walls, and non-rhizosphere exhibit lower enzymatic activity compared to other types. The activity of S-β-GC does not show significant variation across sampling locations (P>0.05). However,

TABLE 3 Comparison of sediment enzymatic activities (U/g dry soil) between different types of sediments collected from mudflats, juvenile crab burrow walls, mature crab burrow walls, rhizosphere and non-rhizosphere.

Tukey's multiple comparisons test	S-CAT			S-β-GC			S-ACP		
	Mean 1	Mean 2	*P*-Value	Mean 1	Mean 2	*P*-Value	Mean 1	Mean 2	*P*-Value
Mudflats vs. Juvenile	33.78	37.99	0.355	16.89	17.91	0.6929	2397	2210	0.9988
Mudflats vs. Mature	33.78	45.26	**<0.0001**	16.89	18.74	0.1368	2397	5432	**0.0003**
Mudflats vs. Rhizo	33.78	51.8	**<0.0001**	16.89	18.12	0.5223	2397	4011	0.1489
Mudflats vs. Nonrhizo	33.78	36.44	0.7715	16.89	17.19	0.995	2397	2306	>0.9999
Juvenile vs. Mature	37.99	45.26	**0.0168**	17.91	18.74	0.8259	2210	5432	**0.0001**
Juvenile vs. Rhizo	37.99	51.8	**<0.0001**	17.91	18.12	0.9988	2210	4011	0.0814
Juvenile vs. Nonrhizo	37.99	36.44	0.9601	17.91	17.19	0.8931	2210	2306	>0.9999
Mature vs. Rhizo	45.26	51.8	**0.0411**	18.74	18.12	0.9323	5432	4011	0.2564
Mature vs. Nonrhizo	45.26	36.44	**0.002**	18.74	17.19	0.2901	5432	2306	**0.0002**
Rhizo vs. Nonrhizo	51.8	36.44	**<0.0001**	18.12	17.19	0.7645	4011	2306	0.1119

The bold numbers indicate significant difference between the two groups.

mature crab burrow walls display significantly higher enzymatic activity of S-CAT and S-ACP compared to the aforementioned sediment types. The only enzyme that exhibits significantly higher activity in the rhizosphere is S-CAT.

3.5 PCA analysis for carbon flux in different sites and sediment zonation

We conducted a principal component analysis (PCA) to examine the invasiveness of salt marsh plants and sediment sources (Figure 7). Figure 7A shows that the invasive *S. alterniflora* and native *P. australis* have distinct traits. The invasive group is positively associated with PC2 and negatively associated with PC1, while the native group is positively associated with PC1 and negatively associated with PC2 (Figure 7A). The invasiveness of the plants is primarily influenced by photosynthesis, with negative effects from ROC, EOC, and TOC. In contrast, the native group is positively influenced by root respiration and negatively influenced by crabs, burrows, AMF, and sprouts.

However, the sediment traits from different sources are not separated (Figure 7B). There is considerable overlap between sediments from mudflat, juvenile crab burrows, and non-rhizosphere, indicating similarity among these sampling types. The rhizosphere is influenced by PC1-related variables, while PC2-related variables influence mature crab burrows. PC1-related variables include photosynthesis and enzymes, while PC2-related variables include the density and size of crabs and burrows, as well as sediment carbon contents (Supplementary Figure S3).

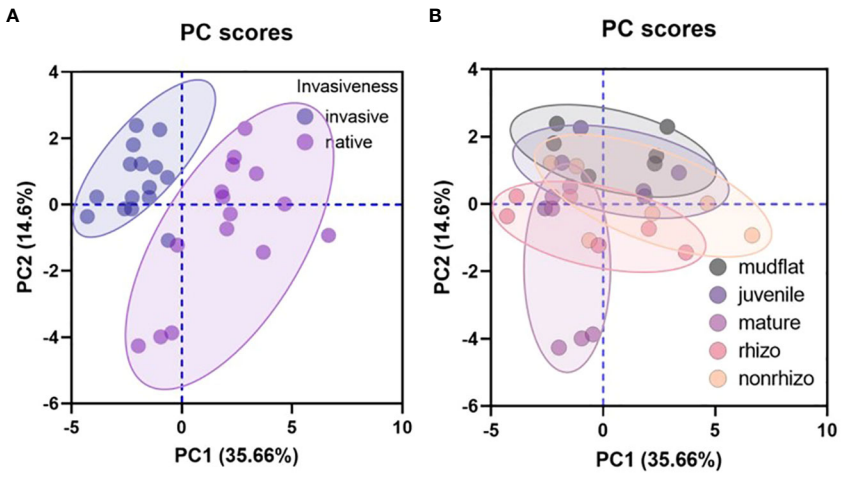

FIGURE 7
Principal component analysis results based on: **(A)** the invasiveness, and **(B)** sediment source.

4 Discussion

4.1 Crab respiration related to dietary preference

To investigate the dietary preferences of crabs, researchers often consider the $\delta^{13}C$ of crabs, plants, and sediments as key parameters. For instance, fiddler crabs in Georgia salt marshes exhibit a biased isotopic composition towards C4 plants (Haines, 1976). *Chiromantes dehaani* crabs show a preference for *P. australis* over sediments. Among various plant tissues, crabs favor sprout leaves (35.7%) the most and falling litter (6.8%) the least (Zhang and Tong, 2018). This difference may be attributed to variations in food sources, as *C. haematocheir* crabs inhabit *P. australis* sites, which have higher crude protein content (Ji et al., 2011). These proteins are more edible but require more energy to be converted into CO_2 through cellular respiration compared to those in *P. australis*. A more efficient and animal-friendly method to determine their food source is by analyzing the isotopic content in their exhaled breath (Ouyang et al., 2021). The CO_2 production of Sesarmid crabs is 0.12 mmol g^{-1} wet wt day^{-1} (Ouyang et al., 2021), while ocypodid crabs range from 0.05 to 0.15 mmol g^{-1} wet wt day^{-1} (Kristensen et al., 2008; Penha-Lopes et al., 2010). These CO_2 production rates are lower than the CO_2 production observed in *Chiromantes* crabs during this experiment (0.960 ± 0.506 µmol/s individual and 0.389 ± 0.188 µmol/s individual for *C. haematocheir* and *C. dehaani*, respectively), which can be attributed to the larger size of *Chiromantes* crabs. By considering the carapace width, the CO_2 production in our study falls within a similar range as other research findings.

The invasion of *S. alterniflora* in mangrove forests has led to significant changes in the diets of crabs and other gastropod species (Feng et al., 2018). Herbivorous and detritus feeders exhibit species-specific changes in their food sources during invasion (Nordström et al., 2015). For instance, herbivorous feeders like *Sesarma plicata* rapidly change their food within three years, while detritus feeders like *Uca arcuata* show no immediate change (Feng et al., 2018).

The invasion of *Spartina* also affects the biodiversity and abundance of benthic macrofauna in seafloor and marsh habitats (Cutajar et al., 2012). However, it has minimal impact on invertebrate and fish richness and diversity in Australia (Neira et al., 2007; Curado et al., 2014; Shin et al., 2022). In salt marshes invaded by Spartina alterniflora and subsequently restored, the biodiversity remains similar or even higher compared to preserved and invaded salt marshes (Curado et al., 2014). Nevertheless, hybrid *Spartina* facilitates the colonization of non-indigenous invertebrate species in edge areas and oligochaetes at higher elevations (Neira et al., 2007).

In China, invasive *S. alterniflora* supports more epiphytic communities compared to the native *P. australis* region. The preference of microbenthic organisms is also influenced by different stand states. For example, dead *S. alterniflora* provides a favorable habitat for bacterivores and fungivores epiphytic species (Chen et al., 2015). However, the additional invasion of hybrid *Spartina* does not necessarily increase biomass and detrital input into the food web (Brusati and Grosholz, 2009), and can even become part of the aquatic food webs in estuarine ecosystems (Li et al., 2009). The interaction between plant invasion and the allocation of microbenthic organisms is species-specific, and further research is needed to understand the general mechanisms and ecosystem functioning processes (Li et al., 2009).

4.2 Crab bioturbation induced change in carbon efflux during invasion

Crab burrows and plant rhizosphere soil had more carbon transfer into easy oxidized carbon (EOC) and labile forms than other soil. Plant invasion can directly and indirectly alter the physical properties of sediment. The focus of this study is the invaded salt marsh site dominated by *S. alterniflora*, a fast-growing plant species with high productivity and well-developed below-ground rhizomes (Li et al., 2009; Feng et al., 2018). This invasion can reduce the energy of tidal flow, leading to decreased detritus transport to the ocean and increased detritus production from litter (Neira et al., 2007). In some of the invaded sites of *S. alterniflora*, the rapid spread can result in the disappearance of mudflats and native vegetation (Lee and Khim, 2017). The change in food sources could significantly affect the functions of the macrobenthos food web (Tue et al., 2012). From Feng et al. (2014) all benthic species switched their heterogenous diet to a homogeneous diet within a short period. This can adversely affect carbon contents in sediments and litter. Crab can also accelerate sediment turnover rate. For example, the net sediment transport to the marsh surface in *Spartina alterniflora* marsh by crabs is 109.54 g m^{-2} d^{-1}, with a corresponding sediment turnover time of 4.07 years.

In addition to consuming salt marsh vegetation, the burrowing activity of crabs also affects the vertical movement of carbon in sediments. Research on fiddler crab burrows has shown that the rate of CO_2 flux is 536.7 nmol g^{-1} h^{-1} for crabs, while the background sediment CO_2 flux is 117.4 nmol g^{-1} h^{-1} (Grow et al., 2022). This rate is similar to the respiration rate of crabs in this experiment. The combination of small fiddler crabs and the sediment matrix leads to a CO_2 flux that is comparable to that of larger *Chiromantes* crabs. In native *S. alterniflora* salt marshes in the United States of America, fiddler crabs can produce approximately 60 mmol m^{-2} d^{-1} more CO_2 than *Chiromantes* crabs, which are smaller in size than fiddler crabs. Both crab respiration and burrowing activities contribute to an increase in CO_2 release (Figure 4).

Salt marshes are highly productive wetlands that export dissolved inorganic and organic carbon into estuaries and oceans (Najjar et al., 2018; Xiao et al., 2021). However, the effects of burrows in these ecosystems are often underestimated and require further observation. In recent years, there has been increased attention on the carbon budget variation in mangrove forests, which is influenced by the large size of burrows and the significant changes caused by oxidation conditions and tidal fluctuations (Guimond et al., 2020). These changing environmental conditions accelerate sediment respiration processes, leading to the release of CO_2, dissolved inorganic carbon (DIC), and dissolved organic carbon (DOC) through burrow walls (Kristensen et al., 2000; Maher et al., 2017). On the other hand, quantifying carbon budgets in salt marshes is

more challenging compared to mangrove forests. This is due to the smaller size of burrows, the complexity of the root system, the salinity and strength of tidal wave fluxes, and the landscape variation in salt marshes. These factors contribute to exacerbated physical and chemical feedback from crab burrowing. Studies have shown that the exchange of porewater from crab burrows to the sediment matrix is lower compared to the opposite direction, and more than 75% of the exchanged carbon is in the form of DIC (Xiao et al., 2021).

4.3 Sediment enzymatic activity during invasion

From our results, sediments collected from mature crab burrow walls showed increased enzymatic activities related to CO2.Plant invasion can have varying effects on carbon-related enzymes, as shown by Zhou and Staver (2019). However, meta-analysis results indicate that invaded sites generally exhibit higher activities of nitrogen and phosphorous-related enzymes. The range of enzyme activity increases from 23% to 69% (Zhou and Staver, 2019). In our experiment, we observed significantly higher activity of the S-ACP enzyme (related to phosphorous cycling) in the rhizosphere of the invaded Spartina salt marsh. However, the activity of S-β-GC (related to carbon cycling) was not enhanced in the invasive site. There are a few possible explanations for this phenomenon. Firstly, since enzymes are proteins that require carbon and nitrogen for synthesis, the nutrient-rich environment may already provide sufficient resources, eliminating the need for increased production (Allison and Vitousek, 2005; Burns et al., 2013). Another explanation is that fast-growing invasive species contribute nitrogen-rich litter to the sediments, which may increase overall enzyme investment (Sardans et al., 2017; Zhou and Staver, 2019). The enhanced activity of sediment enzymes in releasing nutrients accelerates the nutrient cycle and creates a favorable environment for invasion. Although the activity of enzymes in crab burrow walls has not been extensively studied, the higher content of EOC (extractable organic carbon) aligns well with the increased enzymatic activity observed in sediment collected from burrow walls.

4.4 Future expected research

The goal of this research was to study the effects of plant invasiveness and crab on carbon cycling. Salinity levels vary between the sites, influencing the distribution of S. alterniflora in one of the sites due to its high salinity tolerance. The differences between the sites are believed to be primarily attributed to water salinity. Hydrolytic carbon-acquiring and oxidative carbon-acquiring enzyme activities are reduced by 33% and increased by 15%, respectively by under salination conditions. Although we conducted salinity tests at both sites, the samples analyzed for enzymatic activity did not correspond to the sampling period. Currently, it is challenging to assess the site effect, but this could be valuable for future studies.

The phylogenetic tree shows that the crabs inhabiting these sites are closely related, having previously belonged to the same genus before diverging. Sesarma crabs construct intricate and interconnected burrows. Initially, we planned to create casts of these burrows by using epoxy resin; however, the cool and moist conditions within these extensive burrows made it difficult to obtain casts. While we successfully carried out this operation for fiddler crab burrows, no analysis was conducted on soil enzymatic activity or crab respiration at that time. It is unfortunate that we could not investigate the effects of these burrow structures on carbon cycling in our current research. Nevertheless, this perspective presents a promising avenue for further exploration.

5 Conclusion

Our findings indicate that plant invasiveness leads to higher CO_2 efflux in native *P. australis* sites compared to invasive *S. alterniflora* sites. Other factors such as crab bioturbation (respiration, food intake, and burrowing), arbuscular mycorrhiza fungi infection, photosynthetic rate, and changes in organic carbon also contribute to greater carbon sequestration in invasive sites. However, the content and enzymatic activity of EOC does not result in lower carbon sequestration in *P. australis*. We observed significantly higher levels of TC, TN, TOC, ROC, EOC, S-ACT, S-β-GC, and S-ACP activities in mature crab burrows. In contrast, juvenile crab burrows showed no significant differences in biogeochemical properties compared to mudflats and non-rhizosphere sediment. Therefore, the carbon pool and organic carbon fraction vary across different zones. This study emphasizes the importance of understanding below-ground carbon cycling processes concerning crab and plant invasion. Further research on microbial communities and functional groups can provide a better understanding of the mechanisms behind nutrient cycling in crab and plant invasions.

Data availability statement

The original contributions presented in the study are included in the article/Supplementary Material. Further inquiries can be directed to the corresponding author.

Ethics statement

The manuscript presents research on animals that do not require ethical approval for their study.

Author contributions

YH: Conceptualization, Data curation, Formal analysis, Investigation, Methodology, Visualization, Writing – original draft, Writing – review & editing. XL: Conceptualization, Data

curation, Funding acquisition, Methodology, Project administration, Supervision, Validation, Visualization, Writing – review & editing. HC: Data curation, Investigation, Supervision, Writing – review & editing. LR: Conceptualization, Data curation, Supervision, Writing – review & editing. JT: Conceptualization, Funding acquisition, Resources, Writing – original draft.

Funding

The author(s) declare financial support was received for the research, authorship, and/or publication of this article. This research is funded by the National Natural Science Foundation of China (42141016), and Research Program of Shanghai Science and Technology (22dz1209600).

Acknowledgments

XL and JT managed projects and funding. We sincerely thank the reviewers for their insightful comments to improve the manuscript.

Conflict of interest

The authors declare that the research was conducted in the absence of any commercial or financial relationships that could be construed as a potential conflict of interest.

Publisher's note

Supplementary material

The Supplementary Material for this article can be found online at: https://www.frontiersin.org/articles/10.3389/fmars.2024.1413145/full#supplementary-material

References

Agusto, L. E., Qin, G., Thibodeau, B., Tang, J., Zhang, J., Zhou, J., et al. (2022). Fiddling with the blue carbon: Fiddler crab burrows enhance CO_2 and CH_4 efflux in saltmarsh. *Ecol. Indic.* 144, 109538. doi: 10.1016/j.ecolind.2022.109538

Alberti, J., Daleo, P., Fanjul, E., Escapa, M., Botto, F., and Iribarne, O. (2015). Can a single species challenge paradigms of salt marsh functioning? *Estuaries Coast.* 38, 1178–1188. doi: 10.1007/s12237–014-9836-z

Allison, S. D., and Vitousek, P. M. (2005). Responses of extracellular enzymes to simple and complex nutrient inputs. *Soil Biol. Biochem.* 37, 937–944. doi: 10.1016/j.soilbio.2004.09.014

Altieri, A. H., Bertness, M. D., Coverdale, T. C., Herrmann, N. C., and Angelini, C. (2012). A trophic cascade triggers collapse of a salt-marsh ecosystem with intensive recreational fishing. *Ecology* 93, 1402–1410. doi: 10.1890/11-1314.1

Andreetta, A., Fusi, M., Cameldi, I., Cimò, F., Carnicelli, S., and Cannicci, S. (2014). Mangrove carbon sink. Do burrowing crabs contribute to sediment carbon storage? Evidence from a Kenyan mangrove system. *J. Sea Res.* 85, 524–533. doi: 10.1016/j.seares.2013.08.010

Bertness, M. D., and Coverdale, T. C. (2013). An invasive species facilitates the recovery of salt marsh ecosystems on Cape Cod. *Ecology* 94, 1937–1943. doi: 10.1890/12-2150.1

Bortolus, A., and Iribarne, O. (1999). Effects of the SW Atlantic burrowing crab *Chasmagnathus granulata* on a *Spartina* salt marsh. *Mar. Ecol. Prog. Ser.* 178, 79–88. doi: 10.3354/meps178079

Brusati, E. D., and Grosholz, E. D. (2009). Does invasion of hybrid cordgrass change estuarine food webs? *Biol. Invasions* 11, 917–926. doi: 10.1007/s10530-008-9304-4

Bueno De Mesquita, C. P., Knelman, J. E., King, A. J., Farrer, E. C., Porazinska, D. L., Schmidt, S. K., et al. (2017). Plant colonization of moss-dominated soils in the alpine: Microbial and biogeochemical implications. *Soil Biol. Biochem.* 111, 135–142. doi: 10.1016/j.soilbio.2017.04.008

Burns, R. G., Deforest, J. L., Marxsen, J., Sinsabaugh, R. L., Stromberger, M. E., Wallenstein, M. D., et al. (2013). Soil enzymes in a changing environment: Current knowledge and future directions. *Soil Biol. Biochem.* 58, 216–234. doi: 10.1016/j.soilbio.2012.11.009

Chen, H., Zhang, P., Li, B., and Wu, J. (2015). Invasive cordgrass facilitates epifaunal communities in a Chinese marsh. *Biol. Invasions* 17, 205–217. doi: 10.1007/s10530-014-0720-3

Chen, X., He, Q., Xin, P., Gong, Z., Zhou, Z., and Zhang, C. (2021). Research progress on the biological disturbed behavior process of crabs in the tidal flats of estuaries and coasts. *Mar. Sci.* 45, 113–122. doi: 10.11759/hykx20200726001

Chu, W., Lu, F., Zhu, W., and Kang, C. (2011). Isolation and characterization of new potential probiotic bacteria based on quorum-sensing system. *J. Appl. Microbiol.* 110, 202–208. doi: 10.1111/jam.2010.110.issue-1

Coverdale, T. C., Altieri, A. H., and Bertness, M. D. (2012). Belowground herbivory increases vulnerability of New England salt marshes to die-off. *Ecology* 93, 2085–2094. doi: 10.1890/12-0010.1

Curado, G., Sánchez-Moyano, J. E., Figueroa, E., and Castillo, J. M. (2014). Do *spartina maritima* plantations enhance the macroinvertebrate community in European salt marshes? *Estuaries Coast.* 37, 589–601. doi: 10.1007/s12237–013-9713–1

Cutajar, J., Shimeta, J., and Nugegoda, D. (2012). Impacts of the invasive grass *Spartina anglica* on benthic macrofaunal assemblages in a temperate Australian saltmarsh. *Mar. Ecol. Prog. Ser.* 464, 107–120. doi: 10.3354/meps09826

Feng, J., Guo, J., Huang, Q., Jiang, J., Huang, G., Yang, Z., et al. (2014). Changes in the community structure and diet of benthic macrofauna in invasive spartina alterniflora wetlands following restoration with native mangroves. *Wetlands (Wilmington).* 34, 673–83. doi: 10.1007/s13157-014-0533-2

Feng, J., Huang, Q., Chen, H., Guo, J., and Lin, G. (2018). Restoration of native mangrove wetlands can reverse diet shifts of benthic macrofauna caused by invasive cordgrass. *J. Appl. Ecol.* 55, 905–916. doi: 10.1111/1365-2664.12987

Feng, J., Yu, D., Sinsabaugh, R. L., Moorhead, D. L., Andersen, M. N., Smith, P., et al. (2023). Trade-offs in carbon-degrading enzyme activities limit long-term soil carbon sequestration with biochar addition. *Biol. Rev. Camb Philos. Soc.* 98, 1184–1199. doi: 10.1111/brv.12949

Ge, X., Criswold, K. C., and Newman, A. J. (2023). Warmer and more seasonal climates reduce the effect of top-down population control: An example with aphids and ladybirds. *Funct. Ecol.* 37, 1604–1619. doi: 10.1111/1365-2435.14326

Gillis, L. G., Snavely, E., Lovelock, C., and Zimmer, M. (2019). Effects of crab burrows on sediment characteristics in a Ceriops australis-dominated mangrove forest. *Estuarine Coast. Shelf Sci.* 218, 334–339. doi: 10.1016/j.ecss.2019.01.008

Grow, A. K., Schutte, C. A., and Roberts, B. J. (2022). Fiddler crab burrowing increases salt marsh greenhouse gas emissions. *Biogeochemistry* 158, 73–90. doi: 10.1007/s10533-021-00886-5

Guimond, J. A., Seyfferth, A. L., Moffett, K. B., and Michael, H. A. (2020). A physical-biogeochemical mechanism for negative feedback between marsh crabs and carbon storage. *Environ. Res. Lett.* 15, 34024. doi: 10.1088/1748-9326/ab60e2

Gutiérrez, J. L., Jones, C. G., Groffman, P. M., Findlay, S. E. G., Iribarne, O. O., Ribeiro, P. D., et al. (2006). The contribution of crab burrow excavation to carbon availability in surficial salt-marsh sediments. *Ecosystems* 9, 647–658. doi: 10.1007/s10021-006-0135-9

Haines, E. B. (1976). Relation between the stable carbon isotope composition of fiddler crabs, plants, and soils in a salt marsh1. *Limnol. Oceanogr.* 21, 880–883. doi: 10.4319/lo.1976.21.6.0880

Harada, Y., and Lee, S. Y. (2016). Foraging behavior of the mangrove sesarmid crab Neosarmatium trispinosum enhances food intake and nutrient retention in a low-quality food environment. *Estuarine Coast. Shelf Sci.* 174, 41–48. doi: 10.1016/j.ecss.2016.03.017

Hassan, W., Bashir, S., Ahmed, N., Tanveer, M., Shah, A. N., Bano, R., et al. (2016). Labile organic carbon fractions, regulator of co2 emission: effect of plant residues and water regimes. *CLEAN – Soil, Air, Water*. 10, 1268-427. doi: 10.1002/clen.201400405

Hinson, A. L., Feagin, R. A., Eriksson, M., Najjar, R. G., Herrmann, M., Bianchi, T. S., et al. (2017). The spatial distribution of soil organic carbon in tidal wetland soils of the continental United States. *Glob. Chang. Biol.* 23, 5468–5480. doi: 10.1111/gcb.13811

Huhta, V. (2007). The role of soil fauna in ecosystems: A historical review. *Pedobiologia (Jena)* 50, 489–495. doi: 10.1016/j.pedobi.2006.08.006

IPCC. (2013). Climate Change 2013: The Physical Science Basis. (Cambridge: Cambridge University Press).

Ji, Y., Wu, B., Ding, Y., and Qin, P.. (2011). "Nutritional components of Phragmites australis and Spartina alterniflora in Dafeng free range David's Deer habitat of Jiangsu Province, East China: A comparative analysis". *Chin. J. Ecol.* 30, 2240–2244. doi: 10.3724/SP.J.1011.2011.00187

Khoshnevisan, B., Bashir, M. A., Sun, Q., Pan, J., Wang, H., Xu, Y., et al. (2021). Optimal rice-crab co-culture system as a new paradigm to air-water-food nexus sustainability. *J. Clean Prod.* 291, 125936. doi: 10.1016/j.jclepro.2021.125936

Koo, B. J., Kim, S., and Hyun, J. (2019). Feeding behavior of the ocypodid crab Macrophthalmus japonicus and its effects on oxygen-penetration depth and organic-matter removal in intertidal sediments. *Estuarine Coast. Shelf Sci.* 228, 106366. doi: 10.1016/j.ecss.2019.106366

Kristensen, E., Flindt, M. R., Ulomi, S., Borges, A. V., Abril, G., and Bouillon, S. (2008). Emission of CO_2 and CH_4 to the atmosphere by sediments and open waters in two Tanzanian mangrove forests. *Mar. Ecol. Prog. Ser.* 370, 53–67. doi: 10.3354/meps07642

Kristensen, E., Liebezeit, G., Dittmann, S., and Kroencke, I. (2000). Organic matter diagenesis at the oxic/anoxic interface in coastal marine sediments, with emphasis on the role of burrowing animals. *Hydrobiologia* 426, 1–24. doi: 10.1023/A:1003980226194

Lee, S. Y., and Khim, J. S. (2017). Hard science is essential to restoring soft-sediment intertidal habitats in burgeoning East Asia. *Chemosphere* 168, 765–776. doi: 10.1016/j.chemosphere.2016.10.136

Li, B., Liao, C., Zhang, X., Chen, H., Wang, Q., Chen, Z., et al. (2009). *Spartina alterniflora* invasions in the Yangtze River estuary, China: An overview of current status and ecosystem effects. *Ecol. Eng.* 35, 511–520. doi: 10.1016/j.ecoleng.2008.05.013

Li, S., Sun, L., Wu, H., Hu, Z., Liu, W., Li, Y., et al. (2012). The intestinal microbial diversity in mud crab (Scylla paramamosain) as determined by PCR-DGGE and clone library analysis. *J. Appl. Microbiol.* 113, 1341–1351. doi: 10.1111/jam.2012.113.issue-6

Liu, H., Wang, L., Liu, M., Wang, B., Jiang, K., Ma, S., et al. (2011). The intestinal microbial diversity in Chinese shrimp (Fenneropenaeus chinensis) as determined by PCR–DGGE and clone library analyses. *Aquaculture* 317, 32–36. doi: 10.1016/j.aquaculture.2011.04.008

Luo, B., Li, X., Luo, D., Xu, P., Chen, X., and You, W. (2019). *Preference of Helice tientsinensis and Sesarma plicata for typical salt marsh plants in the north of Hangzhou Bay. J. East China Norm. Univ. (Natur. Sci.)* 6, 123–131. doi: 10.3969/j.issn.1000.5641.2019.06.012

Maher, D. T., Santos, I. R., Schulz, K. G., Call, M., Jacobsen, G. E., and Sanders, C. J. (2017). Blue carbon oxidation revealed by radiogenic and stable isotopes in a mangrove system. *Geophys. Res. Lett.* 44, 4889–4896. doi: 10.1002/2017GL073753

McGonigle, T. P., Miller, M. H., Evans, D. G., Fairchild, G. L., and Swan, J. A.. (1990). A new method which gives an objective measure of colonization of roots by vesicular-arbuscular mycorrhizal fungi. *New Phytologist*. 115, 495-501.

Najjar, R. G., Herrmann, M., Alexander, R., Boyer, E. W., Burdige, D. J., Butman, D., et al. (2018). Carbon budget of tidal wetlands, estuaries, and shelf waters of Eastern North America. *Global Biogeochem. Cycles* 32, 389–416. doi: 10.1002/2017GB005790

Neira, C., Levin, L. A., Grosholz, E. D., and Mendoza, G. (2007). Influence of invasive Spartina growth stages on associated macrofaunal communities. *Biol. Invasions* 9, 975–993. doi: 10.1007/s10530-007-9097-x

Nordström, M. C., Demopoulos, A. W. J., Whitcraft, C. R., Rismondo, A., McMillan, P., Gonzalez, J. P., et al. (2015). Food web heterogeneity and succession in created saltmarshes. *J. Appl. Ecol.* 52, 1343–1354. doi: 10.1111/1365-2664.12473

Ouyang, X., and Lee, S. Y. (2014). Updated estimates of carbon accumulation rates in coastal marsh sediments. *Biogeosciences* 11, 5057–5071. doi: 10.5194/bg-11-5057-2014

Ouyang, X., Lee, C. Y., and Lee, S. Y. (2021). Effects of food and feeding regime on CO_2 fluxes from mangrove consumers – Do marine benthos breathe what they eat? *Mar. Environ. Res.* 169, 105352. doi: 10.1016/j.marenvres.2021.105352

Penha-Lopes, G., Kristensen, E., Flindt, M., Mangion, P., Bouillon, S., and Paula, J. (2010). The role of biogenic structures on the biogeochemical functioning of mangrove constructed wetlands sediments – A mesocosm approach. *Mar. Pollut. Bull.* 60, 560–572. doi: 10.1016/j.marpolbul.2009.11.008

Rovira, P., and Vallejo, V. R. (2002). Labile and recalcitrant pools of carbon and nitrogen in organic matter decomposing at different depths in soil; an acid hydrolysis approach. *Geoderma* 107, 109–141. doi: 10.1016/S0016-7061(01)00143-4

Sardans, J., Bartrons, M., Margalef, O., Gargallo-Garriga, A., Janssens, I. A., Ciais, P., et al. (2017). Plant invasion is associated with higher plant-soil nutrient concentrations in nutrient-poor environments. *Glob. Chang. Biol.* 23, 1282–1291. doi: 10.1111/gcb.13384

Sheng, P., Liu, R., and Li, M. (2011). Methodological comparison of observation and colonization measurement of arbuscular mycorrhizal fungi. *Mycosystema* 30, 519–525. doi: 10.13346/j.mycosystema.2011.04.002

Shin, W., Oh, M., Hong, J., Byun, C., and Lee, E. J. (2022). Early invasion of common cordgrass (Spartina anglica) increases belowground biomass and decreases macrofaunal density and diversity in a tidal flat marsh. *Biol. Invasions* 24, 3615–3629. doi: 10.1007/s10530-022-02866-8

Sinsabaugh, R. L., Lauber, C. L., Weintraub, M. N., Ahmed, B., Allison, S. D., Crenshaw, C., et al. (2008). Stoichiometry of soil enzyme activity at global scale. *Ecol. Letter* 11, 1252–1264. doi: 10.1111/j.1461-0248.2008.01245.x

Soti, G. P., Toprak, B., Rosa, D. N., and Jayachandran, K.. (2021) Influence of land use intensity and management on arbuscular mycorrhizal fungi-avocado symbiosis. *J. Agric. Sci.* 12, 3: 10-16. doi: 10.5539/jas.v13n3p10

Stieglitz, T., Ridd, P., and Müller, P. (2000). Passive irrigation and functional morphology of crustacean burrows in a tropical mangrove swamp. *Hydrobiologia* 421, 69–76. doi: 10.1023/A:1003925502665

Tang, J. W., Ye, S. F., Chen, X. C., Yang, H. L., Sun, X. H., Wang, F. M., et al. (2018). Coastal blue carbon: Concept, study method, and the application to ecological restoration. *Sci. China Earth Sci.* 61, 637–646. doi: 10.1007/s11430-017-9181-x

Thongtham, N., Kristensen, E., and Puangprasan, S. (2008). Leaf removal by sesarmid crabs in Bangrong mangrove forest, Phuket, Thailand; with emphasis on the feeding ecology of *Neoepisesarma versicolor*. *Estuarine Coast. Shelf Sci.* 80, 573–580. doi: 10.1016/j.ecss.2008.09.017

Tue, N. T., Hamaoka, H., Sogabe, A., Quy, T. D., Nhuan, M. T., and Omori, K. (2012). Food sources of macro-invertebrates in an important mangrove ecosystem of Vietnam determined by dual stable isotope signatures. *J. Sea Res.* 72, 14–21. doi: 10.1016/j.seares.2012.05.006

Wang, J. Q., Zhang, X. D., Bertness, M. D., Fang, C. M., Chen, J. K., Hara, T., et al (2010). Bioturbation of burrowing crabs promotes sediment turnover and carbon and nitrogen movements in an estuarine salt marsh. *Ecosystems* 13, 586–599. doi: 10.1007/s10021-010-9342-5

Xiao, K., Wilson, A. M., Li, H., Santos, I. R., Tamborski, J., Smith, E., et al. (2021). Large CO_2 release and tidal flushing in salt marsh crab burrows reduce the potential for blue carbon sequestration. *Limnol. Oceanogr.* 66, 14–29. doi: 10.1002/lno.11582

Yang, S., Sun, X., Ding, J., Jiang, Z., Liu, X., and Xu, J. (2020). Effect of biochar addition on CO_2 exchange in paddy fields under water-saving irrigation in Southeast China. *J. Environ. Manage* 271, 111029. doi: 10.1016/j.jenvman.2020.111029

Zhang, Y., and Tong, C. F. (2018). Stomach content characteristics and feeding preference of Chiromantes dehaani in the salt marsh of Yangtze estuary. *Chin. J. Ecol.* 37, 2059–2066. doi: 10.13292/j.1000–4890.201807.022

Zhou, Y., and Staver, A. C. (2019). Enhanced activity of soil nutrient-releasing enzymes after plant invasion: a meta-analysis. *Ecology* 100, e2830. doi: 10.1002/ecy.2830

Zhu, L., Wang, X., Chen, F., Li, C., and Wu, L. (2019). Effects of the successive planting ofEucalyptus urophylla on soil bacterial and fungal community structure, diversity, microbial biomass, and enzyme activity. *Land Degrad. Dev.* 30, 636–646. doi: 10.1002/ldr.3249

frontiers | Frontiers in Marine Science

TYPE Original Research
PUBLISHED 03 July 2024
DOI 10.3389/fmars.2024.1425587

OPEN ACCESS

EDITED BY
Qing Wang,
Beijing Normal University, Zhuhai, China

REVIEWED BY
Fengrun Wu,
Xiamen University of Technology, China
Zhonghua Ning,
Beijing Normal University, China

*CORRESPONDENCE
Youzheng Zhang
zhangyz@sio.org.cn

†These authors share first authorship

RECEIVED 30 April 2024
ACCEPTED 18 June 2024
PUBLISHED 03 July 2024

CITATION
Zhang Y, Guo Y, Wang H, Li N, Xu H, Zhang D, Qian J and Hu Y (2024) Divergence in spatial patterns of leaf stoichiometry between native and non-native plants across coastal wetlands.
Front. Mar. Sci. 11:1425587.
doi: 10.3389/fmars.2024.1425587

Divergence in spatial patterns of leaf stoichiometry between native and non-native plants across coastal wetlands

Youzheng Zhang[1,2*†], Yaolin Guo[3†], Hui Wang[4], Niu Li[5], Hengtao Xu[1,2], Dongrong Zhang[1,2], Jian Qian[1,2] and Yukun Hu[6]

[1]Key Laboratory of Engineering Oceanography, Second Institute of Oceanography, Ministry of Natural Resources, Hangzhou, China, [2]Key Laboratory of Nearshore Engineering Environment and Ecological Security of Zhejiang Province, Second Institute of Oceanography, Ministry of Natural Resources, Hangzhou, China, [3]School of Life Sciences, Fudan University, Shanghai, China, [4]Department of Biogeochemical Processes, Max Planck Institute for Biogeochemistry, Jena, Germany, [5]Wetland Ecosystem Research Station of Hangzhou Bay, Research Institute of Subtropical Forestry, Chinese Academy of Forestry, Hangzhou, China, [6]State Key Laboratory of Herbage Improvement and Grassland Agro-ecosystems, College of Pastoral Agriculture Science and Technology, Lanzhou University, Lanzhou, China

The spatial pattern of leaf stoichiometry is critical in predicting plant palatability and ecosystem productivity and nutrient cycling rates and thus is a major focus of community ecological research. Coastal wetlands as vital blue carbon ecosystems, with high possibility to be vulnerable to plant invasion, studies focused on stoichiometry and its pattern are important to unveil the elements cycling process. However, previous studies have mainly focused on stoichiometry in terrestrial ecosystems, there are few studies conducted on coastal wetland ecosystems, especially the studies that compare leaf stoichiometry between native and non-native plants in coastal wetlands. In this study, we compared the latitudinal patterns of leaf nutrient contents and their stoichiometric ratios between native and non-native plant species across coastal wetland ecosystems and investigated whether leaf stoichiometric patterns were driven by climatic factors. We used a compiled global data set of 954 records to conduct a systematic meta-analysis. The results showed that there were significant differences in latitudinal patterns of leaf carbon (C) and nitrogen (N) contents and C:N ratio between native and non-native species, as well as significant differences in leaf C, N, and phosphorus (P) contents. For native species, we found significant latitudinal patterns in leaf C, N, and P contents and C:N and C:P ratios, whereas for non-native species, we found significant latitudinal patterns in leaf N content and C:P and N:P ratios. Mean annual temperature of the data collection site was a significant predictor of leaf stoichiometry of native plants but only of leaf N content and C:P ratio of non-native plants. Thus, we demonstrated spatial heterogeneity in leaf stoichiometries between native and non-native plants in coastal wetlands, indicating that such differences should be emphasized in future biogeochemical models and plant-herbivore interaction studies owing to the

important role of wetland plants in global C, N, and P cycles. Our findings increase understanding of plant-related nutrient and elements cycling in coastal wetlands, as well as improve predictions of plant growth rates and vegetation productivity across large scales under plant invasion scenarios.

KEYWORDS

biogeography, coastal wetlands, leaf stoichiometry, latitudinal spatial patterns, mean annual temperature, native plants, non-native plants

Introduction

Latitudinal gradients in biotic interactions are a classic paradigm in ecology (Kinlock et al., 2018; Zvereva and Kozlov, 2022). The spatial heterogeneity of both biotic and abiotic factors is largely responsible for latitudinal gradients in plant traits (Abdala-Roberts et al., 2016; Reese et al., 2016; Moreira et al., 2018). For example, plant defensive traits are greater at low latitudes than at high latitudes, mainly due to stronger biotic interactions at low latitudes (Anstett et al., 2014). However, the cost of resource acquisition may also be a key driver of latitudinal variation in plant defenses (Kooyers et al., 2017). Leaf stoichiometry (i.e., leaf carbon (C), nitrogen (N), and phosphorus (P) contents) is also one of the most important plant traits and is an effective predictor of plant palatability, ecosystem function and nutrient cycling rates, and role of plants in global biogeochemical models (Kattge et al., 2009; Chen et al., 2013; Koerselman and Meuleman, 1996; Elser et al., 2003; Güsewell, 2004; Joshi and Vrieling, 2005; Kerkhoff et al., 2006; Leishman et al., 2007; Kattge et al., 2009; Li et al., 2009; Ehrenfeld, 2010; Huang et al., 2010; Kurokawa et al., 2010; Kitajima et al., 2012; Funk, 2013; Funk and Cornwell, 2013; Heberling and Fridley, 2013; Cronin et al., 2015; Funk et al., 2017; Ju et al., 2017; Kooyers et al., 2017; Kinlock et al., 2018; Fox and Weisberg, 2019; Ju et al., 2019; Guo et al., 2020; Harvey and Leffler, 2020; Liu et al., 2020; Hu et al., 2021; Guo et al., 2023; Guo et al., 2024; Liu et al., 2021; Zhang et al., 2021). However, we lack a sufficiently comprehensive research on latitudinal patterns of leaf stoichiometry.

Leaf C is a major component of carbohydrates, representing starch reserves and CO_2 fixation capacity (Rogers et al., 2004), and it is also strongly correlated with cellulose and hemicellulose contents (Kitajima et al., 2012). Leaf N is a major component of amino acids and proteins, and thus, high leaf N indicates high nutrient levels, which lead to high decomposition rates and palatability to herbivores (Schädler et al., 2003; Kurokawa et al., 2010). In addition, many secondary metabolites are also nitrogenous compounds, which can have major effects on plant–insect interactions (Waller, 2012). Leaf P is an important component of nucleotides in genetic materials (e.g., DNA) and energy-transfer compounds (e.g., ATP) (Ågren, 2008; Guo et al., 2020). The leaf stoichiometric ratios of these critical nutrients (i.e., C:N, C:P, and N:P) have been used to indicate ecosystem nutrient limitation (Koerselman and Meuleman, 1996; Güsewell, 2004). Thus, studies of latitudinal patterns in leaf nutrient contents and stoichiometric ratios can significantly improve our understanding of ecosystem processes, including productivity, detritivory and decomposition, herbivory, and energy flow (Güsewell, 2004; Banks and Frost, 2017; Zhang et al., 2021; Guo et al., 2023).

Native and non-native plants have different resource allocation strategies; for example, non-native plants can grow faster and use resources more efficiently than native plants (Huang et al., 2010; Heberling and Fridley, 2013). Because of the differences in strategies, there may be large differences in leaf stoichiometry between non-native and native plants, which can lead to greater competitive capacity of non-natives (Harvey and Leffler, 2020; Zhu et al., 2020). Plant invasions by non-natives are an important component of anthropogenic global climate change and are considered one of the most serious environmental problems (Sala et al., 2000; Vilà et al., 2007; Bradley et al., 2010). At the scale of communities and ecosystems, plant invasions can threaten native community species richness and diversity and alter ecosystem C and N cycling and affect ecosystem structure and function (Ehrenfeld, 2010; Vilà et al., 2011; Pyšek et al., 2012). Therefore, we consider plant stoichiometry to be a useful functional trait for explaining and predicting the status of plant invasions at large scales. However, the differences in biogeographic patterns of leaf stoichiometry between native and non-native plants have not been systematically studied.

Coastal wetland ecosystems are currently one of the most fragile and sensitive ecosystems worldwide and are severely threatened and damaged by invasive plants (Li et al., 2009). In China, for example, coastal salt marshes have suffered from serious plant invasions, and non-native *Spartina alterniflora* has taken over all coastal wetlands in the country (Ju et al., 2017; Xu et al., 2022; Ning et al., 2024). Similarly, over the past century, the invasive plant *Phragmites australis* has steadily invaded the coastal salt marshes of North America, causing severe damage to native plant communities (Silliman and Bertness, 2004; Minchinton et al., 2006; Ning et al., 2021). The few empirical studies that investigated the leaf stoichiometry of salt marsh plants found significant latitudinal differences in leaf stoichiometry patterns between exotic and native plants (Cronin et al., 2015; Zhang et al., 2021). However, previous studies are all limited to a few model species, and the results may not be generalizable across species. Therefore, a

systematic cross-species comparative study is needed on the spatial patterns of leaf nutrient contents and stoichiometric ratios of native and non-native plants across global coastal wetland ecosystems.

Here, we report a meta-analysis of the spatial patterns of leaf stoichiometry between native and non-native plants in coastal wetlands. Plants of the same identity in the same latitude face similar environmental factors, which may result in co-occurring plants with similar ecological strategies (Hu et al., 2021; Guo et al., 2024). This provides an opportunity to conduct cross-species spatial analyses of leaf stoichiometry. In this study, we integrated a data set of leaf stoichiometry from global coastal wetland ecosystems for cross-species ecological modelling. The effect of temperature on leaf stoichiometry was analyzed using linear regression. We hypothesized the following: (1) there are significant differences in leaf stoichiometry between native and non-native plants in coastal wetlands; (2) there are significant differences in spatial patterns of leaf stoichiometry between native and non-native plants in coastal wetlands; and (3) any differences between native and non-native plants are primarily related to differential responses to climatic factors (mainly temperature). We aim to increase understanding of patterns in two kinds of plant leaf stoichiometries and nutrient cycling in coastal wetlands, as well as improve predictions of biogeochemical models across large scales.

Materials and methods

Data collection

We first used a comprehensive dataset of leaf stoichiometry for coastal wetland plants containing six leaf stoichiometric traits (C, N, P, C:N, C:P and N:P) with 698 data points from 205 sites (Hu et al., 2021). This dataset was primarily collected from typical coastal wetlands (including tidal salt marshes and mangroves), and excluded studies of seedlings. This dataset also excluded data from significant disturbances and experimental treatments (e.g., grazing and reclamation), as well as data from greenhouses and common gardens (Hu et al., 2021). We then added some additional studies from recent years with data based on salt marshes on the east coast of China (Xu et al., 2020; Liu et al., 2020). In total, the data set contained 954 records. For all data, we also recorded the name of the plant species and the original location of the data. We used temperature as the climatic factor in the study and extracted mean annual temperature using recorded site information at worldclim.org. We did not include precipitation as a climatic factor in this study, because the focus was on salt marsh ecosystems, which have almost regular tides and are mostly less water-limited. We also determined plant identity (native or non-native) for all plant species in the data set using Plants of the World Online (powo.science.kew.org). In the end, our dataset contained 740 data points for native plants and 214 for non-native plants (Figure 1).

Statistical analyses

As the sample size (N) of the six leaf stoichiometric traits is inconsistent, we performed separate analyses for the six leaf stoichiometric traits in subsequent data analyses. We used the average of the values of leaf element contents (C, N and P) and their ratios (C:N, C:P and N:P) for each species within each site. We then tested the normality of the distributions for these plant characteristics and found that none followed a normal distribution. To normalize the distribution of residuals, all leaf characteristics were log10-transformed to meet the assumption of normality. To determine whether leaf stoichiometries were affected by plant identity (native and non-native) and latitude, we used the lme4 package for linear mixed models (LMMs) to analyze each leaf stoichiometric character (C, N, P, C:N, C:P and N:P). LMMs could accurately assess the effects of different factors on the response

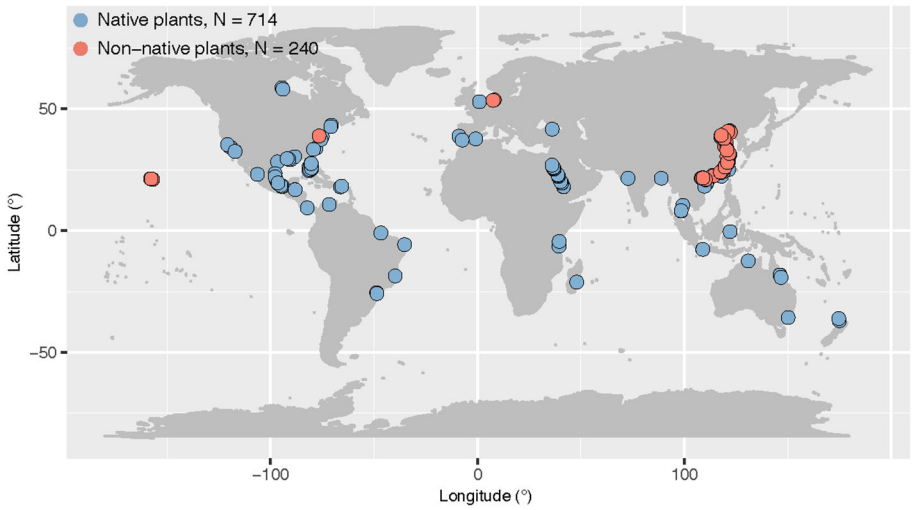

FIGURE 1
Map of original study sites of native and non-native plant leaf stoichiometry across global coastal wetlands. Several studies that only provided latitude without longitude were not included in the map. The sample size (N) was reported.

variables by including interactions (Bolker et al., 2009). Each model included plant identity, latitude, and their interaction as fixed effects and plant species as a random effect (Bates et al., 2015). Inclusion of plant species as a random effect to separately consider correlations for the same plant species and to account for these interdependencies when fitting the model. The significance of fixed effects in a model was assessed by the Type II Wald chi-squared test using the CAR package (Fox and Weisberg, 2019). To further compare differences in latitudinal patterns of leaf stoichiometry between native and non-native plants, linear regression was used to fit the relations between latitude and leaf stoichiometry for each plant type. To investigate the response of leaf stoichiometry to mean annual temperature (MAT), we used linear regression to fit the relations between MAT and leaf stoichiometry for each plant type. All analyses were performed using R v3.6.2 (R Core Team, 2019).

Results

Effects of plant identity and latitude on leaf stoichiometry

In the LMM models, the effect of plant identity was significant for leaf C, N, and P (Table 1), indicating significant differences in leaf stoichiometry between native and non-native plants in coastal wetlands. Latitude was significant for leaf C and N and C:N ratio, indicating significant relations of those variables with latitude (Table 1). Plant identity × latitude interactions were significant for leaf C and C:N ratio, indicating significant latitudinal differences in the relations of the two characteristics between native and non-native plants.

In separate analyses of the relations between leaf stoichiometry and latitude for native and non-native plants, leaf C, N, and P and C:N and C:P ratios of native plant species were significantly correlated with latitude (Figure 2), with leaf C and C:N and C:P ratios decreasing with increasing latitude and leaf N and P increasing. For non-native plants, leaf N and C:P and N:P ratios were significantly related with latitude (Figure 2), with leaf N and N:P ratio increasing with increasing latitude and leaf C:P ratio decreasing.

Relations between leaf stoichiometry and mean annual temperature

For native plants, leaf C, N, and P and C:N and C:P ratios were significantly related with MAT (Figure 3), with leaf C and C:N and C:P ratios increasing with increasing MAT and leaf N and P decreasing. For non-native plants, leaf N and C:P ratio were significantly related with MAT (Figure 3), with leaf N decreasing and leaf C:P ratio increasing with increasing MAT.

Discussion

We investigated the spatial heterogeneity of leaf nutrient contents and stoichiometric ratios between native and non-native plants across global coastal wetland ecosystems. And we found significant latitudinal patterns in leaf C and N and C:N ratio (Table 1). For native plants, latitudinal patterns were significant for most leaf nutrient contents and stoichiometric ratios, whereas for non-native plants, latitudinal patterns were only significant for leaf N and C:P and N:P ratios. In spite of this, striking differences were also found between native and non-native plants in the responses of leaf nutrient contents and stoichiometric ratios to temperature.

According to several studies, non-native plants typically have higher resource acquisition capacity than that of native plants, resulting in significantly higher C, N, and P contents in non-native plants than in native species (Leishman et al., 2007; Funk, 2013; Funk et al., 2017. This general conclusion is consistent with our findings. Although there were significant differences in leaf nutrient contents between native and non-native plants, there were no significant differences in stoichiometric ratios (Table 1; Figure 2). This result may be because leaf stoichiometric ratios are calculated from leaf element contents, which can mask potential differences between native and non-native plants. Nevertheless, our results indicated that non-native plants have higher nutrient acquisition capacity and thus nutrient levels than those of native plants. Such increases in leaf C and N contents may also indicate an increase in contents of structural substances and nitrogenous compounds, which are most likely related to an increase in plant defenses

TABLE 1 Linear mixed models of the effects of plant identity (PI, native or non-native), latitude (L), and their interaction on leaf stoichiometry in global coastal wetlands.

Variable	Plant identity (PI)			Latitude (L)			PI × L		
	χ^2	*df*	*P*	χ^2	*df*	*P*	χ^2	*df*	*P*
C	**10.162**	**1**	**0.001**	**3.962**	**1**	**0.047**	**5.939**	**1**	**0.015**
N	**11.316**	**1**	**0.001**	**16.155**	**1**	< **0.001**	0.396	1	0.529
P	**8.719**	**1**	**0.003**	0.304	1	0.582	0.757	1	0.384
C:N	1.756	1	0.185	**46.098**	**1**	< **0.001**	**4.697**	**1**	**0.030**
C:P	0.496	1	0.482	2.392	1	0.122	0.048	1	0.827
N:P	0.438	1	0.508	2.052	1	0.152	1.781	1	0.182

df, degrees of freedom; χ^2, chi–squared test statistic. Significant effects are shown in bold.

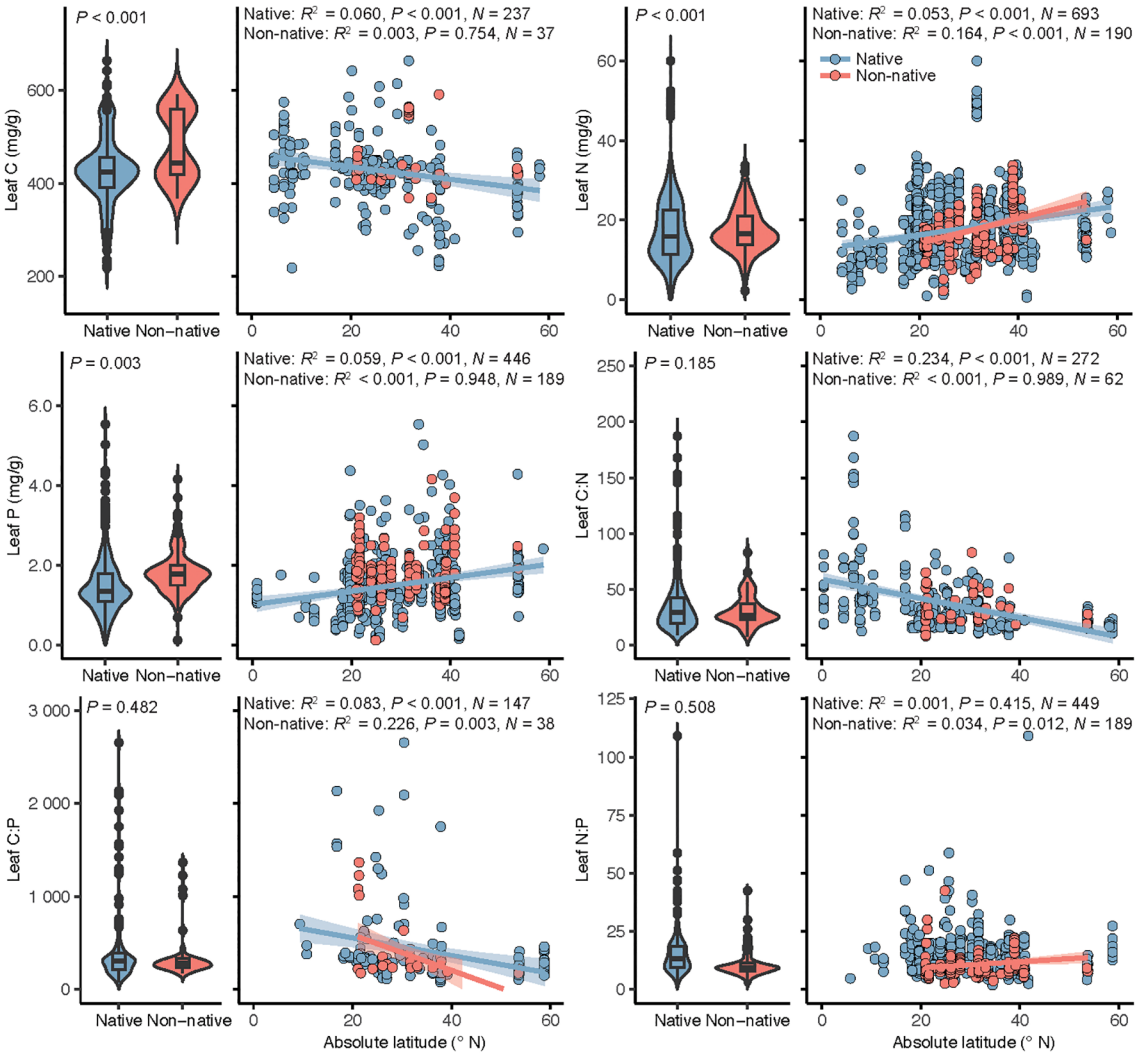

FIGURE 2
Leaf stoichiometry of native and non-native plant species in coastal wetlands and its relation with latitude. Panels, left side: leaf nutrient contents and stoichiometric ratios of native and non-native plant species, with box plots indicating the median and interquartile ranges and violin plots indicating distribution of the data with black dots outliers in the data set. The *P*-values indicate the significance of the effect of plant identity in linear mixed models. Panels, right side: linear regressions of the relations between leaf stoichiometry and latitude for native and non-native plants. When the latitude effect was significant, regression lines were plotted and associated R^2, *P*-values and sample size (N) reported.

(Kitajima et al., 2012; Waller, 2012; Aljbory and Chen, 2018). However, the results of this study do not allow an accurate assessment of leaf palatability of coastal plants. Therefore, because leaf stoichiometry may affect multiple plant performances, further bioassay experiments are needed to determine leaf palatability.

Significant latitudinal patterns were detected in leaf C and N contents and C:N ratio of coastal wetland plants but not in leaf P content and C:P and N:P stoichiometric ratios (Table 1), which are results partially consistent with those of previous findings in coastal wetlands (Hu et al., 2021). This was mainly because in this study, plant identity was set as a random effect in LMMs, and species dependence was accounted for when assessing the significance of fixed effects. Furthermore, our results for leaf P are not fully consistent with those based on terrestrial ecosystems, mainly because of the strong P limitation in terrestrial ecosystems, which gradually increases with increasing latitude and leads to similar gradients of leaf P content (Reich and Oleksyn, 2004; Tian et al., 2018). When we further differentiated plant identities, significant differences were detected between native and non-native plants in latitudinal patterns of leaf nutrient contents and stoichiometric ratios (Figure 2). With the exception of the N:P ratio, all leaf stoichiometries of native plants showed significant latitudinal patterns, whereas in non-native plants, only leaf stoichiometries of N content C:P and N:P ratios showed significant latitudinal gradients. Such non-parallel latitudinal gradients have also been observed with native and invasive lineages of *Phragmites australis*, a model species in North American coastal marshes (Cronin et al., 2015; Bhattarai et al., 2017). Thus, our results extend the applicability of such findings from the level of single species to that of multiple species.

Temperature is one of the most important factors included in the complex factor of latitude. Environmental factors can influence

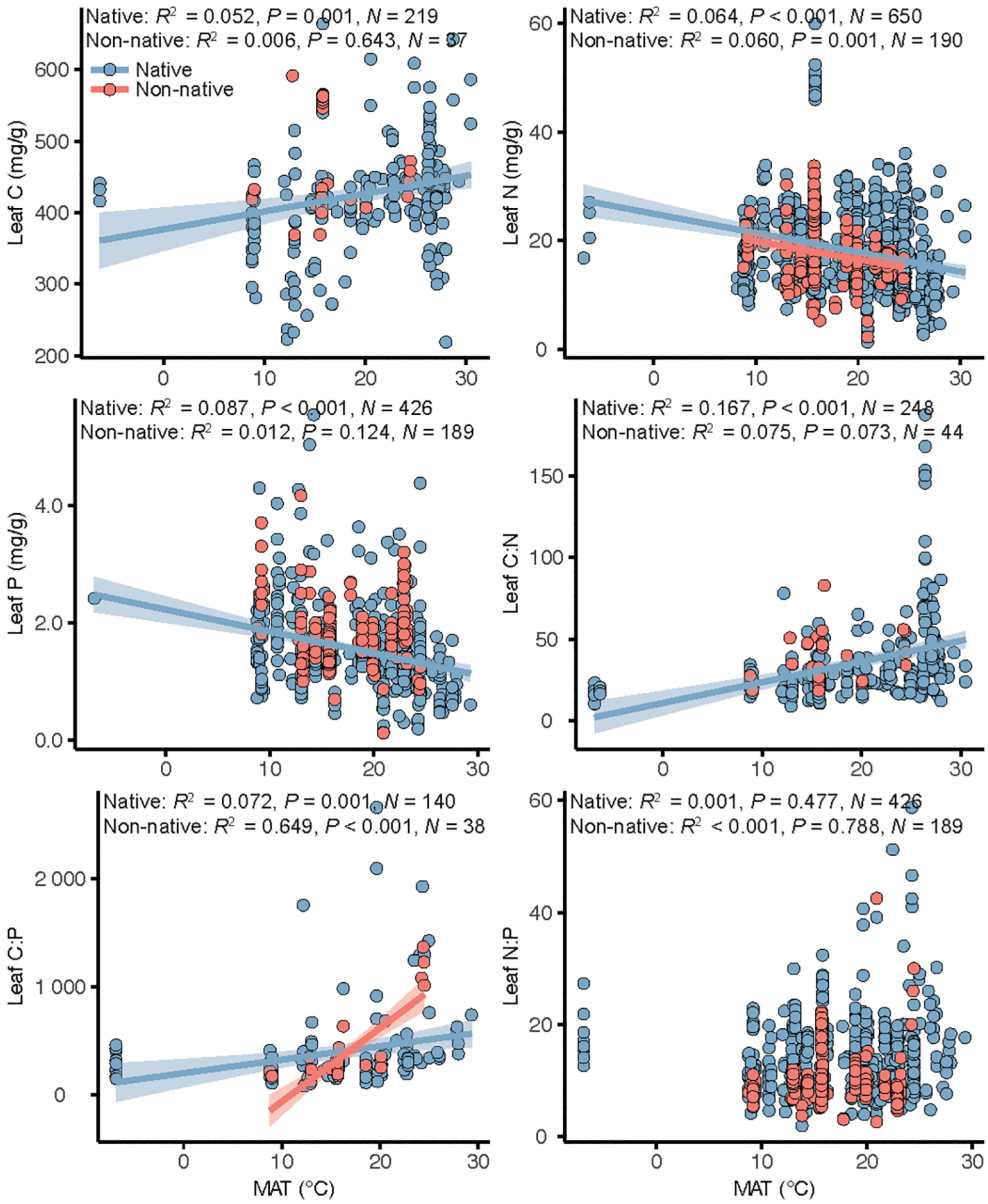

FIGURE 3
Linear regressions of the relations between mean annual temperature (MAT) and leaf stoichiometry in native and non-native plants in global coastal wetlands. When the temperature effect was significant, regression lines were plotted and associated R^2, P-values and sample size (N) reported.

plant traits independently of biotic factors and control the accumulation and removal rates of C, N, and P in leaves at the plant level and therefore also strongly influence plant development and resource use strategies (Moles et al., 2014; Abdala-Roberts et al., 2016; Tian et al., 2018; Wang et al., 2022). We found significant differences in the responses of native and non-native plants to MAT (Figure 3). Except for leaf N:P ratio, all native plants responded significantly to the variation in temperature with latitude, whereas only leaf N and C:P ratio of non-native plants responded to the variation in temperature (Figure 3). This difference in response of leaf stoichiometry to MAT between native and non-native plant species is mainly because non-native plants have been introduced for a short period of time and have not had enough time to adapt to MAT of the introduced range (Guo et al., 2023, 2024).

Temperature directly affects plant physiology and thus regulates plant traits, but it also indirectly mediates biotic factors, such as herbivory, which can cause changes in plant traits (Pennings et al., 2009; Moreira et al., 2018). The latitudinal gradient hypothesis of biotic interactions suggests that biotic interactions are more intense at low latitudes than at high latitudes (Zvereva and Kozlov, 2022; Guo et al., 2024). The increase in intensity of interactions would result in long-term natural selection pressure on plants at lower latitudes for lower palatability and thus resistance to herbivorous consumers, whereas the opposite would be true at higher latitudes (Anstett et al., 2015; Kooyers et al., 2017). We found that compared with non-native plants, native plants had higher leaf C and C:N and C:P ratios and lower leaf P and N at low latitudes (Figure 2). These results suggest that native coastal plants are less palatable at lower

latitudes than at higher latitudes, supporting the latitudinal gradient hypothesis of biotic interactions. However, a similar latitudinal pattern was not detected for non-native coastal plants. This result is mainly because non-native plants have only a short history of coevolution with local herbivores in introduced areas and have not yet developed spatial patterns similar to those of native plants. One caveat is our study only focus the climatic factor as MAT, we suggest future study may have more on exploring the multifactor effect on the leaf stoichiometry in coastal wetlands (e.g. tide undulation, deposit sediment chemistry).

Our study is the most comprehensive study to date comparing the latitudinal patterns of leaf stoichiometry of native and non-native plants in coastal wetland ecosystems. We found significant spatial heterogeneity between native and non-native plants, supporting the previous hypothesis that plant traits of native and exotic plants show non-parallel latitudinal gradients (Cronin et al., 2015; Bhattarai et al., 2017). The differences in spatial patterns in this study may be due to differences in the responses of the two types of plants to temperature drivers. These findings support our first and second hypotheses. Leaf C, N, P and their ratios are the vital indicators of leaf palatability, our results imply there are differences in leaf palatability of coastal wetland plants between high and low latitudes, which indicate that biotic interactions (e.g. herbivory intensity) may vary across spatial scales. Thus, this study can help increase understanding of biotic interactions and nutrient cycling in coastal wetlands, and improve predictions of plant growth rates and vegetation productivity across large scales, as well as be useful in the parameterization of vegetation climate models under plant invasion scenarios (Ågren & Andersson, 2011; Tang et al., 2018). In addition, differences in leaf stoichiometry between native and non-native plants can help to study the effects of exotic plants on native plant communities and improve understanding of plant adaptation and evolution (Kerkhoff et al., 2006).

Data availability statement

The original contributions presented in the study are included in the article/Supplementary Material. Further inquiries can be directed to the corresponding author.

Author contributions

YZ: Conceptualization, Data curation, Formal analysis, Funding acquisition, Methodology, Writing – original draft, Writing – review & editing. YG: Conceptualization, Data curation, Formal analysis, Methodology, Writing – original draft, Writing – review & editing. HW: Writing – original draft, Writing – review & editing. NL: Writing – review & editing. HX: Writing – original draft, Writing – review & editing. DZ: Writing – original draft, Writing – review & editing. JQ: Writing – original draft, Writing – review & editing. YH: Data curation, Writing – original draft, Writing – review & editing.

Funding

The author(s) declare financial support was received for the research, authorship, and/or publication of this article. This study was supported by National Natural Science Foundation of China (grant no. 32301368), the Zhejiang Province Commonwealth Projects (grant no. ZCLQ24C0301 and LQ23C030003), the Scientific Research Fund of the Second Institute of Oceanography, SOA (Grant No. JG2216), and the Cooperation of Zhejiang Province and the Chinese Academy of Forestry (grant no. 2023SY11).

Conflict of interest

The authors declare that the research was conducted in the absence of any commercial or financial relationships that could be construed as a potential conflict of interest.

Publisher's note

Supplementary material

The Supplementary Material for this article can be found online at: https://www.frontiersin.org/articles/10.3389/fmars.2024.1425587/full#supplementary-material

References

Abdala-Roberts, L., Rasmann, S., Berny-Mier y Terán, J. C., Covelo, F., Glauser, G., and Moreira, X. (2016). Biotic and abiotic factors associated with altitudinal variation in plant traits and herbivory in a dominant oak species. *Am. J. Bot.* 103, 2070–2078. doi: 10.3732/ajb.1600310

Ågren, G. I. (2008). Stoichiometry and nutrition of plant growth in natural communities. *Annu. Rev. Ecol. Evol. S* 39, 153–170. doi: 10.1146/annurev.ecolsys.39.110707.173515

Ågren, G. I., and Andersson, F. O. (2011). *Terrestrial ecosystem ecology: principles and applications*. (Cambridge: Cambridge University Press).

Aljbory, Z., and Chen, M. S. (2018). Indirect plant defense against insect herbivores: a review. *Insect Sci.* 25, 2–23. doi: 10.1111/1744-7917.12436

Anstett, D. N., Ahern, J. R., Glinos, J., Nawar, N., Salminen, J. P., and Johnson, M. T. (2015). Can genetically based clines in plant defence explain greater herbivory at higher latitudes? *Ecol. Lett.* 18, 1376–1386. doi: 10.1111/ele.12532

Anstett, D. N., Naujokaitis-Lewis, I., and Johnson, M. T. (2014). Latitudinal gradients in herbivory on *Oenothera biennis* vary according to herbivore guild and specialization. *Ecology* 95, 2915–2923. doi: 10.1890/13-0932.1

Banks, L. K., and Frost, P. C. (2017). Biomass loss and nutrient release from decomposing aquatic macrophytes: effects of detrital mixing. *Aquat. Sci.* 79, 881–890. doi: 10.1007/s00027-017-0539-y

Bates, D., Mächler, M., Bolker, B., and Walker, S. (2015). Fitting linear mixed-effects models using lme4. *J. Stat. Software* 67, 1–48. doi: 10.18637/jss.v067.i01

Bhattarai, G. P., Meyerson, L. A., Anderson, J., Cummings, D., Allen, W. J., and Cronin, J. T. (2017). Biogeography of a plant invasion: genetic variation and plasticity in latitudinal clines for traits related to herbivory. *Ecol. Monogr.* 87, 57–75. doi: 10.1002/ecm.1233

Bolker, B. M., Brooks, M. E., Clark, C. J., Geange, S. W., Poulsen, J. R., Stevens, M. H. H., et al. (2009). Generalized linear mixed models: a practical guide for ecology and evolution. *Trends Ecol. Evol.* 24, 127–135. doi: 10.1016/j.tree.2008.10.008

Bradley, B. A., Blumenthal, D. M., Wilcove, D. S., and Ziska, L. H. (2010). Predicting plant invasions in an era of global change. *Trends Ecol. Evol.* 25, 310–318. doi: 10.1016/j.tree.2009.12.003

Chen, Y., Han, W., Tang, L., Tang, Z., and Fang, J. (2013). Leaf nitrogen and phosphorus concentrations of woody plants differ in responses to climate, soil and plant growth form. *Ecography* 36, 178–184. doi: 10.1111/j.1600-0587.2011.06833.x

Cronin, J. T., Bhattarai, G. P., Allen, W. J., and Meyerson, L. A. (2015). Biogeography of a plant invasion: plant–herbivore interactions. *Ecology* 96, 1115–1127. doi: 10.1890/14-1091.1

Ehrenfeld, J. G. (2010). Ecosystem consequences of biological invasions. *Annu. Rev. Ecol. Evol. S.* 41, 59–80. doi: 10.1146/annurev-ecolsys-102209-144650

Elser, J. J., Acharya, K., Kyle, M., Cotner, J., Makino, W., Markow, T., et al. (2003). Growth rate–stoichiometry couplings in diverse biota. *Ecol. Lett.* 6, 936–943. doi: 10.1046/j.1461-0248.2003.00518.x

Fox, J., and Weisberg, S. (2019). *An R companion to applied regression* (Thousand Oaks, CA, USA: Sage).

Funk, J. L. (2013). The physiology of invasive plants in low-resource environments. *Conserv. Physiol.* 1, cot026. doi: 10.1093/conphys/cot026

Funk, J. L., and Cornwell, W. K. (2013). Leaf traits within communities: context may affect the mapping of traits to function. *Ecology* 94, 1893–1897. doi: 10.1890/12-1602.1

Funk, J. L., Nguyen, M. A., Standish, R. J., Stock, W. D., and Valladares, F. (2017). Global resource acquisition patterns of invasive and native plant species do not hold at the regional scale in Mediterranean type ecosystems. *Biol. Invasions* 19, 1143–1151. doi: 10.1007/s10530-016-1297-9

Guo, Y., Parepa, M., Wang, H., Wang, M., Wu, J., Li, B., et al. (2024). Global heterogeneity of latitudinal patterns in herbivory between native and exotic plants. *bioRxiv*. doi: 10.1101/2024.01.24.576872

Guo, Y., Yan, Z., Gheyret, G., Zhou, G., Xie, Z., and Tang, Z. (2020). The community-level scaling relationship between leaf nitrogen and phosphorus changes with plant growth, climate and nutrient limitation. *J. Ecol.* 108, 1276–1286. doi: 10.1111/1365-2745.13369

Guo, Y., Zhang, Y., Wu, J., Richards, C. L., Bossdorf, O., Li, B., et al. (2023). Geographic variation of litter chemistry and palatability in an invasive plant versus its native competitor. *J. Biogeogr* 50, 1139–1150. doi: 10.1111/jbi.14604

Güsewell, S. (2004). N: P ratios in terrestrial plants: variation and functional significance. *New Phytol.* 164, 243–266. doi: 10.1111/j.1469–8137.2004.01192.x

Harvey, J. T., and Leffler, A. J. (2020). Differential stoichiometric homeostasis and growth in two native and two invasive C_3 grasses. *Oecologia* 193, 857–865. doi: 10.1007/s00442-020-04734-5

Heberling, J. M., and Fridley, J. D. (2013). Resource-use strategies of native and invasive plants in Eastern North American forests. *New Phytol.* 200, 523–533. doi: 10.1111/nph.12388

Hu, Y. K., Liu, X. Y., He, N. P., Pan, X., Long, S. Y., Li, W., et al. (2021). Global patterns in leaf stoichiometry across coastal wetlands. *Global Ecol. Biogeogr* 30, 852–869. doi: 10.1111/geb.13254

Huang, W., Siemann, E., Wheeler, G. S., Zou, J., Carrillo, J., and Ding, J. (2010). Resource allocation to defence and growth are driven by different responses to generalist and specialist herbivory in an invasive plant. *J. Ecol.* 98, 1157–1167. doi: 10.1111/j.1365-2745.2010.01704.x

Joshi, J., and Vrieling, K. (2005). The enemy release and EICA hypothesis revisited: incorporating the fundamental difference between specialist and generalist herbivores. *Ecol. Lett.* 8, 704–714. doi: 10.1111/j.1461-0248.2005.00769.x

Ju, R.-T., Li, H., Shang, L., Qiu, S., Li, J., Nie, M., et al. (2017). "Saltmarsh cordgrass *Spartina alterniflora* Loisel," in *Biological invasions and its management in China*, vol. 2 . Eds. F. H. Wan, M. Jiang and A. Zhan (Springer Nature Singapore Private Ltd, Singapore), 187–198.

Ju, R. T., Ma, D., Siemann, E., Liu, X., Wu, J. H., and Li, B. (2019). Invasive *Spartina alterniflora* exhibits increased resistance but decreased tolerance to a generalist insect in China. *J. Pest Sci.* 92, 823–833. doi: 10.1007/s10340-018-1020-y

Kattge, J., Knorr, W., Raddatz, T., and Wirth, C. (2009). Quantifying photosynthetic capacity and its relationship to leaf nitrogen content for global-scale terrestrial biosphere models. *Global Change Biol.* 15, 976–991. doi: 10.1111/j.1365-2486.2008.01744.x

Kerkhoff, A. J., Fagan, W. F., Elser, J. J., and Enquist, B. J. (2006). Phylogenetic and growth form variation in the scaling of nitrogen and phosphorus in the seed plants. *Am. Nat.* 168, E103–E122. doi: 10.1086/507879

Kinlock, N. L., Prowant, L., Herstoff, E. M., Foley, C. M., Akin-Fajiye, M., Bender, N., et al. (2018). Explaining global variation in the latitudinal diversity gradient: meta-analysis confirms known patterns and uncovers new ones. *Global Ecol. Biogeogr* 27, 125–141. doi: 10.1111/geb.12665

Kitajima, K., Llorens, A. M., Stefanescu, C., Timchenko, M. V., Lucas, P. W., and Wright, S. J. (2012). How cellulose-based leaf toughness and lamina density contribute to long leaf lifespans of shade-tolerant species. *New Phytol.* 195, 640–652. doi: 10.1111/j.1469-8137.2012.04203.x

Koerselman, W., and Meuleman, A. F. (1996). The vegetation N:P ratio: a new tool to detect the nature of nutrient limitation. *J. Appl. Ecol.* 33, 1441–1450. doi: 10.2307/2404783

Kooyers, N. J., Blackman, B. K., and Holeski, L. M. (2017). Optimal defense theory explains deviations from latitudinal herbivory defense hypothesis. *Ecology* 98, 1036–1048. doi: 10.1002/ecy.1731

Kurokawa, H., Peltzer, D. A., and Wardle, D. A. (2010). Plant traits, leaf palatability and litter decomposability for co-occurring woody species differing in invasion status and nitrogen fixation ability. *Funct. Ecol.* 24, 513–523. doi: 10.1111/j.1365-2435.2009.01676.x

Leishman, M. R., Haslehurst, T., Ares, A., and Baruch, Z. (2007). Leaf trait relationships of native and invasive plants: community-and global-scale comparisons. *New Phytol.* 176, 635–643. doi: 10.1111/j.1469-8137.2007.02189.x

Li, B., Liao, C. H., Zhang, X. D., Chen, H. L., Wang, Q., Chen, Z. Y., et al. (2009). *Spartina alterniflora* invasions in the Yangtze River estuary, China: an overview of current status and ecosystem effects. *Ecol. Eng.* 35, 511–520. doi: 10.1016/j.ecoleng.2008.05.013

Liu, C., Li, Y., Yan, P., and He, N. (2021). How to improve the predictions of plant functional traits on ecosystem functioning? *Front. Plant Sci.* 12. doi: 10.3389/fpls.2021.622260

Liu, Y., Xu, X., Liu, H., Li, B., and Nie, M. (2020). Latitude gradient variations of leaf functional traits of *Spartina alterniflora* and *Phragmites australis* along the coastal saltmarshes of China. *J. Fudan Univ. (Nat. Sci.)* 59, 381–389.

Minchinton, T. E., Simpson, J. C., and Bertness, M. D. (2006). Mechanisms of exclusion of native coastal marsh plants by an invasive grass. *J. Ecol.* 94, 342–354. doi: 10.1111/j.1365-2745.2006.01099.x

Moles, A. T., Perkins, S. E., Laffan, S. W., Flores-Moreno, H., Awasthy, M., Tindall, M. L., et al. (2014). Which is a better predictor of plant traits: temperature or precipitation? *J. Veg. Sci.* 25, 1167–1180. doi: 10.1111/jvs.12190

Moreira, X., Castagneyrol, B., Abdala-Roberts, L., Berny-Mier y Teran, J. C., Timmermans, B. G., Bruun, H. H., et al. (2018). Latitudinal variation in plant chemical defences drives latitudinal patterns of leaf herbivory. *Ecography* 41, 1124–1134. doi: 10.1111/ecog.03326

Ning, Z., Chen, C., Xie, T., Zhu, Z., Wang, Q., Cui, B., et al. (2021). Can the native faunal communities be restored from removal of invasive plants in coastal ecosystems? A global meta-analysis. *Global Change Biol.* 27, 4644–4656. doi: 10.1111/gcb.15765

Ning, Z., Cui, B., Chen, C., Xie, T., Gao, W., Zhang, Y., et al. (2024). Tidal channel meanders serve as stepping-stones to facilitate cordgrass landward spread by creating invasion windows. *Ecol. Appl.* 34, e2813. doi: 10.1002/eap.2813

Pennings, S. C., Ho, C. K., Salgado, C. S., Więski, K., Davé, N., Kunza, A. E., et al. (2009). Latitudinal variation in herbivore pressure in Atlantic Coast salt marshes. *Ecology* 90, 183–195. doi: 10.1111/j.1365–2486.2011.02636.x

Pyšek, P., Jarošík, V., Hulme, P. E., Pergl, J., Hejda, M., Schaffner, U., et al. (2012). A global assessment of invasive plant impacts on resident species, communities and ecosystems: the interaction of impact measures, invading species' traits and environment. *Global Change Biol.* 18, 1725–1737. doi: 10.1111/j.1365-2486.2011.02636.x

R Core Team (2019). *R: a language and environment for statistical computing* (Vienna: R for Statistical Computing).

Reese, A. T., Ames, G. M., and Wright, J. P. (2016). Variation in plant response to herbivory underscored by functional traits. *PloS One* 11, e0166714. doi: 10.1371/journal.pone.0166714

Reich, P. B., and Oleksyn, J. (2004). Global patterns of plant leaf N and P in relation to temperature and latitude. *P. Natl. Acad. Sci.* 101, 11001–11006. doi: 10.1073/pnas.040358810

Rogers, A., Allen, D. J., Davey, P. A., Morgan, P. B., Ainsworth, E. A., Bernacchi, C. J., et al. (2004). Leaf photosynthesis and carbohydrate dynamics of soybeans grown throughout their life-cycle under free-air carbon dioxide enrichment. *Plant Cell Environ.* 27, 449–458. doi: 10.1111/j.1365-3040.2004.01163.x

Sala, O. E., Stuart Chapin, F. I. I. I., Armesto, J. J., Berlow, E., Bloomfield, J., Dirzo, R., et al. (2000). Global biodiversity scenarios for the year 2100. *Science* 287, 1770–1774. doi: 10.1126/science.287.5459.1770

Schädler, M., Jung, G., Auge, H., and Brandl, R. (2003). Palatability, decomposition and insect herbivory: patterns in a successional old-field plant community. *Oikos* 103, 121–132. doi: 10.1034/j.1600–0706.2003.12659.x

Silliman, B. R., and Bertness, M. D. (2004). Shoreline development drives invasion of Phragmites australis and the loss of plant diversity on New England salt marshes. *Conserv. Biol.* 18, 1424–1434. doi: 10.1111/j.1523-1739.2004.00112.x

Tang, X., Zhao, X., Bai, Y., Tang, Z., Wang, W., Zhao, Y., et al. (2018). Carbon pools in China's terrestrial ecosystems: New estimates based on an intensive field survey. *Proc. Natl. Acad. Sci*. 115, 4021-4026. doi: 10.1073/pnas.1700291115

Tian, D., Yan, Z., Niklas, K. J., Han, W., Kattge, J., Reich, P. B., et al. (2018). Global leaf nitrogen and phosphorus stoichiometry and their scaling exponent. *Natl. Sci. Rev.* 5, 728–739. doi: 10.1093/nsr/nwx142

Vilà, M., Corbin, J. D., Dukes, J. S., Pino, J., and Smith, S. D. (2007). "Linking plant invasions to global environmental change," in *Terrestrial ecosystems in a changing world* (Springer Berlin Heidelberg, Berlin, Heidelberg), 93–102.

Vilà, M., Espinar, J. L., Hejda, M., Hulme, P. E., Jarošík, V., Maron, J. L., et al. (2011). Ecological impacts of invasive alien plants: a meta-analysis of their effects on species, communities and ecosystems. *Ecol. Lett.* 14, 702–708. doi: 10.1111/ele.2011.14.issue-7

Waller, G. R. (2012). *Alkaloid biology and metabolism in plants*. (New York and London: Springer Science & Business Media).

Wang, J., Wang, X., Ji, Y., and Gao, J. (2022). Climate factors determine the utilization strategy of forest plant resources at large scales. *Front. Plant Sci.* 13. doi: 10.3389/fpls.2022.990441

Xu, X., Liu, H., Liu, Y., Zhou, C., Pan, L., Fang, C., et al. (2020). Human eutrophication drives biogeographic salt marsh productivity patterns in China. *Ecol. Appl.* 30, e02045. doi: 10.1002/eap.2045

Xu, X., Wei, S., Chen, H., Li, B., and Nie, M. (2022). Effects of Spartina invasion on the soil organic carbon content in salt marsh and mangrove ecosystems in China. *J. Appl. Ecol.* 59, 1937–1946. doi: 10.1111/1365-2664.14202

Zhang, Y., Pennings, S. C., Liu, Z., Li, B., and Wu, J. (2021). Consistent pattern of higher lability of leaves from high latitudes for both native *Phragmites australis* and exotic *Spartina alterniflora*. *Funct. Ecol.* 35, 2084–2093. doi: 10.1111/1365-2435.13826

Zhu, D., Hui, D., Wang, M., Yang, Q., and Yu, S. (2020). Light and competition alter leaf stoichiometry of introduced species and native mangrove species. *Sci. Total Environ.* 738, 140301. doi: 10.1016/j.scitotenv.2020.140301

Zvereva, E. L., and Kozlov, M. V. (2022). Meta-analysis of elevational changes in the intensity of trophic interactions: Similarities and dissimilarities with latitudinal patterns. *Ecol. Lett.* 25, 2076–2087. doi: 10.1111/ele.14090

frontiers | Frontiers in Marine Science

TYPE Original Research
PUBLISHED 31 July 2024
DOI 10.3389/fmars.2024.1432106

OPEN ACCESS

EDITED BY
Qin Zhu,
Southern Marine Science and Engineering Guangdong Laboratory (Guangzhou), China

REVIEWED BY
Peng Zhao,
Hainan University, China
Chao Liu,
Sichuan University, China

*CORRESPONDENCE
Yujun Yi
yiyujun@bnu.edu.cn

RECEIVED 13 May 2024
ACCEPTED 24 June 2024
PUBLISHED 31 July 2024

CITATION
Yi Y, Zhao F, Hou C, Zhang C and Tang C (2024) Mechanism and threshold of environmental stressors on seagrass in high-turbidity estuary: case of *Zostera japonica* in Yellow River Estuary, China.
Front. Mar. Sci. 11:1432106.
doi: 10.3389/fmars.2024.1432106

Mechanism and threshold of environmental stressors on seagrass in high-turbidity estuary: case of *Zostera japonica* in Yellow River Estuary, China

Yujun Yi[1,2]*, Fanxuan Zhao[1], Chuanying Hou[1], Chengxiang Zhang[1] and Caihong Tang[3]

[1]State Key Laboratory of Water Environmental Simulation, School of Environment, Beijing Normal University, Beijing, China, [2]Ministry of Education Key Laboratory of Water and Sediment Science, School of Environment, Beijing, China, [3]North China Electric Power University, Beijing, China

Zostera japonica (*Z. japonica*), the most widely distributed seagrass species in temperate estuaries, has experienced a dramatic decline of nearly 75% over the past decade. While previous research has investigated the adaptation of seagrass individuals and populations to single stress factors, the molecular mechanisms underlying the interaction of multiple stressors remain poorly understood. This study conducted laboratory experiments to examine the response of *Z. japonica* at different life stages to environmental pressures, specifically salinity and turbidity, as indicated by changes in free amino acids (FAAs). The results demonstrate that *Z. japonica* exhibits stronger adaptability to high salinity environments but displays weaker adaptability to freshwater conditions. Through single stress experiments, the salinity and turbidity thresholds for FAA homeostatic disturbance in *Z. japonica* were determined at seedling, juvenile, and mature stages. As *Z. japonica* matures, its metabolic pathways expand and diversify, allowing the regulation of key FAAs to enhance stress resistance. Turbidity stress exerts a more pronounced negative impact on the cellular homeostasis of *Z. japonica* compared to salinity stress, and when turbidity levels exceed 150 NTU, they significantly intensify the negative effects of salinity stress on the seagrass. Furthermore, under strong salinity-turbidity interactions, the concentration of key FAAs generally decreases by 20-30%, indicating inhibition of growth and development in *Z. japonica*. These findings have important implications for the conservation of intertidal seagrass beds and estuarine ecosystems in the face of multiple human activities and environmental stressors. The study provides valuable insights into the molecular mechanisms underlying *Z. japonica*'s adaptations to salinity and turbidity stress, contributing to the development of targeted strategies to mitigate the impacts of environmental pressures on seagrass populations and promote the resilience of these critical marine ecosystems.

KEYWORDS

***Zostera japonica*, free amino acids, salinity, turbidity, cumulative effects, seagrass conservation**

1 Introduction

Seagrass, a marine angiosperm that thrives in the intertidal and subtidal zones of temperate and tropical coasts, plays a pivotal role as one of the most important primary producers in coastal ecosystems. Seagrass beds are among the most productive and ecologically valuable coastal ecosystems, providing a wide range of essential services (Orth et al., 2006; Short et al., 2007). These underwater meadows contribute significantly to water quality improvement by reducing suspended particles and removing excess nutrients from the water column and sediments. Moreover, seagrass beds act as natural barriers that attenuate wave energy and mitigate coastal erosion (Cornelisen and Thomas, 2006). In addition to their physical benefits, seagrass beds serve as critical habitats for a diverse array of marine species and provide food sources in the form of leaves, detritus, and epiphytes (Barbier et al., 2011).

Zostera japonica, a eurythermal seagrass species, exhibits a wide distribution along the northwestern Pacific Coast, spanning from the temperate regions of Russia to the tropical waters of southern Vietnam. The Yellow River Delta in China boasts the largest intertidal *Z. japonica* meadow in the country, covering an impressive area of over 1000 hectares (Zhang et al., 2020). This species is characterized by its well-developed and creeping rhizome, which enables both asexual reproduction through underground stems and sexual reproduction via seed germination. As a perennial angiosperm, *Z. japonica* predominantly inhabits the upper reaches of the intertidal zone. The ecological significance of *Z. japonica* lies in its ability to sequester carbon dioxide, store nutrients in sediments, and enhance dissolved oxygen levels in the water column (Park et al., 2011). Furthermore, this species serves as a valuable bioindicator for assessing water eutrophication levels (Han et al., 2017).

Recent studies have highlighted the importance of understanding the factors that influence the growth and distribution of *Z. japonica* in the Yellow River Delta. Environmental variables such as temperature, salinity, light availability, and sediment characteristics have been identified as key drivers of seagrass productivity and spatial patterns (Han et al., 2017; Zhang et al., 2020). Additionally, anthropogenic pressures, including coastal development, pollution, and climate change, pose significant threats to the long-term stability and resilience of these valuable ecosystems (Orth et al., 2006; Short et al., 2007).

Despite their ecological importance, seagrass beds have experienced a significant decline at an alarming annual rate of 7% worldwide since the 1990s, primarily due to the impacts of global warming and human activities (Waycott et al., 2009). *Z. japonica*, in particular, has been widely threatened and has undergone a dramatic decrease in its native range, especially in China (Zhang et al., 2020). In the last decade, the *Z. japonica* seagrass bed area in the Yellow River Delta has degraded by nearly 75% due to increasing human activities, the invasion of *Spartina alterniflora*, and extreme climate events (Zhou et al., 2022; Gao et al., 2023). Consequently, the protection and restoration of seagrass beds have become extremely pressing and challenging.

Previous studies have demonstrated that *Z. japonica* possesses strong self-defense mechanisms to mitigate the damage caused by salinity stress, with its salt tolerance mainly dependent on various physiological and biochemical processes (Canalejo et al., 2014). High salinity poses a significant obstacle to the survival and growth of seagrass by reducing the water potential of leaves and increasing the difficulty of maintaining growth (Cambridge et al., 2017; Blanco-Murillo et al., 2023). Prolonged exposure to saline stress can alter the photosynthetic and respiratory metabolism in seagrass, impairing the carbon balance and leading to complex photosynthetic adjustments (Sandoval-Gil et al., 2014).

In addition to salinity, light is another critical eco-factor influencing the growth of *Z. japonica*. Sediments from land can cause changes in light transmittance (Cussioli et al., 2020), and Hou et al. (2020) found a clear linear relationship between the height and biomass of *Z. japonica* and water turbidity. However, compared to subtidal species, *Z. japonica* exhibits a stronger adaptability to turbidity stress (Shafer and Kaldy, 2014). Under low light conditions, *Z. japonica* increases shoot height and chlorophyll concentration to enhance photosynthetic performance (Kim et al., 2020).

Free amino acids (FAAs) are sensitive to environmental stresses such as drought and cold and can serve as biological indicators to measure the effect of environmental disturbances. Song et al. (2012) discovered that *Z. japonica* typically increases the content of relevant amino acids to stimulate the accumulation of stress-responsive proteins, thereby enhancing its tolerance to stress. Chou et al. (2019) also used FAAs to monitor the stoichiometric characteristics of aquatic *Z. japonica*, finding that the free amino acid content in *Z. japonica* is related to the availability of carbon dioxide and light in the water. These 17 FAAs likely contribute to different aspects of plant defense mechanisms. For instance, proline (Pro) generally increases in response to osmotic and salt stress, while leucine, a branched-chain amino acid, plays a crucial role as an osmotic regulator in plant stress resistance. Methionine (Met) from the aspartate pathway can stimulate metabolic and transcriptomic responses associated with drought stress and mitochondrial energy metabolism, enhancing tolerance to abiotic stressors. Furthermore, the metabolism of cysteine (Cys) is associated with biological pathways such as protein synthesis, DNA repair, and antioxidant responses. Therefore, exploring the response mechanisms of seagrasses to environmental stress by analyzing the metabolism of amino acid components is essential for understanding their adaptations and resilience.

The Yellow River Estuary (YRE) is characterized by complex flow, sediment, and salinity conditions, and is home to an extensive seagrass bed. The annual distribution of water and sediment fluxes from the Yellow River (YR) is extremely uneven. During the flood season, surged runoff with high sediment is injected into the estuary, dramatically reducing salinity and increasing turbidity in the YRE. This unique environment makes the YRE an ideal experimental field for exploring the adaptive mechanisms of *Z. japonica* to salinity and turbidity stress. Through laboratory control experiments, this study aims to answer the following questions: 1) What is the effect mechanism of individual eco-factors on amino

acid homeostasis in *Z. japonica*? 2) What is the synergistic influence mechanism of multiple eco-factors on *Z. japonica* at the molecular level? and 3) What are the responses of *Z. japonica* at different growth stages? To address these questions, *Z. japonica* plants were collected at seedling, juvenile, and mature stages. Stress experiments were conducted under six salinity gradients (0 ppt [fresh water], 5 ppt, 10 ppt, 20 ppt [control group], 25 ppt, and 35 ppt [seawater]) and six turbidity gradients (0 NTU [control group], 50 NTU, 100 NTU, 150 NTU, 200 NTU, and 250 NTU). The concentration of each FAA was determined, and the response mechanisms of *Z. japonica* at different growth stages to external stresses (salinity and turbidity) were further analyzed. This comprehensive approach will provide valuable insights into the adaptations and resilience of *Z. japonica* to the dynamic environmental conditions in the Yellow River Estuary (YRE), contributing to the development of effective conservation and management strategies for this important seagrass species.

2 Materials and methods

2.1 Study area

YRE is located in Dongying, Shandong Province, where the Yellow River discharges into the Bohai Sea (Figure 1). In 2015, the largest seagrass bed of *Z. japonica* in China, covering an area of 1031.8 hectares, was discovered in the intertidal zone of the YRE (Zhou et al., 2015, Zhou et al., 2016). This seagrass bed is interspersed with the invasive species *Spartina alterniflora* and stretches 25-30 km along the coast on both the north and south sides of the estuary, with a width of 200-500 m from the shoreline to the sea. The *Z. japonica* bed provides essential food sources (Li et al., 2019) and habitats for various wetland birds, such as Cygnus, Grus, and Ciconia, as well as fishes and invertebrates.

2.2 Experiment materials

Seagrasses with similar growth (approximately 1000 *Z. japonica*/m^2) were collected from less disturbed tidal flats on the northern shore of the YRE (119°15′10.25′′E, 37°44′17.04′′N), in an area with minimal influence from inflow, as shown in Figure 1. Monitoring of water salinity and turbidity was conducted on-site using the YSI (EXO multiparameter water quality monitor) (Supplementary Table S1). The sampling zone consisted of three belts, each with three sampling points evenly set 50 m apart. At each sampling point, a 1m×1m quadrat was arranged (Figures 1B, 2). Samples were collected during three growth stages: seedling stage (March to April), juvenile stage (May to June), and mature stage (July to August). To minimize ecological damage in the sample area and ensure practicality, the sampling number was kept small. Reusable PP planting basins with 0.8 mm thickness, 6.0 cm bottom diameter, and 8.0 cm height were selected based on the size of the sample area. During sampling, whole *Z. japonica* plants were collected to maintain the integrity of the root system, with approximately 10 plants in each pot covered with topsoil. The pots were placed indoors for a week of preculture, and *Z. japonica* plants with better adaptation were selected and cultivated under improved ventilation and light conditions for a ten-day control experiment.

In this experiment, locally produced marine crystals (origin: Jinan Huili Chemical Technology Co., Ltd., Gudao Town, Hekou District, Dongying City, Shandong Province, China) were used to prepare experimental water with different salinity levels. The marine crystals did not contain nutrients such as nitrogen and phosphorus. Surface sediments were collected from the growing area of *Z. japonica* on the northern shore of the YRE. The sediments were dried, crushed, and sieved through a 100-mesh sieve (< 150 μm) to set different turbidity gradients. This approach ensured that the experimental conditions closely mimicked the natural environment of *Z. japonica*, allowing for

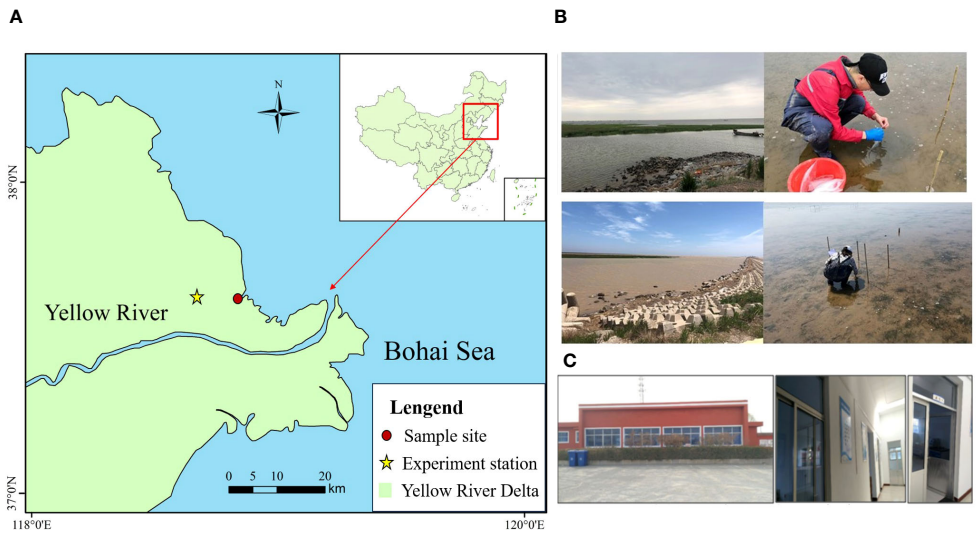

FIGURE 1
Location of the *Zostera japonica* sampling site and experiment station in the Yellow River Delta. **(A)** Study area; **(B)** The sampling setting of *Zostera japonica*; **(C)** Experiment station.

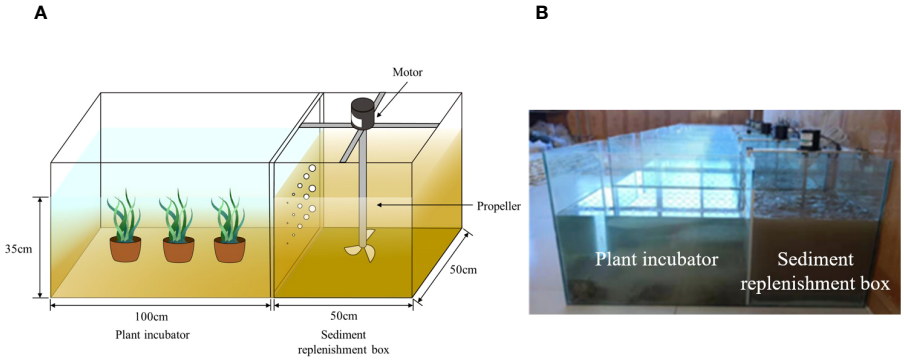

FIGURE 2
Experimental installation **(A)** Schematic diagram of the equipment and experiment. **(B)** Photo of the equipment and experiment.

a more accurate assessment of the species' adaptations to salinity and turbidity stress.

2.3 Experimental design

The laboratory control experiment was conducted at the Yellow River Estuary Wetland Ecosystem Field Scientific Observation and Research Station in Dongying City, Shandong Province (Figure 1). The experimental setup consisted of a water-sand mixing box and an experimental reaction box, both made of 5-mm-thick glass with good transparency. A propeller at the bottom of the glass box, driven by an engine, rotated to ensure thorough mixing of water and sediment. The suspended sediment from the disturbed water flow entered the reaction box through pores, forming different turbidity gradients. During the experiment, the water depth was maintained at 35 cm, and the turbidity in the reaction chamber was adjusted every 4 h. The motor speed was set at 110 r/min, and 15 holes were evenly distributed in a 5/row × 3 rows pattern in the glass between the water-sand mixing box and the experimental reaction box. The hole diameters were 0.2 cm, 0.5 cm, 1.0 cm, 1.2 cm, and 1.5 cm. Figures 2A and 2B illustrate the experimental apparatus.

Based on the actual possible stress range, the experiment included six salinity gradients and six turbidity gradients. The control group was grown in water with a salinity of 20 ppt and a turbidity of 0 NTU, which is considered the most suitable salinity for *Z. japonica* growth (Shafer et al., 2011; Hou et al., 2020). The salinity gradients were divided into two groups: low salinity (0 ppt, 5 ppt, and 10 ppt) and high salinity (25 ppt and 35 ppt). The turbidity gradients were set at 50 NTU, 100 NTU, 150 NTU, 200 NTU, and 250 NTU. Throughout the experiment, the water temperature was maintained at approximately 25°C, consistent with the local temperature, and no nutrients were added. After treating the experimental plants, three planting pots were collected from each experimental device, and the number of surviving *Z. japonica* in each pot was counted. The surviving *Z. japonica* were isolated and washed with distilled water to determine the composition and content of FAAs. The use of multiple salinity and turbidity gradients, along with the inclusion of a control group, allows for a comprehensive assessment of *Z. japonica*'s adaptations to these stressors.

2.4 Free amino acids determination

The collected *Z. japonica* samples were dried in an oven at 70°C until they reached a constant weight. The dried samples were then crushed and filtered through a 250 µm (60 mesh) sieve. A 50 mg portion of each sample was weighed and placed into a 3 ml centrifuge tube, followed by the addition of 1.5 ml of 5% sulfosalicylic acid solution. The samples were centrifuged at 10,000 r/min for 20 min at 20°C. The supernatant was collected and diluted twice with 0.02 mol·L-1 hydrochloric acid solution. The content of FAAs was determined using a Biochrom 30+ automatic amino acid analyzer (BIOCHROM, UK). The experiment utilized the 17 kinds of amino acid mixture standard material GBW(E) 100062 (China, China Institute of Metrology) as the standard solution. The 17 kinds of FAAs in *Z. japonica* tissue were determined, as shown in Supplementary Table S2.

2.5 Data analysis

One-way ANOVA with the least significant difference (LSD) test was employed to assess the significant differences in FAAs of *Z. japonica* under different turbidity and salinity gradients at 95% ($P < 0.05$) and 99% confidence levels ($P < 0.01$). Additionally, two-way analysis of variance was used to analyze the differences in the effects of turbidity-salinity interactions on FAAs in *Z. japonica* at 95% ($P < 0.05$) and 99% confidence levels ($P < 0.01$). These statistical analyses were performed using SPSS 24.0 software (SPSS Inc., Chicago, IL, USA).

Changes in the 17 FAAs of *Z. japonica* at different growth stages under critical salinity/turbidity conditions were analyzed. First, the top 6 FAAs with the highest concentrations in the control group were identified. Then, the key FAAs that played major coordinating roles were determined based on their fold change (FC) values under critical stress conditions. Linear and non-linear trend tests for the

10.3389/fmars.2024.1432106

key FAAs were conducted to reveal the regulatory mechanisms of *Z. japonica* under single and interactive stresses using the R package "ggtrendline" (Version 4.3.1) (Greenwell and Kabban, 2014).

Based on their biosynthetic pathways, the 17 FAAs measured in the experiment were divided into five groups: (1) glutamic-group amino acids (Glu group), containing Glutamic (Glu), Proline (Pro), and Arginine (Arg); (2) aspartate-group amino acids (Asp group), containing Aspartate (Asp), Lysine (Lys), Methionine (Met), and Threonine (Thr); (3) branched-chain amino acids (BCAAs), containing Valine (Val), Leucine (Leu), and Isoleucine (Ile); (4) aromatic-group amino acids (AAAs), containing L-Phenylalanine (Phe), Tyrosine (Tyr), and Histidine (His); and (5) serine-group amino acids (Ser group), containing Glycine (Gly), Serine (Ser), Alanine (Ala), and L-Cysteine (Cys). The composition and content of amino acids in *Z. japonica* tissues under different salinity and turbidity treatments were further analyzed to gain insights into the species' adaptive responses.

3 Result

3.1 Effects of salinity and turbidity on the composition of FAAs

The content and composition of FAAs in *Z. japonica* varied significantly across the three growth stages. As a starting point for investigating the regulatory mechanisms during salinity/turbidity stress, the FAA content and composition of the control group, grown under optimal conditions (salinity at 20 ppt, turbidity at 0 NTU), were analyzed to establish a baseline understanding of their status in the absence of stress (Figure 3). Under optimal conditions, the total amount of FAAs in *Z. japonica* was lowest (12.16 mg/g) at the seedling stage and highest (31.30 mg/g) at the juvenile stage. The composition of FAAs in *Z. japonica* was mainly composed of the Glu group, Asp group, and Ser group. However, the proportion of each amino acid group varied greatly at different growth stages. During the transition from the seedling stage to the mature stage, there was a gradual decrease in the proportion of the Glu group, while that of the Ser group increased.

3.2 Response of FAAs to single stress

Compared to the control group, the stress threshold of *Z. japonica* at different growth stages was determined. When the salinity was 10 ppt, the content of FAAs in the seedling stage significantly decreased ($p < 0.01$), indicating the occurrence of salinity stress (Figure 4A). However, *Z. japonica* at the mature stages only showed salinity stress when the salinity decreased to 0 ppt (Figures 4B, C). Under high salt treatment, FAAs of seedling *Z. japonica* significantly increased at a salinity of 25 ppt ($p < 0.01$) (Figure 4A), indicating hypersaline stress. Interestingly, there were no significant changes in FAAs in juvenile and mature *Z. japonica* under high-salinity treatment (Figures 4B, C). Under the optimal salinity condition (20 ppt), the differences in the total content of FAAs in *Z. japonica* were analyzed between turbidity-free and different turbidity gradients. When the turbidity reached 100 NTU, FAAs in *Z. japonica* significantly increased, indicating an apparent turbidity stress (Figure 4). It indicated that a turbidity level of 100 NTU represents a critical threshold for *Z. japonica*, irrespective of growth stage.

3.3 Cumulative effects under salinity-turbidity interaction treatment

The interaction between salinity and turbidity had a cumulative effect on *Z. japonica*. Two-way ANOVA (Table 1) was used to determine the effect size of salinity, turbidity, and salinity-turbidity interaction, represented by partial eta squared (η^2). Compared to the single-stress treatments, salinity-turbidity interaction had a stronger explanatory power for the variations in FAAs of *Z. japonica* at the seedling and juvenile stages. At the seedling stage, the content of FAAs in *Z. japonica* was the lowest and fluctuated sharply with changes in salinity and turbidity (Figure 4A). At the juvenile stage, increased water turbidity exacerbated the stress of salinity on *Z. japonica*. With a 100 NTU turbidity treatment, FAAs of *Z. japonica* in the juvenile stage showed a significant decrease under 25 ppt salinity ($p < 0.05$), which was not observed under turbidity-free conditions. For mature *Z. japonica*, turbidity stress

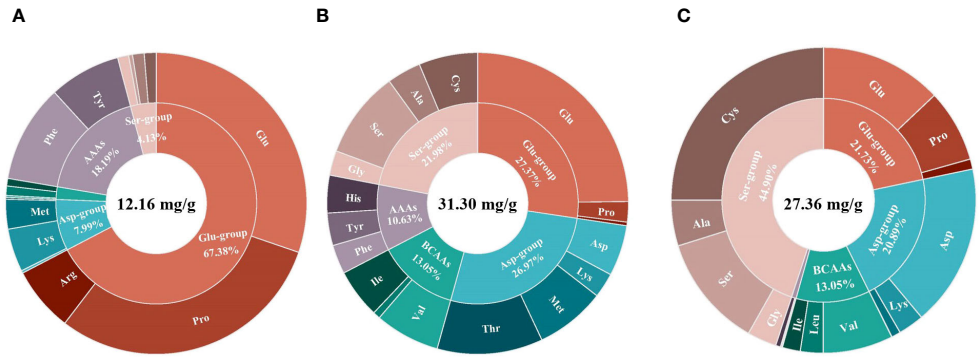

FIGURE 3
The proportion of FAAs in *Z. japonica* under different salinity and turbidity treatments. **(A)** Seedling stage. **(B)** Juvenile stage. **(C)** Mature stage.

10.3389/fmars.2024.1432106

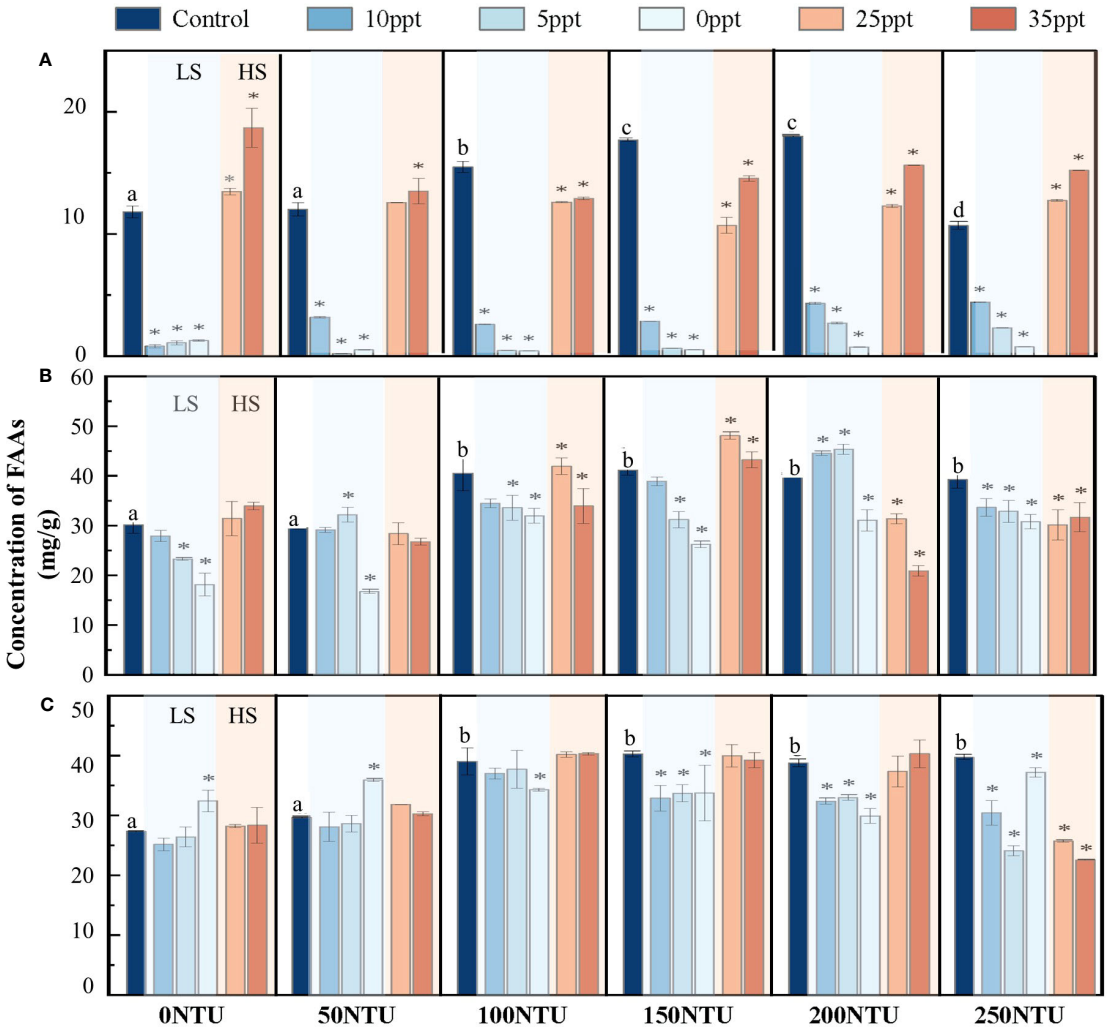

FIGURE 4
Changes of total concentration of FAAs in *Z. Japonica* at different growth stages under different salinity gradients. **(A)** Seedling stage. **(B)** Juvenile stage. **(C)** Mature stage. One-way ANOVA was constructed between control group and each experiment group: "*" represents FAAs concentration in this salinity condition significantly different from that in control group [95% confidence level]; Alphabet (e.g. a, b, c, ...) represents FAAs concentration in this turbidity condition significantly different from that in control group [95% confidence level].

contributed more to the changes in FAAs than salinity stress and salinity-turbidity interaction (Table 1). FAAs were relatively higher under the treatment of high salinity-medium turbidity (Figure 4C). Furthermore, at a turbidity of 150 NTU, the impact of salt stress on mature *Z. japonica* was intensified.

These findings highlight the complex interplay between salinity and turbidity in shaping the stress responses of *Z. japonica* at different growth stages. The stronger explanatory power of salinity-turbidity interaction for FAA variations in seedling and juvenile plants suggests that these earlier life stages are more sensitive to the cumulative effects of multiple stressors. The sharp fluctuations in FAA content under varying salinity and turbidity levels at the seedling stage further support this notion of heightened sensitivity during early development. The observation that increased turbidity exacerbates the impact of salinity stress on juvenile *Z. japonica* underscores the importance of considering the synergistic effects of environmental factors when assessing the adaptive capacity of this species. The significant decrease in FAAs under high salinity (25 ppt) and moderate turbidity (100 NTU) conditions, which was not detected under turbidity-free conditions, indicates that the combined stress exceeds the tolerance threshold of juvenile plants, leading to a more pronounced metabolic response.

In contrast, the greater contribution of turbidity stress to FAA changes in mature *Z. japonica* suggests a shift in the relative importance of individual stressors as the plants age. The higher FAA levels observed under high salinity-medium turbidity and medium salinity-high turbidity treatments in mature plants may reflect an adaptive response to maintain osmotic balance and protect cellular functions under these challenging conditions.

3.4 Recognition of key FAAs involved with stress resistance

Considering that high turbidity treatment exacerbated the effect of salinity stress on *Z. japonica*, the differences in the change trends

10.3389/fmars.2024.1432106

TABLE 1 Statistical results of the two-way ANOVA analyses examining the effects of Salinity (S), Turbidity (T) and Salinity-turbidity interaction (S*T) treatment on the content of FAAs in *Z. Japonica*.

Stage	Factor	Freedom	FAA		Glu group		Asp group		BCAAs		AAAs		Ser group	
			F	η^2	F	η^2	F	η^2	F	η^2	F	η^2	F	η^2
Seedling stage	S	5	133.539**	0.949	1111.170**	0.994	423.695**	0.983	150.603**	0.954	15.652**	0.685	45.591**	0.864
	T	5	28.464**	0.798	513.025**	0.986	144.580**	0.953	74.882**	0.912	32.191**	0.817	12.170**	0.628
	S*T	25	44.629**	0.969	750.854**	0.998	128.290**	0.989	38.287**	0.964	16.941**	0.922	14.552**	0.910
Juvenile stage	S	5	5.041**	0.412	6.446**	0.472	11.486**	0.615	12.761**	0.639	34.274**	0.826	15.402**	0.681
	T	5	6.855**	0.488	66.134**	0.902	2.578*	0.264	43.895**	0.859	28.067**	0.796	23.295**	0.764
	S*T	25	2.564**	0.640	19.581**	0.931	11.531**	0.889	23.890**	0.943	12.796**	0.899	4.899**	0.773
Mature stage	S	5	1.930	0.211	4.819**	0.401	0.533	0.069	0.764	0.096	1.750	0.196	0.928	0.114
	T	5	13.09**	0.645	27.831**	0.794	8.686**	0.547	1.617	0.183	6.080**	0.458	4.294**	0.374
	S*T	25	1.245	0.464	2.661**	0.649	1.085	0.430	0.980	0.405	1.238	0.462	2.025*	0.584

η^2 represents the effect size, **represents significant correlation at 99% confidence level (2- tailed), *represents significant correlation at 95% confidence level (1-tailed).

of regulatory FAAs under single salinity stress and interactive stress were compared to reveal the regulatory mechanisms of *Z. japonica* under interactive stress. For *Z. japonica* at the seedling stage, Pro, Met, and Val served as the key regulatory FAAs (Figure 5). Under turbidity stress, the concentrations of Met (FC=2.63) and Val (FC=3.15) initially increased and then decreased with increasing turbidity, exceeding twice that of the control group at the critical point (100 NTU) (Figures 5, 6A). Under low salinity conditions, all FAAs decreased to nearly 0. Under high salinity stress, the concentrations of 14 FAAs, primarily Val (FC=1.54), Pro (FC=1.58), and Met (FC=1.79), increased (Figure 6B). Under salinity-turbidity interaction, the contents of the three key FAAs decreased overall and exhibited a decreasing trend with increasing intensity of salinity stress (Figure 6C).

For *Z. japonica* at the juvenile stage, the key regulatory FAAs were Cys, Thr, Val and Glu. Under the critical turbidity condition (100 NTU), Cys (FC=7.20) and Met (FC=2.13) concentrations were up-regulated, while Glu concentration was down-regulated by 2/3 (Figure 7). Under single turbidity stress, Cys concentration first increased and then decreased with increasing turbidity, while Glu concentration showed an opposite trend, with a turning point at 150 NTU (Figure 8A). Under single salinity stress, FAA concentrations generally decreased (Figure 8B). Under freshwater conditions, only a few FAAs showed an increase, with Cys (FC=2.43) concentration reaching more than double that of the control group (Figure 7). Under high salinity stress, concentrations of Val (FC=1.89) and Thr (FC=1.82) increased, while Cys showed an opposite trend (Figure 8B). With the salinity-turbidity interaction treatment (turbidity at 150 NTU), the variations in Cys and Val concentrations were significantly influenced by turbidity stress, exhibiting altered patterns. Cys concentration showed a significant decreasing trend in response to hypersaline stress, while Val concentration showed an opposite trend (Figure 8C).

For mature *Z. japonica*, the key regulatory FAAs were Ser, Glu and Pro. When turbidity stress (150 NTU) occurred, Pro (FC=2.84) played a major regulating role and was positively correlated with water turbidity (Figures 9, 10A). The concentrations of other main FAAs fluctuated less. When salinity stress occurred at 0 ppt, most FAAs exhibited an upward trend. Notably, Ser (FC=2.44) and Glu (FC=1.91) played crucial roles in the resistance to salinity stress, as they were up-regulated with decreasing salinity levels (Figure 10B). However, the interaction exacerbated the impact of salinity stress, as evidenced by the contrasting trends in Ser and Glu concentrations and an overall decrease (Figure 10C). Interestingly, high turbidity-high salinity conditions increased the performance levels of key FAAs.

4 Discussion

Z. japonica, an intertidal seagrass species, has evolved remarkable adaptations to the highly variable environmental conditions in its habitat, exhibiting high desiccation tolerance, salinity adaptation, and light adaptation (Shafer and Kaldy, 2014; Kim et al., 2020). As crucial organic solutes, amino acids play a pivotal role in *Z. japonica*'s ability to cope with stress conditions by

10.3389/fmars.2024.1432106

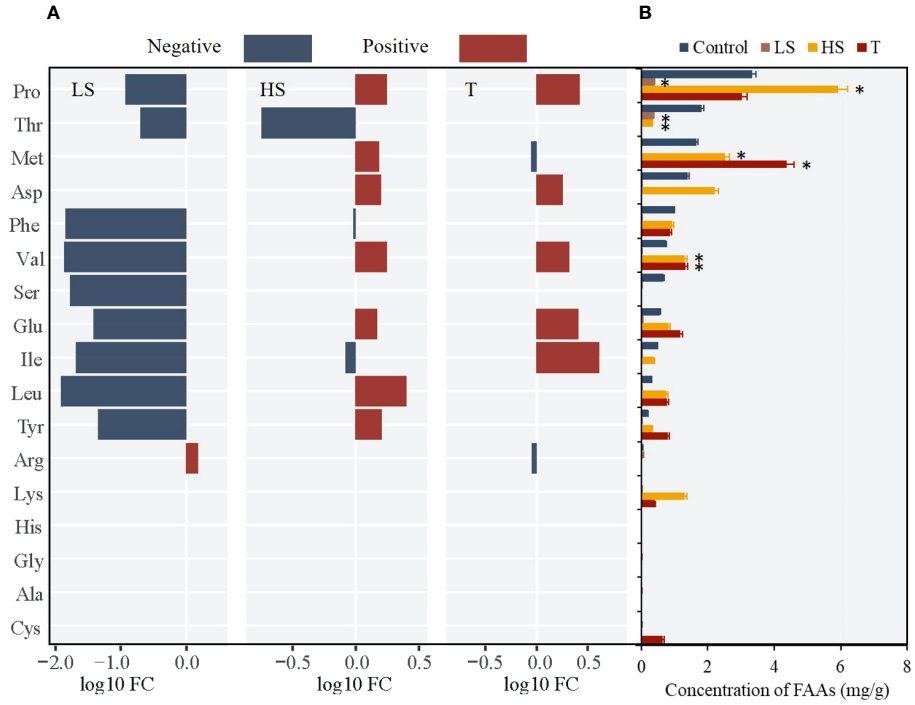

FIGURE 5
Changes of 17 FAAs in seedling *Z. Japonica* with low salinity (LS), high salinity (HS) and turbidity(T) treatments comparing with control group (* represents significant differences of major FAAs contents between experimental group and control group).

participating in osmotic pressure adjustments, photogrammetry responses, and nitrogen metabolism maintenance (Sandoval-Gil et al., 2014; Cambridge et al., 2017). The composition of amino acid groups in *Z. japonica* varies significantly across its life cycle, reflecting the changing metabolic demands and physiological processes associated with each growth stage. In the seedling stage, glutamic acid group (Glu group) constitutes more than 30% of the total amino acid content (Figure 3), which can be attributed to the

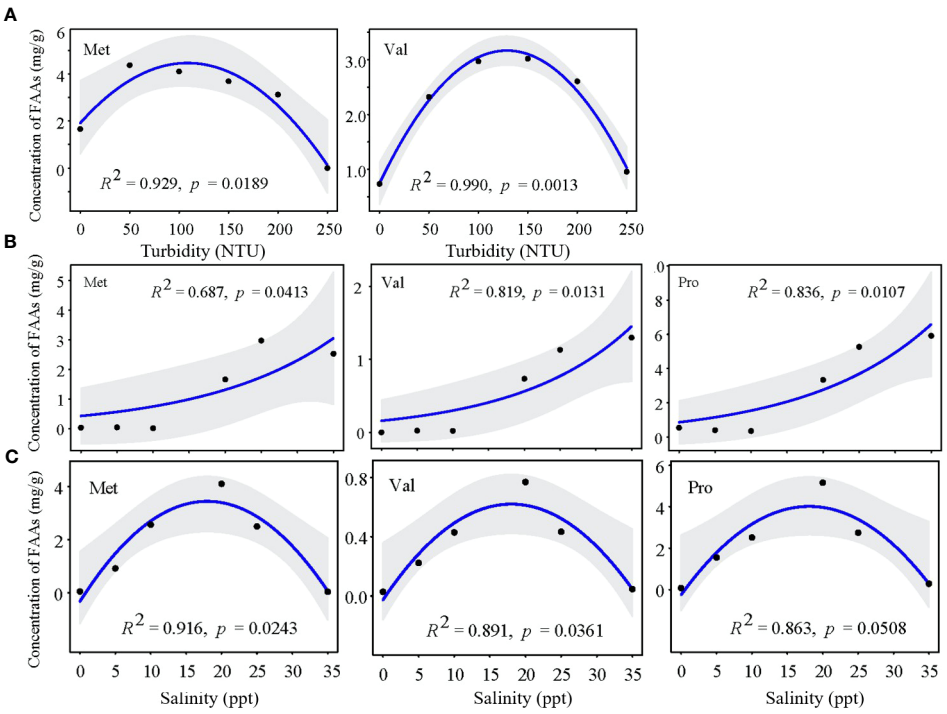

FIGURE 6
Change trend in key FAAs of seedling *Z. Japonica* with **(A)** turbidity, **(B)** salinity and **(C)** salinity-turbidity interaction treatments(Turbidity = 100NTU).

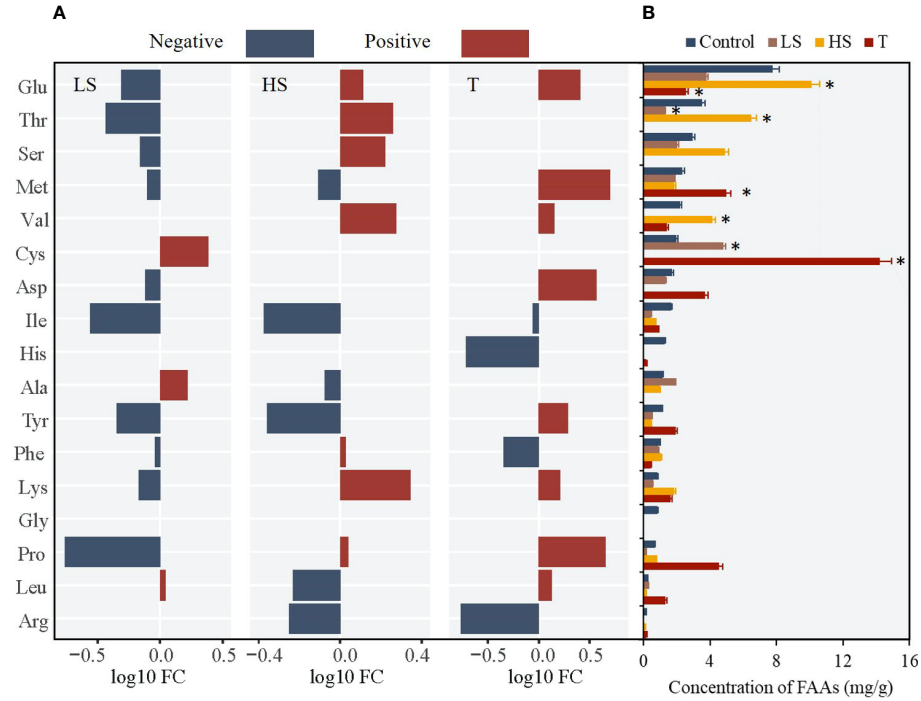

FIGURE 7
Changes of 17 FAAs in juvenile *Z. Japonica* with low salinity (LS), high salinity (HS) and turbidity(T) treatments comparing with control group (* represents significant differences of major FAAs contents between experimental group and control group).

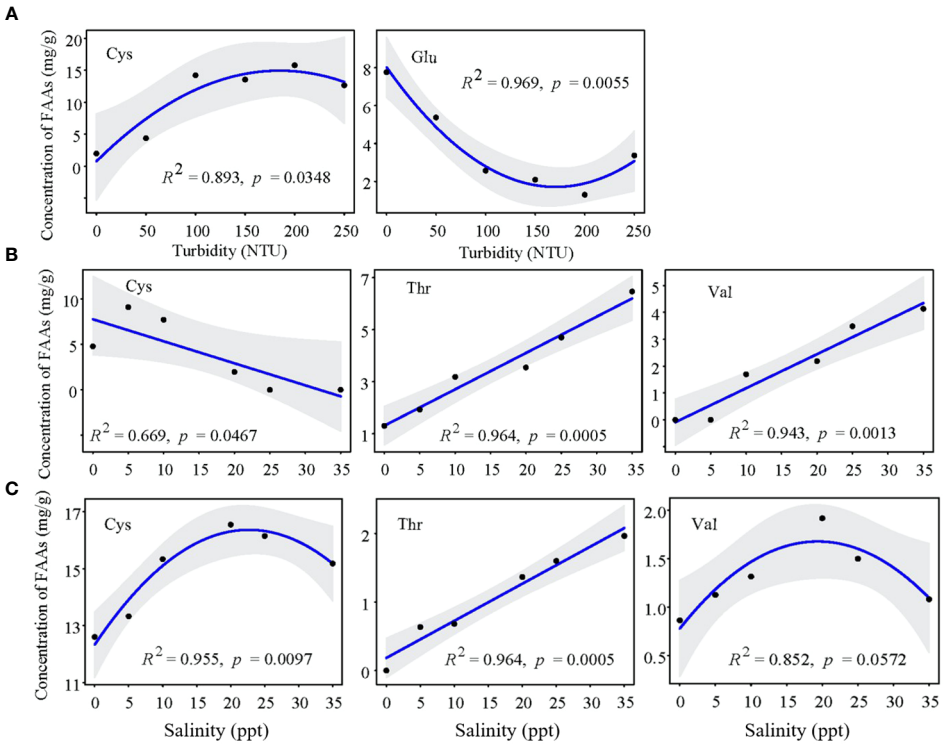

FIGURE 8
Change tendency of key FAAs concentration in juvenile *Z. Japonica* with **(A)** turbidity, **(B)** salinity and **(C)** salinity-turbidity interaction treatments (Turbidity = 150NTU).

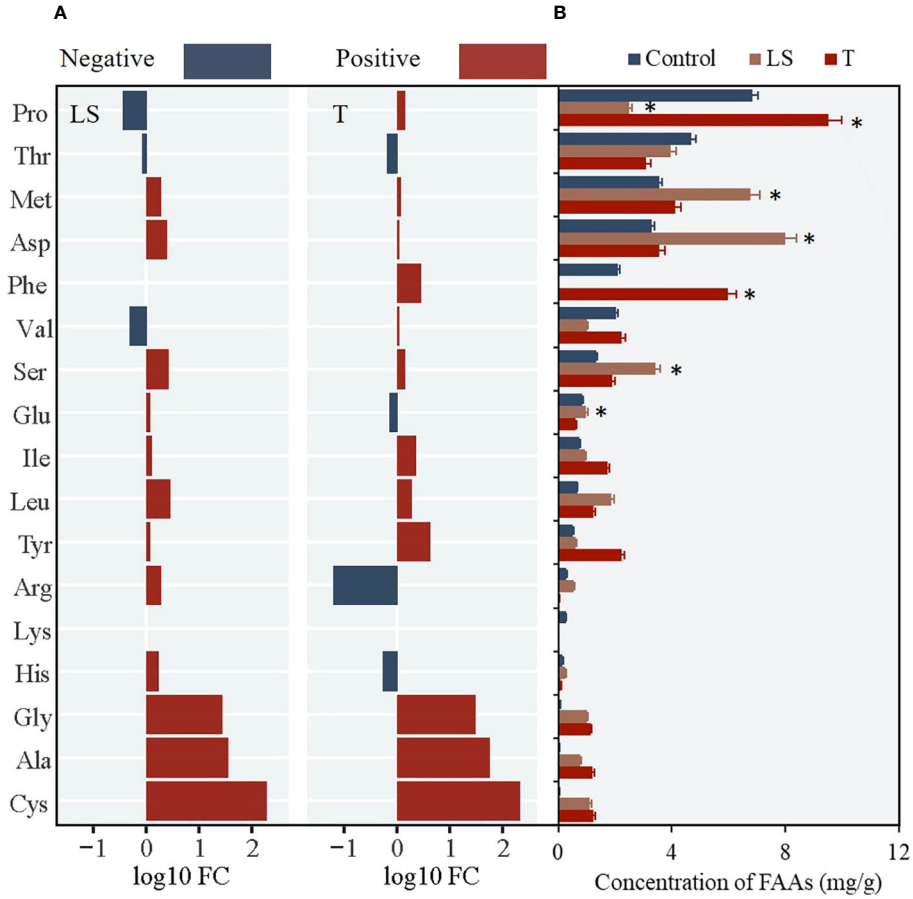

FIGURE 9
Changes of 17 FAAs in juvenile *Z. Japonica* with low salinity (LS), high salinity (HS) and turbidity(T) treatments comparing with control group (* represents significant differences of major FAAs contents between experimental group and control group).

high organic nitrogen requirements for the rapid development of leaves and stems. Glutamic acid serves as a primary amino donor for the synthesis of other amino acids and nitrogen-containing compounds, facilitating the seedlings' growth and development (Griffiths et al., 2020). As *Z. japonica* matures, the proportion of serine group amino acids (Ser group) becomes the highest (Figure 3), supporting chlorophyll synthesis and maintaining homeostasis in the fully developed plants. The varying amino acid composition across growth stages highlights the seagrass's ability to fine-tune its metabolic processes in response to changing developmental needs and environmental conditions. *Z. japonica* exhibits distinct adjustment mechanisms to external stress at different life stages, which can be attributed to the morphological and physiological variations associated with its development. When exposed to salinity and/or turbidity stress, mature *Z. japonica* maintains metabolic balance by altering the composition of FAAs within a narrow range (Figure 3), demonstrating an enhanced tolerance to these environmental challenges compared to earlier growth stages. This adaptive capacity allows mature plants to better cope with the dynamic conditions in their intertidal habitat, ensuring their survival and persistence.

As intermediates in specific metabolic pathways, FAAs serve a crucial regulatory function in plants by influencing multiple metabolic, physiological, and biochemical processes. Consequently, changes in FAA content and composition can act as reliable indicators of cellular homeostasis and abiotic stress in plants. In this study, molecular analysis was employed to determine the environmental threshold at which cellular homeostasis is disturbed in *Z. japonica* (Figure 4). *Z. japonica* exhibits varying stress thresholds for salinity and turbidity at different growth stages. The seedling stage appears to be the most sensitive to salinity stress, with significant changes in FAA content observed at both low (10 ppt) and high (25 ppt) salinity levels. In contrast, juvenile and mature plants only showed significant responses to extremely low salinity (0 ppt), suggesting a higher tolerance to salinity fluctuations at these later growth stages. Remarkably, this threshold was found to be narrower than the range of conditions that elicit significant morphological changes at each growth stage (Hou et al., 2020). This finding underscores the potential of FAAs as highly sensitive indicators of abiotic stress in seagrasses inhabiting the intertidal zones of high-turbidity estuaries. By detecting stress responses at the molecular level before visible morphological changes occur, FAA analysis can provide early warning signals of environmental perturbations and facilitate timely management interventions to protect these valuable coastal ecosystems.

Z. japonica exhibits a remarkable capacity to adapt to high salinity, which strengthens as the plant matures. The absence of

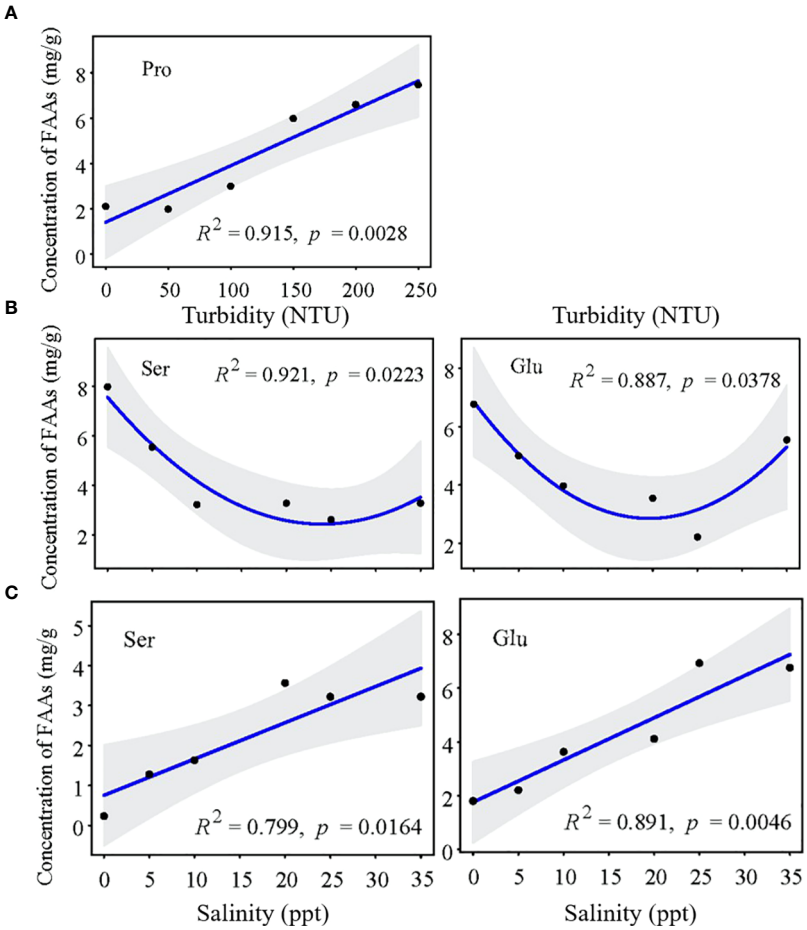

FIGURE 10
Change tendency of key FAAs concentration in mature *Z. Japonica* with **(A)** turbidity, **(B)** salinity and **(C)** salinity-turbidity interaction treatments (Turbidity = 150NTU).

significant changes in FAA content under high-salinity treatment in juvenile and mature plants further supports this notion of increased salinity tolerance with age. Salinity affects seagrass metabolism by altering osmotic pressure and ion concentrations in *Z. japonica* (Galvan-Ampudia and Testerink, 2011; Canalejo et al., 2014; Julkowska and Testerink, 2015). FAAs play a crucial role in maintaining the metabolic balance of *Z. japonica* under different salinity conditions through continuous synthesis, accumulation, and transformation. Under freshwater conditions, a notable decrease in FAA concentration was observed in both seedling and juvenile *Z. japonica*. However, under hypersaline stress, seedling-stage *Z. japonica* adapted by upregulating FAAs related to osmotic regulation (e.g., Pro) and cellular energy metabolism (e.g., Val, Met) (Cohen et al., 2014). The increased expression of ornithine ω-transaminase under osmotic stress leads to Pro synthesis (Delauney et al., 1993), which prevents ion outflow. Additionally, due to the increased demand for proteins and energy under adverse conditions, BCAAs like Val, Leu, and Ile participate in the tricarboxylic acid cycle (TAC) for mitochondrial respiration. Val degradation, in particular, produces energy comparable to carbohydrate metabolism (Heinemann et al., 2021). As *Z. japonica* matures, its metabolic pathways expand and diversify, enhancing stress resistance by upregulating certain FAAs involved in chlorophyll synthesis (e.g., Glu, Ser, Thr), thereby improving photosynthetic rates (Figure 6B, Figure 8B, Figure 10B) (Xu et al., 2020). Simultaneously, the conversion from Gly to Ser can provide ATP for plants, enhancing photorespiration and protecting the seagrass against external stress (Ehlting et al., 2007).

Compared to saline stress, light suppression might trigger more severe inhibition of *Z. japonica*'s metabolism. Underwater light conditions affect the photosynthetic rate of *Z. japonica*, and increased water turbidity can lead to water hypoxia, allowing gaseous H_2S to invade the seagrass (Borum et al., 2005), inhibiting seaweed metabolism and increasing mortality (Pérez-Pérez et al., 2012; Lamers et al., 2013). However, *Z. japonica*, known as a highly light-adapted species with significant morphological and physiological plasticity, can thrive under highly variable environmental conditions. Under moderate turbidity (100~150 NTU), key FAAs in *Z. japonica* accumulate to maintain homeostasis by participating in various metabolic pathways.

During energy deficiency, *Z. japonica* relies on BCAA catabolism pathways (e.g., Val, Leu, and Ile) to supply energy and maintain basic cellular metabolism. Juvenile and mature *Z. japonica* accumulate specific FAAs (e.g., Pro and Cys) related to protein synthesis and detoxification of organic peroxides to sustain cellular function and enhance resistance to turbidity stress (Figure 6A, Figure 8A, Figure 10A) (Yang et al., 2020). This indicates that *Z. japonica* demonstrates increased physiological plasticity in response to external stress as it matures. The long-term survival of *Z. japonica* in highly turbid water may lead to genetic improvements that enhance resistance to turbidity stress. However, when water turbidity exceeds 150 NTU, it becomes unsuitable for *Z. japonica* growth. The concentration of FAAs in *Z. japonica* generally declines, indicating a disruption in the resistance response and potential impacts on cellular homeostasis (Figure 4) (Heinemann et al., 2021).

Turbidity exacerbates the negative effects of salinity stress on *Z. japonica*. In highly turbid water, the limited photosynthesis of *Z. japonica* results in a restricted energy supply, rendering it more susceptible to salinity changes. The significant increase in FAA content at this turbidity level suggests that the plants are experiencing stress and adjusting their metabolic processes in response to the reduced light availability and altered sediment conditions. The identification of key regulatory FAAs at each growth stage provides valuable insights into the specific metabolic pathways and adaptive strategies employed by the plant to cope with these environmental challenges. The up-regulation of Pro in mature *Z. japonica* under turbidity stress and the increased concentrations of Ser and Glu under low salinity conditions underscore the importance of these FAAs in maintaining metabolic homeostasis and coping with environmental challenges in later life stages. Through FAA synthesis and transformation, *Z. japonica* continuously supplies energy to activate resistance responses to salinity stress, maintaining homeostasis, growth, and development. This includes the catabolism of BCAAs and the Asp group, as well as the conversion between the Ser group and Asp group (Song et al., 2013). However, increased turbidity imposes more severe light restrictions on *Z. japonica*, intensifying the inhibition of the photosynthesis pathway and blocking the organism's energy generation pathway, leading to an insufficient energy supply. Moreover, *Z. japonica* requires more energy for resistance responses to maintain homeostasis, depleting organic matter within the cell and impeding normal physiological functions. These combined pressures degrade the adaptability of *Z. japonica* to salt stress, and even slight changes in salinity can cause drastic fluctuations in FAA composition and content within the seagrass, altering the environmental threshold (Figure 4). The exacerbated impact of salinity stress under salinity-turbidity interaction, as evidenced by the contrasting trends in key FAAs concentrations, suggests that the combined stress may strain the mature plants' adaptive capacity. It is worth noting that juvenile and mature *Z. japonica* mitigate the negative effects of other side effects by elevating the content of FAAs associated with antioxidant responses and activating protective mechanisms, including Cys and Glu (Figure 8C, Figure 10C). This suggests that salinity-turbidity interaction may induce a progressive increase in glutathione synthesis (γ-glutathione + glycine, GSH), which can remove reactive oxygen species (ROS) to maintain redox status and increase chlorophyll content to restore photosynthesis (Gill and Tuteja, 2010; Son et al., 2014; Capó et al., 2020). However, the increased performance levels of key FAAs under high turbidity-high salinity conditions indicate a potential synergistic effect that enhances the plant's stress tolerance.

To better understand the mechanisms underlying these stage-specific responses to salinity and turbidity stress, future studies should focus on integrating metabolomic, transcriptomic, and proteomic data to develop a more comprehensive understanding of the complex interplay between amino acid metabolism and stress responses in seagrasses. Comparative analyses of the metabolomic and transcriptomic profiles of *Z. japonica* at different growth stages and under various stress conditions could provide valuable insights into the adaptive strategies employed by this species throughout its life cycle. Furthermore, YRE has complex hydrodynamic and water environmental conditions, with many factors affecting the growth and development of *Z. japonica*. Assessing the impact of other environmental factors, such as total nitrogen, total phosphorus and dissolved oxygen, could help further elucidate the resistance mechanism of external stress on *Z. japonica*.

5 Conclusion

This study utilized laboratory control experiments to investigate the physiological mechanisms of *Z. japonica* under varying salinity and turbidity conditions. The results provide valuable insights into the adaptive capacity and vulnerability of *Z. japonica* to environmental stressors, highlighting the potential use of FAAs as sensitive biomarkers for monitoring seagrass health in high-turbidity estuaries. These findings contribute to effective conservation and management strategies for protecting these important marine ecosystems. The three main findings of this study are as below:

(1) FAAs can serve as highly sensitive indicators of abiotic stress in seagrasses within the intertidal zone of high-turbidity estuaries. Through single stress experiments, the salinity and turbidity thresholds for FAA homeostatic disturbance in *Z. japonica* were determined at seedling, juvenile, and mature stages.

(2) *Z. japonica* exhibits strong adaptability to high salinity environments but displays weaker adaptability to freshwater conditions. Interaction experiments further revealed that turbidity has a more pronounced negative impact on the cellular homeostasis of *Z. japonica* compared to salinity, and the two stressors have a cumulative effect. The negative effects of salinity stress on *Z. japonica* were significantly intensified when turbidity levels exceeded 150 NTU.

(3) Under the interaction of high turbidity and high salinity, the concentration of key FAAs in *Z. japonica* generally showed a downward trend. This decline in FAA concentration could contribute to the degradation of cellular energy metabolism, protein synthesis, stress resistance, and other physiological processes, ultimately inhibiting the growth and development of *Z. japonica*.

Data availability statement

The original contributions presented in the study are included in the article/supplementary material, further inquiries can be directed to the corresponding author/s.

Author contributions

YY: Conceptualization, Funding acquisition, Writing – original draft, Writing – review & editing. FZ: Formal analysis, Investigation, Methodology, Writing – original draft, Writing – review & editing. CH: Formal analysis, Investigation, Methodology, Writing – original draft, Writing – review & editing. CZ: Writing – original draft, Writing – review & editing. CT: Formal analysis, Validation, Writing – review & editing.

Funding

The author(s) declare financial support was received for the research, authorship, and/or publication of this article. This study was supported by the National Natural Science Foundation of China (U2243236, 52025092), and the National Key Research and Development Program of China (2022YFC3202002).

Conflict of interest

The authors declare that the research was conducted in the absence of any commercial or financial relationships that could be construed as a potential conflict of interest.

Publisher's note

Supplementary material

The Supplementary Material for this article can be found online at: https://www.frontiersin.org/articles/10.3389/fmars.2024.1432106/full#supplementary-material

References

Barbier, E. B., Hacker, S. D., Kennedy, C., Koch, E. W., Stier, A. C., and Silliman, B. R. (2011). The value of estuarine and coastal ecosystem services. *Ecol. Monogr.* 81, 169–193. doi: 10.1890/10-1510.1

Blanco-Murillo, F., Díaz, M. J., Rodríguez-Rojas, F., Navarrete, C., Celis-Plá, P. S. M., Sánchez-Lizaso, J. L., et al. (2023). A risk assessment on *Zostera chilensis* the last relict of marine angiosperms in the South-East Pacific Ocean, due to the development of the desalination industry in Chile. *Science of the Total Environment* 883, 163538. doi: 10.1016/j.scitotenv.2023.163538

Borum, J., Pedersen, O., Greve, T. M., Frankovich, T. A., Zieman, J. C., Fourqurean, J. W., et al. (2005). The potential role of plant oxygen and sulphide dynamics in die-off events of the tropical seagrass, Thalassia testudinum. *J. Ecol.* 93, 148–158. doi: 10.1111/j.1365-2745.2004.00943.x

Cambridge, M. L., Zavala-Perez, A., Cawthray, G. R., Mondon, J., and Kendrick, G. A. (2017). Effects of high salinity from desalination brine on growth, photosynthesis, water relations and osmolyte concentrations of seagrass Posidonia australis. *Mar. pollut. Bull.* 115, 252–260. doi: 10.1016/j.marpolbul.2016.11.066

Canalejo, A., Martínez-Domínguez, D., Córdoba, F., and Torronteras, R. (2014). Salt tolerance is related to a specific antioxidant response in the halophyte cordgrass. *Estuar. Coast. Shelf* S 146, 68–75. doi: 10.1016/j.ecss.2014.05.017

Capó, X., Tejada, S., Ferriol, P., Pinya, S., Mateu-Vicens, G., Montero-González, I., et al. (2020). Hypersaline water from desalinization plants causes oxidative damage in Posidonia oceanica meadows. *Sci. Of Total Environ.* 736, 139601. doi: 10.1016/j.scitotenv.2020.139601

Chou, Q. C., Cao, T., Ni, L. Y., Xie, P., and Jeppesen, E. (2019). Leaf soluble carbohydrates, free amino acids, starch, total phenolics, carbon and nitrogen stoichiometry of 24 aquatic macrophyte species along climate gradients in China. *Front. Plant Sci.* 10. doi: 10.3389/fpls.2019.00442

Cohen, H., Israeli, H., Matityahu, I., and Amir, R. (2014). Seed-specific expression of a feedback-insensitive form of CYSTATHIONINE-γ-SYNTHASE in arabidopsis stimulates metabolic and transcriptomic responses associated with desiccation stress. *Plant Physiol.* 166, 1575–1592. doi: 10.1104/pp.114.246058

Cornelisen, C. D., and Thomas, F. I. M. (2006). Water flow enhances ammonium and nitrate uptake in a seagrass community. *Mar. Ecol. Prog. Ser.* 312, 1–13. doi: 10.3354/meps312001

Cussioli, M. C., Seeger, D., Pratt, D. R., Bryan, K. R., Bischof, K., de Lange, W. P., et al. (2020). Spectral differences in the underwater light regime caused by sediment types in New Zealand estuaries: implications for seagrass photosynthesis. *Geo-Mar Lett.* 40, 217–225. doi: 10.1007/s00367-020-00640-0

Delauney, A. J., Hu, C. A., Kishor, P. B., and Verma, D. P. (1993). Cloning of ornithine delta-aminotransferase cDNA from Vigna aconitifolia by trans-complementation in Escherichia coli and regulation of proline biosynthesis. *J. Biol. Chem.* 268 (25), 18673–18678. doi: 10.1016/S0021-9258(17)46682-8

Ehlting, B., Dluzniewska, P., Dietrich, H., Selle, A., Teuber, M., Hansch, R., et al. (2007). Interaction of nitrogen nutrition and salinity in Grey poplar (Populus tremula x alba). *Plant Cell Environ.* 30, 796–811. doi: 10.1111/j.1365-3040.2007.01668.x

Galvan-Ampudia, C. S., and Testerink, C. (2011). Salt stress signals shape the plant root. *Curr. Opin. In Plant Biol.* 14, 296–302. doi: 10.1016/j.pbi.2011.03.019

Gao, Y., Yi, Y., Chen, K., and Xie, H. (2023). Simulation of suitable habitats for typical vegetation in the Yellow River Estuary based on complex hydrodynamic processes. *Ecol. Indic.* 154, 110623. doi: 10.1016/j.ecolind.2023.110623

Gill, S. S., and Tuteja, N. (2010). Reactive oxygen species and antioxidant machinery in abiotic stress tolerance in crop plants. *Plant Physiol. Bioch* 48, 909–930. doi: 10.1016/j.plaphy.2010.08.016

Greenwell, B. M., and Kabban, C. M. S. (2014). investr: an R package for inverse estimation. *R J.* 6, 90–100. doi: 10.32614/RJ-2014-009

Griffiths, L. L., Melvin, S. D., Connolly, R. M., Pearson, R. M., and Brown, C. J. (2020). Metabolomic indicators for low-light stress in seagrass. *Ecol. Indic.* 114, 106316. doi: 10.1016/j.ecolind.2020.106316

Han, Q. Y., Soissons, L. M., Liu, D. Y., van Katwijk, M. M., and Bouma, T. J. (2017). Individual and population indicators of *Zostera japonica* respond quickly to experimental addition of sediment-nutrient and organic matter. *Mar. pollut. Bull.* 114, 201–209. doi: 10.1016/j.marpolbul.2016.08.084

Heinemann, B., Künzler, P., Eubel, H., Braun, H. P., and Hildebrandt, T. M. (2021). Estimating the number of protein molecules in a plant cell: protein and amino acid homeostasis during drought. *Plant Physiol.* 185, 385–404. doi: 10.1093/plphys/kiaa050

Hou, C. Y., Song, J., Yan, J. G., Wang, K., Li, C. H., and Yi, Y. J. (2020). Growth indicator response of *Zostera japonica* under different salinity and turbidity stresses in the Yellow River Estuary, China. *Mar. Geology* 424, 106169. doi: 10.1016/j.margeo.2020.106169

Julkowska, M. M., and Testerink, C. (2015). Tuning plant signaling and growth to survive salt. *Trends In Plant Sci.* 20, 586–594. doi: 10.1016/j.tplants.2015.06.008

Kim, S. H., Kim, J. W., Kim, Y. K., Park, S. R., and Lee, K. S. (2020). Factors controlling the vertical zonation of the intertidal seagrass, *Zostera japonica* in its native range in the northwestern Pacific. *Mar. Environ. Res.* 157, 104959. doi: 10.1016/j.marenvres.2020.104959

Lamers, L. P. M., Govers, L. L., Janssen, I., Geurts, J. J. M., van der Welle, M. E. W., Van Katwijk, M. M., et al. (2013). Sulfide as a soil phytotoxin-a review. *Front. Plant Sci.* 4. doi: 10.3389/fpls.2013.00268

Li, X. W., Hou, X. Y., Song, Y., Shan, K., Zhu, S. Y., Yu, X. B., et al. (2019). Assessing changes of habitat quality for shorebirds in stopover sites: a case study in yellow river delta, China. *Wetlands* 39, 67–77. doi: 10.1007/s13157-018-1075-9

Orth, R. J., Carruthers, T. J. B., Dennison, W. C., Duarte, C. M., Fourqurean, J. W., Heck, K. L., et al. (2006). A global crisis for seagrass ecosystems. *Bioscience* 56, 987–996. doi: 10.1641/0006-3568(2006)56[987:AGCFSE]2.0.CO;2

Park, S. R., Kim, Y. K., Kim, J. H., Kang, C. K., and Lee, K. S. (2011). Rapid recovery of the intertidal seagrass *Zostera japonica* following intense Manila clam (Ruditapes philippinarum) harvesting activity in Korea. *J. Of Exp. Mar. Biol. And Ecol.* 407, 275–283. doi: 10.1016/j.jembe.2011.06.023

Pérez-Pérez, M. E., Lemaire, S. D., and Crespo, J. L. (2012). Reactive oxygen species and autophagy in plants and algae. *Plant Physiol.* 160, 156–164. doi: 10.1104/pp.112.199992

Sandoval-Gil, J. M., Ruiz, J. M., Marin-Guirao, L., Bernardeau-Esteller, J., and Sanchez-Lizaso, J. L. (2014). Ecophysiological plasticity of shallow and deep populations of the Mediterranean seagrasses *Posidonia oceanica* and *Cymodocea nodosa* in response to hypersaline stress. *Mar. Environ. Res.* 95, 39–61. doi: 10.1016/j.marenvres.2013.12.011

Shafer, D. J., and Kaldy, J. E. (2014). Comparison of photosynthetic characteristics of the seagrass congeners *Zostera marina* L. and *Zostera japonica* Ascher. & Graeb. *Aquat. Bot.* 112, 91–97. doi: 10.1016/j.aquabot.2013.09.002

Shafer, D. J., Kaldy, J. E., Sherman, T. D., and Marko, K. M. (2011). Effects of salinity on photosynthesis and respiration of the seagrass *Zostera japonica*: A comparison of two established populations in North America. *Aquat. Bot.* 95, 214–220. doi: 10.1016/j.aquabot.2011.06.003

Short, F., Carruthers, T., Dennison, W., and Waycott, M. (2007). Global seagrass distribution and diversity: A bioregional model. *J. Of Exp. Mar. Biol. And Ecol.* 350, 3–20. doi: 10.1016/j.jembe.2007.06.012

Son, J. A., Narayanankutty, D. P., and Roh, K. S. (2014). Influence of exogenous application of glutathione on rubisco and rubisco activase in heavy metal-stressed tobacco plant grown in *vitro*. *Saudi J. Biol. Sci.* 21, 89–97. doi: 10.1016/j.sjbs.2013.06.002

Song, Q., Cao, F., Gong, Y., Cheng, X., Bi, X., and Liu, L. (2012). Current research progresses of amino acids uptake,transport and their biological roles in higher plants. *Plant Nutr. Fertitizer Sci.* 18, 1507–1517.

Song, S. K., Hou, W. S., Godo, I., Wu, C. X., Yu, Y., Matityahu, I., et al. (2013). Soybean seeds expressing feedback-insensitive cystathionine -synthase exhibit a higher content of methionine. *J. Exp. Bot.* 64 (7), 1917–1926. doi: 10.1093/jxb/ert053

Waycott, M., Duarte, C. M., Carruthers, T. J. B., Orth, R. J., Dennison, W. C., Olyarnik, S., et al. (2009). Accelerating loss of seagrasses across the globe threatens coastal ecosystems. *P Natl. Acad. Sci. U.S.A.* 106, 12377–12381. doi: 10.1073/pnas.0905620106

Xu, S. C., Wang, P. M., Wang, F., Liu, P., Liu, B. J., Zhang, X. M., et al. (2020). In situ Responses of the Eelgrass *Zostera marina* L. @ to Water Depth and Light Availability in the Context of Increasing Coastal Water Turbidity: Implications for Conservation and Restoration. *Front. Plant Sci.* 11. doi: 10.3389/fpls.2020.582557

Yang, Q. Q., Zhao, D. S., and Liu, Q. Q. (2020). Connections between amino acid metabolisms in plants: Lysine as an example. *Front. Plant Sci.* 11. doi: 10.3389/fpls.2020.00928

Zhang, X. M., Zhou, Y., Adams, M. P., Wang, F., Xu, S. C., Wang, P. M., et al. (2020). Plant morphology and seed germination responses of seagrass (*Zostera japonica*) to water depth and light availability in Ailian Bay, northern China. *Mar. Environ. Res.* 162, 105082. doi: 10.1016/j.marenvres.2020.105082

Zhou, Q., Ke, Y., Wang, X., Bai, J., Zhou, D., and Li, X. (2022). Developing seagrass index for long term monitoring of *Zostera japonica* seagrass bed: A case study in Yellow River Delta, China. *Isprs J. Photogramm* 194, 286–301. doi: 10.1016/j.isprsjprs.2022.10.011

Zhou, Y., Xu, J., Wang, D., Zhao, X., and Yang, C. (2015). Rechecking the characteristic flood levels of a built reservoir after extending the hydrologic time series. *River Basin Manage. Viii* 197, 81–90. doi: 10.2495/RM150081

Zhou, Y., Zhang, X., Xu, S., Song, X., Lin, H., Wang, P., et al. (2016). New discovery of larger seagrass beds with areas > 50 ha in temperate waters of China: An unusual large seagrass (*Zostera japonica*) bed in the Yellow River estuary. *Mar. Sci.* 40, 95–97.

frontiers | Frontiers in Marine Science

TYPE Original Research
PUBLISHED 29 August 2024
DOI 10.3389/fmars.2024.1433104

OPEN ACCESS

EDITED BY
Charitha Bandula Pattiaratchi,
University of Western Australia, Australia

REVIEWED BY
Shiquan Chen,
Hainan Academy of Ocean and Fisheries Sciences, China
Jennifer Li Ruesink,
University of Washington, United States

*CORRESPONDENCE
Dacheng Wang
wangdacheng@mail.cgs.gov.cn
Guowei Fu
fuguowei@mail.cgs.gov.cn

†These authors have contributed equally to this work and share first authorship

RECEIVED 15 May 2024
ACCEPTED 12 August 2024
PUBLISHED 29 August 2024

CITATION
Fu M, Jiang J, Wang D, Fu G, Song Y, Wang H and Zhang D (2024) Assessment of the community status of seagrass bed and its relationship with environmental characteristics in Wenchang, Hainan Island, China.
Front. Mar. Sci. 11:1433104.
doi: 10.3389/fmars.2024.1433104

Assessment of the community status of seagrass bed and its relationship with environmental characteristics in Wenchang, Hainan Island, China

Miao Fu†, Junyi Jiang†, Dacheng Wang*, Guowei Fu*, Yanwei Song, Hongbing Wang and Daheng Zhang

Haikou Marine Geological Survey Center, China Geological Survey, Haikou, China

As one of the typical coastal ecosystems, seagrass bed has important ecological service functions. In order to enrich the basic data of multispecies tropical seagrass beds, the main controlling factors affecting the community status of seagrass were identified. In this study, the species, distribution and community characteristics of seagrass in Wenchang were investigated at five stations in 2023, and Spearman correlation analysis and Redundancy analysis were used to investigate the relationship between seagrass and environmental characteristics. The results showed that there were 7 species of seagrass belonging to 5 genera in 2 families along Wenchang coast, including *Enhalus acoroides*, *Thalassia hemprichii*, *Cymodocea rotundata*, *Cymodocea serrulata*, *Halophila ovalis*, *Halophila minor* and *Halodule uninervis*. The distribution of seagrass beds in Wenchang showed an obvious trend of degradation. Except for the relatively stable of seagrass beds in the central part of Wenchang, the seagrass beds on both the north and south sides decreased significantly, and the coverage of seagrass beds decreased from 24.31% in 2016 to 21.0% in 2020, and further decreased to 20.67% in 2023. The data showed that the coverage and aboveground biomass of seagrass were significantly positively correlated with temperature, and the density of seagrass was significantly positively correlated with DO, but significantly negatively correlated with COD. In addition, increased nutrient salts in the water column could negatively affect seagrass bed. In order to promote the sustainable development of seagrass ecosystem and enhance the stability of seagrass habitat, it is suggested to rationally plan the aquaculture scale of the surrounding area; flexibly manage the rake snail, rake clam and other fishing activities, appropriately reduce the frequency of mining; and scientifically plan marine engineering to reduce the damage to seagrass bed.

KEYWORDS

seagrass beds, community characteristics, environmental characteristics, community status, assessment index

1 Introduction

As one of the most important coastal ecosystems in the world, seagrass has high productivity and important ecosystem service value (Scott et al., 2018). It can not only purify water quality, but also fix sediment (McKenzie et al., 2021). It is also a food source, habitat and shelter for a variety of marine organisms (Jiang et al., 2020). In addition, seagrass bed is one of the most efficient carbon sequestration systems on earth, holding more than 10% of the ocean's carbon reserves (Howard et al., 2020). However, with the interference of human activities and the intensification of environmental pressure, the degradation of seagrass bed has increased globally (Short et al., 2011).

The growth and distribution of seagrass are affected by a variety of environmental factors, including temperature, light, salinity and nutrient (Lee et al., 2007; Suykerbuyk et al., 2018). Suitable water temperature and light conditions have important effects on the photosynthesis and growth of seagrass (Collier and Waycott, 2014; Bertelli and Unsworth, 2018), while excessive nutrient content and suspended matter concentration may lead to deterioration of water quality, which affects the growth and development of seagrass (Bertelli et al., 2020). Therefore, exploring the relationship between seagrass and environmental factors is of great significance for understanding the stability and vulnerability of seagrass ecosystems.

Wenchang is located in the northeastern part of Hainan Province, which is rich in seagrass resources and is the largest seagrass distribution area in Hainan Province (Wang et al., 2012). According to data records, there were eight species of seagrass belonging to six genera along Wenchang seagrass distribution area, including *Enhalus acoroides*, *Thalassia hemprichii*, *Cymodocea rotundata*, *Cymodocea serrulata*, *Syringodium isoetifolium*, *Halophila ovalis*, *Halophila minor* and *Halodule uninervis* (Wang et al., 2012). In recent years, the growth of seagrass bed in Wenchang has been affected to varying degrees, with the phenomenon of seagrass degradation has gradually emerged (Chen et al., 2015; Xu et al., 2022). With the reduction of seagrass habitats, *Thalassodendron ciliatum* and *Halophila decipiens*, which were historically recorded in Hainan, were not found in the corresponding distribution areas during surveys in the 21st century (Zheng et al., 2013). The degradation and reduction of seagrass bed area has seriously threatened the species diversity of seagrass. Therefore, in-depth understanding of the community status and ecological characteristics of the seagrass bed in Wenchang and analysis of the main factors affecting the degradation of the seagrass bed can not only enhance the public's attention to the conservation of seagrass, but also provide the scientific basis for the protection, restoration and effective management of seagrass beds in Wenchang.

2 Materials and methods

2.1 Study area

Wenchang is a tropical oceanic monsoon climate with sufficient sunshine and rainfall. The unique climate environment provides superior conditions for the development of seagrass. In recent years, seagrass habitats along the coast of Wenchang have been degraded and reduced, and seagrass beds that were originally distributed in sheets have gradually been distributed in patches or scattered. A total of five survey stations were deployed in this survey, covering Longlou Town (HC01), Yelin Bay (HC02), Gangdong Village (HC03), Changpi Port (HC04) and Fengjiawan (HC05) in Wenchang from north to south (Figure 1).

2.2 Survey method

During May and June 2023, seagrass beds would be surveyed and samples collected during the ebb tide period when seagrass was exposed to the surface. According to the distribution of seagrass, survey sections were arranged perpendicular to the shoreline of each survey station, from the intertidal zone to the subtidal zone, through the distribution of seagrass beds. The section layout covers the upper limit, lower limit and distribution center of seagrass. Transects parallel to the shoreline were laid on each section according to the upper limit, center and lower limit of seagrass distribution, and three 25cm×25cm quadrats were randomly placed on each transect. Each survey station has 3 transects and 9 quadrats. A total of 5 survey stations with 45 quadrats were set up in the study area. The investigation and analysis methods were carried out according to the《Technical guideline for investigation and assessment of coastal ecosystem—Part 6: Seagrass bed》(T/CAOE 20.6-2020).

Using the 25cm×25cm quadrat frame, the species of seagrass in the quadrat were identified on site, and the coverage of seagrass was estimated according to the distribution of seagrass in each quadrat. All seagrass plants in the quadrat were removed completely during sampling, washed and brought back to the laboratory for determination and analysis. Species were identified in each quadrat, and species were combined for shoot counts and biomass. Then all the seagrass plants in the quadrat were divided into aboveground and underground parts, dried at 60 °C to constant weight, and the biomass of seagrass per unit area (g/m^2) was measured.

The temperature (Temp), pH, salinity (Sal) and dissolved oxygen (DO) of seawater were measured on-site using the DZB-712F portable multi-parameter water quality analyzer in the areas where transects were laid out at each survey station, and water samples for laboratory testing were collected. The water samples were then transported to the laboratory for determination of and chemical oxygen demand (COD), nitrate (NO_3^-), nitrite (NO_2^-), total nitrogen (TN), active phosphate (PO_4^{3-}), total phosphorus (TP) and active silicate (SiO_3^{2-}). The collection, transportation and analysis of seawater samples were carried out in accordance with《The requirements of the specification for marine monitoring》(GB 17378-2007) and《The specification for marine investigation》(GB 12763-2007).

2.3 Methods for assessing the community status of seagrass bed

According to the《Technical guideline for investigation and assessment of coastal ecosystem—Part 6: Seagrass bed》(T/CAOE

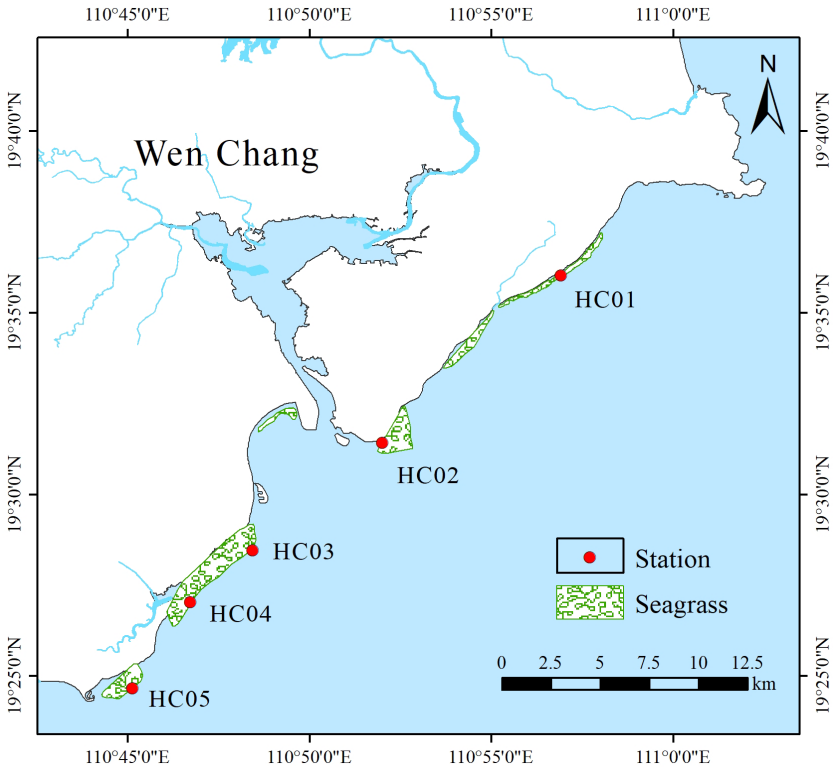

FIGURE 1
Investigation stations of seagrass in Wenchang, Hainan.

20.6-2020), the community status of seagrass bed in Wenchang was assessed, and the community characteristics of seagrass were assigned according to the degree of change (Table 1).

The change in the coverage of seagrass (V_1) was calculated according to the Equation 1:

$$V_1 = \frac{\bar{C} - C_0}{C_0} \times 100\,\% \quad (1)$$

Where V_1 is the rate of change in the coverage of seagrass, unit is percentage; $\bar{C}$. is the monitoring average of seagrass coverage; and C_0 is the historical reference data.

The change in the density of seagrass (V_2) was calculated according to the Equation 2:

$$V_2 = \frac{\bar{D} - D_0}{D_0} \times 100\,\% \quad (2)$$

Where V_2 is the rate of change in the density of seagrass, unit is percentage; $\bar{D}$ is the monitoring average of seagrass density; and D_0 is the historical reference data.

The assessment index (I_V) of seagrass bed was calculated according to the Equation 3:

$$I_V = \frac{\sum_1^q V_i}{q} \quad (3)$$

Where I_V is the seagrass bed assessment index; V_i is the value assigned to the ith seagrass bed assessment indicator; and q is the total number of seagrass bed assessment indicators.

When $37 \le I_V \le 50$, the seagrass bed is stable; when $30 \le I_V < 37$, the seagrass bed is damaged; when $10 \le I_V < 30$, the seagrass bed is severely damaged.

2.4 Data processing

In this study, SPSS 26.0 software was used to process and analyze the data. Based on the 2023 survey data of seagrass resources in Wenchang at five stations, combined with the data of the "Marine Biodiversity Survey of Hainan Province" from 2016 to 2020, the community status of seagrass beds was assessed, and the assessment map of seagrass community status along Wenchang was drawn by ArcGIS 10.2 Kriging interpolation. Spearman correlation analysis and Redundancy analysis were used to analyze the potential relationship between community characteristics of seagrass and environmental factors, and the significance level was $P<0.05$.

TABLE 1 Assessment indicators and assigned values of seagrass beds.

Indicator	Stable	Damaged	Severely damaged
Change in area	≥-10%	≥-30%~<-10%	<-30%
Change in coverage	≥-10%	≥-30%~<-10%	<-30%
Change in density	≥-10%	≥-30%~<-10%	<-30%
Assigned index	50	30	10

Smaller sample size may lead to significant relationships by chance. Therefore, we will report all statistical results, including both significant and non-significant findings, in the hope of providing preliminary insights for further research.

3 Results and analysis

3.1 Current status of seagrass bed resources

3.1.1 Composition of seagrass species

Seven species of seagrasses belonging to two families and five genera were surveyed along the coast of Wenchang in 2023. They were *Enhalus acoroides*, *Thalassia hemprichii*, *Cymodocea rotundata*, *Cymodocea serrulata*, *Halophila ovalis*, *Halophila minor* and *Halodule uninervis*. The survey area is rich in seagrass species, accounting for 70% of the seagrass species in Hainan Island. Among all surveyed stations, HC02 had the highest number of seagrass species (5 species) and HC01 had the lowest number (1 specie). *T. hemprichii* was present in all surveyed stations, followed by *E. acoroides* with a higher frequency (Table 2).

3.1.2 Community characteristics of seagrass

The coverage of seagrass beds in Wenchang ranges from 10.22% to 42.78%, with HC02 being the largest, followed by HC03 (Figure 2A). The mean density of seagrass bed was 334.58 ind/m^2, and the mean density of HC02 was significantly higher than that of the other four stations (P<0.05) (Figure 2B). Aboveground biomass ranged from 32.05 g/m^2 to 142.38 g/m^2, and the average aboveground biomass was 92.72 g/m^2, with the overall pattern of HC02>HC03>HC04>HC05>HC01 (Figure 2C). The underground biomass ranged from 105.05 g/m^2 to 514.06 g/m^2, and the average underground biomass was 274.85 g/m^2, with no significant difference among different stations (P>0.05) (Figure 2D).

3.1.3 Assessment of seagrass community status

In this study, combined with the survey data of seagrass beds along Wenchang from 2016 to 2020, the community characteristics of seagrass beds were assigned and evaluated (Table 3). The results of the study showed that HC01 and HC05 seagrass beds were severely damaged with an assessment index (I_V) of 10, which was consistent with the high level of habitat destruction of seagrass beds in the region. HC03 and HC04 seagrass beds were assessed as damaged with an index (I_V) of 30, which may be related to the high density of local aquaculture activities and frequent fishing activities. HC02 seagrass beds had an assessment index (I_V) of 50, which was a stable condition with abundant and well-established seagrass species. It could be seen that the community status of seagrass beds in the central part of the coastal of Wenchang were better than that of the north and south sides (Figure 3).

TABLE 2 Distribution of seagrass species.

Seagrass species	Survey area				
	HC01	HC02	HC03	HC04	HC05
Enhalus acoroides	––	––	+	+	+
Thalassia hemprichii	+	+	+	+	+
Cymodocea rotundata	––	+	––	––	––
Cymodocea serrulata	––	+	––	––	––
Halophila ovalis	––	+	––	+	––
Halophila minor	––	––	––	+	––
Halodule uninervis	––	+	––	––	––
Number of species	1	5	2	4	2

"+" indicates that the distribution of the species is surveyed in the region, and "––" indicates that the distribution of the species is not surveyed in the region.

3.2 Environmental factors of seagrass bed

The seawater temperature at each station ranges from 30.8°C to 31.6°C, the salinity ranges from 32.6‰ to 33.3‰, and the pH ranges from 7.97 to 8.62 (Table 4). The DO content of seawater ranged from 6.34 mg/L to 6.78 mg/L, and the COD concentration ranged from 0.48 mg/L to 0.91 mg/L, which met the first water quality standard. The contents of NO_3^- and NO_2^- were the highest in HC01 and the lowest in HC05. The content of SiO_3^{2-} was the highest in HC05 and the lowest in HC02. The content of PO_4^{3-} ranged from 0.002 mg/L to 0.107 mg/L, and the content of PO_4^{3-} varied greatly among different stations. The highest contents of total nitrogen and total phosphorus were found in HC04, which were 1.12 mg/L and 1.22 μ mol/L respectively.

3.3 Relationship between community characteristics of seagrass and environmental factors

3.3.1 Spearman correlation analysis

Spearman correlation analysis was conducted on the community characteristics of seagrass and environmental factors in Wenchang (Figure 4), and the results showed that there was a strong correlation between the community characteristics of seagrass and environmental factors. The coverage and aboveground biomass of seagrass were significantly positively correlated with temperature (P<0.05). The density of seagrass was positively and negatively correlated with salinity and pH, respectively. There was a significant positive correlation between the density of seagrass and DO content (P<0.05). The coverage and density of seagrass were significantly negatively correlated with COD (P<0.05). The coverage, density, and biomass of seagrass were negatively correlated with NO_3^- and NO_2^-. The density of seagrass was negatively correlated with the TN and TP content. The density

10.3389/fmars.2024.1433104

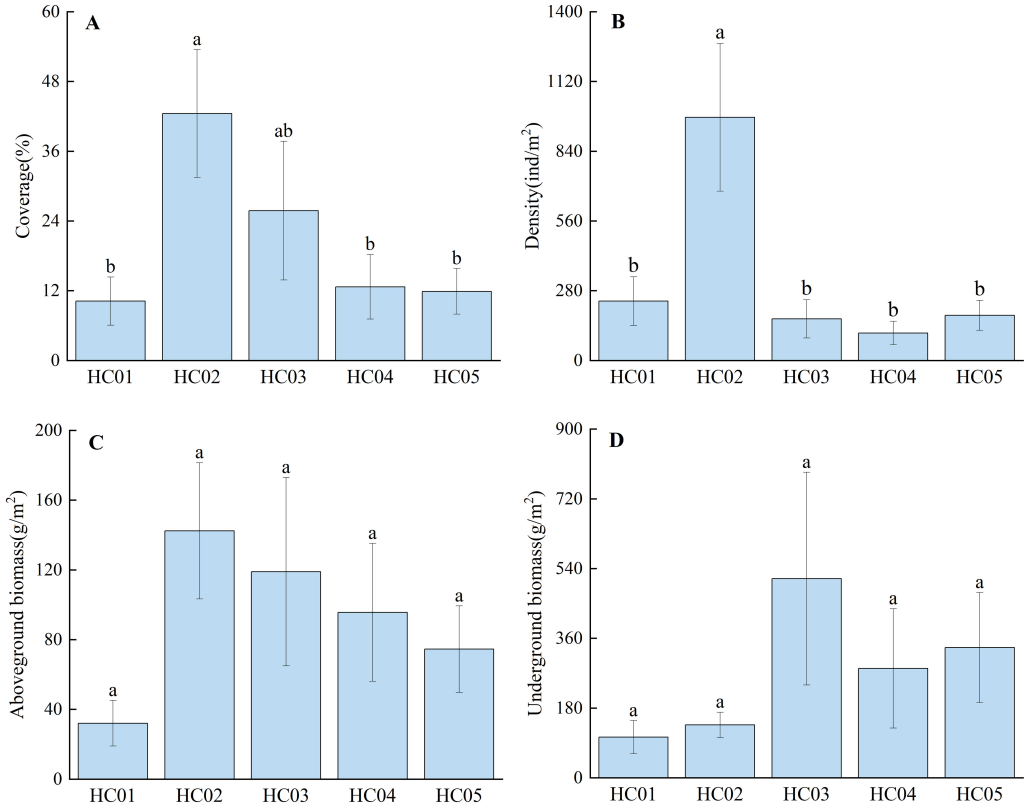

FIGURE 2
Community characteristics of seagrass. **(A)** coverage; **(B)** density; **(C)** aboveground biomass; **(D)** underground biomass. The sample sizes for the community characteristic of seagrass in each station is 9; error bars denote the standard error of the mean; different lowercase letters (a, b) in the same graph indicate significant differences (P<0.05).

of seagrass was significantly negatively correlated with SiO_3^{2-} and PO_4^{3-} (P<0.05).

3.3.2 Redundancy analysis

Redundancy analysis was applied to seagrass bed, in which environmental factors were used as explanatory variables and seagrass community characteristics were used as response variables. The eigenvalues of the first and second spindles were 0.8716 and 0.1235, respectively, which explained 99.51% of the variation in seagrass indicators, and the adjusted variance explanation was 98.1% (Figure 5). The interpretation rates of DO, temperature and COD were 66.9%, 31.3% and 1.3%, respectively. Among them, the coverage and aboveground biomass of seagrass were significantly positively correlated with temperature, while the density of seagrass was significantly positively correlated with DO, but significantly negatively correlated with COD. In addition, the density, coverage, and aboveground biomass of seagrass were relatively close to each other in the diagram, there was a positive correlation between them.

TABLE 3 Assessment of seagrass community status.

Station	Coverage (%)		Assignment value for change in coverage	Density (ind/m^2)		Assignment value for change in density	I_V
	C_0	$\bar{C}$		D_0	$\bar{D}$		
HC01	21.00	10.22	10	590.70	238.22	10	10
HC02	14.35	42.78	50	362.00	976.00	50	50
HC03	25.55	25.78	50	857.00	167.11	10	30
HC04	11.25	12.67	50	586.00	110.22	10	30
HC05	25.00	11.89	10	471.00	181.33	10	10

$\bar{C}$ is the monitoring average of seagrass coverage, and C_0 is the historical reference data; $\bar{D}$ is the monitoring average of seagrass density; and D_0 is the historical reference data. The lower I_V of the seagrass bed, the more serious the damage condition of seagrass bed.

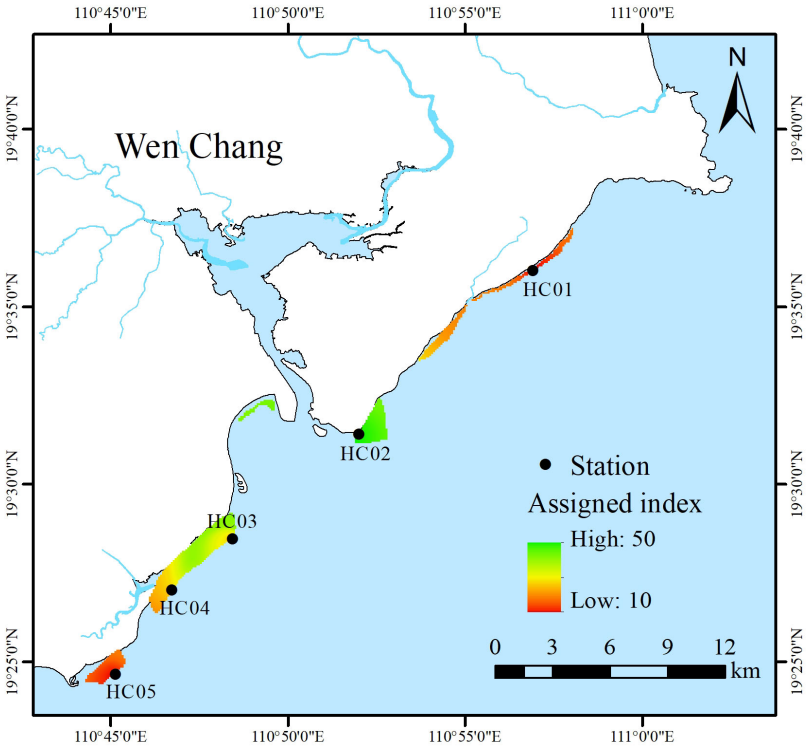

FIGURE 3
Community status of seagrass beds in Wenchang.

4 Discussion

4.1 Analysis of the community status of seagrass beds in Wenchang

In this survey of seagrass in Wenchang, 7 species of seagrass were found in 2 families and 5 genera. Compared with previous surveys (Wang et al., 2012; Zhu et al., 2017), *S. isoetifolium* was not found in this survey. Historical records *S. isoetifolium* was mainly distributed in the Fengjiawan. Fengjiawan is a sewage outlet for many cultured shrimp ponds, and the active phosphate and total phosphorus in this area are at a high level. Under the condition of nutrient enrichment, the seagrass ecosystem will produce a large amount of organic matter, resulting in low oxygen in the ecosystem, reducing the utilization rate of phosphate in the seagrass, and thus limiting the metabolism and energy transfer process of the seagrass

TABLE 4 Environmental characteristics of seagrass bed.

Environmental factor	HC01	HC02	HC03	HC04	HC05
Temp (°C)	30.8 ± 0.00	31.6 ± 0.00	31.4 ± 0.00	30.9 ± 0.00	30.9 ± 0.00
pH	8.27 ± 0.00	8.05 ± 0.00	8.28 ± 0.00	7.97 ± 0.00	8.62 ± 0.00
Sal (‰)	33.3 ± 0.00	33.2 ± 0.00	33.1 ± 0.00	32.6 ± 0.00	32.7 ± 0.00
DO (mg/L)	6.62 ± 0.00	6.78 ± 0.00	6.34 ± 0.00	6.52 ± 0.00	6.52 ± 0.00
COD (mg/L)	0.91 ± 0.02	0.48 ± 0.06	0.71 ± 0.12	0.74 ± 0.02	0.67 ± 0.01
NO_3^- (mg/L)	0.60 ± 0.00	0.12 ± 0.04	0.44 ± 0.23	0.49 ± 0.29	0.07 ± 0.03
NO_2^- (mg/L)	0.53 ± 0.00	<0.001	<0.001	0.23 ± 0.10	<0.001
TN (mg/L)	0.71 ± 0.00	0.84 ± 0.61	0.89 ± 0.01	1.12 ± 0.06	0.57 ± 0.11
SiO_3^{2-} (mg/L)	0.38 ± 0.01	0.37 ± 0.02	0.55 ± 0.09	0.41 ± 0.02	0.63 ± 0.12
PO_4^{3-} (mg/L)	0.014 ± 0.00	0.002 ± 0.00	0.107 ± 0.04	0.091 ± 0.01	0.034 ± 0.00
TP (μ mol/L)	0.32 ± 0.13	0.97 ± 0.28	0.99 ± 0.02	1.22 ± 0.27	1.16 ± 0.43

The sample sizes of environmental characteristic in each station is 3; "±" denotes the standard error of the mean.

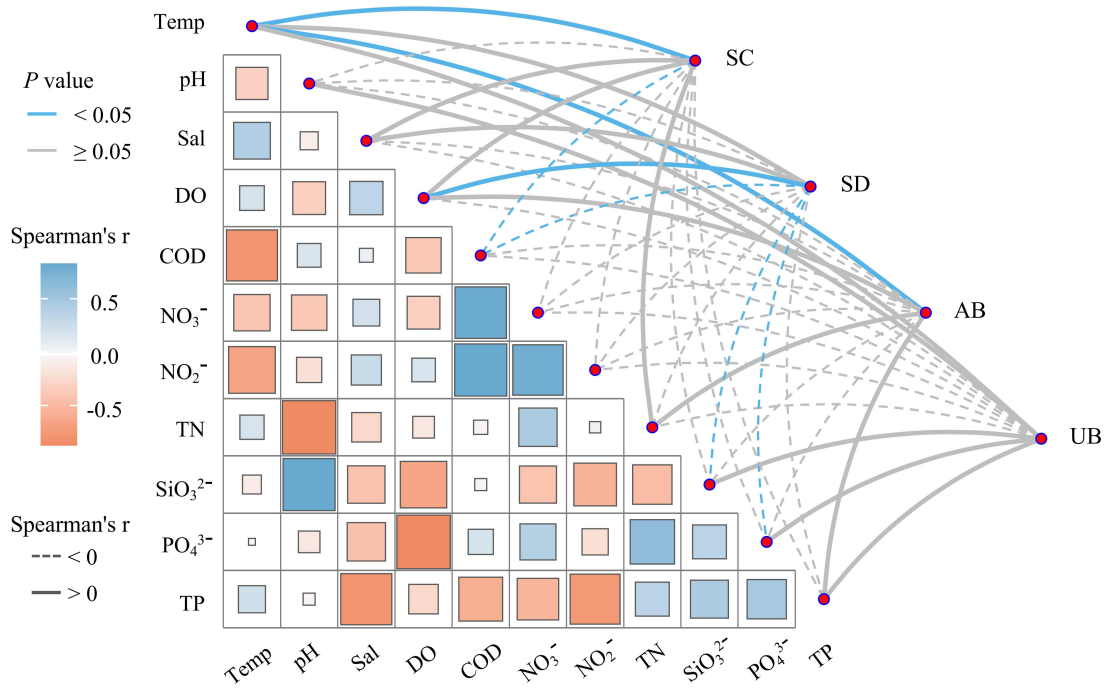

FIGURE 4
Correlation analysis between seagrass community characteristics and environmental factors.

(Han et al., 2017). In addition, a large-scale water intake project has been constructed along the coast of Fengjiawan, and the layout of water intake pipes would destroy the habitat of seagrass and change the dynamic characteristics of water flow, including the speed and direction of water flow, which may affect the seed dispersal and the selection of developmental sites of seagrass. Compared with *E. acoroides* and *T. hemprichii* from Fengjiawan, *S. isoetifolium* belongs to small seagrass, which was more sensitive to environmental changes and difficult to survive in harsh environments (Cai et al., 2017).

The survey found that the average coverage of seagrass bed in Wenchang was 20.67%, which was similar to the survey results in 2020 (21%) (Xu et al., 2022). Studies have shown that the average density of seagrass bed in Hainan Province reached 1753.39 ind/m^2

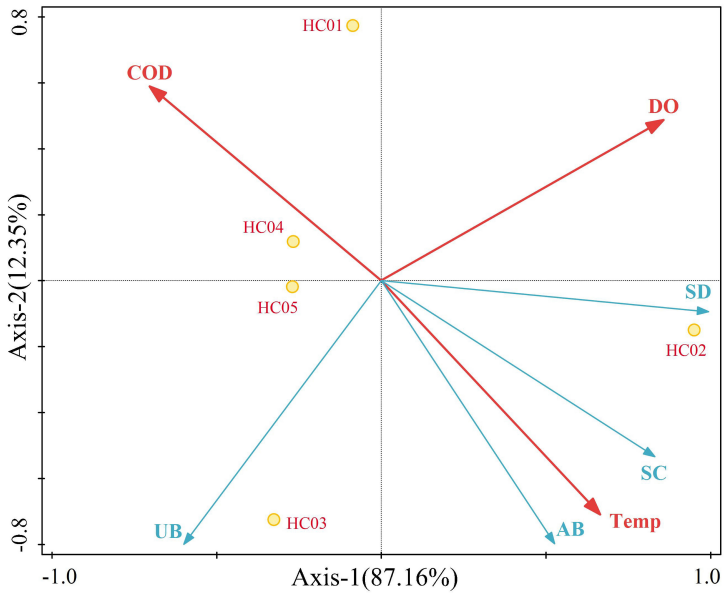

FIGURE 5
Redundancy analysis between seagrass community characteristics and environmental factors.

from 2004 to 2009, among which the average density of seagrass bed in Changpi Port was 585.85 ind/m^2 (Wang et al., 2012), whereas the average density of seagrass beds in Changpi Port in the present survey was only 110.22 ind/m^2. The estuary of the Changpi Port was a navigable area, and the navigation of fishing vessels cut seagrass while stirring up the substrate of the seagrass beds, caused irreversible damage to seagrass habitats (Neckles et al., 2005). In addition, fishing activities such as raking snails and clams were relatively common along the whole coast of Wenchang, especially in Gangdong Village, Changpi Port and Fengjiawan. High-intensity fishing activities dug seagrasses out by the roots, which directly caused the reduction of seagrass resources (Chen et al., 2020).

The average biomass of *T. hemprichii* in Longlou Town was the smallest because the morphology of *T. hemprichii* was generally small and the defect of stems and leaves was serious. Field investigations have found that algae were widely distributed in this region, which not only competed with seagrass for habitat and nutrient resources, but also shaded seagrass and inhibit its photosynthesis (Huang et al., 2017). In addition, the low DO and high COD environment caused by algae blooms would also have a negative impact on the growth and reproduction of seagrass (Liu et al., 2016). Seagrass in the Yelin Bay was mainly found in the reef area, where seagrass was distributed in a wide variety of species. It was mainly related to the clearer water and slower currents at coral reef margins, which was conducive to the photosynthesis of seagrass. However, the growth of seagrass in Yelin Bay was under some threat due to coastal erosion and a few fishing activities (Guo et al., 2009). By compared with the historical survey data of seagrass bed in Wenchang, the average coverage, density and biomass of seagrass bed showed a decreasing trend, indicated that the seagrass in Wenchang was in a serious decline.

4.2 Effects of environmental characteristics on seagrass

Gene and environmental factors are the main causes of species differences, and the same species may also show certain differences in performance under different environments (Palacio-López et al., 2015). We used Spearman correlation analysis and Redundancy analysis to analyze the relationship between environmental factors and the community characteristics of seagrass. Since our survey stations were only five, this may limit the strength of our interpretation of the results. Therefore, we report all statistical findings in our results, including significant and non-significant findings, with a view to providing initial insights for further research. Among them, Spearman correlation analysis showed that seagrass was sensitive to environmental changes, and its community characteristics were affected by many environmental factors. RDA analysis indicated that the coverage and aboveground biomass of seagrass were significantly positively correlated with temperature, while the density of seagrass was significantly positively correlated with DO, but significantly negatively correlated with COD.

4.2.1 Effect of temperature on seagrass

Seagrass is broadly thermophilic plants but it is very sensitive to changes in temperature (Jiang et al., 2012). In this study, the temperature of seawater was significantly and positively correlated with the coverage and aboveground biomass of seagrass. At suitable temperatures, higher temperatures have a positive effect on the enzymatic mechanism of photosynthesis (Egea et al., 2018). Different seagrass species have different sensitivity to temperature. The optimum temperature for photosynthesis in tropical and subtropical seagrass is between 27°C and 33°C, and the optimum growth temperature of temperate seagrass is between 11.5°C and 26°C (Liu W. et al., 2017). The temperature of seawater in the investigated area ranged from 30.8°C to 31.6°C, which was a suitable temperature for photosynthesis of tropical seagrass, and the coverage and aboveground biomass of seagrass increased with the increase of seawater temperature. However, data from Odense, Denmark, showed that *Zostera marina*, a temperate seagrass, has significantly lower stem survival rate as well as leaf growth at 27°C (Höffle et al., 2011). In the context of global climate change, even if the impact of temperature change on seagrass is relatively slow, the impact on seagrass bed cannot be ignored. The temperature above or below the appropriate temperature for seagrass may reduce photosynthesis, and its increased respiration rate can break the balance between photosynthesis and respiration, which in turn affects the synthesis and storage of non-structural carbohydrates (Han et al., 2023).

4.2.2 Effects of DO and COD on seagrass

DO plays the role of oxidant in the chemical purification process of water, and abundant DO content can effectively accelerate the degradation rate of organic matter and improve the purification capacity of seawater (He et al., 2012). The study in Zhelin Bay showed that the NH_3-N in aquaculture area was higher than that in non- aquaculture area, while the DO content was at a lower level, indicating that the large amount of NH_3-N produced by culture activities would consume more DO (Du et al., 2006). It has been demonstrated that the reduction of DO content caused by aquaculture will lead to excess organic matter remaining in the sediment, and then inhibit the growth of the erect stems of seagrasss (Marbà et al., 2006). In addition, during the investigation of seagrass beds in Liusha Bay, it was found that the biomass of seagrass was significantly positively correlated with the concentration of DO (Zhong et al., 2019). In this study, DO content was significantly and positively correlated with the coverage of seagrass, indicating that the aquaculture activity and marine engineering around Wenchang not only affected nutrient salt in the water and sediment, but also caused hypoxia in the water. Anoxic environment will increase the energy demand of seagrass photosynthesis, which will affect the material circulation of seagrass ecosystem.

During the investigation of the seagrass bed in Liusha Bay, it was found that *H. ovalis* was suitable for living in the sea with the high concentration of COD (Zhong et al., 2019). However, in this study, the concentration of COD was significantly negatively correlated with the coverage and density of seagrass. On the one hand, the high COD

values are usually accompanied by water eutrophication, which increases the primary productivity of algae and the activity of microorganisms (Liu S. et al., 2017). When strongly stimulated, the microorganisms in the rhizosphere of seagrass accelerates the oxygen consumption and the anaerobic metabolic processes of the bacterial community, thereby releasing toxic by-products such as sulfide and methane (Terrados et al., 1999). On the other hand, higher COD will cause hypoxia in the water and increase the energy demand for photosynthesis in seagrass, which affecting the absorption of nutrients by seagrass, and ultimately impacting the cycle of nutrient in the seagrass ecosystem (Liu W. et al., 2017).

4.2.3 Effects of other environmental factors on seagrass

Influenced by the input of freshwater from the terrestrial domain, there are obvious spatial and seasonal differences in the salinity of seagrass bed in the coastal waters (Wu et al., 2017). Long-term low salinity environment could reduce the leaf growth rate of *T. hemprichii* (Jiang et al., 2013). On the contrary, within an appropriate salinity, the increase of salinity can promote the growth of seagrass and increase the biomass of seagrass (Zhong et al., 2019). This was consistent with the conclusion in this study that salinity was positively correlated with the density of seagrass. However, it has also been shown that photosynthesis and respiration of seagrass is often inhibited in the environments with extreme high salinity, and that the increase in salinity leads to a decrease in chlorophyll content and enzyme activities in the plant, which in turn affects its growth and physiological processes (Kahn and Durako, 2006). Whether the seagrass bed is in a high salinity or low salinity environment, large amounts of energy are required to maintain the osmotic pressure of intracellular and the integrity of cell membrane, thus affecting the growth and metabolic processes of the seagrass bed (Atkinson and Smith, 1983).

Nutrient salt is one of the main factors limiting the growth and reproduction of seagrass (Lee et al., 2007). Under the condition of nutrient deficiency, reduced nutrient salt is the main environmental factor limiting the development of seagrass. However, under the condition of eutrophication, excessive concentration of the nutrient will have a negative impact on the growth of seagrass (Burkholder et al., 2007). In this study, the density of seagrass was significantly and negatively correlated with SiO_3^{2-} and PO_4^{3-}. The coastal area of Wenchang is densely populated, and the aquaculture area of shrimp ponds has been increasing year by year. Among them, the aquaculture scale from Gangdong Village to Fengjiawan has been maintained at a high level (Zhang et al., 2022). The discharge of domestic sewage and aquaculture wastewater introduce significant inputs of nutrients such as nitrogen and phosphorus to seagrass bed. A small amount of nitrogen and phosphorus input can provide nutrients for the growth of seagrass, but excess nutrients can cause the outbreak of algae, thus affecting the growth of seagrass (Han et al., 2016). Furthermore, in the eutrophic environment, seagrass needs to continuously consume carbohydrates to meet their carbon requirements (Alexandre et al., 2015), and extracellular enzyme activities associated with seagrass cellulose as well as lignin decomposition are significantly increased, which accelerates the decomposition of organic matter, which in turn negatively impacts seagrass beds (Liu et al., 2022).

Studies have shown that seagrass exposed to alkaline environment will be inhibited in growth with increasing pH (Invers et al., 1997). The overall water environment in Wenchang was weakly alkaline, and the coverage and density of seagrass were negatively correlated with pH, indicated that the change of pH caused by exogenous pollution could negatively affect the seagrass. The productivity and carbon sequestration capacity of seagrass increased with the decrease of pH, which was mainly related to the concentration of HCO_3^- in seawater, and the increase of HCO_3^- concentration was conducive to promoting the photosynthesis of seagrass (Palacios and Zimmerman, 2007; Liu et al., 2020).

5 Conclusion

In 2023, a total of seven species of seagrasses belonging to two families and five genera were investigated in the Wenchang of Hainan Province, Among them, *T. hemprichii* was the most widely distributed, followed by *E. acoroides*. According to the historical data, the species, coverage, density and biomass of seagrass beds in Wenchang showed a decreasing trend. The community status of seagrass beds in the central part of Wenchang were relatively stable, while the seagrass beds in the north and south were damaged.

Through the study on the community status and environmental characteristics of seagrass in Wenchang, it was found that the seagrass was sensitive to environmental changes, which the coverage and aboveground biomass of seagrass were significantly positively correlated with temperature, and the density of seagrass was significantly positively correlated with DO, but significantly negatively correlated with COD. In addition, due to the influence of fishery production, aquaculture activities and marine engineering, the increase of nutrient in the seawater of Wenchang will have a negative impact on the seagrass bed. In order to further analyze the effects of environmental changes on seagrass, we will expand the scope of our research and increase the frequency of monitoring, and strengthen the study on the growth and physiological level of seagrass from the interaction of multiple factors, to understand the long-term changes of seagrass in different environments, and explore the mechanism of its response to the external environmental changes.

In view of the degradation of seagrass resources in Wenchang, it is hoped that all sectors of society should pay attention to the conservation of seagrass, in particular, by rationally planning the scale of aquaculture; flexibly managing fishery activities such as raking snails and clams, appropriately reducing the frequency of digging; scientifically planning the construction of water intake projects, so as to reduce the damage to the seagrass bed.

Data availability statement

The raw data supporting the conclusions of this article will be made available by the authors, without undue reservation.

Author contributions

MF: Conceptualization, Writing – original draft, Writing – review & editing. JJ: Data curation, Investigation, Writing –

original draft. DW: Supervision, Writing – review & editing. GF: Funding acquisition, Supervision, Writing – review & editing. YS: Writing – review & editing. HW: Writing – review & editing. DZ: Software, Writing – review & editing.

Funding

The author(s) declare financial support was received for the research, authorship, and/or publication of this article. We acknowledge the financial support from the Comprehensive Survey of Natural Resources in "Hai Cheng Wen" Coastal Zone (DD20230414), the Comprehensive Survey of Natural Resources in Huizhou-Shanwei Coastal Zone (DD20230415).

Conflict of interest

The authors declare that the research was conducted in the absence of any commercial or financial relationships that could be construed as a potential conflict of interest.

Publisher's note

References

Alexandre, A., Hill, P. W., Jones, D. L., and Santos, R. (2015). Dissolved organic nitrogen: A relevant, complementary source of nitrogen for the seagrass *Zostera marina*. *Limnol. Oceanogr.* 60, 1477–1483. doi: 10.1002/lno.10084

Atkinson, M. J., and Smith, S. V. (1983). C: N: P ratios of benthic marine plants. *Limnol. Oceanogr.* 28, 568–574. doi: 10.4319/lo.1983.28.3.0568

Bertelli, C. M., Creed, J. C., Nuuttila, H. K., and Unsworth, R. K. F. (2020). The response of the seagrass *Halodule wrightii* Ascherson to environmental stressors. *Estuarine Coast. Shelf Sci.* 238, 106693. doi: 10.1016/j.ecss.2020.106693

Bertelli, C. M., and Unsworth, R. K. F. (2018). Light stress responses by the eelgrass, *zostera marina* (L). *Front. Environ. Sci.* 6. doi: 10.3389/fenvs.2018.00039

Burkholder, J. M., Tomasko, D. A., and Touchette, B. W. (2007). Seagrasses and eutrophication. *J. Exp. Mar. Biol. Ecol.* 350, 46–72. doi: 10.1016/j.jembe.2007.06.024

Cai, Z., Chen, S., Wu, Z., Liang, D., Yin, F., Tong, Y., et al. (2017). Distribution differences and environmental effects of seagrasses between Bays and Lagoons of Hainan Island. *Trans. Oceanol. Limnol.* 3), 74–84. doi: 10.13984/j.cnki.cn37-1141.2017.03.011

Chen, S., Pang, Q., Cai, Z., Wu, Z., Shen, J., Wang, D., et al. (2020). Analysis of distribution characteristics, health status, and influencing factors of seagrass bed in Lian lagoon, Hainan Island. *Mar. Sci.* 44, 57–64. doi: 10.11759/hykx20200426004

Chen, S., Wang, D., Wu, Z., Zhang, G., Li, Y., Tu, Z., et al. (2015). Discussion of the change trend of the seagrass beds in the east coast of Hainan Island in nearly a decade. *Mar. Environ. Sci.* 34, 48–53. doi: 10.13634/j.cnki.mes20150109

Collier, C. J., and Waycott, M. (2014). Temperature extremes reduce seagrass growth and induce mortality. *Mar. pollut. Bulletin.* 83, 483–490. doi: 10.1016/j.marpolbul.2014.03.050

Du, H., Huang, C., and Dong, Q. (2006). Distribution of dissolved oxygen in zhelin Bay and its relationship with nutrients. *J. oceanogr. Taiwan strait.* 25, 188–193. doi: 10.3969/j.issn.1000-8160.2006.02.006

Egea, L. G., Jiménez-Ramos, R., Vergara, J. J., Hernández, I., and Brun, F. G. (2018). Interactive effect of temperature, acidification and ammonium enrichment on the seagrass *Cymodocea nodosa*. *Mar. Pollut. Bulletin.* 134, 14–26. doi: 10.1016/j.marpolbul.2018.02.029

Guo, Z., Huang, D., Huang, Z., Qi, S., and Yu, X. (2009). Study on investigation and evolution of seagrass bed in Yelin Bay of Hainan Province. *Mar. Environ. Sci.* 28, 706–709. doi: 10.3969/j.issn.1007-6336.2009.06.026

Han, Q., Soissons, L. M., Bouma, T. J., van Katwijk, M. M., and Liu, D. (2016). Combined nutrient and macroalgae loads lead to response in seagrass indicator properties. *Mar. pollut. Bulletin.* 106, 174–182. doi: 10.1016/j.marpolbul.2016.03.004

Han, Q., Soissons, L. M., Liu, D., van Katwijk, M. M., and Bouma, T. J. (2017). Individual and population indicators of *Zostera japonica* respond quickly to experimental addition of sediment-nutrient and organic matter. *Mar. pollut. Bulletin.* 114, 201–209. doi: 10.1016/j.marpolbul.2016.08.084

Han, Q., Zeng, W., Ye, J., Qiu, C., Shi, Y., and Zhao, M. (2023). Characteristics of morphological and physiological indicators of *Thalassia hemprichii* and environmental factors in Xincun Bay, Haiman Island. *Prog. Fishery Sci.* 44, 225–238. doi: 10.19663/j.issn2095-9869.20230330001

He, B., Wei, M., and Li, Z. (2012). Relations of water self-purify ability with water dynamics, biological and chemical factor in sea grass bed ecosystem in Tieshan Bay. *Mar. Environ. Sci.* 31, 662–666, 673.

Höffle, H., Thomsen, M. S., and Holmer, M. (2011). High mortality of Zostera marina under high temperature regimes but minor effects of the invasive macroalgae *Gracilaria vermiculophylla*. *Estuarine Coast. Shelf Sci.* 92, 35–46. doi: 10.1016/j.ecss.2010.12.017

Howard, J. L., Lopes, C. C., Wilson, S. S., McGee-Absten, V., Carrión, C. I., and Fourqurean, J. W. (2020). Decomposition rates of surficial and buried organic matter and the lability of soil carbon stocks across a large tropical seagrass landscape. *Estuaries Coasts* 44, 846–866. doi: 10.1007/s12237-020-00817-x

Huang, C., Zhang, J., Jiang, Z., and Huang, X. (2017). Nutrients uptake processes of seagrass and its competition with epiphytic algae. *J. Fisheries Res.* 39, 222–228. doi: 10.14012/j.cnki.fjsc.2017.03.009

Invers, O., Romero, J., and Pérez, M. (1997). Effects of pH on seagrass photosynthesis: a laboratory and field assessment. *Aquat. Botany* 59, 185–194. doi: 10.1016/s0304-3770(97)00072-7

Jiang, Z., Huang, D., Fang, Y., Cui, L., Zhao, C., Liu, S., et al. (2020). Home for marine species: Seagrass leaves as vital spawning grounds and food source. *Front. Mar. Sci.* 7. doi: 10.3389/fmars.2020.00194

Jiang, Z., Huang, X., and Zhang, J. (2012). Effect of environmental stress on non-structural carbohydrates reserves and transfer in seagrasses. *Acta Ecologica Sinica* 32, 6242–6250. doi: 10.5846/stxb201108311275

Jiang, Z., Huang, X., and Zhang, J. (2013). Effect of nitrate enrichment and salinity reduction on the seagrass *Thalassia hemprichii* previously grown in low light. *J. Exp. Mar. Biol. Ecol.* 443, 114–122. doi: 10.1016/j.jembe.2013.02.034

Kahn, A. E., and Durako, M. J. (2006). *Thalassia testudinum* seedling responses to changes in salinity and nitrogen levels. *J. Exp. Mar. Biol. Ecol.* 335, 1–12. doi: 10.1016/j.jembe.2006.02.011

Lee, K. S., Park, S. R., and Kim, Y. K. (2007). Effects of irradiance, temperature, and nutrients on growth dynamics of seagrasses: A review. *J. Exp. Mar. Biol. Ecol.* 350, 144–175. doi: 10.1016/j.jembe.2007.06.016

Liu, P.-J., Ang, S.-J., Mayfield, A. B., and Lin, H.-J. (2020). Influence of the seagrass *Thalassia hemprichii* on coral reef mesocosms exposed to ocean acidification and experimentally elevated temperatures. *Sci. Total Environment* 700, 134464. doi: 10.1016/j.scitotenv.2019.134464

Liu, W., Han., Q., Tang, Y., and Sun, X. (2017). Review of nutrient enrichment and global warming effects on seagrasses. *Chin. J. Ecol.* 36, 1087–1096. doi: 10.13292/j.1000-4890.201704.027

Liu, S., Jiang, Z., Wu, Y., Zhang, J., Zhao, C., and Huang, X. (2017). Mechanisms of sediment carbon sequestration in seagrass meadows and its responses to eutrophication (in Chinese). *Chin. Sci. Bulletin.* 62, 3309–3318. doi: 10.1360/N972017-00376

Liu, S., Jiang, Z., Zhang, J., Wu, Y., Lian, Z., and Huang, X. (2016). Effect of nutrient enrichment on the source and composition of sediment organic carbon in tropical seagrass beds in the South China Sea. *Mar. pollut. Bulletin.* 110, 274–280. doi: 10.1016/j.marpolbul.2016.06.054

Liu, S., Trevathan-Tackett, S. M., Jiang, Z., Cui, L., Wu, Y., Zhang, X., et al. (2022). Nutrient loading decreases blue carbon by mediating fungi activities within seagrass meadows. *Environ. Res.* 212, 113280. doi: 10.1016/j.envres.2022.113280

Marbà, N., Santiago, R., Díaz-Almela, E., Álvarez, E., and Duarte, C. M. (2006). Seagrass (*Posidonia oceanica*) vertical growth as an early indicator of fish farm-derived stress. *Estuarine Coast. Shelf Sci.* 67, 475–483. doi: 10.1016/j.ecss.2005.11.034

McKenzie, L. J., Yoshida, R. L., Aini, J. W., Andréfouet, S., Colin, P. L., Cullen-Unsworth, L. C., et al. (2021). Seagrass ecosystem contributions to people's quality of life in the Pacific Island countries and territories. *Mar. pollut. Bulletin.* 167, 203–223. doi: 10.1016/j.marpolbul.2021.112307

Neckles, H. A., Short, F. T., Barker, S., and Kopp, B. S. (2005). Disturbance of eelgrass *Zostera marina* by commercial mussel Mytilus edulis harvesting in Maine: dragging impacts and habitat recovery. *Mar. Ecol. Prog. Series* 285, 57–73. doi: 10.3354/MEPS285057

Palacio-López, K., Beckage, B., Scheiner, S., and Molofsky, J. (2015). The ubiquity of phenotypic plasticity in plants: a synthesis. *Ecol. Evolution* 5, 3389–3400. doi: 10.1002/ece3.1603

Palacios, S., and Zimmerman, R. (2007). Response of eelgrass *Zostera marina* to CO_2 enrichment: possible impacts of climate change and potential for remediation of coastal habitats. *Mar. Ecol. Prog. Series* 344, 1–13. doi: 10.3354/meps07084

Scott, A. L., York, P. H., Duncan, C., Macreadie, P. I., Connolly, R. M., Ellis, M. T., et al. (2018). The role of herbivory in structuring tropical seagrass ecosystem service delivery. *Front. Plant Sci.* 9. doi: 10.3389/fpls.2018.00127

Short, F. T., Polidoro, B., Livingstone, S. R., Carpenter, K. E., Bandeira, S., Bujang, J. S., et al. (2011). Extinction risk assessment of the world's seagrass species. *Biol. Conserv.* 144, 1961–1971. doi: 10.1016/j.biocon.2011.04.010

Suykerbuyk, W., Govers, L., van Oven, W. G., Giesen, K., Giesen, W. B. J. T., de Jong, D. J., et al. (2018). Living in the intertidal: Desiccation and shading reduce seagrass growth but high salinity or population of origin have no additional effect. *PeerJ.* 6, 52341. doi: 10.7717/peeri.5234

Terrados, J., Duarte, C., Kamp-Nielsen, L., Agawin, N. S., Gacia, E., Lacap, D., et al. (1999). Are seagrass growth and survival constrained by the reducing conditions of the sediment? *Aquat. Botany* 65, 175–197. doi: 10.1016/s0304-3770(99)00039-x

Wang, D., Wu, Z., Chen, C., Lan, J., Wu, R., Chen, X., et al. (2012). Distribution of seagrass resources and existing threat in Hainan Island. *Mar. Environ. Sci.* 31, 34–38. doi: 10.3969/j.issn.1007-6336.2012.01.008

Wu, Y., Jiang, Z., Liu, S., Zhang, J., Lian, Z., and Huang, X. (2017). Effects of salinity on the photodegradation of chromophoric dissolved organic matter (CDOM) released by seagrass *Enhalus acoroides* and *Thalassia hemprichii* leaf litter. *Chin. J. Ecol.* 36, 687–694. doi: 10.13292/j.1000-4890.201703.012

Xu, B., Zhang, J., Lang, S., Chen, S., Wu, Z., and Wang, D. (2022). Ecological status and degradation factors in seagrass beds along the coast of Wenchang, Hainan. *J. Appl. Oceanogr.* 41, 614–624. doi: 10.3969/J.ISSN.2095-4972.2022.04.007

Zhang, J., Xu, B., Lang, S., Chen, S., and Wu, Z. (2022). Resource changes of macroalgae and analysis of their influencing actors in Wenchang coast of Hainan province. *Trans. Oceanol. Limnol.* 4, 9–138. doi: 10.13984/j.cnki.cn37-1141.2022.03.018

Zheng, F., Qiu, G., Fan, H., and Zhang, W. (2013). Diversity, distribution and conservation of Chinese seagrass species. *Biodiversity Sci.* 21, 517–526. doi: 10.3724/SP.J.1003.2013.10038

Zhong, C., Sun, K., Liao, Y., Qi, S., Chen, Q., Yin, Q., et al. (2019). Distribution status of seagrass and its relationship with different habitat types in Liusha bay of Guangdong province. *Mar. Environ. Sci.* 38, 521–527. doi: 10.13634/j.cnki.mes.2019.04.006

Zhu, Z., Ma, K., Fang, Z., Cai, Z., and Chen, S. (2017). Distribution of seagrass resources of Eucheuma nature reserve of Hainan province and its protection suggestions. *Guangdong Agric. Sci.* 44, 90–98. doi: 10.16768/j.issn.1004-874X.2017.04.014

frontiers | Frontiers in Marine Science

TYPE Original Research
PUBLISHED 19 September 2024
DOI 10.3389/fmars.2024.1460272

OPEN ACCESS

EDITED BY
Qing Wang,
Beijing Normal University, China

REVIEWED BY
Jia Jia,
Yellow River Institute of Hydraulic Research, China
Zhengyi Liu,
Chinese Academy of Sciences (CAS), China

*CORRESPONDENCE
Kai Liu
kliu@yic.ac.cn

RECEIVED 05 July 2024
ACCEPTED 21 August 2024
PUBLISHED 19 September 2024

CITATION
Liu K, Gao W, Yu Z, Hu Y, Zuo M, Sun C, Zou X and Wang L (2024) The effect of *Sesuvium portulacastrum* for reducing inorganic nitrogen pollution in coastal mariculture wetland.
Front. Mar. Sci. 11:1460272.
doi: 10.3389/fmars.2024.1460272

The effect of *Sesuvium portulacastrum* for reducing inorganic nitrogen pollution in coastal mariculture wetland

Kai Liu[1]*, Wei Gao[1], Zhenzhen Yu[1], Yongchao Hu[1], Ming Zuo[1], Chen Sun[1], Xiaotao Zou[2] and Lizhi Wang[3]

[1]Sea and Island Research Laboratory, Dongying Institute of Marine Development Research, Dongying, China, [2]Dongying Haimu Agricultural Technology Co., Ltd., Dongying, China, [3]Faculty of Hydraulic Engineering, Environment and Oceanography, Ludong University, Yantai, China

Mariculture ponds are essential components of the coastal wetland, which are often criticized by eutrophication risk for the dissolved inorganic nitrogen (DIN) input to the coastal zone by the culture tailwater. However, the reduce of this DIN pollution was difficult because the tailwater is hard to collect and the treatment is inefficient and expensive. *Sesuvium Portulacastrum* is a coastal vegetation which has high efficiency in DIN absorption from the seawater and sediment. In this study, we use *Sesuvium Portulacastrum* as a tool species to study the control behavior of the DIN in mariculture ponds wetland. The change trend of DIN in pond water and benthic species in pond sediment was investigated. The results showed that *Sesuvium Portulacastrum* reduced NH_{4+}, NO_{3-}, and NO_{2-} in the pond water by 83.21%, 95.22%, and 91.32%, respectively. The species number of benthic organisms was enhanced from 2 to 5 and the species structure was more optimized in *Sesuvium Portulacastrum* pond than control pond. At the end of the experiment, eutrophication indicator species (*Capitella capitata*) was disappeared in the *Sesuvium Portulacastrum* pond. Those suggest that the coastal vegetation (*Sesuvium Portulacastrum*) have great potential to eliminate DIN pollutants in mariculture pond wetland.

KEYWORDS

***Sesuvium portulacastrum*, reduction, inorganic nitrogen, mariculture, pond water**

1 Introduction

Mariculture ponds is an essential component of the coastal wetland because the large water body and proximity the coastal area. It supplies a large amount of quality protein for human about 30% of global mariculture production (The State of World Fisheries and Aquaculture, 2022). Meanwhile, it is often criticized by eutrophication risk for the input the effluents rich in N and P to the adjacent coastal zone. According to the World Food and Agriculture Organization (FAO), the growth in global marine and coastal aquaculture production will mainly come from mariculture in the next 30 years. With this rapid

development trend, adjacent coastal zones would receive a large amount of mariculture tailwater, which enhance the eutrophication risk in this area (Levy et al., 2017). However, human activities such as overfishing, especially the overharvesting of shellfish, have excessive destructed the coastal sediments. It resulted in the disappearance of indigenous habitats such as seagrass beds, macroalgae bed, and oyster reefs which express the key buffering and degradation capacity of coastal zones for the N and P pollutants (Planque et al., 2010). Furthermore, the restoration of indigenous habitats in coastal zone is often slow and difficult. Therefore, it is important to control the N and P level in mariculture pond wetlands to reduce the input of this contaminant to coastal zone.

Currently, the treatment of mariculture tailwater is difficult because it is rich in variety of pollutants including N, P, and a larger number of organic pollutants such as bait and animal limbs (Chen et al., 2016). These pollutants are prone to clogging treatment equipment, which increases the equipment consumed and cost. Furthermore, the high salinity of the tailwater will corrode treatment equipment made of steel. Taking the normal industrial treatment model, the cost of tailwater treatment is 1.47 RMB m^{-3} which could increase the cost of mariculture about 17.6 RMB kg^{-1}, about 50% of the original culture cost (Zeng et al., 2019). Hence, industrial treatment model is unsustainable which tends to reduce the expansion of mariculture by the high culture cost. Therefore, it is urgent to develop a low-costly and eco-friendly method to control the N and P pollution level of mariculture tailwater.

Artificial wetlands constructed by the salt marsh vegetations are often eco-friendly method applied for mariculture tailwater treatment (Hu et al., 2017; Cai et al., 2022). The removal rates of N and P pollution can be up to 92% and 72% or more in this kind of system (Wang et al., 2014). High removal capacity of N and P are form two pathways. First are the abundant microorganisms such as *Phytophthora nitrite*, *Vibrio vulnificus*, and *Platyhelminthes* supply by the root system of the salt marsh vegetation. Another was the uptake of N and P by the growth of salt marsh vegetation in wetland. The combination and cooperative interaction of microorganisms and the growth of salt marsh vegetation would make the efficiently removal capacity of artificial wetlands. In addition, the macro-vegetation surviving in salt marshes, such as *Salicornia europaea L*, *Suaeda salsa (L.) Pall.*, and *Sesuvium portulacastrum*, has evolved the ability to absorb multiple forms of elemental N. Those vegetations could directly utilize peptide organic nitrogen in seawater, which is important for scavenging N in mariculture tailwater (Quintã et al., 2015; Zheng et al., 2016). However, there are still intractable limits for the application of artificial wetland in treatment mariculture ponds tailwater which constructed based by salt marsh vegetations. For example, the high temperatures and salinity of mariculture water make the salt marsh vegetations difficult survival in this harsh environment. It is necessary to select and breed of vegetations tolerant to high temperatures, high salinity, and high stress tolerance for application in the control of pollutants in mariculture wetland.

Sesuvium portulacastrum is a perennial herbaceous saline vegetations that grows in tropical and subtropical coastal areas (Fan et al., 2010). It often grows in high temperature, high salinity, and long-term flooding adverse environments and have potential to select as the contaminant control species in mariculture wetlands. Some applications of the *Sesuvium portulacastrum* in mariculture tailwater treatment have been conducted. For example, wetlands constructed based by *Sesuvium portulacastrum* could increase the removal efficiency of DIN in mariculture effluents (Ma et al., 2021). *Sesuvium portulacastrum* could remove 98.5% of NH_4^+ and 55.9% of total nitrogen in mariculture tailwater (Ying et al., 2018). In addition, the use of *Sesuvium portulacastrum* in a recirculating aquaculture system integrating *Chanos chanos* and *Holothuria scabra* allowed ammonia levels to be controlled and reliably decreased to < 1 mg L^{-1} (Senff et al., 2015). Hence, *Sesuvium portulacastrum* has great potential applications for controlling N pollution in mariculture water environment.

In this work, we select open-air *Holothuria scabra* mariculture ponds in the Yellow River Delta as the study area. The role of *Sesuvium portulacastrum* in controlling inorganic nitrogen (NH_4^+, NO_3^-, and NO_2^-) in pond water during the summer and early autumn growth season of *Holothuria scabra* was observed. Biodiversity parameters were investigated for the pond substrate. Meanwhile, the water temperature in this system was monitored because it is the key factor in ensuring that the *Holothuria scabra* safely survives in growing season in summer and early autumn.

2 Materials and methods

2.1 Study location

The Yellow River Delta is the important coastal *Holothuria scabra* culture zone in China. The culture scale has exceeded 333 km^2 and accounts for more than half of the pond culture area of sea cucumbers in Shandong Province. This region has become the largest sea cucumber pond culture area in China (Wang and Liu, 2023). However, the temperatures and rainfall are variable in the Yellow River Delta, which pose a potential threat to sea cucumber mariculture. In the summers of 2013, 2016, and 2017, the production of *Holothuria scabra* mariculture was significantly decreased due to the high temperatures and lack of oxygen by the short-time strong rainfall. It had seriously affected the development of *Holothuria scabra* mariculture and the living of mariculturist in this area. Meanwhile, the discharge of tailwater would be urgent problem for the culture of *Holothuria scabra* with the gradual tightening of environmental protection policies for mariculture. The experiment was conducted in the *Holothuria scabra* culture ponds in Dongying Kenli District Huilu Aquaculture Co. in the coastal area of Laizhou Bay (E 118°57′50.39″, N 37°37′12.00″) (Figure 1).

2.2 Experimental setup

2.2.1 *Sesuvium portulacastrum*

In summer, *Holothuria scabra* ponds are characterized by high temperature and salinity. Hence, we collected *Sesuvium portulacastrum* near the subtidal zone in Wenchang City, Hainan Province, which also has higher temperature and salinity. It is unable to overwinter and will not impact the local ecosystem in the Yellow River Delta. To maintain the activity of the *Sesuvium*

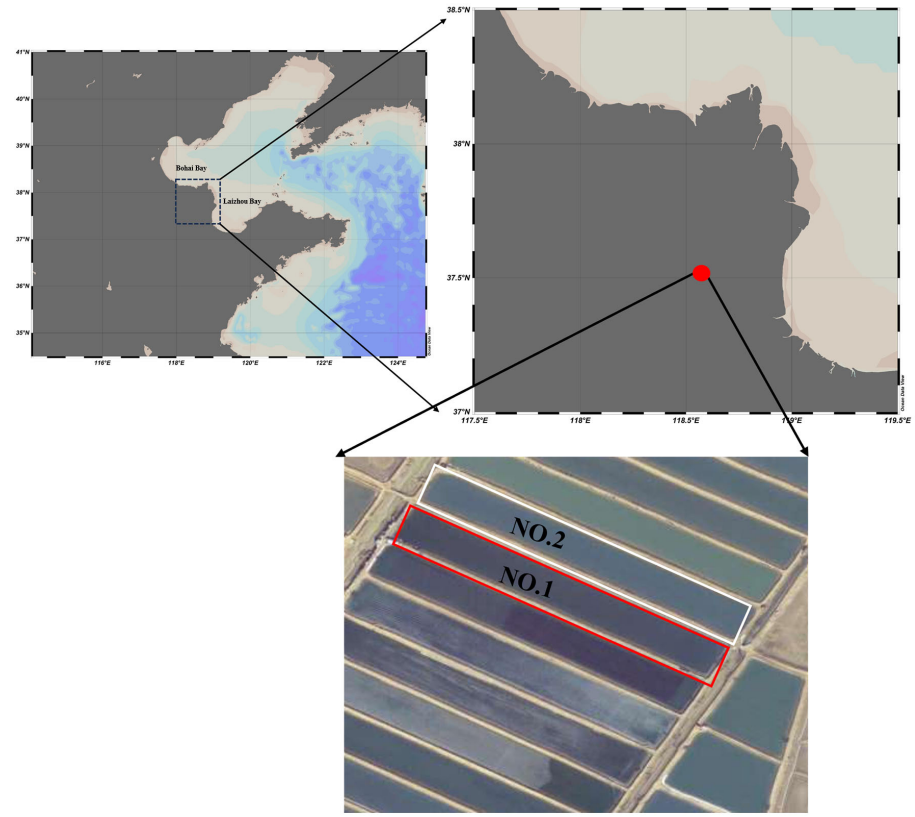

FIGURE 1
The location of the experiment in the sea cucumber ponds in Dongying Kenli District Huilu Aquaculture Co. in the coastal area of Laizhou Bay (E 118°57′50.39″, N 37°37′12.00″). The red boxes in the figure represent the experimental area (NO. 1). The white boxes in the figure represent the control area (NO. 2).

portulacastrum seedlings, we conducted acclimatization process before the begin of the experiment in sea cucumber ponds for 15 d. The brief process was below: *Sesuvium portulacastrum* were staged in 30 L high-density polyethylene square boxes (60cm×50cm×10cm) contain about 20 L seawater. We used air to supply the dissolved oxygen for the *Sesuvium portulacastrum* at a rate of 1.5 m^3 h^{-1} and a light period of 16h:8h. Thick and stout *Sesuvium portulacastrum* with fat leaves was selected for the experiment.

2.2.2 Experiment in the ponds

The experiment was carried out over a period of 120 d from June 5 to October 5 in 2023. The steps were as follows: Two ponds with the same area (1 hm^2), specifications, and facilities were selected to carry out the experiment. Pond No. 1 served as the experiment pond and Pond No. 2 was as the control pond (Figure 1). The experimental ponds were rectangular in shape, east-west oriented, water depth up to 2.5 m, and water quality in accordance with The Water Quality Standards for Fishery (GB 11607-89). Six fish cages were set up in the experimental ponds, with specifications of 3m×1.5m×1m and a 30-purpose polyethylene mesh as the cage coat. Cages were fixed using bamboo poles and ropes, with a foam float tied to each of the four corners of the nets. The distance between every fish cage was 6m. The control pond also comprised six fish cages. At the beginning of June (June 5), we used a bench scale (AHC-WL, T-scale®) to weigh about 0.25kg of *Holothuria scabra* seeding (0.08g/ins-0.10g/ins) and put into every cage. *Sesuvium portulacastrum* with robust plants and fat leaves were selected and transplanted onto XPS (extruded polystyrene foam board) floating beds in June 10. The floating beds were secured together with ties and then fixed above the *Holothuria scabra* seeding cages. About 30% of the surface water of the sea cucumber culture cages was covered by floating beds. The same process was followed for the control pond. The initial concentration of DIN in control pond and experiment pond was 0.927 mg L^{-1} and 0.944 mg L^{-1}, respectively. Figure 2 shows a brief flow of the experiment.

2.3 Sampling and analysis

2.3.1 Sampling

The sampling process is according our previous study and briefly described below (Wang and Liu, 2023). The sample system consists of a collection unit, a filtration unit, and a sampling unit. The collection unit was 125 ml HDPE bottles (Nalgene™, Thermo Fisher Scientific Inc., USA). The filtration unit was a pressure filtration unit (YY3014236, Filter Holder, Millipore®). Since the pond waters contained high concentrations of suspended particulate matter and organic matter, the diameter of the filter

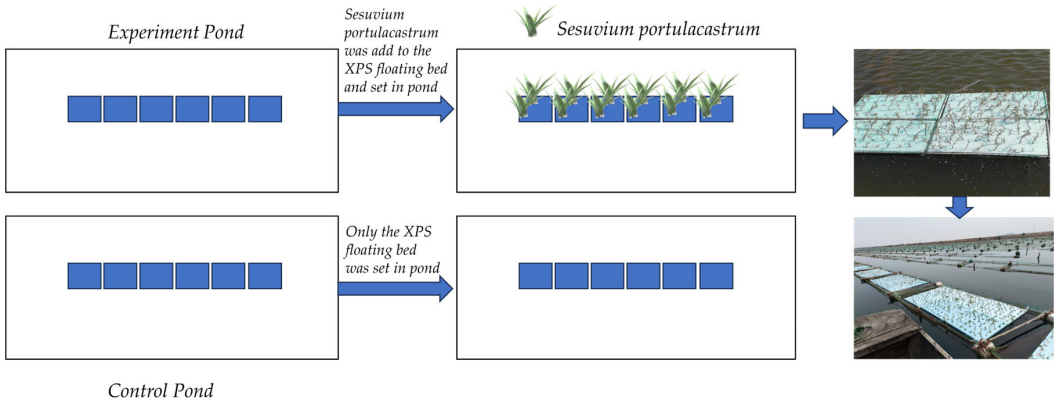

FIGURE 2
The brief flow of the experiment.

membrane (0.22 μm, GPWP14250, Millipore®) was 142 mm. The units were fixed using a C-Flex tube. When sampling, the C-Flex-tube-fixed water intake was directly inserted into the pond water to collected the samples. Two parallel samples were collected. The fixed water intake sampling tubes were attached to a disc filter unit, and washed with ultrapure water before and after each sample. The collected water samples were stored in self-sealing PE bag at -20°C. Sampling devices and bottles were soaked in 3% HNO_3 for 48 h and then rinsed five times with ultra-pure water (>18.2 Ω) and blown dry on an ultra-clean table (Class-100). Water samples were collected every 10 days from June 5 to September 5. The last sample was collected every 30d from September 5 to October 5 because the culture in the pond was over.

Benthic organisms were sampled according to the quantitative sampling method in the Zhang et al., 2007. The collection gear was a QNC7-1 box-type mud collector, the sampling area was 0.25m^2, and each station was sampled 4 times. Samples were eluted with a 0.5 mm mesh set sieve and macrobenthic samples were collected and stored in 500 ml HDPE bottles containing formaldehyde solution. The samples were preserved, categorized, and weighed in accordance with the Specifications for oceanographic survey-Part 6: Marine biological survey (GB/T 12763.3-2007).

2.3.2 Analysis

Regular parameters such as temperature (T), salinity (S), and dissolved oxygen (DO) were collected using a multiparameter water quality analyzer (ProQuatro, YSI®). The concentrations of DIN (NH_4^+-N, NO_2^-N, and NO_3^-N), active phosphate (PO_4^{3-}), and DSi (SiO_2) of the samples were detected by a continuous-flow nutrient analysis (AutoAnalyzer III, SEAL Analytical™). The quantification limit of the nutrient analysis method for DIN, active phosphate (PO_4^{3-}), and DSi was 0.012 mg L^{-1}, 0.008 mg L^{-1}, 0.011 mg L^{-1} and the recoveries ranged from 95.5% to 101.2%. The samples were analyzed three times and the error must be less than 5%.

Indicator of coastal eutrophication potential (ICEP) was used to measure the nutrients risk of the N and P in the *Sesuvium portulacastrum* ponds to the coastal zone. This index was proposed by Billen and Garnier (2007) and modified it to suit the study because the pond water was not exchanged with the coastal area in the culture process. The modified equation is as follows:

$$ICEP(N) = \left(\frac{C_N}{14 \times 16} - \frac{C_{Si}}{28 \times 20}\right) \times 106 \times 12 \quad (1)$$

$$ICEP(P) = \left(\frac{C_p}{31 \times 16} - \frac{C_{Si}}{28 \times 20}\right) \times 106 \times 12 \quad (2)$$

In this study, benthic community compositional diversity was expressed using the Shannon–Wiener species diversity index (H'), the Margaief species abundance index (D), and the Pielou species evenness index (J) (Lobon-Cervia et al., 2012). The following formula was used:

$$H' = -\sum_{i=1}^{a} N_i \ln N_i \quad (3)$$

$$J = \frac{H'}{\ln S} \quad (4)$$

$$D = \frac{S-1}{\ln N} \quad (5)$$

N_i is the ratio of the number of individuals of species i to the total number of individuals of all captured organisms (n_i/N); N is the total number of individuals of all captured organisms; and S is the total number of species of all captured organisms.

The Mcnaughton dominance index was used to determine the dominant species in the pond sediment (Lobon-Cervia et al., 2012). Community dominance was calculated using the following formula:

$$W = \frac{S_1 + S_2}{ST} \quad (6)$$

S_1 and S_2 are the biotic densities of the two most abundant species in the community; ST is the total benthic density.

3 Results

3.1 Basic geochemical parameters

The temperature (T), salinity (S), pH, and dissolved oxygen (DO) are key geochemical parameters related to the stability of the environment in *Holothuria scabra* pond. Especially for the temperature, it is related to the survival rate of the *Holothuria scabra* seedlings cultured in the pond. Figure 3 shows the change trend of basic geochemical parameters throughout the culture process. In all the ponds, the water temperature showed a trend of increasing and then decreasing, which was similar to the weather temperature changes during the experiment. However, changing amplitude of temperature was different from the experimental and control ponds (Figure 3A). In the control pond, the water temperature increased from 25°C to 30.9°C, whereas that of the experimental pond increased to 29.2°C. This indicates that the *Sesuvium portulacastrum* floating bed can effectively reduce the pond water temperature. It is important for the *Holothuria scabra* in the pond to survive the high temperature period in summer and early autumn.

Changes in DO are strongly influenced by the external environment such as wind around the pond because the water depth of the pond was only about 2m. In the *Sesuvium portulacastrum* pond, the average concentration of DO fluctuate around 4.53 mg L^{-1}, with a concentration fluctuation range of 0.32 mg L^{-1} (Figure 3B). However, in the control pond, the average concentration of DO was 4.35 mg L^{-1}, with a fluctuation range of 0.65 mg L^{-1}. This fluctuation mainly occurred around 60d and 70d, and the lowest concentration of DO was 3.04 mg L^{-1} (Figure 3B). pH showed similar changes trend to DO (Figure 3C). In the *Sesuvium portulacastrum* pond, pH varied from 8.01 to 8.23 with a fluctuation of 0.06. However, in the control ponds, pH varied from 7.89 to 8.24 with a fluctuation of 0.09, and the severe changes were observed around 60 d and 70 d. For salinity, the change trend was almost identical between different ponds (Figure 3D). Salinity ranged from 30-34 and the highest salinity occurring during the maximum temperature in almost 32°C. Evaporation from the pond water body was high during high-temperature periods, resulting in higher salinity in the pond water (Figure 4D). During this period, *Sesuvium portulacastrum* still grew vigorously which indicating the salt and heat tolerance of this plant.

3.2 Dissolved inorganic nitrogen and reactive phosphate

Nitrate nitrogen (NO_3^-N) is the most essential forms for vegetation uptake in the pond. It is also one of the more stable states of elemental N. Figure 4A. shows the changes in NO_3^-N concentration in ponds with or without *Sesuvium portulacastrum*. The concentration of NO_3^-N varied with different ponds. In the *Sesuvium portulacastrum* pond, NO_3^-N was continued declining but the decrease rate gradually slowed with the decrease in temperature. The maximum concentration of NO_3^-N was found in June, about 0.625 ± 0.005 mg L^{-1}. During the culture process, the concentration of NO_3^-N showed three change stages (Figure 4A). There was rapid decline phase from 0 to 40d, a slow decline phase from 40 to 60d, and an equilibrium rise phase from 60 to 90d. About 88.12% of the NO_3^-N was eliminated in the rapid decline phase, while there was only 5% in the slow decline stage. In the control pond, the minimum concentration of NO_3^-N was 0.195 ± 0.002 mg L^{-1} in August and was essentially unchanged by September. Notably, a strenuous fluctuation in NO_3^-N

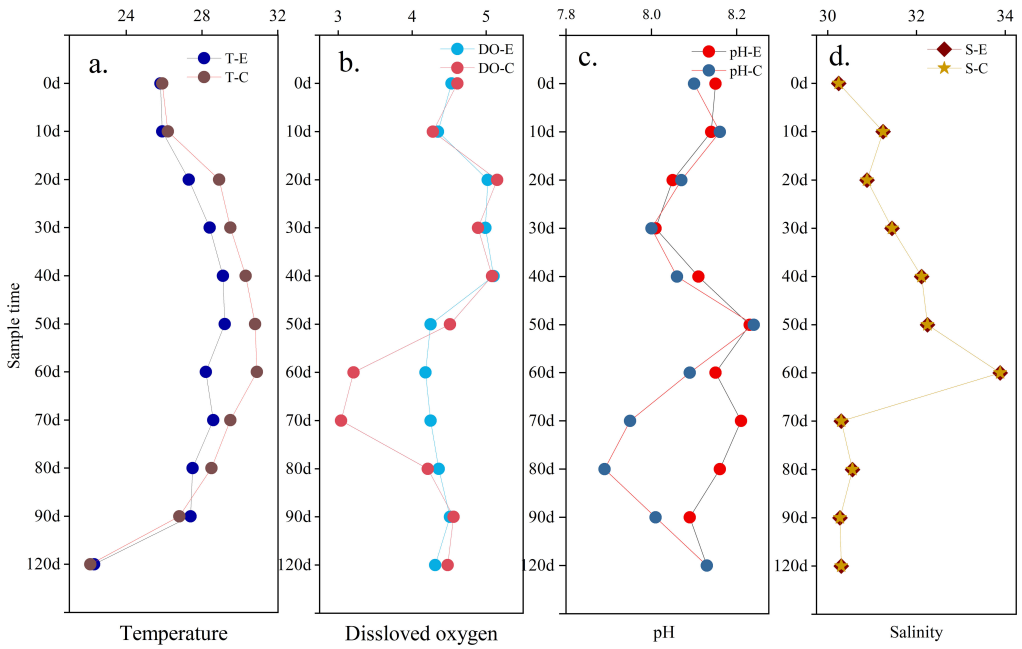

FIGURE 3
Change trend of basic biogeochemical parameters in ponds with or without *Sesuvium portulacastrum*.

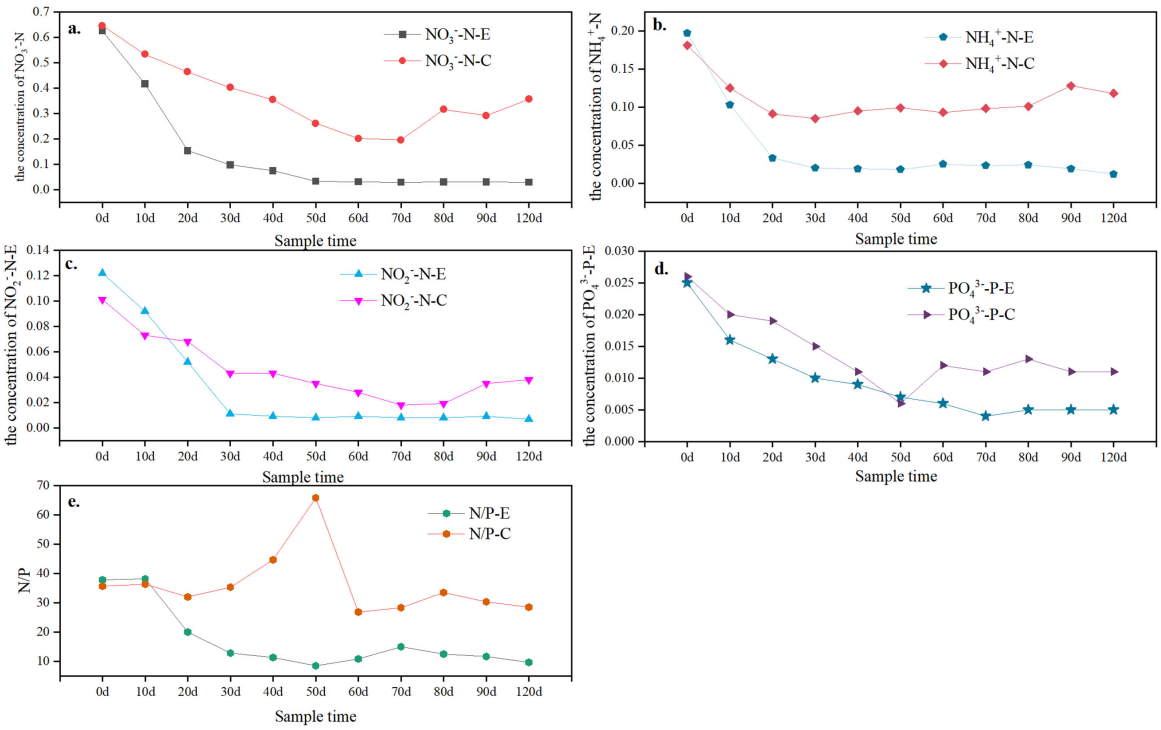

FIGURE 4
Concentration trend of dissolved inorganic nitrogen in the culture system with or without *Sesuvium portulacastrum*: **(A)** NO_3^-N variation; **(B)** NO_2^-N variation; **(C)** NH_4^+-N variation; **(D)** PO_4^{3-}P variation; **(E)** N/P ration variation. X-E represent the pond with *Sesuvium portulacastrum*; X-C represent the pond without *Sesuvium portulacastrum*..

concentration was observed (about 0.356 ± 0.011 mg L^{-1}) in October. However, the NO_3^-N in the *Sesuvium portulacastrum* pond was lower and more stable in the same period than the control pond. The elimination rate of NO_3^-N was 95.22% in the *Sesuvium portulacastrum* system but it was 42.56% in the control pond.

The variation of NO_2^-N was similar to NO_3^-N but more drastic in the culture system. Figure 4B shows the changes in NO_2^-N in the culture system with or without *Sesuvium portulacastrum*. A rapid decline stage was found from 0 to 30d in the *Sesuvium portulacastrum* system about 0.029 ± 0.003 mg L^{-1} (Figure 4B). However, in the control pond, this decline continued to 60d at a concentration amplitude of 0.019 ± 0.006 mg L^{-1}. There was no increase in NO_2^-N in the *Sesuvium portulacastrum* pond during September and October. However, for the control ponds, NO_2^-N showed a significant increase and fluctuation. About 91.32% of the NO_2^-N was consumed in the *Sesuvium portulacastrum* system in the rapid decline stage (0-30d). However, the removal rate was 81.67% in the control pond.

The change trend of NH_4^+-N in the culture system was different to that of DIN in other forms. Figure 4C. shows the trend of NH_4^+-N in the culture system with or without *Sesuvium portulacastrum*. In the *Sesuvium portulacastrum* system, NH_4^+-N showed a very rapid decrease from 0 to 20d, and about 83.21% was removed. After this stage, NH_4^+-N showed a slow removal rate of only 8-10% from 20d to 40d. After 40d, the NH_4^+-N stably fluctuated around 0.19 ± 0.07 mg L^{-1} in the experimental pond. In the control pond, NH_4^+-N also showed a relatively intense decline, about 50% in 20d. However, the concentration of NH_4^+-N stably fluctuated around 0.10 ± 0.05 mg L^{-1} with the culture process.

Reactive phosphate levels in pond water were consistently low (Figure 4D). At the beginning of the experiment, the phosphate concentrations in the two ponds were 0.025 mg L^{-1} and 0.026 mg L^{-1}, respectively. In the *Sesuvium portulacastrum* ponds, reactive phosphate had a rapid declining phase from 0 to 30d. It then gradually decreased to minimum of 0.005 mg L^{-1} in 30-70d stage. After 70d, the phosphate concentration in the ponds fluctuated around 0.005 mg L^{-1}. In the control ponds, different trends of changes in phosphate concentration were observed. A sharp decline in phosphate occurred during the 0-50d period, although most of the decline was lower than in the experimental ponds. At 50d, the phosphate concentration reached minimum concentration (about 0.006mg L^{-1}). However, after 50 days, there was a significant increase in phosphate concentration in the control pond. It eventually rose to 0.18 mg L^{-1}. This trend was similar to the changes in DIN in the control system. The N/P ratio was also express extremely varied in the ponds with the culture (Figure 4E). In the control ponds, the N/P ratio was changed from 26.8 to 65.8 and maximum value was observed in 40d to 50d. It was no found a clear change trend in the N/P ratio. However, in the experiment ponds, the N/P ratio decreased with the culture time. Furthermore, the after 30d, the N/P was maintained in 11.5 ± 1.9. Moreover, the N/P ratio in the experiment pond was lower than in the control pond.

3.3 Eutrophication risk

The ICEP index indicated the eutrophication risk of the water in *Holothuria scabra* ponds and could use to measuring the impact of *Holothuria scabra* culture tailwater on the offshore environment. The maximum eutrophication index of DIN (about 4.63) in the *Sesuvium portulacastrum* pond appeared at the beginning of the experiment (Figure 5). With the culture process, the ICEP gradually decreased until the index became negative after up to 50 d in the experiment pond. It is notably indicated that the eutrophication risk of the experimental ponds disappeared. In the control ponds, the change trend of ICEP was in another way. During the 0-60d, the ICEP changed similarly to the experimental ponds, which gradually decreased but the decreased amplitude was smaller. However, a significant increase of the ICEP about 6.43 was observed in the control ponds at 70d (Figure 5). And the ICEP then decreased and finally stabilized at about 2.4. In the whole experiment process, the ICEP of the control ponds was higher than that in the experimental ponds. These results suggest that *Sesuvium portulacastrum* plays an important role in controlling eutrophication risk in *Holothuria scabra* ponds. The ICEP index for phosphate was consistently negative in both the experimental and control ponds. This result clarified that the *Holothuria scabra* ponds are phosphate-limited in the Yellow River Delta. It is noteworthy that ICEP index for phosphate fluctuated less in the experimental ponds than in the control ponds. It also indicates that *Sesuvium portulacastrum* plays an important role in phosphate stabilization in *Holothuria scabra* pond like the control behavior in DIN.

3.4 Benthos community

The acquisition of benthic species in different ponds was compared at 0d, 30d, 60d, and 90d (Table 1 and Figure 6). In the control pond, only two benthic species was observed, which mainly dominated by *Capitella capitata* and with a small number of *Minicoraphium insidiosum*. The composition of benthic species was not change in this pond and the biodiversity parameters at low level. The Shannon–Wiener diversity index (H') was about 0.13-0.16, the Pielou evenness index (J) was about 0.24-0.26, and the Margaief species abundance index (D) was about 0.19-0.22. It indicated that the control pond was undergoing persistently eutrophication. In the *Sesuvium portulacastrum* pond, the benthic species was changed with the experiment process. The benthic species was consistent to the control pond in the preliminary stage of the experiment, dominated by *Capitella capitata* and small number of *Minicoraphium insidiosum*. However, as the experiment continued, the number of species increased to 3 and *Capitella capitata* was about 45.23% lower than in the control pond in 30d. The Shannon–Wiener diversity index (H') increased from 0.17 to 1.06, the Pielou evenness index (J) from 0.24 to 0.96, and the Margaief species abundance index (D) from 0.21 to 0.46. The change of benthic organisms in the *Sesuvium portulacastrum* pond was shown in Figure 6. Significant variations in species structure occurred during the 60 d. Although the number of species was decreased from 3 to 2, the *Capitella capitata*, a species indicative of eutrophication, decreased from 38.79% to 0% (Silva et al., 2017). *Capitella capitata* was replaced by the *Perinereis aibuhitensis* and *Pseudopolydora paucibranchiata*. Over the 90d, the number of species increased to 5 and some shellfish such as *Theora lata* appeared.

3.5 *Holothuria scabra* seedling

At 80 d, five *Holothuria scabra* fishfly cages were randomly selected for weighing in the experiment and control ponds, respectively. This result would best reflect the role of the *Sesuvium portulacastrum* system in protection of *Holothuria scabra* seedlings because the high temperature period has just

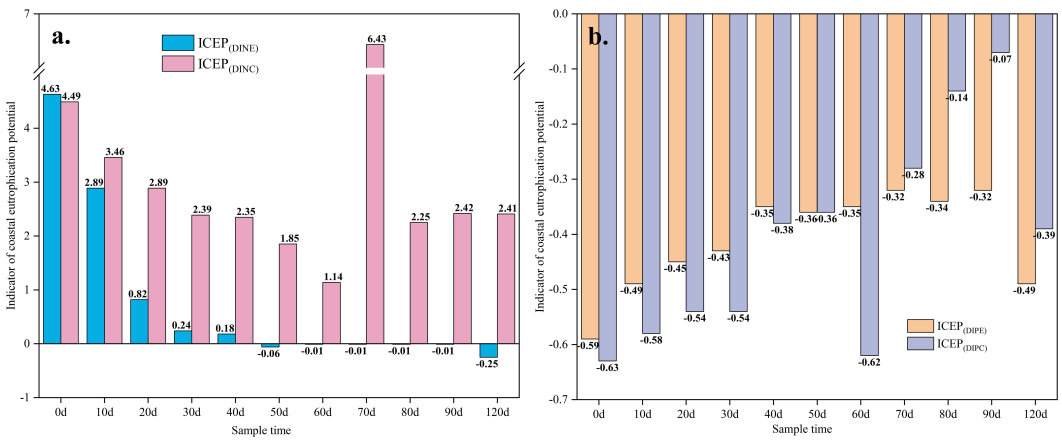

FIGURE 5
Indicator of coastal eutrophication potential in the culture system with or without *Sesuvium portulacastrum*. **(A)** $ICEP_{(DINE)}$ and $ICE_{P(DINC)}$ are the indicators of coastal eutrophication potential of dissolved inorganic nitrogen in the *Sesuvium portulacastrum* and control systems, respectively; **(B)** $ICEP_{(DIPE)}$ and $ICEP_{(DIPC)}$ are the indicators of coastal eutrophication potential of active phosphate in the *Sesuvium portulacastrum* and control systems, respectively.

TABLE 1 Structural parameters of benthic organisms in the *Sesuvium portulacastrum* pond and control pond at different times.

Sample time (d)	Species		Shannon–Wiener diversity index (H')		Pielou evenness index (J)		Margaief species abundance index (D)		Simpson dominance index (W)	
0	2^{c}	2^{e}	0.13^{c}	0.17^{e}	0.24^{c}	0.24^{e}	0.22^{c}	0.21^{e}	1.00^{c}	1.00^{e}
30	2^{c}	3^{e}	0.16^{c}	1.06^{e}	0.24^{c}	0.96^{e}	0.19^{c}	0.46^{e}	1.00^{c}	0.98^{e}
60	2^{c}	2^{e}	0.15^{c}	0.28^{e}	0.25^{c}	0.26^{e}	0.21^{c}	0.20^{e}	1.00^{c}	1.00^{e}
90	2^{c}	5^{e}	0.16^{c}	2.04^{e}	0.26^{c}	1.35^{e}	0.20^{c}	0.92^{e}	1.00^{c}	0.35^{e}

c is control pond; e is Sesuvium portulacastrum pond.

passed. The survival rate was calculated according to the seedling casting of 0.25 kg and the specification of 11,000 heads/kg. The survival rate results are shown in Table 2. In the experiment pond, the average harvest was 2.313 kg, with a single weight of 1.732 g ins^{-1} and a survival rate of 61.45%. In the control pond, the average harvest was 1.762 kg, with an average weight of 1.598 g ins^{-1} and a survival rate of 40.29%. The average harvest of the experimental pond was increased by 0.551 kg, the average weight of every seedling was increased by 0.078 g, and the survival rate was increased by 21.16% compared with the control pond.

4 Discussion

From the experiment results, the *Sesuvium portulacastrum* system in the *Holothuria scabra* ponds expressed positive influences in reducing pond eutrophication, increasing pond ecological stability, and conserving *Holothuria scabra* seedlings under high temperatures in summer and early autumn. The *Sesuvium portulacastrum* might be the key factor to induce those positive influences in the mariculture pond system. Figure 7 shows the potential ecological cycle built by *Sesuvium portulacastrum*.

4.1 For the dissolved inorganic nitrogen

In the begin of the experiment, the initially high concentration of NO_3^-N reflected the transformation of NH_4^+-N and NO_2^-N by microorganisms in the pond water (Diab et al., 1993). NO_3^-N is the most stable state of elemental N and was more conservative removal compared to other forms (NH_4^+-N and NO_2^-N) in the seawater. It was mainly accomplished through the uptake behavior of algae and vegetations in the pond water (Pereira et al., 2020). Generally, the higher concentration of NO_3^-N the faster uptake of *Sesuvium portulacastrum* in the pond water (Hao et al., 2024). When the NO_3^-N in the system declines to certain level, the uptake of this form will gradually become slower (Pereira et al., 2020; Hao et al., 2024). However, when the NO_3^-N is gradually depleted, the concentration balance between the sediment-water was broken induced the release of NO_3^-N from sediment to water (Khoi et al., 2006). This release process is mainly dominated by the microbial activities in the sediment (Zhang et al., 2015). Under the strong adsorption and uptake of the *Sesuvium portulacastrum* system, the released nitrate will be rapidly consumed (Peng et al., 2022). NO_3^-N in the pond will eventually reach the equilibrium with a relatively low concentration. In addition, epiphytic algae appeared on the roots of *Sesuvium portulacastrum* in the late stage of the experiment. This indicated that not only the *Sesuvium portulacastrum* but also the epiphytic environment created by the root system have an important influence on the NO_3^-N removal in the system (Dou et al., 2011; Liu et al., 2019). Hence, *Sesuvium portulacastrum* play powerful absorber for NO_3^-N in the mariculture pond because this form of nitrogen was easily and rapidly uptake by vegetations (Cai et al., 2022).

As an important intermediate state of nitrification in the *Sesuvium portulacastrum* pond system, the concentration of NO_2^-N reflects the influence of the whole system on the cycling of

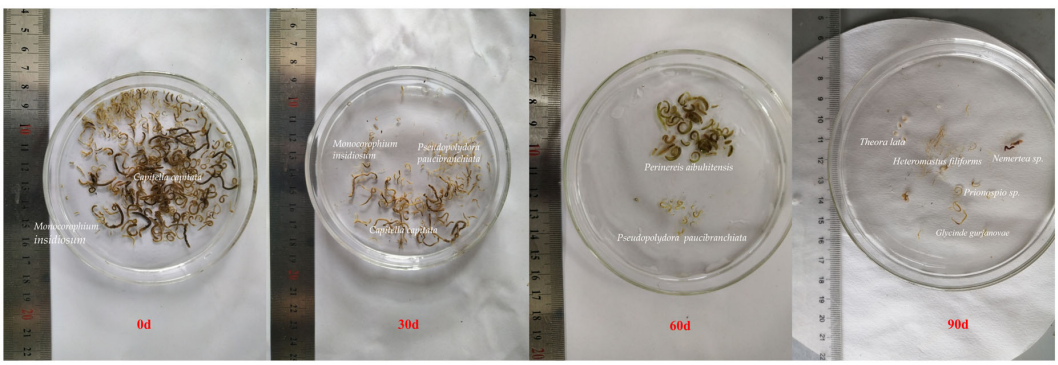

FIGURE 6
Change trend of benthic organisms in the Sesuvium portulacastrum pond.

TABLE 2 The total biomass, individual weight, and survival rate in the different ponds.

Pond	total biomass (kg)	individual weight (g/ins)	survival rate (%)
Experiment pond	2.313 ± 0.056	1.676 ± 0.155	61.45 ± 1.36
Control pond	1.762 ± 0.085	1.598 ± 0.187	40.17 ± 1.50

elemental N (Beman et al., 2013). The concentration of NO_2^-N was in the rapid decline stage (0-20d) when the dissolved oxygen increased in the pond water. High dissolved oxygen would promote more active microbial activity, which lead to the conversion of NO_2^-N to stable NO_3^-N and N_2 (Rosamond et al., 2012). However, in this study, the decline in NO_2^-N was smaller in the experimental pond than that in the control pond. This might be the *Sesuvium portulacastrum* system consumed a certain amount of dissolved oxygen during the early growth stages of this plants. It results in partial hypoxia in the pond where the *Sesuvium portulacastrum* are deployed which could reduce the level of nitrification and denitrification (Ni et al., 2021). After 20d of the experiment, the level of NO_2^-N in the *Sesuvium portulacastrum* system decreased sharply. The nitrification system in the *Sesuvium portulacastrum* system was being constructed, resulting in a low level of intermediate nitrogen conversion in the system (Dou et al., 2011; Liu et al., 2019). Meanwhile, the damage of plant root by transplant during the construction of the *Sesuvium portulacastrum* system also caused the release and formation of nitrite in the pond water. When the construction of the microbial nitrification system was completed, the NO_2^-N was rapidly removed. With the culture process, the free NO_2^-N was transformed into a complete form in the pond water, and only a small amount was left to decompose continuously. This stable nitrification system would also continuously eliminate NH_4^+-N in the water, which was rapidly converted to NO_3^-N and NO_2^-N under sufficient oxygen (Dou et al., 2011). In addition, the *Sesuvium portulacastrum* would directly utilize the ammonium nitrogen in the water as a nutrient source for plant growth. The *Sesuvium portulacastrum* system not only an absorber of the NH_4^+-N but also comprises a healthy nitrification system to maintain the cycling between different forms of DIN in the pond. This stable cycle would make the changes in nitrate nitrogen, nitrite nitrogen, and ammonia nitrogen leveled off.

4.2 For the microalgae

The *Sesuvium portulacastrum* system also maintained the microalgae balance in the pond. During the 60d-70d period, abnormal changes in dissolved oxygen, pH, and DIN occurred in the control pond. We believe that this phenomenon is mainly related to the massive death of microalgae in the *Holothuria scabra* ponds, i.e., algal inversion. Microalgae blooms easily induced a sharp decrease of nutrients in the pond by rapid multiplication uptake amount of nutrients (Bell et al., 2015). However, disordered proliferation of microalga was not stable and often exceeded the survival capacity of the pond which could induce the mass and rapid death of this organism (Silva et al., 2017). In addition, sudden rainstorm following persistent high temperature also induced the algal inversion in the pond (Tayaban et al., 2018). The decomposition of microalgae led to sharply decrease in dissolved oxygen and the release of nutrient. Meanwhile, the microalgae gradually entered extinction also caused decrease in DO and pH in September (Sanchis-Perucho et al., 2018). However, this phenomenon did not occur in the *Sesuvium portulacastrum* system. This might because the nutrient uptake behavior of *Sesuvium portulacastrum* suppressed the microalgae in the pond and make them could not disorderly growth (Smith and Horne, 1988). *Sesuvium portulacastrum* could balance the

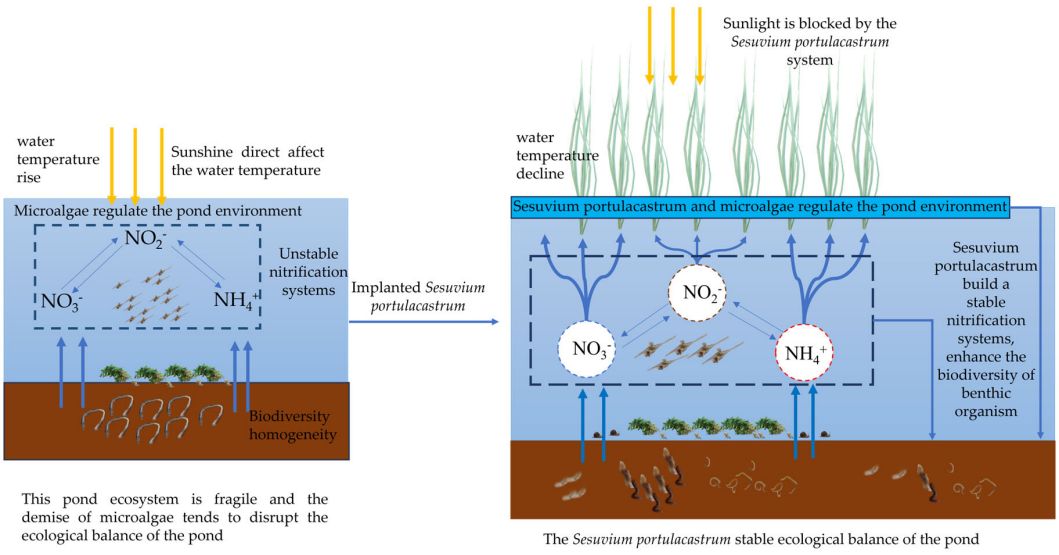

FIGURE 7
The ecological cycle built by Sesuvium portulacastrum in sea cucumber pond.

changes in pH, dissolved oxygen, and nutrients timely when partial algal collapse or algal die-off in the pond. The ecosystem became more stable and the ecological buffering capacity for the DIN pollution were stronger in the *Sesuvium portulacastrum* pond.

4.3 For the organism

The *Sesuvium portulacastrum* system played a beneficial role and made positive influence on both cultured and benthic organisms. The continuous high temperature was often fatal to *Holothuria scabra*. In general, the pond water temperature once exceeded 33°C for more than 2d, the *Holothuria scabra* cultured in the pond would extinction due to intolerance to high temperatures (≥33°C) (Dong and Dong, 2009; Zhang et al., 2022). Meanwhile, the high temperature would also induce hypoxia of the pond water further leading to the death of *Holothuria scabra* (Unmuth et al., 2000; Zhang et al., 2022; Hoblyn and Iversen, 2024). *Sesuvium portulacastrum* community could suppression of high temperatures of pond water by covering water surface to reduce water temperature in the pond. The *Sesuvium portulacastrum* system diminished the water temperature by 1-2°C to enhance the *Holothuria scabra* survival rate about 21.6%. Notably, the *Sesuvium portulacastrum* system changed the organism species and structure in the pond. Aquatic vegetation cover was a significant environmental variable to influence the variance in aquatic organisms in pond sediment (Natsumeda et al., 2015). The vegetation could primarily affect the chemistry characters of pond sediment such as uptake more N and P, and then manage the evolution of ponds benthic species for the direction more species and prefer the vegetation (Sinclair et al., 2021). Hence, the *Sesuvium portulacastrum* system will induce the ponds environment more biodiversity.

In general, the strong uptake behavior of *Sesuvium portulacastrum* diminished the DIN in the mariculture pond, which created nutrient deficit between surface waters. This deficit induced the release of DIN, DIP, and other eutrophication factors from sediment (Wu et al., 2021). Meanwhile, it also increased the decomposition of organic debris in sediments. Changes in sediment composition would cause variations in benthos species structure (Posey et al., 1993; Ni et al., 2021). In mariculture pond, the benthic organisms in pond sediment were often single and mostly represented by eutrophication indicator species such as *Capitella capitata*. The establishment of the *Sesuvium portulacastrum* system led to a succession of benthic organisms in the mariculture pond (Kaenel et al., 1998). For example, the replacement of the *Capitella capitata* by the *Perinereis aibuhitensis* in the pond sediment indicated more stable and health pond depositional environment with the *Sesuvium portulacastrum*.

5 Conclusions

The *Sesuvium portulacastrum* system established in the *Holothuria scabra* ponds demonstrated a very positive impact on the pond and around environment. It reduced the NH_4^+, NO_3^-, and NO_2^- in the pond water by 83.21%, 95.22%, and 91.32%, respectively. Active phosphate was suppressed to low levels (<0.005 mg L^{-1}) in the pond water. The number of pond benthic organism species was enhanced from 2 to 5. *Capitella capitata*, the eutrophication indicator organism, was disappeared and *Perinereis aibuhitensis* appeared. These results suggest that the *Sesuvium Portulacastrum* could both reduce DIN pollutants in *Holothuria scabra* culture pond and regulate the pond environment. However, studies on the effects of *Sesuvium portulacastrum* and other aquatic vegetations on the stability of mariculture pond ecosystems are still few and focused on nutrient depletion. Its effects on the microbial, microalgal, and elemental geochemical cycles and biodiversity in mariculture ponds still need to be further investigated. In addition, the wetland function of the mariculture pond around the coastal area should be taken seriously in future.

Data availability statement

The raw data supporting the conclusions of this article will be made available by the authors, without undue reservation.

Author contributions

KL: Writing – original draft, Writing – review & editing, Funding acquisition, Methodology, Software. WG: Formal analysis, Investigation, Visualization, Writing – review & editing. ZY: Investigation, Validation, Writing – review & editing. YH: Formal analysis, Investigation, Writing – review & editing. MZ: Formal analysis, Investigation, Writing – review & editing. CS: Investigation, Writing – review & editing. XZ: Investigation, Writing – review & editing. LW: Writing – original draft, Writing – review & editing, Conceptualization.

Funding

The author(s) declare financial support was received for the research, authorship, and/or publication of this article. This research was funded by the Natural Science Foundation of Dongying in China (2023ZR01) and the Foundation of State Environmental Protection Key Laboratory of Marine Ecosystem Restoration (202302).

Acknowledgments

We would like to thank all the group members for their constant field and laboratory assistance, helpful advice, and in-depth discussion. Special thanks to JunQi Chen for the tremendous work on the furthered English-editing and polishing on the manuscript. The Prof. Bingchen Wang and Dr. Fei Cheng were given amount of assistance in sampling and sample analysis.

Conflict of interest

Author XZ was employed by the company Dongying Haimu Agricultural Technology Co., Ltd.

The remaining authors declare that the research was conducted in the absence of any commercial or financial relationships that could be construed as a potential conflict of interest.

Publisher's note

References

Bell, T., Bruyn, W., Marandino, C., Miller, S., Law, C., Smith., M., et al. (2015). Dimethylsulfide gas transfer coefficients from algal blooms in the Southern Ocean. *Atmo. Chem. Phys.* 15, 1783–1794. doi: 10.5194/acp-15-1783-2015

Beman, J. M., Shih, J. L., and Popp, B. N. (2013). Nitrite oxidation in the upper water column and oxygen minimum zone of the eastern tropical North Pacific Ocean. *ISME J.* 7, 2192–2205. doi: 10.1038/ismej.2013.96

Billen, G., and Garnier, J. (2007). River basin nutrient delivery to the coastal sea: assessing its potential to sustain new production of non-siliceous algae. *Mar. Chem.* 106, 148–160. doi: 10.1016/j.marchem.2006.12.017

Cai, Z., Li, Q., Bai, H., Zhu, C., Tang, G., Zhou, H., et al. (2022). Interactive effects of aquatic nitrogen and plant biomass on nitrous oxide emission from constructed wetlands. *Environ. Res.* 213, 113716. doi: 10.1016/j.envres.2022.113716

Chen, Y. B., Song, G. B., Zhao, W. X., and Chen, J. W. (2016). Estimating pollutant loadings from mariculture in China. *Mar. Envir. Sci.* 35, 1–12. doi: 10.13634/j.cnki.mes.2016.01.001

Diab, S., Kochba, M., and Avnimelech., Y. (1993). Nitrification pattern in a fluctuating anaerobic-aerobic pond environment. *Water Res.* 27, 1469–1475. doi: 10.1016/0043-1354(93)90027-F

Dong, Y. W., and Dong, S. L. (2009). Advances of ecological physiology in sea cucumber, *apostichopus japonicus selenka*. *Period Ocean U. China* 39, 908–912. doi: 10.16441/j.cnki.hdxb.2009.05.017

Dou, B. X., Huang, J. R., Li, L. C., Qu, H. T., Zhou, Q. Y., and Li, Z. F. (2011). Research on Effects of nutrient and phosphate removal from marine aquaculture system by Sesuvium portulacastru. *J. Hydroecol.* 32, 94–99. doi: 10.15928/j.1674-3075.2011.05.012

Fan, W., Li, W. J., Fu, G., and Zhang, Z. L. (2010). Sesuvium portulacastrum L., A promising halophyte in research and application. *J. Trop. Subtrop. Bot.* 18, 689–695. doi: 10.3969/j.issn.1005-3395.2010.06.017

Hao, M. M., Li, B., Li, H. J., Qiao, P., Zhang, M. L., Xiang, Z. W., et al. (2024). Effects of salinity and nitrogen and phosphorus concentrations on water quality and growth of Sesuvium portulacastrum. *Trans. Oceanol. Limnol.* 46, 125–133. doi: 10.13984/j.cnki.cn37-1141.2024.02.015

Hoblyn, A., and Iversen, L. L. (2024). Effects on local oxygen conditions by the invasive macrophyte Myriophyllum spicatum. *Aquat. Bot.* 192, 103739. doi: 10.1016/j.aquabot.2023.103739

Hu, J., Liu, J., Fan, J., Hu, Z., Xie, H., Wang, S., et al. (2017). Effect of salinity on the performance of constructed wetlands treating mariculture wastewater with different halophytes and its molecular biological mechanism. *Desalin. Water Treat.* 99, 255–265. doi: 10.5004/dwt.2017.21702

Kaenel, B. R., Kaenel, B. R., Matthaei, C. D., and Uehlinger, U. (1998). Disturbance by aquatic plant management in streams: effects on benthic invertebrates. *Regul. Rivers Res. Manage.* 14, 341–356. doi: 10.1002/(ISSN)1099-1646

Khoi, C. M., Guong, V. T., and Merckx, R. (2006). Predicting the release of mineral nitrogen from hypersaline pond sediments used for brine shrimp Artemia franciscana production in the Mekong Delta. *Aquaculture* 257, 221–231. doi: 10.1016/j.aquaculture.2006.02.075

Levy, A., Milstein, A., Neori, A., Harpaz, S., Shpigel, M., and Guttman, L. (2017). Marine periphyton biofilters in mariculture effluents: Nutrient uptake and biomass development. *Aquaculture* 473, 513–520. doi: 10.1016/j.aquaculture.2017.03.018

Liu, X., Pu, X., Luo, D., Lu, J., and Liu, Z. L. (2019). Model assessment of nutrient removal via planting Sesuvium portulacastrum in floating beds in eutrophic marine waters: the case of aquaculture areas of Dongshan Bay. *Acta Oceanol. Sin.* 38, 91–100. doi: 10.1007/s13131-019-1492-5

Lobon-Cervia, J., Rezende, C. F., and CastelLaos, C. (2012). High species diversity and low density typify drift and benthos composition in neotropical streams. *Fund. Appl. Limnol.* 181, 129–142. doi: 10.1127/1863-9135/2012/0242

Ma, X. N., Li, X., Li, J., Ren, J. L., Chi, L., and Cheng, X. W. (2021). Iron-carbon could enhance nitrogen removal in Sesuvium portulacastrum constructed wetlands for treating mariculture effluents. *Biores. Technol.* 352, 124602. doi: 10.1016/j.biortech.2020.124602

Natsumeda, T., Takamura, N., Nakagawa, M., Kadono, Y., Tanaka, T., and Mitsuhashi, H. (2015). Environmental and biotic characteristics to discriminate farm ponds with and without exotic largemouth bass and bluegill in western Japan. *Limnology* 16, 139–148. doi: 10.1007/s10201-015-0453-8

Ni, M., Liang, X., Hou, L. J., Li, W. P., and He, C. Q. (2021). Submerged macrophytes regulate diurnal nitrous oxide emissions from a shallow eutrophic lake: A case study of Lake Wuliangsuhai in the temperate arid region of China. *Sci. Total Environ.* 811, 152451. doi: 10.1016/j.scitotenv.2021.152451

Peng, C., Gao, Y., Tan, Y., Sheng, G., Yang, Y., Huang, J., et al. (2022). Pollution and release characteristics of nitrogen, phosphorus and organic carbon in pond sediments in a typical polder area of the Lake Taihu Basin. *Water* 14, 820. doi: 10.3390/w14050820

Pereira, D. T., Ouriques, L. C., Bouzon, Z. L., and Simioni, C. (2020). Effects of high nitrate concentrations on the germination of carpospores of the red seaweed *Pyropia acanthophora* var. *brasiliensis* (Rhodophyta, Bangiales). *Hydrobiologia* 847, 217–228. doi: 10.1007/s10750-019-04083-2

Planque, B., Fromentin, J. M., Cury, P., Drinkwater, K. F., Jennings, S., Perry, R. I., et al. (2010). How does fishing alter marine populations and ecosystems sensitivity to climate? *J. Mar. Syst.* 79, 403–417. doi: 10.1016/j.jmarsys.2008.12.018

Posey, M. H., Wigand, C., and Stevenson, J. C. (1993). Effects of an introduced aquatic plant, hydrilla verticillata, on Benthic Communities in the upper Chesapeake Bay. *Estuar. Coast. Shelf S.* 37, 539–555. doi: 10.1006/ecss.1993.1072

Quintã, R., Hill, P. W., Jones, D. L., Santos, R., Thomas, D. N., and LeVay, L. (2015). Uptake of an amino acid (alanine) and its peptide (trialanine) by the saltmarsh halophytes Salicornia europaea and Aster tripolium and its potential role in ecosystem N cycling and marine aquaculture wastewater treatment. *Ecol. Eng.* 75, 145–154. doi: 10.1016/j.ecoleng.2014.11.049

Rosamond, M. S., Thuss, S. J., and Schiff, S. L. (2012). Dependence of riverine nitrous oxide emissions on dissolved oxygen levels. *Nat. Geosci.* 5, 715–718. doi: 10.1038/ngeo1556

Sanchis-Perucho, P., Duran, F., Barat, R., Pachés, M., and Aguado, D. (2018). Microalgae population dynamics growth with AnMBR effluent: effect of light and phosphorus concentration. *Water Sci. Technol.* 77, 2566–2577. doi: 10.2166/wst.2018.207

Senff, P., Blanc, P. P., Slater, M., and Kunzmann, A. (2015). Low-technology recirculating aquaculture system integrating milkfish Chanos chanos, sea cucumber Holothuria scabra and sea purslane Sesuvium portulacastrum. *Aquac. Environ. Interact.* 75, 145–154. doi: 10.3354/aei00377

Silva, C. F., Seixas, V. C., Barroso, R., Di Domenico, M., Amaral, A. C. Z., and Paiva, P. C. (2017). Demystifying the Capitella capitata complex (Annelida, Capitellidae) diversity by morphological and molecular data along the Brazilian coast. *Plos. One* 12, e0177760. doi: 10.1371/journal.pone.0177760

Sinclair, J. S., Reisinger, L. S., Adams, C. R., Bean, E., Reisinger, A. J., and Iannone, B. V. (2021). Vegetation management and benthic macroinvertebrate communities in urban stormwater ponds: implications for regional biodiversity. *URBAN Ecosyst.* 24, 725–735. doi: 10.1007/s11252-020-01072-5

Smith, D. W., and Horne, A. J. (1988). Experimental measurement of resource competition between planktonic microalgae and macroalgae (seaweeds) in mesocosms simulating the San Francisco Bay-Estuary, California. *Hydrobiologia* 159, 259–268. doi: 10.1007/BF00008239

Tayaban, K. M. M., Pintor, K. L., and Vital, P. G. (2018). Detection of potential harmful algal bloom-causing microalgae from freshwater prawn farms in Central Luzon, Philippines, for bloom monitoring and prediction. *Environ. Dev. Sustain.* 20, 1134–1328. doi: 10.1007/s10668-017-9942-8

The State of World Fisheries and Aquaculture (2022). Available online at: https://www.fao.org/family-farming/detail/ru/c/1565527/ (accessed 2024/5/15).

Unmuth, J. M. L., Lillie, R. A., Dreikosen, D. S., and Marshall, D. W. (2000). Influence of dense growth of Eurasian watermilfoil on lake water temperature and dissolved oxygen. *J. Freshwater Ecol.* 15, 497–503. doi: 10.1080/02705060.2000.9663772

Wang, J. P., Cui, Z. G., Zhou, Q., Ma, S. S., Qu, K. M., and Mao, C. Q. (2014). Removal effect of mariculture wastewater and analysis of microbial communities in constructed wetlands. *Prog. Fish. Sci.* 35, 1–9. doi: 10.11758/yykxjz.20140601

Wang, Z. H., and Liu, K. (2023). Nutrients transport behavior in Inlet River in the Yellow River Delta in winter. *Mar. Pollut. Bull.* 197, 115815. doi: 10.1016/j.marpolbul.2023.115815

Wu, H. P., Hao, B. B., Cai, Y. P., Liu, G. H., and Xing, W. (2021). Effects of submerged vegetation on sediment nitrogen-cycling bacterial communities in Honghu Lake (China). *Sci. Total Environ.* 755, 142541. doi: 10.1016/j.scitotenv.2020.142541

Ying, R., Chen, J. F., Gao, S. S., Li, Z. F., and Feng, J. X. (2018). Single and synergistic effects of Ulva lactuca and Sesuvium portulacastrum on the purification of mariculture wastewater. *Chin. J. Ecol.* 37, 2745–2753. doi: 10.13292/j.1000-4890.201809.014

Zeng, D., Lin, F. M., Wu, G. Y., Hu, L. Q., Shen, K. J., Zhou, C. Y., et al. (2019). Mariculture wastewater treatment by integrated process of hybridmesh, continuous flow sand filter, and activated carbon adsorption. China. *Water Wastewater* 35, 97–102. doi: 10.19853/j.zgjsps.1000-4602.2019.16.020

Zhang, Y. S., Yang, Q. L., and Chen, R. X. (2007). Specifications for oceanographic survey - Part 6: Marine biological survey. (GB/T 12763.6-2007). Available online at: https://std.samr.gov.cn/gb/search/gbDetailed?id=71F772D788FDD3A7E05397BE0A0AB82A (accessed 2023/04/13).

Zhang, Y. Y., Yu, S. E., Liao, M. L., and Dong, Y. W. (2022). Evaluation and prediction of the effects of extreme high temperatures on sea cucumber (*Apostichopus japonicus*) pond aquaculture in China. *J. Fish. Sci. China* 29, 408–420. doi: 10.12264/JFSC2021-0376

Zhang, Z., Lo, I. M. C., Zheng, G. Y., Woon, K. S., and Rao, P. H. (2015). Effect of autotrophic denitrification on nitrate migration in sulfide-rich marine sediments. *J. Soil Sediment* 15, 1019–1028. doi: 10.1007/s11368-015-1078-6

Zheng, D., Gao., M., Wang., Z., She, Z., Jin, C., and Chang, Q. (2016). Performance comparison of biofilm and suspended sludge from a sequencing batch biofilm reactor treating mariculture wastewater under oxytetracycline stress. *Environ. Technol.* 37, 2391–2404. doi: 10.1080/09593330.2016.1150353

frontiers | Frontiers in Marine Science

TYPE Original Research
PUBLISHED 23 September 2024
DOI 10.3389/fmars.2024.1478599

OPEN ACCESS

EDITED BY
Qin Zhu,
Southern Marine Science and Engineering Guangdong Laboratory (Guangzhou), China

REVIEWED BY
Jiakai Liu,
Beijing Forestry University, China
Zhiyuan Zhao,
Royal Netherlands Institute for Sea Research (NIOZ), Netherlands
Limin Sun,
University of Maryland, United States
Zhe Huang,
Tianjin Universityn, China

*CORRESPONDENCE
Zezheng Liu
zezhengliu@hotmail.com
Yunjing Li
306270856@qq.com

RECEIVED 10 August 2024
ACCEPTED 03 September 2024
PUBLISHED 23 September 2024

CITATION
Xu T, Ma X, Li Y, Xue H, Zhao S and Liu Z (2024) Coastal exotic plant serves as a habitat for a notorious wetland pest in unfavorable seasons: A case study of exotic *Spartina alterniflora* in China.
Front. Mar. Sci. 11:1478599.
doi: 10.3389/fmars.2024.1478599

Coastal exotic plant serves as a habitat for a notorious wetland pest in unfavorable seasons: A case study of exotic *Spartina alterniflora* in China

Tianping Xu[1], Xu Ma[2], Yunjing Li[3]*, Hao Xue[4], Shilin Zhao[2] and Zezheng Liu[1]*

[1]School of Marine Sciences, Sun Yat-Sen University and Southern Marine Science and Engineering Guangdong Laboratory (Zhuhai), Zhuhai, China, [2]Department of Water Ecology and Environment, China Institute of Water Resources and Hydropower Research, Beijing, China, [3]Jiangxi Key Laboratory of Watershed Soil and Water Conservation, Jiangxi Academy of Water Science and Engineering, Nanchang, China, [4]State Key Laboratory of Environmental Criteria and Risk Assessment, Chinese Research Academy of Environmental Sciences, Beijing, China

Coastal biological invasions pose a wide-reaching threat to various ecosystems, affecting both vegetation and herbivores in native communities. Although herbivores often exert strong top-down control on vegetation, the impact of invasive species on consumers that strongly regulate native species in invaded ecosystems remains unclear. Therefore, through field surveys and feeding preference experiments, this study examined the effects of the invasive *Spartina alterniflora* Loisel. (hereafter, Spartina) on the native moth Laelia coenosa Hübner (hereafter, *Laelia*), a notorious pest that has been documented to cause significant damage to native *Phragmites australis* (Cav.) Trin. ex Steud. (hereafter, *Phragmites*) marshes in coastal wetlands of China. Field surveys showed that Laelia larvae were more abundant and had higher grazing rates in *Phragmites* than in *Spartina* marshes in summer, but these patterns reversed in autumn. Feeding experiments consistently showed that the dietary preference of Laelia larvae switched from *Phragmites* in summer to Spartina in autumn, likely because Spartina has a longer growing season and relatively higher nutritional quality than Phragmites in autumn. Thus, by providing shelters (i.e., dietary sources and habitats) during unfavorable seasons, *Spartina* invasions may facilitate this insect pest *Laelia* and potentially amplify its damage to native wetland vegetation. Our work reveals a novel, indirect mechanism of coastal invasion impacts and highlights the importance of incorporating seasonal variation in plant-herbivore interactions.

KEYWORDS

salt marshes, Coastal invasions, insect, plant-herbivore interactions, *Phragmites australis*, *Spartina alterniflora*

1 Introduction

Coastal biological invasions pose a significant threat to biodiversity and ecosystem function (Vila et al., 2011; Tekiela and Barney, 2015), as well as the economy and human health (Mack et al., 2000; Liao et al., 2008; Pejchar and Mooney, 2009; Ehrenfeld, 2010; Pysek et al., 2012). Recently, a growing body of literature has demonstrated that consumers may drive the success of invading species in colonizing new areas (Agrawal and Kotanen, 2003; Strauss et al., 2012; Li et al., 2014; Zhai et al., 2024). Invasive plants may facilitate changes in consumer pressure by offering new food sources or protective cover as refuges for native consumers (Dutra et al., 2011; Stewart et al., 2021; Peller and Altermatt, 2024). One of the predominant, and most extensively tested hypotheses linking herbivores and invasion processes is the Enemy Release Hypothesis (ERH). This hypothesis indicates that invasive species release from natural enemies (i.e. herbivores, pathogens) and gain a competitive advantage in their introduced ranges compared to their co-occurring native counterparts (Keane and Crawley, 2002). While a rapidly increasing number of studies have been conducted to test this hypothesis, the conclusions drawn from different studies appear to be mixed. Several empirical studies support this hypothesis (Keane and Crawley, 2002; Agrawal et al., 2005; Parker and Gilbert, 2007), however, numerous exceptions exist (Agrawal and Kotanen, 2003; Colautti et al., 2004; Parker and Hay, 2005; Chun et al., 2010). There is still no general pattern for explaining the interactions between invasive species and native herbivores and the ERH is a context-dependent hypothesis.

Therefore, understanding the impact of invasive plants on native consumers is important, as the indirect effects mediated by consumers can alter the dynamics of coexistence within native communities. Whether the invasive species are released from herbivores may depend on an array of physical and biological factors: environmental conditions (e.g. light, latitudinal gradients, the presence and absence of neighboring plants, etc.) (Bezemer et al., 2014; Biswas et al., 2015), plant conditions (e.g. the degree of invasiveness, residence time, range sizes spread, the density of the host plant, plant diversity, etc.) (Cappuccino and Carpenter, 2005; Pearse and Hipp, 2014; Biswas et al., 2015; Schultheis et al., 2015), herbivores characteristics (specialists and generalists' native herbivores) (Harvey et al., 2010a; Fortuna et al., 2012), and herbivores' natural enemies such as parasitoids and predators (Ode, 2006; Harvey et al., 2010b). However, comparisons of herbivores on invasive vegetation and natives overlooks the growing season variability of invasive plants and natives, especially in autumn. Autumn is a hugely important season in plant leaf senescence, insect migration and diapause in temperate and arctic ecosystems (Fridley, 2012; Gallinat et al., 2015). For instance, many invasive plants extend their growing season in comparison with natives in autumn; insects can add generations, delayed migration and diapause in warmer autumn (Bale et al., 2002; Fridley, 2012; Gallinat et al., 2015). In addition, some studies also suggested vegetation quality and dietary selection of insects have seasonal changes (Awmack and Leather, 2002; Bale et al., 2002). However, season variability has received less attention in invasion ecology.

Spartina alterniflora, one of the most aggressive invasive species in coastal wetlands around the world, has been well-studied for its impact on native ecosystems and the mechanisms behind these effects (Zhao et al., 2015; Ma et al., 2019; Sun et al., 2020). *Spartina* species not only occupies a space where the native salt marshes vegetation is absent, representing an "empty niche", but also competes with native species (e.g. *Phragmites australis*, *Suaeda salsa* (L.) Pall. and *Scirpus mariqueter* Tang & F. T. Wang) for space in coastal wetlands (Tang et al., 2016; Ma et al., 2020; Zheng et al., 2022). Therefore, *Spartina* invasions significantly affect the physical structures of the native ecosystems and biotic communities. The invasion of *Spartina* in coastal marshes has been reported to cause distribution and dietary changes of herbivores, however, the results from past studies are mixed. Some studies suggested that herbivores prefer native vegetation to invasive *Spartina* in coastal wetlands: insect community (e.g. *Calliptamus barbarus* Costa, *Protohermes costalis* Walker and *Rhopalosiphum rufiabdominalis* S.) (Gao et al., 2006; Peng et al., 2006; Wu et al., 2009), crabs species (e.g. *Helicana wuana* Rathbun) (Zhang et al., 2023); but others advocated that herbivores prefer invasive *Spartina* to native species: crabs species (e.g. *Sesarma dehaani* H.Milne Edwards, *Helice tientsinensis* Rathbun) (Wang et al., 2008; Qin et al., 2010), nekton species (e.g. *Chelon haematocheilus* Temminck & Schlegel, *Synechogobius ommaturus* Richardson) (Quan et al., 2007); and some studies found that it is not distinctly different: snail species (e.g. *Assiminea latericea* H. Adams & A. Adams and *Cerithidea largillierti* R. A. Philippi) (Wang et al., 2014). Therefore, there is an ongoing debate as to the relative importance of invasive *Spartina* and native species to herbivores in coastal wetlands.

Here, we examined how the abundance and diet of the native insect *Laelia coenosa* are affected by the invasive *Spartina* from summer to autumn in coastal marshes through laboratory and field experiments. The salt marsh is located in the Yancheng National Nature Reserve of China and has been heavily invaded by *Spartina*. First, we monitored the density of *Laelia coenosa* larvae on *Phragmites* and *Spartina* from summer to autumn in high, middle and low marshes. Next, we compared the degree of leaf damaged by *Laelia coenosa* larvae for *Phragmites* and *Spartina* to examine whether the native insect *Laelia coenosa* prefers native *Phragmites* to invasive *Spartina* to support the Enemy Release Hypothesis. Finally, we explored whether the Enemy Release Hypothesis is constant in summer and autumn. Specifically, we assessed the larval feeding preference of *Laelia coenosa* on *Spartina* and native *Phragmites* in the laboratory in the different growing seasons.

2 Materials and methods

2.1 Study sites

The study was conducted at the Yancheng National Nature Reserve in Yancheng city of Jiangsu Province of China (32°20′–34°37′N, 119°29′–121°16′E) (Figure 1A), which has experienced the widest and most extensive areal coverage of *Spartina* in China (Zuo

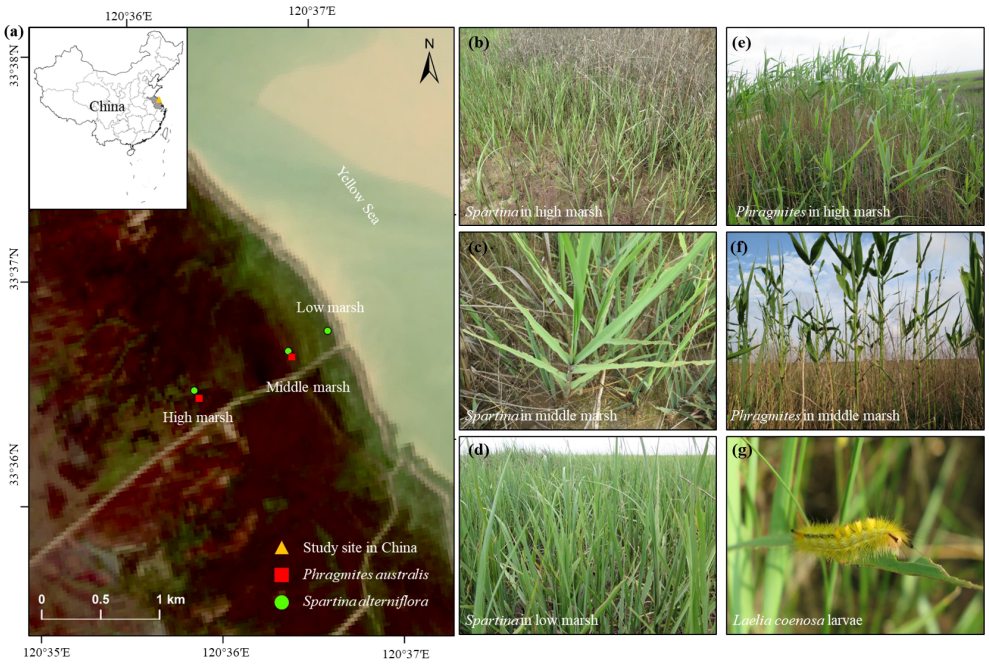

FIGURE 1
Location of the Yancheng National Nature Reserve in Jiangsu Province of China and sampling sites in the Yancheng National Nature Reserve with a true color remote sensing image on August 28, 2016 **(A)**. Photographs of sample sites in summer: **(B)** the high marsh dominated by *Spartina* monoculture; **(C)** the middle marsh dominated by *Spartina* monoculture; **(D)** the low marsh dominated by *Spartina* monoculture; **(E)** the high marsh dominated by *Phragmites* monoculture and **(F)** the middle marsh dominated by *Phragmites* monoculture. Photograph of *Laelia coenosa* larvae in summer **(G)**. Photographs were taken by Zezheng Liu.

et al., 2012). The Yancheng National Nature Reserve lies in the transition belt between subtropical and warm-temperate zones with distinctive seasons and a rainy summer. The average annual temperature and precipitation are 11.4–13.8°C and 1000-1080 mm, with 54% of precipitation occurring in summer (June-August) (Liu et al., 2007; Zhou et al., 2009). The average seasonal precipitation of Yancheng city amounts to 545.56 mm in summer (June-August) and 203.03 mm in autumn (September-November) from 1960 to 2020, respectively (Qi et al., 2023). The average seasonal temperature of Yancheng city amounts to 25.8°C in summer (June-August) and 16.70°C in autumn (September-November) from 1981 to 2018, respectively (Sheng, 2019). The salt marsh is dominated by native *Phragmites australis*, *Suaeda salsa* and by exotic *Spartina alterniflora*. The distribution of vegetation succession from land to seaward is *Phragmites australis*, *Suaeda salsa*, *Spartina alterniflora*, and tidal flat (Zhang et al., 2013). The three species have some overlap in their distribution zones.

2.2 Study species

Laelia coenosa, a generalist herbivorous insect, is a moth of the *Lepidoptera* order, *Lymantriidae* family found in North Africa, southern and central Europe, through Russia and eastern Asia up to Japan (Zeng et al., 1988). It is common and widespread in China, and widely distributed in inland (e.g. Hunan, Hubei, Anhui, and Jiangxi Province) and coastal (e.g. Hebei, Shandong, Jiangsu, and Shanghai Province) zones (Zeng et al., 1988; Xia et al., 1993; Ma et al., 2015). It generally produces two or three generations per year (Supplementary Table S1) and each generation has a four-stage life cycle: egg, larva, pupa and adult (Figure 2). In our study sites, the larvae of *Laelia coenosa* occurred during two periods: from mid-April to mid-June for the first generation, and from mid-June to late September for the second generation (Supplementary Table S1) (Xia et al., 1993). Hibernation takes place as an egg or larvae between the middle of October and early March of next year (Zeng et al., 1988). *Laelia coenosa* has long larvae life stages (Figure 1G), which primarily feed on a wide range of host plants including *Poaceae* and some *Cyperaceae*, especially *Phragmites* and *Miscanthus*, and 30%~40% production of reeds lost mainly by late-instar larvae (Zeng et al., 1988).

2.3 Sampling and analysis

To examine the spatial-temporal distribution of native insect *Laelia coenosa*, five distinct zones (habitats) were delimited based on elevation and vegetation type in June (summer) and September (autumn): (1) the high marsh dominated by *Phragmites* monoculture; (2) the high marsh dominated by *Spartina* monoculture; (3) the middle marsh dominated by *Phragmites* monoculture; (4) the middle marsh dominated by *Spartina* monoculture; (5) the low marsh dominated by *Spartina* monoculture (Figures 1B–F). In each sampling habitat at each

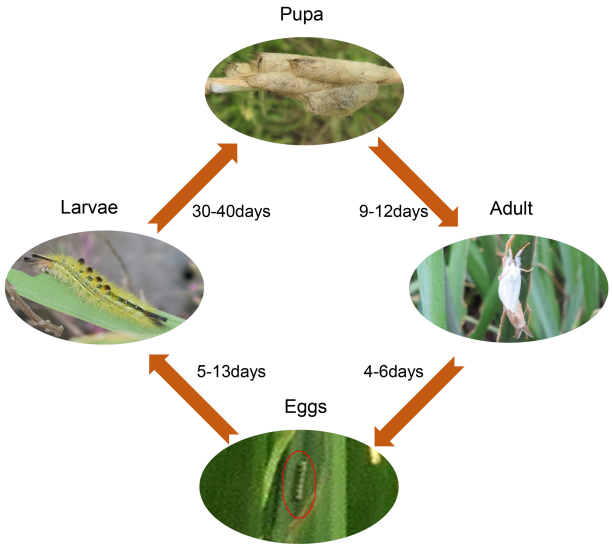

FIGURE 2
Basic life cycle model of *Laelia coenosa*. Date from Zeng et al., 1988. Photographs were taken by Zezheng Liu.

sampling season, 0.5×0.5 m quadrat was randomly placed for sampling. The sample sizes are 16 except those in *Phragmites* marsh whose sample sizes are 8. From the quadrat, numbers of native insect *Laelia coenosa* were counted, and leaves of five plants randomly selected were collected. In summer, all leaves of selected plants were collected, whereas only the up leaves were collected in autumn because the other leaves obviously were not consumed by the second-generation larvae in autumn, but consumed by the first generation in summer. Samples were stored on ice during transportation to the laboratory.

To assess the degree of leaf damage, the area of leaf damaged and percentage of leaf area damaged were calculated. The area of leaf damaged was calculated for each leaf as "complete area of damaged leaves" minus "remaining leaf area". The complete area of damaged leaves was estimated separately for *Phragmites* and *Spartina* by using regression equations between leaf area and length × width from 115 and 59 undamaged leaves of *Phragmites* and *Spartina* from the Yancheng National Nature Reserve salt marshes (Figure 3). When leaves width and length are not available because leaves are severely damaged, we used "average complete area of damaged leaves" minus "remaining leaf area" as the area of leaf damaged. The average complete area of damaged leaves is the mean value of undamaged leaf area in the same habitat as damaged area calculated. The percentage of leaf area damaged was calculated as "area of leaf damaged" divided by "complete area of damaged leaves" or "average complete area of damaged leaves". The length, width, and area of leaves were measured with a Yaxin-1241 leaf area meter. In autumn, we also calculated the percentage of leaf number damaged between *Spartina*-invaded and non-invaded *Phragmites* habitats by dividing the number of damaged leaves by the total number of leaves.

2.4 Dietary preferences experiment

The two-choice experiment was designed to investigate the feeding preference of *Laelia coenosa* between native *Phragmites*

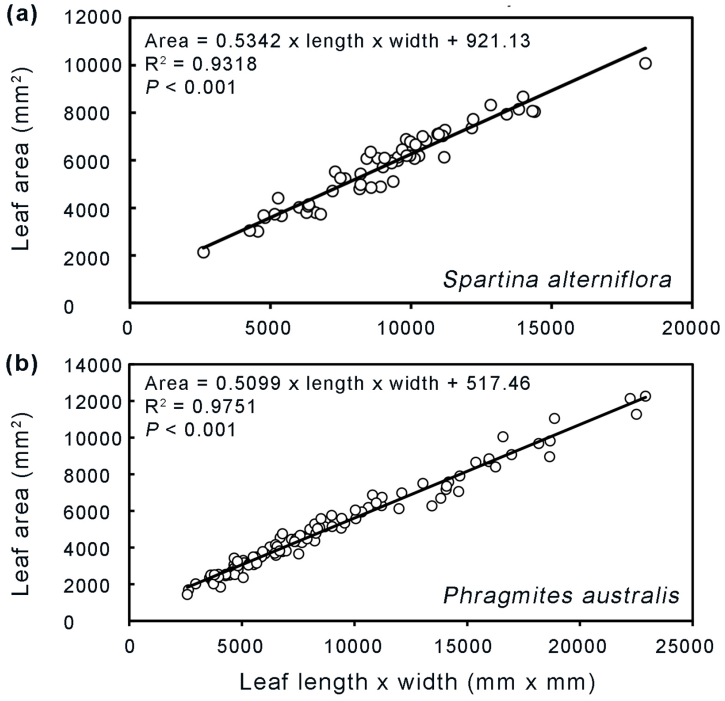

FIGURE 3
Relationship between leaf area and length×width for *Spartina alterniflora* **(A)** and *Phragmites australis* **(B)**.

and exotic *Spartina*. One larva of *Laelia coenosa* and two leaves of each plant species were placed in a loosely capped 1500 mL wide-mouthed plastic bottle, covering the top with a gauze net in case larvae escaped. To keep the experiment systems moist, pure water (10-20mL) was added to the jar at a depth of approximately 0.5 cm. All the plastic jars were subjected to 24 hours' nature photoperiod in June and September at field temperature. All larvae of *Laelia coenosa* were collected from the same area of the middle marsh zone, and the length and color were approximately consistent. The mean length of *Laelia coenosa* was 37.18 ± 4.96 mm and 30.1 ± 5.86 mm in June and September respectively (Supplementary Figure S1). While collecting the larvae in June and September, we also collected the top leaves of t *Spartina alterniflora* and *Phragmites australis* and trimmed them to a length of 20 cm. The feeding experiment was used with twelve replicates, however, only eight replicates data are available, due to the death of *Laelia coenosa*. The leaf area of damaged was calculated as the leaf area before the experiment minus the remaining leaf area after experiment. The percentage of damaged was calculated as the leaf area of damaged divided by leaf area before the experiment. The leaf area was measured before and after feeding trials with a Yaxin-1241 leaf area meter.

2.5 Statistical analysis

The density of *Laelia coenosa* larvae and degree of leaf area damaged for different habitat treatments at the same season were subjected to one-way ANOVAs. *Laelia coenosa* feeding preferences were examined using paired t-tests (two-sided). Before statistical analyses, all data were checked for normality and were log-transformed to improve the normality distribution. The results are represented as means and SE, and the level of statistical significance was set at $P < 0.05$. All statistical analyses were performed with the statistical package SPSS NLN, 15.0 (SPSS Inc., Chicago, USA).

3 Results

3.1 Spatial-temporal distribution pattern of *Laelia* larvae

In total, 582 larvae of *Laelia coenosa* were surveyed in sampling sites in this study. Distribution pattern of larvae at all five sampling plots in two sampling seasons is shown in Figure 4. *Laelia coenosa* showed significantly different along the sampling plots among the two growing seasons. Generally, the density of larvae in summer was higher than in autumn in five sampling sites ($P < 0.01$). We surveyed 523 larvae of *Laelia coenosa* in summer, while the number of larvae in autumn was 59 in all sampling sites. In summer (the first generation of *Laelia coenosa*), *Laelia coenosa* exhibited the highest level in *Phragmites* middle marsh, reaching a density of 23.38 ± 6.22 ind./0.25 m^2. The lowest density also appeared in the middle marsh, however, in *Spartina* habitat with a density of 3.31 ± 0.45 ind./0.25 m^2. Compared to the middle marsh, the density of the native insect *Laelia coenosa* did not significantly differ among the two habitats in the high marsh, with the density of 6.00 ± 0.65 and 6.25 ± 0.87 ind./0.25 m^2 in *Phragmites* and *Spartina* habitats, respectively (Figure 4). The density of larvae in *Spartina* low marsh is second to that in *Phragmites* middle marsh, with a density of 8.44 ± 1.34 ind./0.25 m^2 (Figure 4). However, *Laelia coenosa* preferred *Spartina* marsh, and was absent from *Phragmites* habitat in autumn (the second generation of *Laelia coenosa*) (Figure 4). *Laelia coenosa* exhibited the highest level in *Spartina* low marsh, reaching a density of 2.50 ± 0.30 ind./0.25 m^2. Therefore, season and vegetation species significantly affected the abundance of the native insect *Laelia coenosa*.

3.2 Degree of leaf damage for *Phragmites* and *Spartina*

Similar to the spatial-temporal distribution pattern of larvae, the degree of leaf damage also exhibited significant differences along the sampling habitats between the two growing seasons (Figure 5). In summer, leaves damaged by the first generation of *Laelia coenosa* showed the highest average extent of damage in the middle marsh area of the *Phragmites* community (72.41 ± 2.11%) (Figure 5B), with a damaged area of 5810.28 ± 173.91 mm^2 for each leaf (Figure 5A). In the middle marsh, the area of leaf damaged and percentage of leaf area damaged in *Phragmites* community were significantly higher than in *Spartina* community ($P < 0.05$) (Figure 5). In the high marsh, however, there was no significant difference in the area of leaf damaged and percentage of leaf area damaged between *Phragmites* community and *Spartina* community ($P > 0.05$) (Figure 5). The area of leaf damaged in *Spartina* community did not significantly differ in the high and low marshes, with 1778.66 ± 86.96 mm^2 and 1138.34 ± 134.39 mm^2 for each leaf, respectively ($P > 0.05$) (Figure 5). In autumn, the degree of leaf damage by the second generation of *Laelia coenosa* in the middle marsh area of the *Spartina* community reached the highest level (1478.26 ± 189.72 mm^2), which was significantly higher in the high and low marshes ($P < 0.05$) (Figure 5). However, native *Phragmites* didn't provide food for the native insect *Laelia coenosa* in autumn.

In autumn, more than 60% of the leaves were affected by leaves of *Laelia coenosa* (Figure 6). In general, the proportion of damaged *Spartina* leaves was significantly higher than that of the *Phragmites* community ($P < 0.001$). The proportions of damaged *Spartina* leaves were more than 90% at different elevation levels, with 90.63 ± 1.90%, 97.98 ± 0.95% and 92.16 ± 1.89% in high, middle and low marshes, respectively. The proportions of damaged *Phragmites* leaves were significantly higher in the middle elevation marsh (86.58 ± 2.28%) than in the high elevation marsh (65.97 ± 2.39%) ($P < 0.001$) (Figure 6).

3.3 Feeding preference for *Phragmites* and *Spartina*

In the lab feeding trial, the amount of *Phragmites* consumed by *Laelia coenosa* was significantly higher than *Spartina* in summer, whereas *Laelia coenosa* preferred *Spartina* in autumn (Figure 7). In

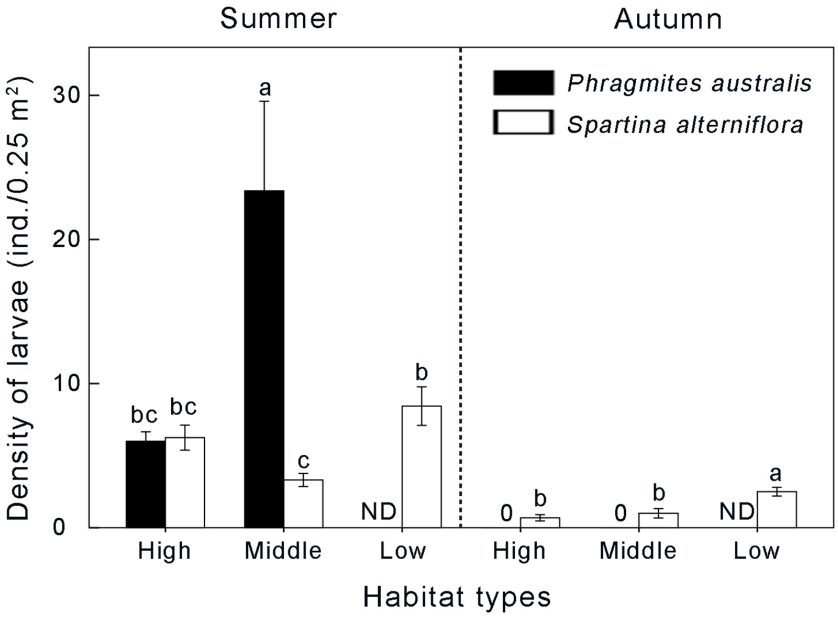

FIGURE 4
Differences in density of native insect *Laelia coenosa* between *Spartina*-invaded and non-invaded *Phragmites* habitats in summer and autumn. Data are shown as means ± SE. ND indicates no data. Different letters indicate significant differences ($P < 0.05$).

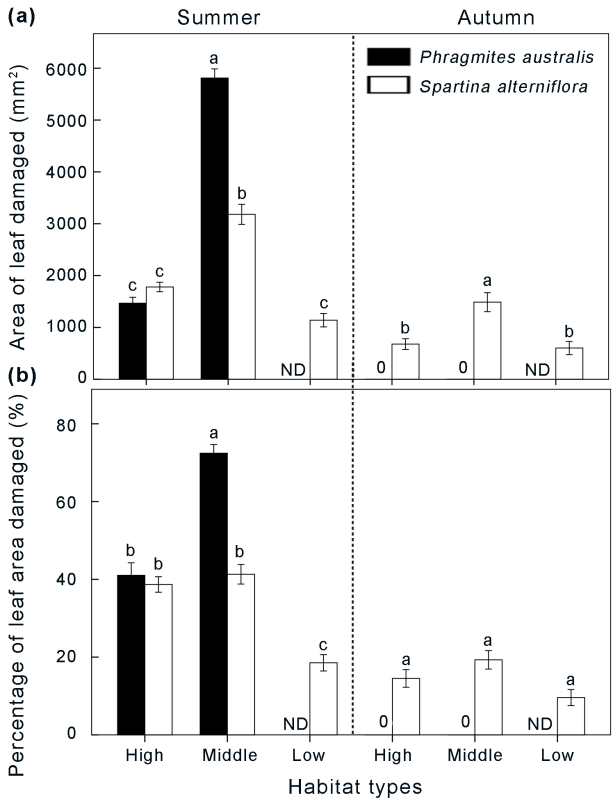

FIGURE 5
Differences in area of leaf damaged **(A)** and percentage of leaf area damaged **(B)** between *Spartina*-invaded and non-invaded *Phragmites* habitats in summer and autumn. Data are shown as means ± SE. ND indicates no data. Different letters indicate significant differences ($P < 0.05$).

summer, the leaf area of *Phragmites* consumed by larvae was 2433.88 ± 410.10 mm^2, more than six times higher than that of *Spartina* (378.9 ± 106.98 mm^2, $P < 0.001$) (Figure 7A). The percentage of *Phragmites* consumed by *Laelia coenosa* was also higher than that of *Spartina* (39.48 ± 6.72% vs. 10.57 ± 3.01%, $P < 0.001$) (Figure 7B). In autumn, however, the leaf area of *Phragmites* consumed by larvae was only a quarter as high as that of *Spartina* (187.22 ± 133.73 mm^2 vs. 851.41 ± 218.43 mm^2, $P < 0.001$) (Figure 7A). Therefore, we could predict a shift in feeding preference by *Laelia coenosa* depending on the growing seasons.

4 Discussion

This study revealed the effects of an invasive *Spartina* on insect species and related the changes in distributions and dietary breadth across two seasons in coastal wetlands. In our survey, the percentage of damaged leaves across the five sampling plots exceeded 60%, and in some cases, approached nearly 100% (Figure 6). This may significantly underestimate the true extent of leaf damage by herbivores, as it fails to include leaves that were entirely eaten or abscised prematurely due to heavy damage, particularly in *Phragmites* marshes. Our findings also indicated that *Laelia coenosa* larvae preferred *Phragmites* habitats over the invasive *Spartina* communities in summer, while the preference was reversed in autumn (Figure 4). The characteristics of leaf damaged and the spatial-temporal distribution pattern of the native insect *Laelia coenosa* exhibited similar patterns of change (Figure 5). Feeding experiments consistently showed that the dietary preference of *Laelia* larvae switched from *Phragmites australis* in summer to *Spartina alterniflora* in autumn (Figure 7).

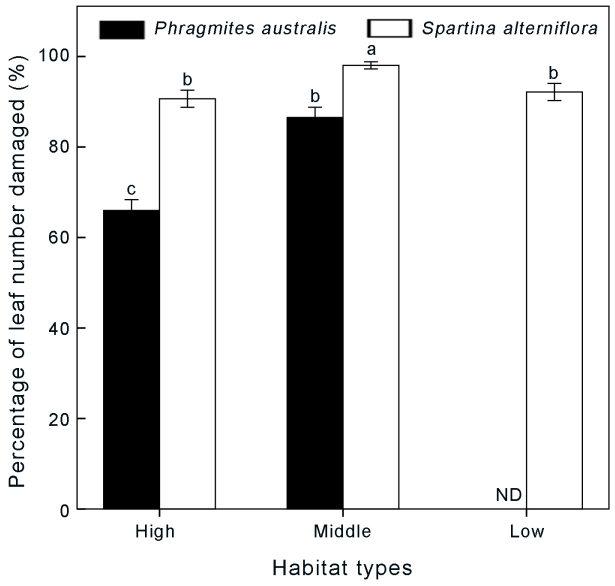

FIGURE 6
Differences in percentage of leaf number damaged between *Spartina*-invaded and non-invaded *Phragmites* habitats in autumn. Data are shown as means ± SE. ND indicates no data. Different letters indicate significant differences ($P < 0.05$).

From these findings, we consistently concluded that *Laelia coenosa* has recently expanded its habitat range, now inhabiting not only native *Phragmites* communities but also invasive *Spartina* communities in coastal wetlands.

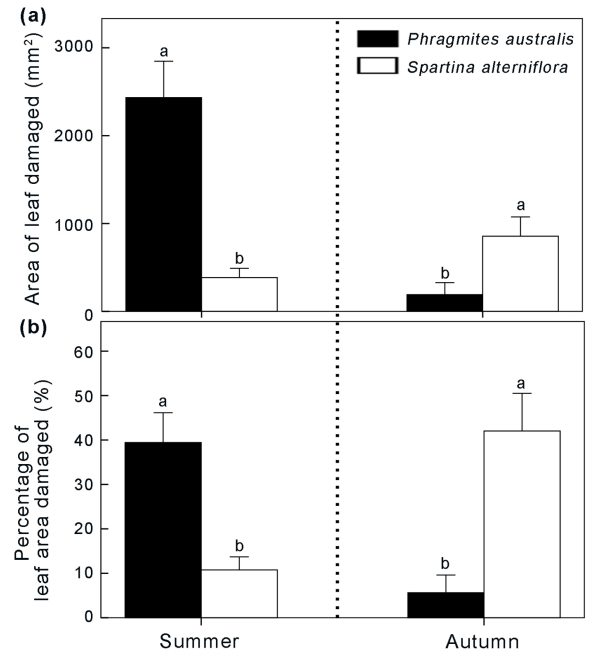

FIGURE 7
Feeding preference of *Laelia coenosa* for *Phragmites* and *Spartina* in summer and autumn. Data are shown as means ± SE. Different letters indicate significant differences ($P < 0.05$).

Invasive plants can affect the spatial and temporal dynamics of native insect populations by disrupting a wide range of trophic interactions (Harvey et al., 2010a; Bezemer et al., 2014). Previous studies have consistently concluded that food source is a primary factor affecting the distribution and survival of herbivorous insects. For example, the invasive *Phragmites australis* offers a more favorable feeding habitat for the dominant grazers (e.g. *Physella gyrina* Say and *Fossaria* (Bakerlymnaea) *bulimoides* group), increasing their density along the southern shoreline of Lake Erie in the USA (Holomuzki and Klarer, 2010). The introduction of *Spartina* in salt marshes has also led to dietary shifts in crab species such as *Helice tientsinensis* and *Chiromantes dehaani* H. Milne Edwards (Qin et al., 2010). The non-native bryozoan *Membranipora membranacea* can serve as a new food source for the native nudibranch *Onchidoris muricata* in the summer and fall in the Gulf of Maine of the USA (Pratt and Grason, 2007). Additionally, invasive predators can disrupt food webs by forcing native predators to feed on suboptimal food sources, and reorganize the low-trophic-level communities, thereby causing significant disruption to native food web structures (Wainright et al., 2021). Thus, invasive species have the potential to alter the resource utilization patterns of native species, leading to both direct and indirect modifications in food web dynamics.

A wide variety of plant traits, such as carbon and nitrogen content, defensive metabolites, morphological characteristics, and phenological traits, are known to significantly influence the preferences for host plants and the associated distribution of herbivorous insects (Awmack and Leather, 2002; Salgado and Saastamoinen, 2019; Bovay et al., 2024). In general, larvae of the *Lepidoptera* order prefer leaves with high nitrogen and water content and low toughness (Peng et al., 2006; Ma et al., 2015). Native herbivores tend to prefer native plants, because exotic species may not provide a suitable diet (Tallamy and Shropshire, 2009). Previous studies have suggested native insect species (*Laelia coenosa*) prefer native *Spartina* in the USA to invasive *Spartina* in China through greenhouse experiments, due to differences in leaf nitrogen content and toughness rather than volatile compounds (Ma et al., 2015). Some studies suggested that the leaf total nitrogen of *Spartina* was significantly lower than that of *Phragmites* in summer in coastal wetlands (Jiang et al., 2009; Guo et al., 2023). In addition, some previous studies indicated that leaves of *Spartina* are more thickness and toughness than those of *Phragmites* in coastal wetlands (Hendricks et al., 2011; Guo et al., 2023). *Spartina* species, known for their salt-secreting capability, have leaves containing salt particles that can reduce the palatability of their diet for herbivorous insects (Smart and Barko, 1978; Smit et al., 2024). Therefore, insects *Laelia coenosa* tend to prefer feeding on native *Phragmites* over exotic species *Spartina* during the summer when food is abundant.

Furthermore, *Spartina* species have a longer growing season compared to the native *Phragmites* in China's salt marshes (Jiang et al., 2009; Wang et al., 2006). The growing season lengths for *Spartina* and *Phragmites* were 270 days and 220 days in the Yangtze Estuary of China, respectively (Liao et al., 2007). In autumn, *Spartina* exhibits higher leaf total nitrogen values and plant tissue water content than *Phragmites* (Wang et al., 2008; Jiang et al., 2009),

which tends to make it a more attractive food source for insects. In September, total plant C and N stock of *Spartina* stands in the Yangtze Estuary of China were 3.83 kg m^{-2} and 57.21 g m^{-2}, respectively, while the values for *Phragmites* stands were significantly lower, at 0.89 kg m^{-2} and 15.86 g m^{-2}, respectively (Liao et al., 2007). Consequently, the invasive *Spartina* creates a more palatable diet for insects, enhancing their density and effectively buffering against food deprivation stress in autumn in coastal wetlands. Similarly, many woody invasive plants in North America retained their leaves later in the autumn than native plants, resulting in extended leaf phenology. The extended leaf phenology of invasive species enhances their competitive advantage over native species by providing increased access to understory light (O'Connell and Savage, 2020). Therefore, there is a seasonal shift in insect habitat selection from *Phragmites* in summer to *Spartina* in autumn in coastal wetlands.

The invasive *Spartina*, characterized by its extended growing season, offers a dietary source and habitat for herbivorous insects in autumn. This additional resource may support an extra generation of insects in the fall and be advantageous for their overwintering, resulting in a shorter overwintering period and a higher survival rate of insects in spring. Consequently, this could lead to an increase in both the frequency and intensity of insect outbreaks in coastal wetlands. In turn, these outbreaks may facilitate further invasion of *Spartina* by causing significant damage to native species, as native insects could contribute to the decline of native species that otherwise might have competed with *Spartina*. Thus, the differences in damaging ability between the invasive and native plants by the native herbivorous may hinder the conservation and restoration of the invaded ecosystem. Looking ahead, additional research is necessary to validate these assumptions and to achieve a more comprehensive understanding of the impact of *Spartina* invasion on various insect behaviors, including oviposition preferences and the selection of overwintering sites.

5 Conclusions

In conclusion, our results suggest that the native insect *Laelia coenosa* preferentially consumes native *Phragmites* over invasive *Spartina* in summer, which may contribute to the decline of native *Phragmites*. Thus, the interaction between invasive *Spartina* and native insects appears to support the Enemy Release Hypothesis in summer. However, this pattern is not consistent in autumn. The invasive *Spartina* offers a dietary source and habitat for herbivorous insects *Laelia coenosa* in autumn with its extended growing season. These differences are anticipated to alter the trophic interactions within the invaded ecosystem, potentially aiding in the further spread of the exotic *Spartina* and hindering the reestablishment of native *Phragmites* populations. This finding helps explain the mixed results often observed in hypothesis tests and enhances our understanding of the mechanisms behind coastal invasions. Such insights will aid in understanding and predicting the success of invasive species in natural ecosystems.

Data availability statement

The raw data supporting the conclusions of this article will be made available by the authors, without undue reservation.

Author contributions

TX: Conceptualization, Data curation, Methodology, Software, Visualization, Writing – original draft, Writing – review & editing. XM: Writing – original draft, Writing – review & editing. YL: Supervision, Writing – original draft, Writing – review & editing. HX: Writing – original draft, Writing – review & editing. SZ: Writing – original draft, Writing – review & editing. ZL: Conceptualization, Formal analysis, Funding acquisition, Investigation, Supervision, Writing – original draft, Writing – review & editing.

Funding

The author(s) declare financial support was received for the research, authorship, and/or publication of this article. This work is financially supported by the National Natural Science Foundation of China (42306187, 42176202), the Guangdong Provincial Department of Science and Technology, China (2024B1515020066, 2019ZT08G090), the Innovation Group Project of Southern Marine Science and Engineering Guangdong Laboratory, China (Zhuhai; Grant no. 311021004).

Conflict of interest

The authors declare that the research was conducted in the absence of any commercial or financial relationships that could be construed as a potential conflict of interest.

Publisher's note

Supplementary material

The Supplementary Material for this article can be found online at: https://www.frontiersin.org/articles/10.3389/fmars.2024.1478599/full#supplementary-material

References

Agrawal, A. A., and Kotanen, P. M. (2003). Herbivores and the success of exotic plants: a phylogenetically controlled experiment. *Ecol. Lett.* 6, 712–715. doi: 10.1046/j.1461-0248.2003.00498.x

Agrawal, A. A., Kotanen, P. M., Mitchell, C. E., Power, A. G., Godsoe, W., and Klironomos, J. (2005). Enemy release? An experiment with congeneric plant pairs and diverse above- and belowground enemies. *Ecology* 86, 2979–2989. doi: 10.1890/05-0219

Awmack, C. S., and Leather, S. R. (2002). Host plant quality and fecundity in herbivorous insects. *Annu. Rev. Entomology* 47, 817–844. doi: 10.1146/annurev.ento.47.091201.145300

Bale, J. S., Masters, G. J., Hodkinson, I. D., Awmack, C., Bezemer, T. M., Brown, V. K., et al. (2002). Herbivory in global climate change research: direct effects of rising temperature on insect herbivores. *Glob. Change Biol.* 8, 1–16. doi: 10.1046/j.1365-2486.2002.00451.x

Bezemer, T. M., Harvey, J. A., and Cronin, J. T. (2014). Response of native insect communities to invasive plants. *Ann. Rev. Entomol.* 59, 119. doi: 10.1146/annurev-ento-011613-162104

Biswas, S. R., Kotanen, P. M., Kambo, D., and Wagner, H. H. (2015). Context-dependent patterns, determinants and demographic consequences of herbivory in an invasive species. *Biol. Invasions* 17, 165–178. doi: 10.1007/s10530-014-0715-0

Bovay, B., Descombes, P., Chittaro, Y., Glauser, G., Nomoto, H., and Rasmann, S. (2024). Adapting to change: Exploring the consequences of climate-induced host plant shifts in two specialist Lepidoptera species. *Ecol. Evol.* 14, e11596. doi: 10.1002/ece3.11596

Cappuccino, N., and Carpenter, D. (2005). Invasive exotic plants suffer less herbivory than non-invasive exotic plants. *Biol. Lett.* 1, 435–438. doi: 10.1098/rsbl.2005.0341

Chun, Y. J., van Kleunen, M., and Dawson, W. (2010). The role of enemy release, tolerance and resistance in plant invasions: linking damage to performance. *Ecol. Lett.* 13, 937–946. doi: 10.1111/j.1461-0248.2010.01498.x

Colautti, R. I., Ricciardi, A., Grigorovich, I. A., and MacIsaac, H. J. (2004). Is invasion success explained by the enemy release hypothesis? *Ecol. Lett.* 7, 721–733. doi: 10.1111/j.1461-0248.2004.00616.x

Dutra, H. P., Barnett, K., Reinhardt, J. R., Marquis, R. J., and Orrock, J. L. (2011). Invasive plant species alters consumer behavior by providing refuge from predation. *Oecologia* 166, 649–657. doi: 10.1007/s00442-010-1895-7

Ehrenfeld, J. G. (2010). Ecosystem consequences of biological invasions. *Annu. Rev. ecology evolution systematics* 41, 59–80. doi: 10.1146/annurev-ecolsys-102209-144650

Fortuna, T. M., Vet, L. E. M., and Harvey, J. A. (2012). Effects of an invasive plant on the performance of two parasitoids with different host exploitation strategies. *Biol. Control* 62, 213–220. doi: 10.1016/j.biocontrol.2012.05.003

Fridley, J. D. (2012). Extended leaf phenology and the autumn niche in deciduous forest invasions. *Nature* 485, 105–359. doi: 10.1038/nature11056

Gallinat, A. S., Primack, R. B., and Wagner, D. L. (2015). Autumn, the neglected season in climate change research. *Trends Ecol. Evol.* 30, 169–176. doi: 10.1016/j.tree.2015.01.004

Gao, H., Peng, X., Li, B., Wu, Q., and Dong, H. (2006). Effects of the invasive plant *Spartina alterniflora* on insect diversity in Jiuduansha wetlands in the Yangtze River Estuary. *Chin. Biodiversity* 14, 400–409. doi: 10.1360/biodiv.060025

Guo, Y., Zhang, Y., Wu, J., Richards, C. L., Bossdorf, O., Li, B., et al. (2023). Geographic variation of litter chemistry and palatability in an invasive plant versus its native competitor. *J. Biogeography* 50, 1139–1150. doi: 10.1111/jbi.14604

Harvey, J. A., Biere, A., Fortuna, T., Vet, L. E. M., Engelkes, T., Morrien, E., et al. (2010a). Ecological fits, mis-fits and lotteries involving insect herbivores on the invasive plant, *Bunias orientalis*. *Biol. Invasions* 12, 3045–3059. doi: 10.1007/s10530-010-9696-9

Harvey, J. A., Bukovinszky, T., and van der Putten, W. H. (2010b). Interactions between invasive plants and insect herbivores: A plea for a multitrophic perspective. *Biol. Conserv.* 143, 2251–2259. doi: 10.1016/j.biocon.2010.03.004

Hendricks, L. G., Mossop, H. E., and Kicklighter, C. E. (2011). Palatability and Chemical Defense of *Phragmites australis* to the Marsh Periwinkle Snail *Littoraria irrorata*. *J. Chem. Ecol.* 37, 838–845. doi: 10.1007/s10886-011-9990-8

Holomuzki, J. R., and Klarer, D. M. (2010). Invasive reed effects on benthic community structure in Lake Erie coastal marshes. *Wetlands Ecol. Manage.* 18, 219–231. doi: 10.1007/s11273-009-9161-7

Jiang, L., Luo, Y., Chen, J., and Li, B. (2009). Ecophysiological characteristics of invasive *Spartina alterniflora* and native species in salt marshes of Yangtze River estuary, China. *Estuar. Coast. Shelf Sci.* 81, 74–82. doi: 10.1016/j.ecss.2008.09.018

Keane, R. M., and Crawley, M. J. (2002). Exotic plant invasions and the enemy release hypothesis. *Trends Ecol. Evol.* 17, 164–170. doi: 10.1016/S0169-5347(02)02499-0

Li, H., Zhang, X., Zheng, R., Li, X., Elmer, W. H., Wolfe, L. M., et al. (2014). Indirect effects of non-native *Spartina alterniflora* and its fungal pathogen (*Fusarium palustre*) on native saltmarsh plants in China. *J. Ecol.* 102, 1112–1119. doi: 10.1111/1365-2745.12285

Liao, C., Luo, Y., Jiang, L., Zhou, X., Wu, X., Fang, C., et al. (2007). Invasion of Spartina alterniflora enhanced ecosystem carbon and nitrogen stocks in the Yangtze Estuary, China. *Ecosystems* 10, 1351–1361. doi: 10.1007/s10021-007-9103-2

Liao, C. Z., Peng, R. H., Luo, Y. Q., Zhou, X. H., Wu, X. W., Fang, C. M., et al. (2008). Altered ecosystem carbon and nitrogen cycles by plant invasion: a meta-analysis. *New Phytol.* 177, 706–714. doi: 10.1111/j.1469-8137.2007.02290.x

Liu, J., Zhou, H., Qin, P., and Zhou, J. (2007). Effects of *spartina alterniflora* salt marshes on organic carbon acquisition in intertidal zones of Jiangsu province, China. *Ecolo. Eng.* 30, 240–249. doi: 10.1016/j.ecoleng.2007.01.010

Ma, D., Ju, R., and Li, B. (2015). Preference of Laelia coenosa for native and introduced populations of invasive *Spartina alterniflora*. *Biodiversity Sci.* 23, 101–108. doi: 10.17520/biods.2014156

Ma, X., Qiu, D., Wang, F., Jiang, X., Sui, H., Liu, Z., et al. (2020). Tolerance between non-resource stress and an invader determines competition intensity and importance in an invaded estuary. *Sci. Total Environ.* 724, 138225. doi: 10.1016/j.scitotenv.2020.138225

Ma, X., Yan, J., Wang, F., Qiu, D., Jiang, X., Liu, Z., et al. (2019). Trait and density responses of Spartina alterniflora to inundation in the Yellow River Delta, China. *Mar. pollut. Bull.* 146, 857–864. doi: 10.1016/j.marpolbul.2019.07.022

Mack, R. N., Simberloff, D., Lonsdale, W. M., Evans, H., Clout, M., and Bazzaz, F. A. (2000). Biotic invasions: causes, epidemiology, global consequences, and control. *Ecol. Appl.* 10, 689–710. doi: 10.1890/1051-0761(2000)010[0689:BICEGC]2.0.CO;2

O'Connell, E., and Savage, J. (2020). Extended leaf phenology has limited benefits for invasive species growing at northern latitudes. *Biol. Invasions* 22, 2957–2974. doi: 10.1007/s10530-020-02301-w

Ode, P. J. (2006). Plant chemistry and natural enemy fitness: Effects on herbivore and natural enemy interactions. *Annu. Rev. Entomology* 51, 163–185. doi: 10.1146/annurev.ento.51.110104.151110

Parker, I. M., and Gilbert, G. S. (2007). When there is no escape: The effects of natural enemies on native, invasive, and noninvasive plants. *Ecology* 88, 1210–1224. doi: 10.1890/06-1377

Parker, J. D., and Hay, M. E. (2005). Biotic resistance to plant invasions? Native herbivores prefer non-native plants. *Ecol. Lett.* 8, 959–967. doi: 10.1111/j.1461-0248.2005.00799.x

Pearse, I. S., and Hipp, A. L. (2014). Native plant diversity increases herbivory to non-natives. *Proc. R. Soc. B: Biol. Sci.* 281(1794):20141841. doi: 10.1098/rspb.2014.1841

Pejchar, L., and Mooney, H. A. (2009). Invasive species, ecosystem services and human well-being. *Trends Ecol. Evol.* 24, 497–504. doi: 10.1016/j.tree.2009.03.016

Peller, T., and Altermatt, F. (2024). Invasive species drive cross-ecosystem effects worldwide. *Nat. Ecol. Evol.* 8, 1087–1097. doi: 10.1038/s41559-024-02380-1

Peng, X. W., Gao, H., Dong, H. Q., and Qian-Hong, W. U. (2006). Study on diurnal insect communities in different habitats at the jiuduansha wetland national nature reserve. *J. Fudan Univ.* 45, 783–790. doi: 10.15943/j.cnki.fdxb-jns.2006.06.017

Pratt, M. C., and Grason, E. W. (2007). Invasive species as a new food source: does a nudibranch predator prefer eating an invasive bryozoan? *Biol. Invasions* 9, 645–655. doi: 10.1007/s10530-006-9065-x

Pysek, P., Jarosik, V., Hulme, P. E., Pergl, J., Hejda, M., Schaffner, U., et al. (2012). A global assessment of invasive plant impacts on resident species, communities and ecosystems: the interaction of impact measures, invading species' traits and environment. *Global Change Biol.* 18, 1725–1737. doi: 10.1111/j.1365-2486.2011.02636.x

Qi, T., Li, Y., Zhu, C., Hao, W., and Hu, C. (2023). Variation law of precipitation in Yancheng from 1960 to 2020. *Environ. Prot. Sci.* 49, 115–120. doi: 10.16803/j.cnki.issn.1004-6216.2022070028

Qin, H., Chu, T., Xu, W., Lei, G., Chen, Z., Quan, W., et al. (2010). Effects of invasive cordgrass on crab distributions and diets in a Chinese salt marsh. *Mar. Ecol. Prog. Ser.* 415, 177–187. doi: 10.3354/meps08771

Quan, W., Fu, C., Jin, B., Luo, Y., Li, B., Chen, J., et al. (2007). Tidal marshes as energy sources for commercially important nektonic organisms: stable isotope analysis. *Mar. Ecol. Prog. Ser.* 352, 89–99. doi: 10.3354/meps07160

Salgado, A. L., and Saastamoinen, M. (2019). Developmental stage-dependent response and preference for host plant quality in an insect herbivore. *Anim. Behav.* 150, 27–38. doi: 10.1016/j.anbehav.2019.01.018

Schultheis, E. H., Berardi, A. E., and Lau, J. A. (2015). No release for the wicked: enemy release is dynamic and not associated with invasiveness. *Ecology* 96, 2446–2457. doi: 10.1890/14-2158.1

Sheng, Y. (2019). Characteristics of Climate Change in Yancheng City and lts lmpact on Agricultural Production. *J. Agric. Catastrophology* 9, 53–54. doi: 10.19383/j.cnki.nyzhyj.2019.06.019

Smart, R. M., and Barko, J. W. (1978). Influence of sediment salinity and nutrients on the physiological ecology of selected salt marsh plants. *Estuar. Coast. Mar. Sci.* 7, 487–495. doi: 10.1016/0302-3524(78)90125-1

Smit, L. A., Adams, J. B., Hawkes, S. A., Peer, N., and Rishworth, G. M. (2024). Proportional top-down effects of grapsoid crabs on growth of Spartina maritima cordgrass in southern African salt marshes. *Mar. Ecol. Prog. Ser.* 739, 49–64. doi: 10.3354/meps14612

Stewart, P. S., Hill, R. A., Stephens, P. A., Whittingham, M. J., and Dawson, W. (2021). Impacts of invasive plants on animal behavior. *Ecol. Lett.* 24, 891–907. doi: 10.1111/ele.13687

Strauss, A., White, A., and Boots, M. (2012). Invading with biological weapons: the importance of disease-mediated invasions. *Funct. Ecol.* 26, 1249–1261. doi: 10.1111/1365-2435.12011

Sun, L., Shao, D., Xie, T., Gao, W., Ma, X., Ning, Z., et al. (2020). How does spartina alterniflora invade in salt marsh in relation to Tidal Channel networks? *Patterns processes. Remote Sens.* 12, 2983. doi: 10.3390/rs12182983

Tallamy, D. W., and Shropshire, K. J. (2009). Ranking lepidopteran use of native versus introduced plants. *Conserv. Biol.* 23, 941–947. doi: 10.1111/j.1523-1739.2009.01202.x

Tang, L., Gao, Y., Li, B., Wang, Q., Wang, C. H., and Zhao, B. (2016). *Spartina alterniflora* with high tolerance to salt stress changes vegetation pattern by outcompeting native species. *Ecosphere* 5, 1–18. doi: 10.1890/ES14-00166.1

Tekiela, D. R., and Barney, J. N. (2015). System-level changes following invasion caused by disruption of functional relationships among plant and soil properties. *Ecosphere* 6, 1–16. doi: 10.1890/ES15-00412.1

Vila, M., Espinar, J. L., Hejda, M., Hulme, P. E., Jarosik, V., Maron, J. L., et al. (2011). Ecological impacts of invasive alien plants: a meta-analysis of their effects on species, communities and ecosystems. *Ecol. Lett.* 14, 702–708. doi: 10.1111/ele.2011.14.issue-7

Wainright, C. A., Muhlfeld, C. C., Elser, J. J., Bourret, S. L., and Devlin, S. P. (2021). Species invasion progressively disrupts the trophic structure of native food webs. *Proc. Natl. Acad. Sci.* 118, e2102179118. doi: 10.1073/pnas.2102179118

Wang, S., Chu, T., Huang, D., Li, B., and Wu, J. (2014). Incorporation of Exotic *Spartina alterniflora* into Diet of Deposit-Feeding Snails in the Yangtze River Estuary Salt Marsh: Stable Isotope and Fatty Acid Analyses. *Ecosystems* 17, 567–577. doi: 10.1007/s10021-013-9743-3

Wang, Q., Wang, C. H., Zhao, B., Ma, Z. J., Luo, Y. Q., Chen, J. K., et al. (2006). Effects of growing conditions on the growth of and interactions between salt marsh plants: implications for invasibility of habitats. *Biol. Invasions* 8, 1547–1560. doi: 10.1007/s10530-005-5846-x

Wang, J., Zhang, X., Nie, M., Fu, C., Chen, J., and Li, B. (2008). Exotic *Spartina alterniflora* provides compatible habitats for native estuarine crab *Sesarma dehaani* in the Yangtze River estuary. *Ecol. Eng.* 34, 57–64. doi: 10.1016/j.ecoleng.2008.05.015

Wu, Y., Wang, C., Zhang, X., Zhao, B., Jiang, L., Chen, J., et al. (2009). Effects of saltmarsh invasion by *Spartina alterniflora* on arthropod community structure and diets. *Biol. Invasions* 11, 635–649. doi: 10.1007/s10530-008-9279-1

Xia, B., Zhao, Y., Shen, B., Zhang, J., Gu, B., and Yan, T. (1993). The ecological control of pests and diseases of reed in Sheyang beach. *J. Plant Resour. Environ.* 2, 31–36.

Zeng, X. S., Xu, G. J., Zhang, G. A., and Zhang, Z. G. (1988). Biological study and precautions of *Laelia coenosa*. *Hubei Agricultural Sciences* 08, 27–30.

Zhai, J., Hou, B., Hu, F., Yu, G., Li, Z., Palmer-Young, E. C., et al. (2024). Active defense strategies for invasive plants may alter the distribution pattern of pests in the invaded area. *Front. Plant Sci.* 15, 1428752. doi: 10.3389/fpls.2024.1428752

Zhang, Y., Li, Y., Jia, Y., Qiu, C., Wang, Y., Huang, W., et al. (2023). Impact factors on distribution and habitat of crab in coastal wetland in tiaozini, Jiangsu, China. *Oceanologia Et Limnologia Sinica.* 54, 1383–1394.

Zhang, H., Liu, H., and Hou, M. (2013). Spatiotemporal characteristics of Spartina alterniflora marsh change in the coastal wetlands of Yancheng caused by natural processes and human activities. *Acta Ecologica Sin.* 33, 4767–4775. doi: 10.5846/stxb201205050649

Zhao, H., Yang, W., Xia, L., Qiao, Y., Xiao, Y., Cheng, X., et al. (2015). Nitrogen-enriched eutrophication promotes the invasion of *spartina alterniflora* in coastal China. *CLEAN - Soil Air Water* 43, 244–250. doi: 10.1002/clen.201300844

Zheng, S., Shao, D., Gao, W., Nardin, W., Ning, Z., Liu, Z., et al. (2022). Drainage efficiency and geometric nuances of tidal channel network mediate Spartina alterniflora landward invasion in marsh-channel system. *Front. Mar. Sci.* 9, 888597. doi: 10.3389/fmars.2022.888597

Zhou, C., An, S., Deng, Z., Yin, D., Zhi, Y., Sun, Z., et al. (2009). Sulfur storage changed by exotic *Spartina alterniflora* in coastal saltmarshes of China. *Ecol. Eng.* 35, 536–543. doi: 10.1016/j.ecoleng.2008.01.004

Zuo, P., Zhao, S., Liu, C., Wang, C., and Liang, Y. (2012). Distribution of Spartina spp. along China's coast. *Ecol. Eng.* 40, 160–166. doi: 10.1016/j.ecoleng.2011.12.014

frontiers | Frontiers in Marine Science

TYPE Original Research
PUBLISHED 27 September 2024
DOI 10.3389/fmars.2024.1466629

OPEN ACCESS

EDITED BY
Qin Zhu,
Southern Marine Science and Engineering Guangdong Laboratory (Guangzhou), China

REVIEWED BY
Shunqi Pan,
Cardiff University, United Kingdom
Zhe Huang,
Tianjin University, China

*CORRESPONDENCE
Yan Li
yantai_fan@163.com

RECEIVED 18 July 2024
ACCEPTED 09 September 2024
PUBLISHED 27 September 2024

CITATION
Xue H, Shi H, Zhan C, Wang Q, Li Y and You Z (2024) Study on the three-dimensional numerical simulation of concentrated brine dispersal processes in estuarine bays. *Front. Mar. Sci.* 11:1466629. doi: 10.3389/fmars.2024.1466629

Study on the three-dimensional numerical simulation of concentrated brine dispersal processes in estuarine bays

Huaiyuan Xue[1], Hongyuan Shi[1,2], Chao Zhan[1,2], Qing Wang[1,2], Yan Li[1,2]* and Zaijin You[1,3]

[1]Institute of Coastal Research, Ludong University of China, Yantai, China, [2]School of Hydraulic and Civil Engineering, Ludong University of China, Yantai, China, [3]School of Civil Engineering, University of Queensland, St Lucia, QLD, Australia

As a new type of liquid discharged into the sea, concentrated brine exhibits complex mixing and stratification patterns due to changes in its density and hydrodynamic properties. This complexity impacts salinity transmission and can result in brine intrusion disasters, directly affecting both ecosystem and human life. This research adopted brine discharge into Dingzi Bay, Shandong Peninsula, a typical estuarine bay, as a case study. 3D convective diffusion numerical simulation techniques were applied to investigate the pathways, salinity rise, impact range, and overall effects on brine dispersal in marine water environments under the combined influence of river flow and tides. The results indicated the followings: (1) Significant spatial variations were observed in flow velocities within Dingzi Bay, with higher velocities near Xiang Island (where river flow turned into the bay) and at bay mouth; (2) The brine discharge point is influenced by complex hydrographic terrain and the combined effects of river flow and tidal movements, resulting in the formation of a high salinity area at the base of the discharge point, where salinity increases by more than 4 PSU within a 100-meter radius.; (3) During high tides, high-concentration brine was clearly transported upstream along the tidal channel, with a salinity increase of ≥3psu covering an area of 5.72×10^4 m^2, extending up to 270 m upstream and 180 m downstream. Brine discharge led to significant mixing of concentrated seawater with seawater within the bay, altering the spatial and temporal distributions of salinity in Dingzi Bay and consequently affecting local sensitive marine species and water environment safety. This study systematically investigated the process of brine discharge into the ocean and its impact range. It was found that discharging brine in areas with higher currents promotes the mixing and dispersion of brine. Additionally, a seasonal discharge plan should be established to avoid discharges during periods of low runoff (such as winter) to minimize negative impacts on aquatic ecosystems and promote the health and diversity of marine ecosystems.

KEYWORDS

concentrated brine discharge, three-dimensional numerical simulation, salinity rise, diffusion range, estuarine bay

1 Introduction

Brine discharge typically involves returning the byproduct of the desalination process (high salinity water) back into the ocean. This can lead to a phenomenon known as "brine underflow," where the denser, saltier water sinks and forms a layer on the seabed, potentially causing low-oxygen conditions that can suffocate benthic life (Lee et al., 2020). Marine water environment problems caused by brine discharge into the sea has attracted widespread attention in recent years; especially the issue of increased salinity in receiving waters has spurred extensive research (Purnalna et al., 2003; Zheng et al., 2014). With rapid progress of industrialization and urbanization, human activities have given rise to the discharge of large amounts of brine, significantly changing the spatial distribution of salinity in recipient marine areas (Lin et al., 2015). In addition, some research works have revealed that high-salinity water bodies have altered local marine ecological environments (Ye et al., 2018), directly threatening the survival and reproduction of some sensitive marine species (Chang-Feng et al., 2014). This ecological imbalance can impact on not only the natural habitats of marine life, but also fishery resources and human economic activities (Zhi-Guo et al., 2018). Therefore, in-depth research on the process and pathways of brine dispersion into the sea, consequent salinity increase, impact range, and effects on marine ecosystems, as well as finding effective mitigation and resolution measures for the stability of marine ecological environments in brine discharge areas is of significant scientific and practical importance (Kowalski and Mazierski, 2008).

Malfeito et al. (2005) studied the environmental impacts of Javea reverse osmosis seawater desalination plant in Alicante, Spain. They found that specific brine discharge treatment methods effectively mitigated environmental impacts, maintained salinity and water quality within the safe limits, and prevented damage to local marine ecosystems. Ruso et al. (2007) revealed that benthic communities near brine discharge outlets were homogeneous and the originally diverse communities had been replaced by communities dominated by nematodes. To alleviate the effect of brine discharge into the sea, some researchers have proposed to improve discharge methods and increase brine-seawater mixing ratios (Voutchkov, 2009). Kelaher et al. (2020) performed a long-term study on the impacts of desalination brine discharge on sensitive fish populations and found that initial brine discharge had positive impacts on surrounding fish communities, increasing fish number and diversity, but these changes were temporary. Once the discharge was stopped, fish community structures tended to revert to their original state, which indicated that the environmental impacts of brine discharge were reversible, with further monitoring and management required to ensure ecological balance. Therefore, to understand the impact of concentrated brine discharge on the salinity of receiving marine areas and to reduce the harmful effects of salinity changes on organisms, it is crucial to utilize numerical models to simulate and predict the variations in the diffusion process before and after brine discharge (Pérez-Díaz et al., 2019; Zhang et al., 2023).

After brine discharge, fan-shaped distribution patterns form near discharge outlets (Del Bene et al., 1994); although these discharge patterns have relatively limited impact ranges, they significantly increase salinity in local marine areas (Ahmad and Baddour, 2014). Purnama and Al-Barwani (2006) applied a 2D convection-diffusion equation to evaluate the environmental impacts of brine discharge from desalination plants in Oman Bay. The obtained results indicated that under specific conditions, tidal oscillations could rapidly increase salinity on both sides of the discharge point, emphasizing on the significant role of tides in brine dispersion processes near discharge outlets. In addition, increase of salinity was found to affect the growth of phytoplankton in the area. Fernández-Torquemada et al. (2019) investigated three reverse osmosis desalination plants in southeastern Spain through field observations and statistical data analyses to explore spatial and temporal distribution patterns following brine discharge. They found that brine dispersion was closely related to the discharge depth, dilution ratio, and seabed topography. Furthermore, increase of the dilution ratio of brine to raw seawater before discharge could significantly decrease the impact range of brine dispersion into the sea (Fernández-Torquemada et al., 2009). Sun et al. (2012) applied COHERENS model to deeply investigate the patterns of brine dispersion into the sea from a desalination plant in Laizhou Bay and analyzed the effects of tidal fluctuations on the variations of temperature and salinity. They showed that the convective dispersion pattern of brine was closely related to periodic fluctuations of tides, playing a key role in brine transportation and dispersion. Wang et al. (2009) applied POM model to set various discharge volumes and analyze temporal changes and distribution of salinity. Their research showed that during February, May, August, and October, there were significant increases in salinity near brine discharge points. In February, salinity could increase by 8.73psu, affecting the growth process of phytoplankton in that marine area.

This research adopted Dingzi Bay on Shandong Peninsula in China as research area. Dingzi Bay is a typical narrow estuarine bay, compared to the open sea areas, its complex bathymetry and relatively poor hydrodynamic conditions can create difficulties in convective dispersion of brine. The local marine areas surrounding the brine discharge zones experience significant salinity increase, affecting local ecological safety, particularly for certain salt-sensitive marine species (Al-Kasbi and Purnama, 2022). An in-depth study on the convective dispersion process of brine into the sea along with its salinity increase, and impact range will aid in the standardized management of brine discharge and protection of ecosystem stability in receiving marine areas (Malcangio and Petrillo, 2010). This study employs a three-dimensional convective diffusion numerical model to focus on the diffusion process, impact range, salinity increase, and its effects on the marine ecological environment following brine discharge into the sea.

2 Materials and methods

2.1 Regional background

Dingzi Bay is located in the southern marine area of Shandong Peninsula, China (Figure 1), connecting upstream to Wulong River estuary and downstream to Yellow Sea (Zhan et al., 2017). This bay is the largest and most representative ria-type tidal channel bay on

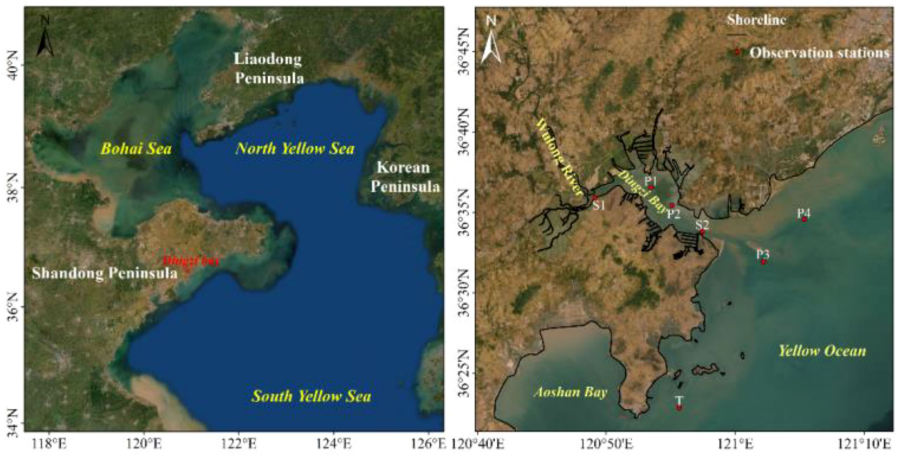

FIGURE 1
Research area and observation station map (P is tidal current observation point, S is salinity observation point, and T is tidal level observation point).

Shandong Peninsula (Tian et al., 2017). It has unique geomorphological properties, with contours resembling "small mouth and big belly" shape. The northwestern area is the estuarine section of Wulong River, while the central to southeastern areas extend into coastal regions outside Wulong River estuary (Wang et al., 2023). During high tide in Dingzi Bay, the area of the bay reaches 143.75 km², with an intertidal zone covering about 119.01 km² and bay mouth width of about 6.0 km. During low tide, seawater mainly covers tidal channel areas, with tidal flats exposed on both sides.

Geomorphological pattern of Dingzi Bay is characterized as "intertidal flats with a tidal channel." A large ebb-tide delta, with bay mouth as its apex, develops outside the bay entrance. Tidal channel is less than 1000 m wide and about 15 km long above the bottom of the channel and channel sidewall slopes range from 0.9 to 5.2% (Figure 2). The area around the brine discharge outlet, located in tidal channel, features a seabed geomorphological pattern of "two channels with a sandbank in between." In the middle section of cross-section DM11, central sandbank top rises about 3.4 m above the western ebb-tide channel and 6.0 m above the eastern flood-tide channel (Figure 2). In cross-section DM16, central sandbank top is 3.4 m above the bottom of the northwest ebb-tide channel and 2.5 m above the bottom of the southeast flood-tide channel.

The tidal characteristics of Dingzi Bay are typical of regular semidiurnal tides, with a maximum tidal range of 4.7 meters. The tidal currents of the bay are primarily due to the narrow, elongated shoreline and the topographic effects of tidal channel, predominantly presenting a reciprocating flow from southeast to northwest. Regarding the waves outside the bay, the primary wave direction is from southeast. In summer, typhoons often cause high waves outside the bay entrance, with wave heights typically exceeding 1.5 m and reaching up to 3.5 m. However, these Most of the waves have minimal impacts inside the bay; therefore, this research model did not consider wave effects (Zhan et al., 2024).

Wulong River at the head of Dingzi Bay is a monsoon rain-fed river, with an average annual runoff of 92.7×10^8 m³, accounting for 70-80% of the total annual runoff during flood season (Figure 3). Based on the data observed at Tuanwang station (hydrological station) from 2000 to 2022, the average monthly discharge of Wulong River into the sea was 10.71 m³/s, with multi-year average daily flow in winter being 3.21 m³/s, which was significantly increased to 24.28 m³/s in summer. On August 12th, 2006, the highest daily flow of 1870 m³/s was recorded.

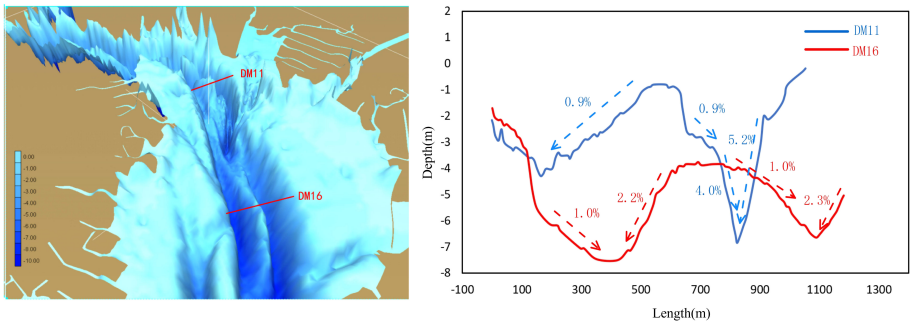

FIGURE 2
Topographic map near the outfall (DM11 represents the section where the outfall is located, and DM16 represents the section within the bay).

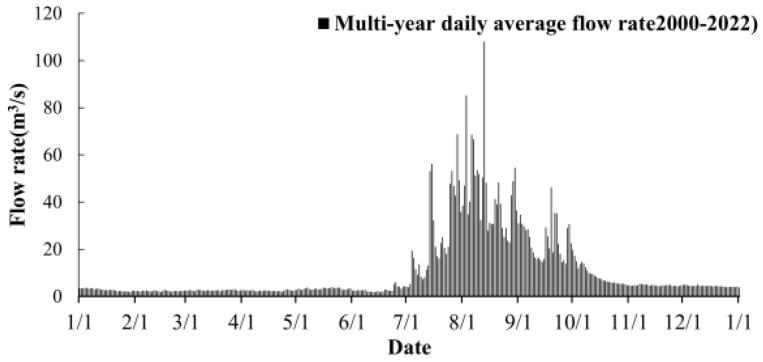

FIGURE 3
Multi-year daily average flow rate of Wulong River.

2.2 Model setup

Research area was located between latitudes 36.1°N and 36.8°N and longitudes 120.6°E and 121.5°E, including Wulong River Estuary, Dingzi Bay, and parts of Yellow River marine area. Bathymetric data for Wulong River Estuary and Dingzi Bay area were collected by onsite measurements with precision of 1:5000. Bathymetric data for areas outside Dingzi Bay were obtained from ETOPO global bathymetric dataset.

Considering the complex topography of Dingzi Bay coastline, to more accurately simulate natural shoreline, the developed model employed an unstructured triangular mesh (Fowler et al., 2016) to delineate the computational area and utilized dynamic boundaries to handle wet-dry grid transformations (Guo et al., 2021). Computational area included 41,866 grids and 23,393 nodes (Figure 4), divided vertically into 6 Sigma layers. To precisely calculate salinity variations near discharge outlets, the grids near these outlets were refined (Zhang et al., 2023), with the smallest grid scale in the refined area being 2 m. Using a bilinear interpolation method (Minh et al., 2024), bathymetric scatter data were applied to grid points to obtain distributions of water depths, as illustrated in Figure 5. The model has a minimum time step of 0.05 seconds and a maximum time step of 30 seconds. The boundary conditions for the Wulong River use runoff input, while the ocean boundary conditions are driven by water levels. The water levels are forecasted based on harmonic constants of various tidal constituents assimilated from satellite altimetry data using the Tide Model Driver (TMD) (Ma et al., 2024).

Seawater salinity data for Dingzi Bay included measurements from two tidal stations (S1 and S2 as shown in Figure 1) collected between December 25th, 2022, and January 1st, 2023. Remote sensing imagery from the same period was used to obtain the spatial distribution of surface salinity in Dingzi Bay.

Brine discharge outlet was located within the main tidal channel of Dingzi Bay, significantly affected by the upstream flow of Wulong River. The salinity of the estuarine area varied greatly in different seasons. During the dry seasons of winter and spring, salinity in the estuary was higher while In the wet seasons of summer and autumn, increased river flow led to a significant decrease in salinity due to seawater dilution by freshwater. Considering the impact of brine discharge on ecological environments, marine biomass in Dingzi Bay reached its peak in autumn, when salinity variations have the most significant impact. Furthermore, the average river flow in September was at its highest. After considering seasonal variations in Wulong River flow into the sea and biomass in Dingzi Bay, winter and autumn were selected as the representative seasons for 3D numerical simulations. The average river flows in December and September served as runoff input conditions for the model.

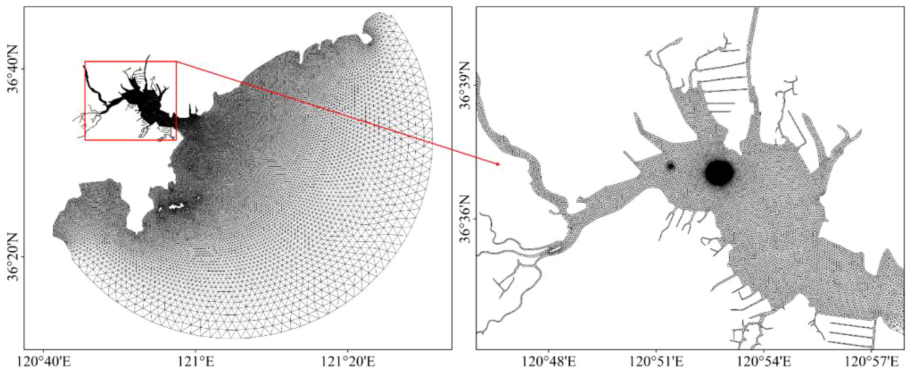

FIGURE 4
Dingzi Bay grid map.

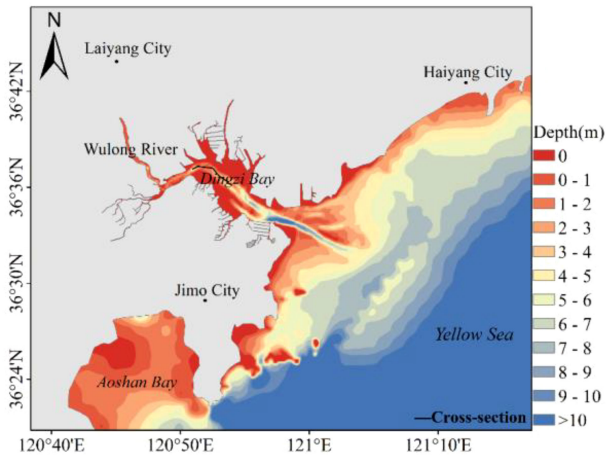

FIGURE 5
Dingzi Bay topographic map.

The water intake during autumn and winter is 15.52 m^3/s and 11.12 m^3/s, respectively, while the discharge rates are 9.99 m^3/s and 7.16 m^3/s, respectively.

2.3 Model validation

To verify the feasibility and accuracy of the developed model, comprehensive validation was performed considering various parameters such as tide level, flow speed, flow direction, and salinity. Figure 6 compares simulated and observed tide levels at Nvdao Station (Figure 1, Station T) from July 16th to July 23rd, 2022, with results indicating good consistency in tide amplitude and phase. The speed and direction of flow at measurement points P1, P2, P3, and P4 from December 29th to December 30th, 2022, are also compared (Figure 7). It was found that simulation results matched well with the experimental values and flow directions were almost identical, proving that the model could accurately reflect the hydrodynamic characteristics of Dingzi Bay. Figure 8 compares the observed and simulated salinity results at measurement points S1 and S2, from December 29th to December 30th, 2022. The calculated values strong agreement with the observed data, ensuring the accuracy of subsequent model calculations.

3 Results analysis

3.1 Characteristics of flow field changes

Dingzi Bay is a narrow estuarine tidal channel bay with seabed geomorphological pattern of "two channels with a sandbank in between." Flood tide flows propagate upstream along the eastern side of the main tidal channel, while ebb tide flows move downstream along the western side of the channel (Figure 9). Figure 10 shows a depth average flow speed map of Dingzi Bay. In this area, the highest flow speeds are typically concentrated near the bay mouth and within the internal tidal channels of the bay. Maximum surface flow speed during flood tide is about 75-85 cm/s and during ebb tide, it is about 70-80 cm/s. Ebb tide duration (6 h 25 min) is longer than that of flood tide (5 h 58 min). Flow speeds in other bay areas are relatively lower, with flood tide flows generally stronger and of shorter duration compared to ebb tide flows.

After entering from the open sea through Dingzi Bay mouth, the tidal flow progresses from southeast to northwest, turns west at the west side of Magu Island, and then north past the west side of Xiang Island into narrow Wulong River. Because of the narrowing of the tidal channels upstream, flood tidal currents downstream of Xiang Island are strong, presenting distinct reverse flow properties. On tidal flats on both sides of the channels, flow speeds are relatively lower and flow direction includes components moving towards the shore.

3.2 Distribution characteristics of salinity increase

As shown in Figure 11, high salinity variation zones are primarily concentrated near discharge outlets, which are affected

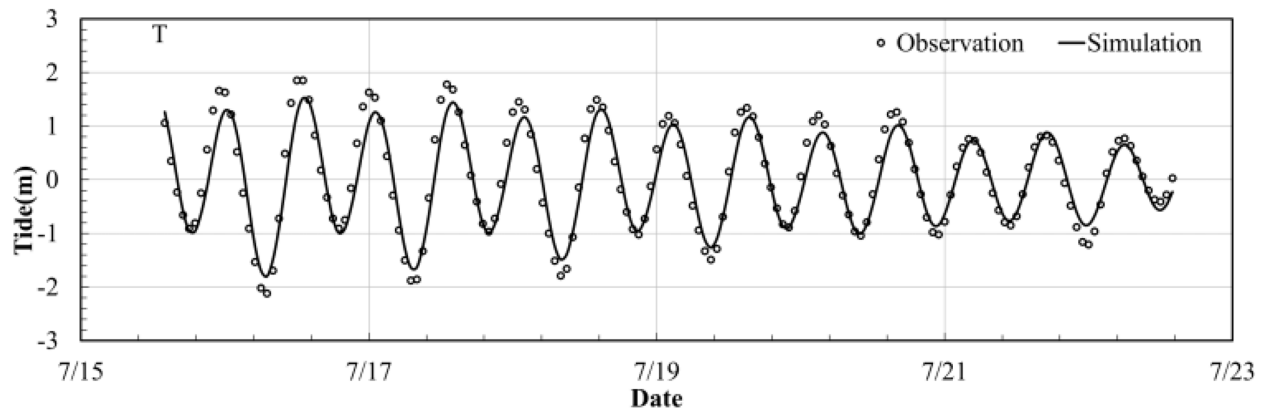

FIGURE 6
Comparison of calculated and measured tide levels.

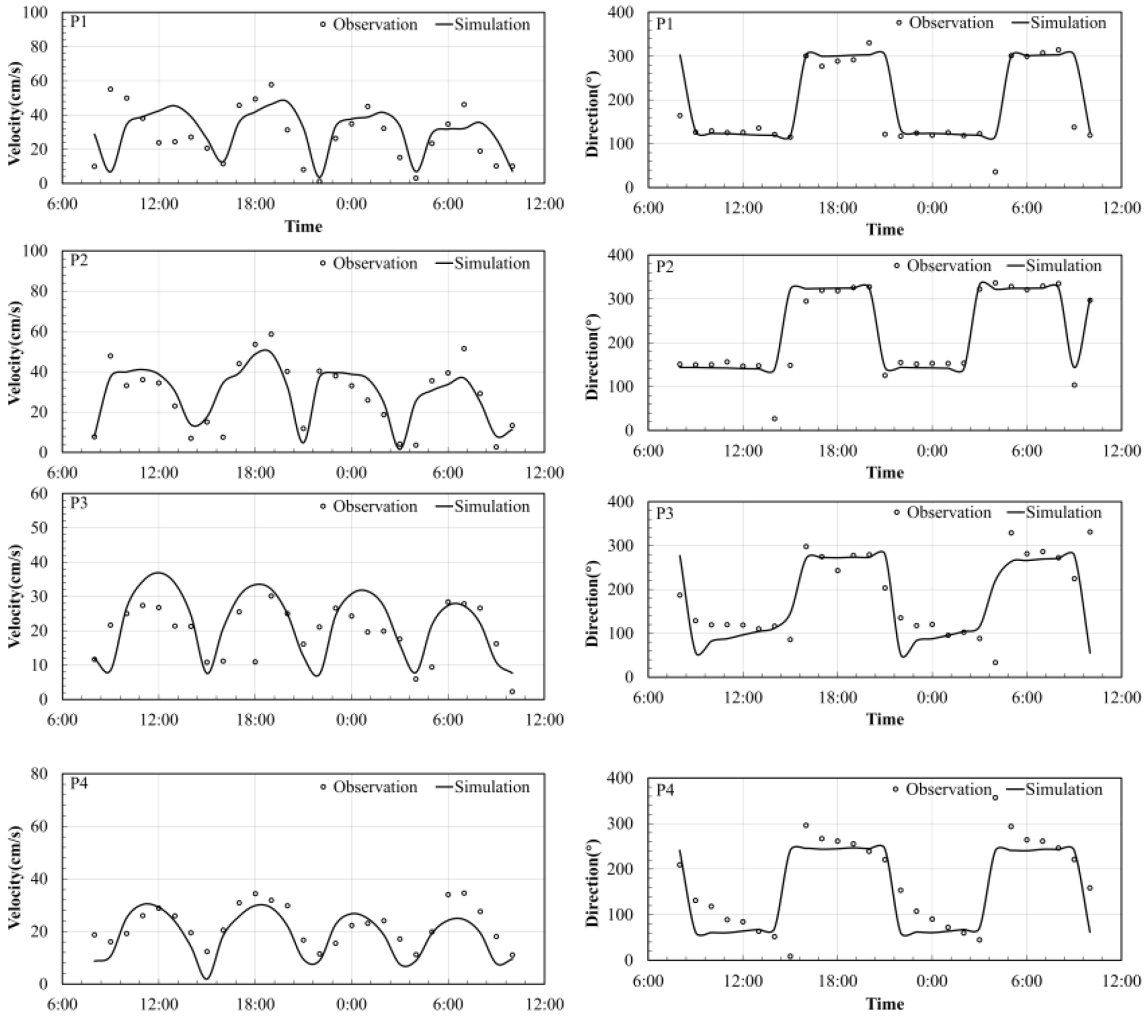

FIGURE 7
Tidal current verification (The left figure shows the flow velocity verification, and the right figure shows the flow direction verification).

by the tidal channels of Dingzi Bay and dynamic geomorphological conditions near these outlets, giving rise to the formation of a narrow strip extending in NW-SE direction. The magnitude of salinity variation after brine discharge was changed with season, tidal pattern, tidal phase, water layer, and specific location. Numerical simulations on Dingzi Bay indicated that in both winter and autumn, areas within the bay and near the bay mouth experienced varying degrees of salinity increase. By analyzing maximum salinity changes in vertical envelopes, it was observed that in winter, most areas had salinity increase values of less than 3psu, particularly in the narrow regions of tidal channel at discharge outlets where increases exceeded 3psu, the statistics for the area of salinity increase are shown in Table 1. In autumn, increase in most areas did not exceed 2psu, with a large area southwest of the discharge outlet experiencing 2psu increase with no instances exceeding 3psu. Seasonal variations showed that high salinity areas near the discharge outlets were more concentrated in winter, possibly due to stronger tidal effects and hydrodynamics

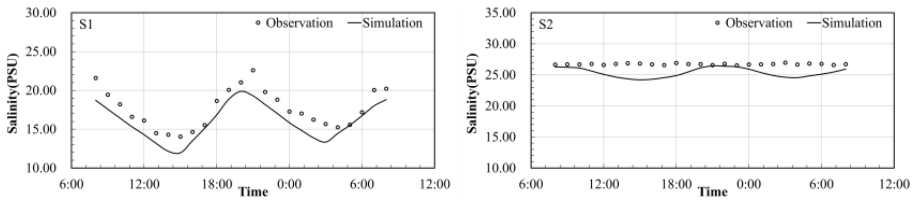

FIGURE 8
Salinity verification.

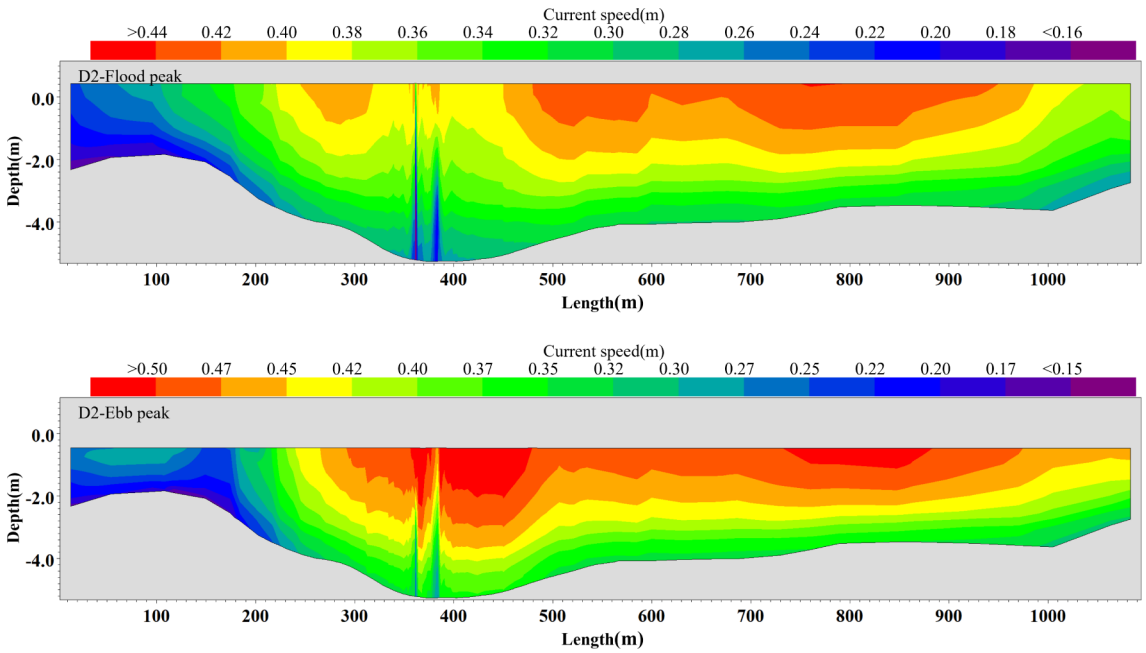

FIGURE 9
Vertical distributions of the flow velocity along cross-section: MD16.

during this season. However, areas with increased salinity in autumn were more dispersed. Although some marine communities can adapt to salinity variation exceeding 3psu, long-term and widespread ecological impacts still require thorough assessment, particularly in winter, where the ecological impacts of high salinity in tidal channel areas should be carefully considered.

By comparing the distribution maps of increased salinity after freshwater discharge in winter (Figure 12) and autumn (Figure 13), distribution characteristics of high-concentration saline water under the effect of Wulong River runoff and tidal action were further investigated. Salinity increase distributions during the four typical tidal phases of flood rapid, flood slack, ebb rapid, and ebb slack in winter and autumn were evaluated. The areas affected by salinity increases were significantly changed with tides, especially in regions where salinity was increased by more than 2psu. During flood rapid, areas with salinity increase of more than 2psu were located at the bend of tidal channel near the discharge outlet, which roughly corresponded to the central marine area of the bay. During flood slack, they were located in the tidal channel near the discharge outlet and at bay top. During ebb rapid, they were upstream of discharge outlet in the tidal channel and at bay top while during ebb slack, they were near tidal channel close to discharge outlet.

3.3 Temporal changes of salinity

Statistical analysis of cumulative durations for salinity increases of over 2psu and 3psu in winter and that over 2psu in autumn showed the temporal patterns of salinity changes (Figures 14, 15). In winter, most areas with salinity increase of 2psu had cumulative duration of less than 150 h, but within 300 m range from discharge outlet, there were areas where cumulative duration exceeded 180 h. Areas with salinity increases of over 3psu and cumulative durations

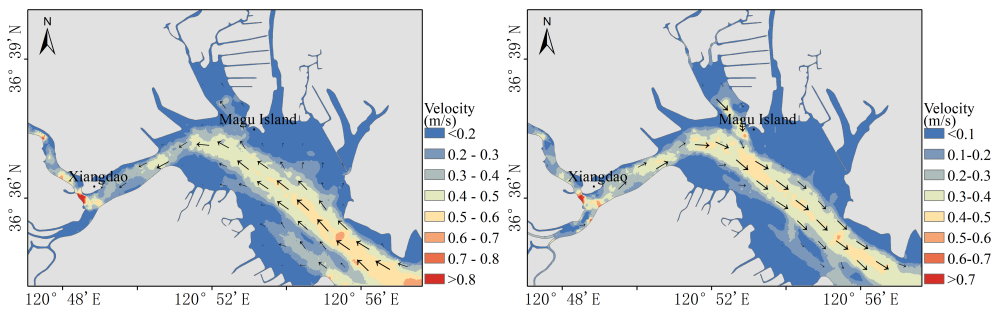

FIGURE 10
Flow field distribution in Dingzi Bay, **(A)** flood current field, and **(B)** ebb current field.

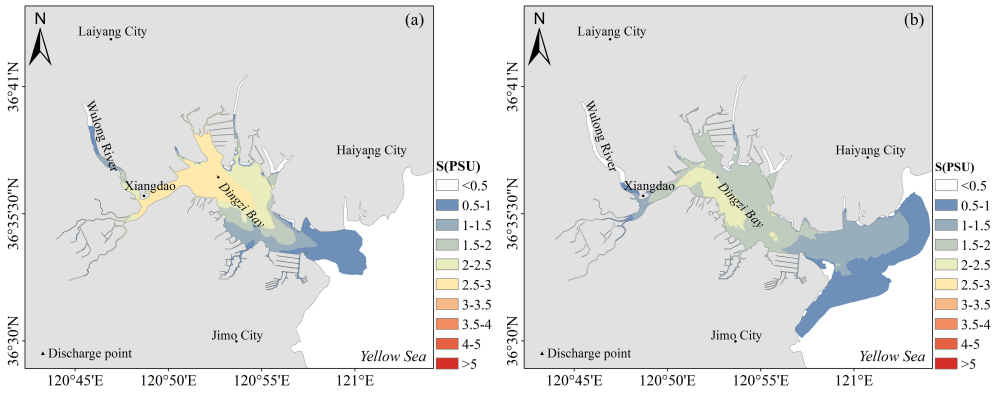

FIGURE 11
Distribution of salinity increase in Dingzi Bay, **(A)** winter and **(B)** autumn.

exceeding 60 h were mainly concentrated near the discharge outlet. Areas with 3psu increase in salinity lasting over 30 h were almost entirely within 200 m of the discharge outlet, while most areas had cumulative durations of less than 120 h, with only the area around the discharge outlet presenting durations exceeding 120 h. In autumn, due to higher Wulong River runoff and the effect of water dilution due to runoff, no high-concentration salinity increase areas occurred and overall salinity increases within the bay were lower. Areas with salinity increases of over 2psu and cumulative durations exceeding 30 h showed elliptical spatial distributions, primarily around the discharge outlet. Most areas with over 2psu increase in autumn had cumulative durations of less than 30 h, with those exceeding 30 h mainly concentrating within tidal channels. In summary, regardless of the season, the areas near the discharge outlets were key regions for the accumulation of increased salinity durations. Especially in winter, due to decreased runoff, areas with prolonged salinity increases might have more significant impacts on marine communities. In contrast, salinity increases in autumn were more gradual with fewer long-duration areas, mainly distributed in tidal channels with stronger water dynamics.

4 Discussion

4.1 Impact of depth and flow speed changes on salinity increase

Figure 16 illustrates the cross-section (Figure 5) of depth -tide-salinity increase relationship. The figure revealed that flow speeds at surface exceeded those at mid-depths and bottom layers. Under the effect of topography, in 0-500 m depth range, due to deeper water and gentle slope, the flow was slow and steady. In 500-1000 m depth range, where the topography was more variable and water was shallower, flow speed was increased. Near discharge outlet at 1000 m depth, flow speeds were smooth but fluctuated significantly near the outlet due to discharged water and density currents. Furthermore, as the terrain flattens and water body widens, flow speeds were gradually stabilized. The vertical distribution of salinity increase was similar to those found by Tsiourtis (2001), who investigated the impacts of brine discharge from desalination plants near Garin Islands. The results revealed that while brine dispersed well at surface layer, its higher density caused it to accumulate in deep water sections, resulting in the formation of high-salinity zones, which in this research were also affected by the terrain near discharge outlets. Research has shown that since natural seawater salinity could fluctuate by ±10psu of the average annual salinity of the area, marine organisms had natural adaptability to these fluctuations. A 10psu increase in seawater salinity could be applied as a conservative estimate of the tolerance of marine organisms to salinity increase (Gao and Ruan, 2004). Monitoring results of brine discharge into the sea indicated that most marine communities could tolerate salinity increases of 2-3psu, some even up to 10psu; therefore, a 2-3psu increase had no impact on the ecosystem (Jenkins et al., 2012). Therefore, we identified areas with 3psu increase as high-concentration salinity zones. The dispersion of high-concentration saline water was found to mainly occur near incoming tide peak moments, indicating a close relationship between brine dispersion and flow speed. At low speeds, high-density brine gathered together under the effect of density gradients, dispersing to other areas near the discharge outlet when flow speed was increased. During ebb tide, the area affected by high-concentration saline water was smaller because, as the tide fell, freshwater from Wulong River diluted the water near the intake, decreasing the salinity of the brine discharged from the outlet and preventing the formation of large high-salinity zones near the outlet.

TABLE 1 Vertical envelop area of salinity increase (km^2).

Season/Salinity Increase	5psu	4psu	3psu	2psu
Winter	3.33×10^{-3}	9.29×10^{-3}	5.72×10^{-2}	33.10
Autumn	0	0	0	10.04

After brine discharge, it rapidly diffused. To investigate salinity diffusion after brine discharge, a statistical analysis was performed on the attenuation process of salinity increases along four directions (E, W, S and N) within a 500 m range from the discharge point during winter (Figure 17). Following discharge, there was a rapid

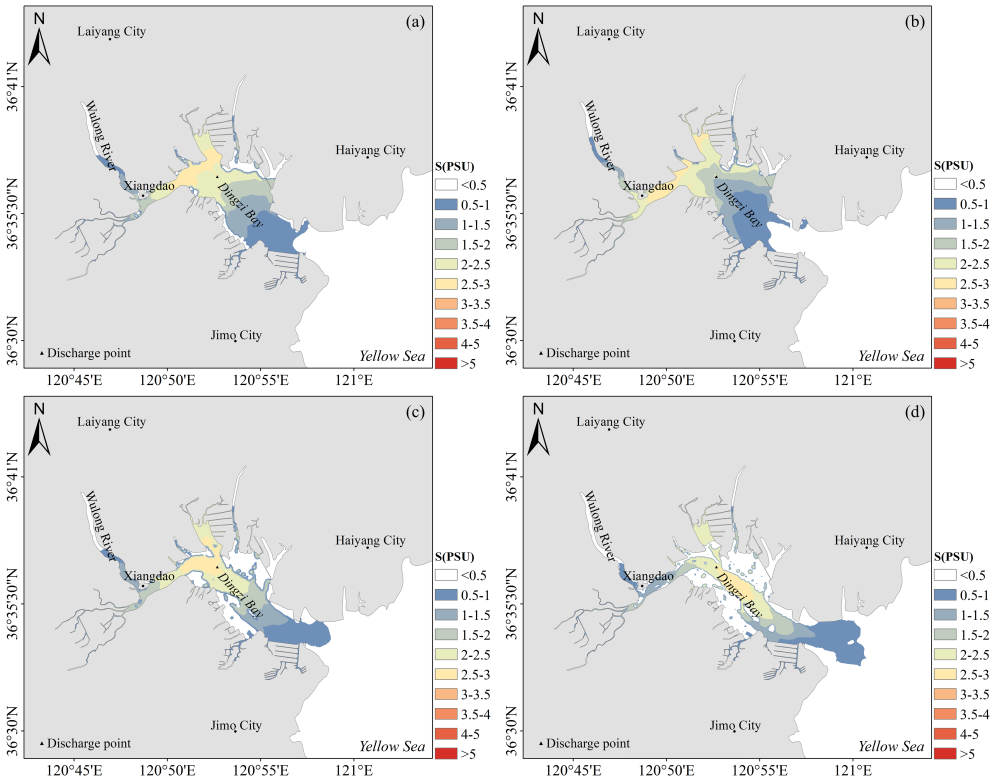

FIGURE 12
Typical tidal salinity increase distribution in Dingzi Bay during winter, **(A)** flood peak, **(B)** high tide slack, **(C)** ebb peak, and **(D)** low tide slack.

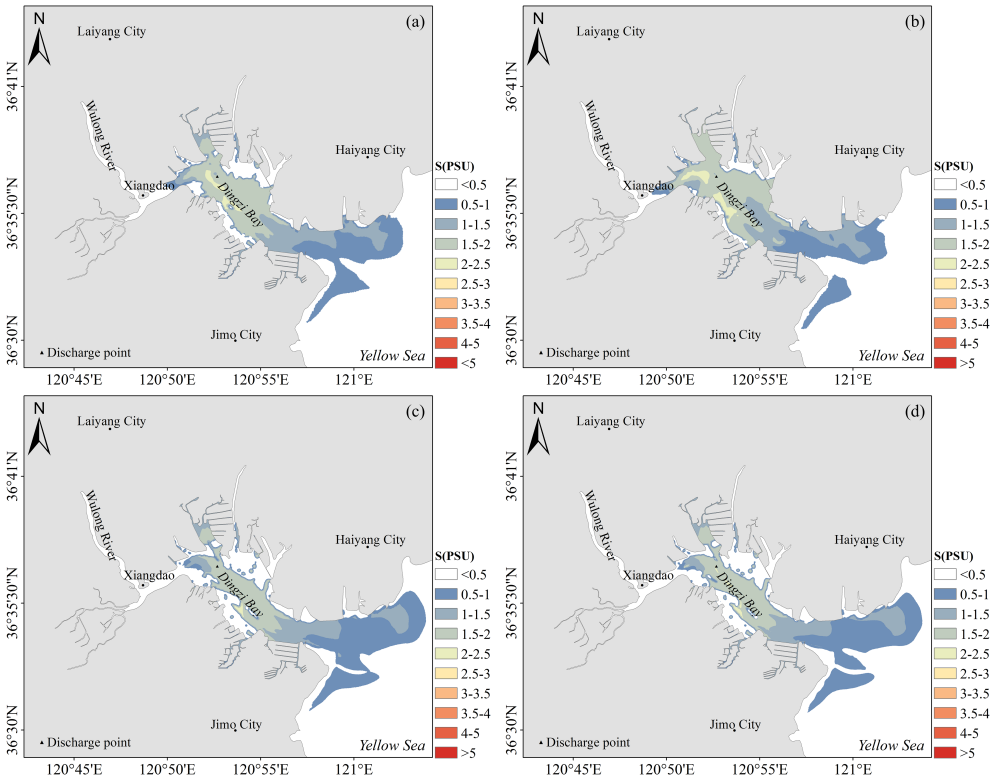

FIGURE 13
Typical tidal salinity increase distribution in Dingzi Bay during autumn, **(A)** flood peak, **(B)** high tide slack, **(C)** ebb peak, and **(D)** low tide slack.

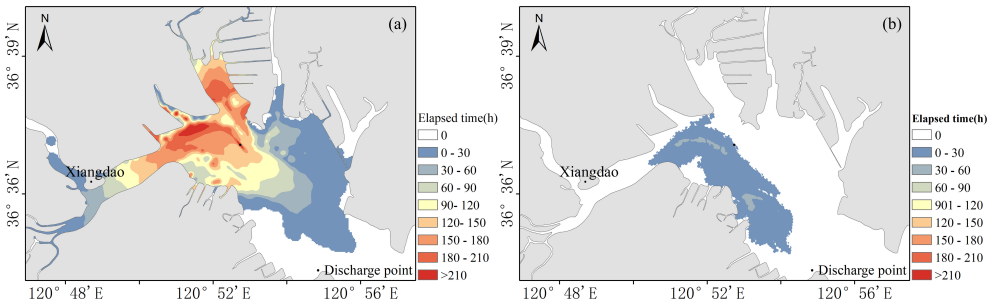

FIGURE 14
Duration of salinity increase of greater than 2% in Dingzi Bay, **(A)** winter and **(B)** autumn.

attenuation of salinity within a 50-100 m range near the discharge outlet, with attenuation rates reaching 42-59% within 100 m along all four directions, with maximum attenuation rate being 0.03799 psu/m (Table 2). Within 100-500 m range, the attenuation of salinity increases was more gradual, due to the brine being sufficiently diluted and oscillating within the bay under tidal effects.

Field simulation results were generally consistent with the findings of most previous researchers (Aljohani et al., 2022), indicating that brine discharge led to significant increases in local salinity, which could potentially impact marine communities (Flavin et al., 2023). This research showed that the amount of salinity changes was related to other factors such as runoff and tides. Under the effect of tidal dynamics, the diffusion characteristics and impact ranges of brine varied between winter and autumn; therefore, when planning and managing brine discharge into the sea, it was necessary to consider the effect mechanisms of these natural conditions on discharge to adopt more effective management strategies to minimize environmental impacts.

4.2 Impact of runoff and tidal volume on salinity increase

The water in estuarine bays is supplied by rivers and the open sea and salinity variations are jointly affected by runoff and tidal flows. Due to the offsetting effects of tidal actions, the effect of tides on salt intrusion was not significant (Uncles and Stephens, 2011). He et al. (2018) analyzed historical data and numerical simulation results and found that an increase in runoff decreased salinity in estuarine areas. When freshwater flow was increased, more freshwater entered the estuary, diluting saline water and thus reducing salinity. By integrating observed data and numerical model results, Chang et al. (2024) found that with the increase of runoff, mixing of salinity intensified, leading to a significant decrease in salinity in estuary areas. In Dingzi Bay, there was a significant seasonal variation in runoff. With high runoff in autumn, salinity within the bay was decreased, resulting in a lower degree of salinity increase from brine discharge into the sea during autumn compared to winter.

Saltwater intrusion is a common phenomenon in estuarine areas (Liu et al., 2011; Jiang et al., 2024), with river runoff being the main factor affecting saltwater intrusion changes (Tian, 2019). In this research, due to internal water extraction and drainage within the bay, where extraction volume exceeded drainage volume, concentrated brine discharge decreased total water volume inside the bay, thereby increasing tidal volume within the bay and intensifying saltwater intrusion. Seawater entered freshwater areas through tidal forces and since seawater salinity outside the bay far exceeded that of freshwater, this led to significant variations in the salinity and its spatial-temporal distribution in Dingzi Bay and nearby maritime areas. The average salinity of seawater outside the bay was 28psu in winter and 27psu in autumn. Reductions of freshwater volume within the bay due to neap tides in winter and autumn were 5132160 and 7039872 m^3, respectively. Based on these figures, the areas where salinity was increased by more than 0.1psu (0.1psu salinity increase zones) and salinity changes due to additional seawater intrusion within the bay were determined (Table 3).

Additional seawater intrusion resulted in average salinity increases of 0.36psu in winter and 0.28psu in autumn for 0.1psu

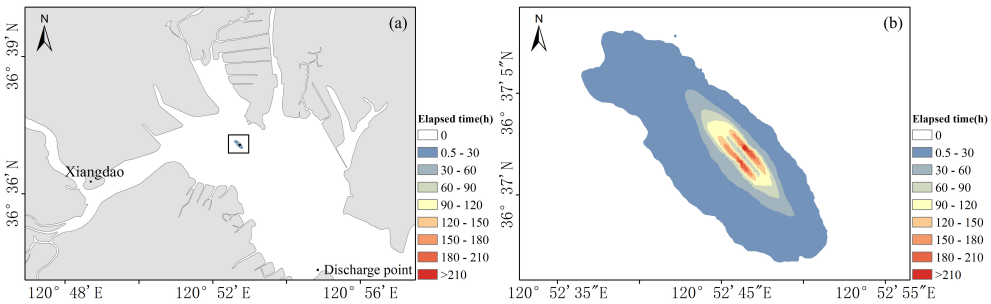

FIGURE 15
Duration map of salinity increase of greater than 3% in Dingzi Bay during winter.

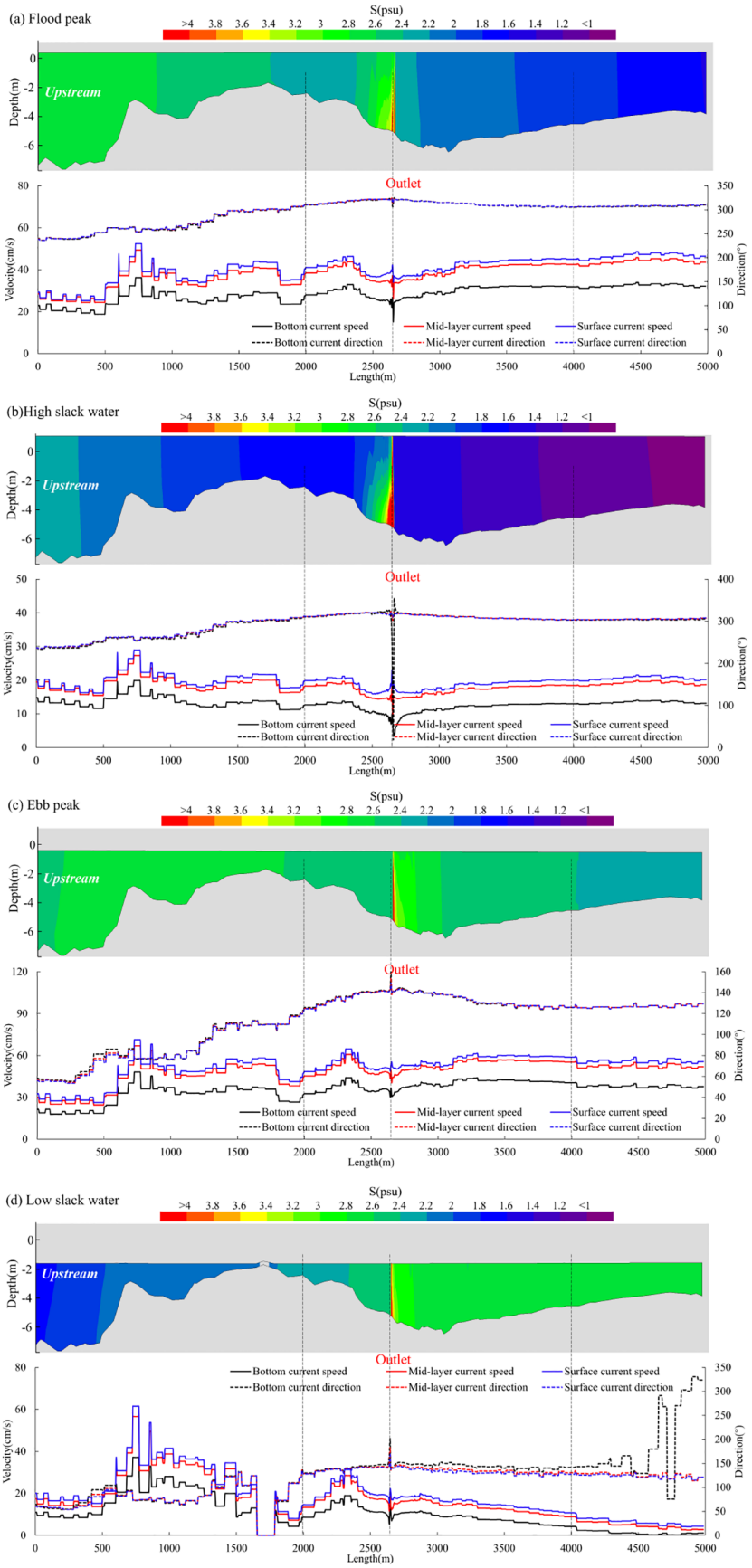

FIGURE 16
(A–D) Flow speed-salinity increase-topography cross-section diagram.

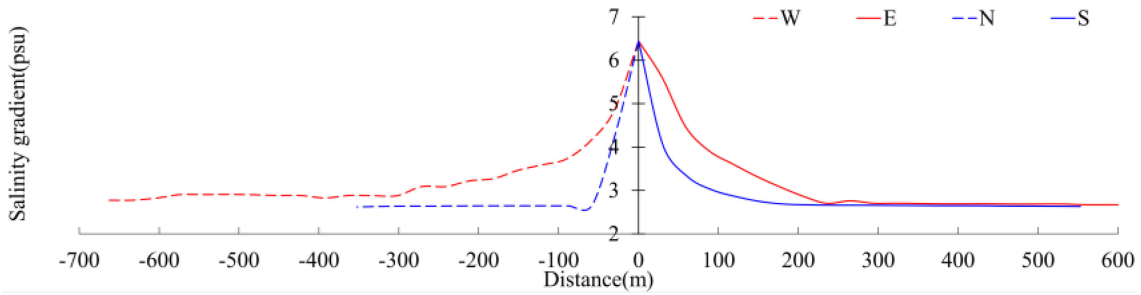

FIGURE 17
Salinity increase attenuation process near discharge outlet.

salinity increase zones during neap tides. Average increases in bay salinity due to additional seawater intrusion during neap tides were 0.80psu in winter and 1.05psu in autumn. Therefore, brine extraction and discharge did not alter the total amount of salt in the original seawater of the bay and only reduced the amount of freshwater within the bay resulting in the addition of higher-salinity seawater from outside the bay, thus increasing total salinity within the bay. Redistribution of original salt due to concentrated brine discharge only had a certain impact on the existing salinity distribution patterns and their dynamics within the bay.

Paparella et al. (2022) showed that the Arabian Gulf was a natural extreme marine system where marine organisms had adapted to high and variable natural salinity. Minor salinity changes due to concentrated brine discharge from desalination plants did not impact the marine environment of the gulf. Even under most dire climate predictions, increase of seawater salinity and tendency toward more desalination over the coming decades are likely to have minimal impacts on gulf salinity. Furthermore, an increase in salinity could lead to greater flow through the Strait of Hormuz, thereby accelerating the renewal of water in the gulf. This accelerated water exchange process might increase high-concentration saline water influx from outside Dingzi Bay, potentially leading to further salinity increase in the bay. This issue requires continued research in future works.

5 Conclusion

This research focused on Dingzi Bay in southern Shandong Peninsula and utilized a 3D hydrodynamic numerical model to systematically simulate brine dispersion into the sea, investigating the dispersion paths, impact scope, degree of salinity increase, and effects on nearby marine ecosystems. The following key insights were obtained:

1. Flow speeds within Dingzi Bay showed significant spatial variability under the effect of topography, especially in tidal channels and nearby areas. Near the bay mouth and within bay tidal channels, flow speeds were high. Incoming tidal flows mainly propagated upstream along the eastern side of the main tidal channel, while outgoing tidal flows moved downstream along the western side.
2. Salinity near brine discharge outlet was significantly increased, forming high salinity zones at the bottom of the outlet. The extent of impact and degree of salinity changes were closely related to natural factors such as season and tide, particularly in winter, where local marine areas around the discharge zone experienced significant salinity increases, forming a conical high-salinity water body within a 20 m range of the outlet.
3. Brine discharge had not changed the total amount of salt in the original seawater of the bay, but by decreasing the amount of the freshwater within the bay, it had led to the intrusion of higher salinity seawater from outside the bay, thus increasing total salinity within the bay. Although the discharged concentrated seawater itself did not change average bay salinity, it altered the spatial and temporal distributions of the original salinity in the bay, affecting salinity distribution patterns in Dingzi Bay.
4. In winter, small areas with salinity increase of over 3psu appeared near discharge outlets, potentially significantly affecting indigenous marine organisms within these areas,

TABLE 2 Attenuation coefficient of salinity increase near the discharge outlet (psu/m) direction (S).

Direction	Outlet(0-100m)	Outlet (100-500m)
W	0.02849	0.00171
E	0.02849	0.00251
N	0.03799	–
S	0.03507	0.00074

TABLE 3 Average salinity increase due to salt intrusion(psu).

	0.1 psu salinity increase area		Salinity increase area within the bay	
	winter	autumn	winter	autumn
Salinity increase caused by seawater exchange/psu	0.3639	0.2759	0.8000	1.0539
Simulated salinity increase/psu	0.4106	0.3624	0.8544	1.0486

while organisms in other marine areas were largely unaffected. The 1, 2, and 3psu salinity increase contour lines from brine discharge did not reach the mouth of Dingzi Bay; therefore, they had no impact on offshore aquaculture.

5. Based on the numerical model results, to reduce the impact of brine discharge, the discharge location should first be optimized by strategically placing discharge points in areas with higher flow rates to enhance the mixing and dispersion of the saline water. This approach aims to minimize high salinity zones near the discharge point. Additionally, a seasonal discharge plan should be implemented, avoiding discharge operations during periods of low runoff (e.g., winter), as these times have the most significant impact on local salinity and marine life.

Dingzi Bay flow field characteristics were complex and were affected by tides, topography, and runoff. There were significant spatial and temporal differences in tidal and ebb flow fields, particularly high salinity areas and flow velocity changes near the discharge outlets, which had significant impacts on local environments. These findings provided important scientific insights to understand the hydrodynamic characteristics of Dingzi Bay and their impact on salinity distribution, supporting the optimization of brine discharge strategies to minimize environmental impacts and protect the health and diversity of marine ecosystems.

Data availability statement

The raw data supporting the conclusions of this article will be made available by the authors, without undue reservation.

Author contributions

HX: Conceptualization, Data curation, Methodology, Software, Validation, Writing – original draft, Writing – review & editing. HS: Data curation, Investigation, Writing – original draft, Writing – review & editing. CZ: Project administration, Supervision, Writing – review & editing. QW: Data curation, Formal analysis, Project administration, Supervision, Writing – review & editing. YL: Funding acquisition, Investigation, Methodology, Resources, Visualization, Writing – original draft, Writing – review & editing. ZY: Conceptualization, Methodology, Supervision, Writing – review & editing.

Funding

The author(s) declare financial support was received for the research, authorship, and/or publication of this article. This research was funded by the Major Research Grant (42330406) from the Natural Science Foundation of China (NSFC), Shandong Provincial Natural Science Foundation, China (No.ZR2023QE310), Yantai Science and Technology Innovation Project (2023JCYJ097, 2023JCYJ094) and Supported by the Innovation Project for graduate students of Ludong University (119-810201).

Conflict of interest

The authors declare that the research was conducted in the absence of any commercial or financial relationships that could be construed as a potential conflict of interest.

Publisher's note

References

Ahmad, N., and Baddour, R. E. (2014). A review of sources, effects, disposal methods, and regulations of brine into marine environments. *Ocean Coast. Manage.* 87, 1–7. doi: 10.1016/j.ocecoaman.2013.10.020

Aljohani, N. S., Kavil, Y. N., Shanas, P. R., Al-Farawati, R. K., Shabbaj, Ii, Aljohani, N. H., et al. (2022). Environmental impacts of thermal and brine dispersion using hydrodynamic modelling for yanbu desalination plant, on the eastern coast of the red sea. *Sustainability* 14, 18. doi: 10.3390/su14084389

Al-Kasbi, A., and Purnama, A. (2022). Behavior of effluents discharged into shallow coastal waters under the influence of spring-neap tidal currents. *Environ. Fluid Mechanics* 22, 5–32. doi: 10.1007/s10652-021-09826-1

Chang, Y., Li, X. Y., Wang, Y. P., Klingbeil, K., Li, W. H., Zhang, F., et al. (2024). Salinity mixing in a tidal multi-branched estuary with huge and variable runoff. *J. Hydrology* 634, 16. doi: 10.1016/j.jhydrol.2024.131094

Chang-Feng, Q., Jin-Ming, S., and Ning, L. (2014). Causes of jellyfish blooms and their influence on marine environment. *Yingyong Shengtai Xuebao* 25, 3701–3712. doi: 10.13287/j.1001-9332.20141009.005

Del Bene, J., Jirka, G., and Largier, J. (1994). Ocean brine disposal. *Desalination* 97, 365–372. doi: 10.1016/0011-9164(94)00100-6

Fernández-Torquemada, Y., Carratalá, A., and Lizaso, J. L. S. (2019). Impact of brine on the marine environment and how it can be reduced. *Desalination Water Treat* 167, 27–37. doi: 10.5004/dwt.2019.24615

Fernández-Torquemada, Y., Gónzalez-Correa, J. M., Loya, A., Ferrero, L. M., Díaz-Valdés, M., and Sánchez-Lizaso, J. L. (2009). Dispersion of brine discharge from seawater reverse osmosis desalination plants. *Desalination Water Treat* 5, 137–145. doi: 10.5004/dwt.2009.576

Flavin, M. T., Fernandes, J., Alqabandi, R., Adams, E., Han, J., and Al-Anzi, B. (2023). Numerical modeling of plunging jets of brine: Mass transport and implications for desalination plant outfalls. *Desalination* 568, 10. doi: 10.1016/j.desal.2023.116996

Fowler, S. J., Kosakowski, G., Driesner, T., Kulik, D. A., Wagner, T., Wilhelm, S., et al. (2016). Numerical simulation of reactive fluid flow on unstructured meshes. *Transport Porous Media* 112, 283–312. doi: 10.1007/s11242-016-0645-7

Gao, C. J., and Ruan, G. L. (2004). *Desalination technology and engineering* (Chemical Industry Press). 978-7-122-22837-6(in China).

Guo, W. W., Xu, H. S., and Hu, Z. J. (2021). *Comparative research on the mesh generating of temperature difference induced heterogeneous flow with MIKE3* (China Rural Water and Hydropower). doi: 10.3969/j.issn.1007-2284.2021.06.005

He, W., Zhang, J., Yu, X. D., Chen, S., and Luo, J. (2018). Effect of runoff variability and sea level on saltwater intrusion: A case study of nandu river estuary, China. *Water Resour. Res.* 54, 9919–9934. doi: 10.1029/2018wr023285

Jenkins, S., Paduan, J., Roberts, P., Schlenk, D., and Weis, J. (2012). *Management of brine discharges to coastal waters recommendations of a science advisory panel* (Mesa, CA, USA: Southern California Coastal Water Research Project Costa). Costa Mesa: Control Board 101.

Jiang, D. S., Dong, C. Y., Ma, Z. M., Wang, X. W., Lin, K. R., Yang, F., et al. (2024). Monitoring saltwater intrusion to estuaries based on UAV and satellite imagery with machine learning models. *Remote Sens. Environ.* 308, 13. doi: 10.1016/j.rse.2024.114198

Kelaher, B. P., Clark, G. F., Johnston, E. L., and Coleman, M. A. (2020). Effect of desalination discharge on the abundance and diversity of reef fishes. *Environ. Sci. Technol.* 54, 735–744. doi: 10.1021/acs.est.9b03565

Kowalski, E., and Mazierski, J. (2008). Effects of cooling water discharges from a power plant on reservoir water quality. *Oceanological Hydrobiological Stud.* 37, 107–118. doi: 10.2478/v10009-008-0001-5

Lee, M. E., Lee, J., and Al-Osairi, Y. (2020). Study on the local sea water temperature variation for the industrial water use of Al-Zour coastal area in Kuwait. *Desalination Water Treat* 176, 9–17. doi: 10.5004/dwt.2020.25488

Lin, J., Yan, Q., and Chen, B. (2015). Ecological impact of thermal discharge from coastal power plants on plankton biomass in Xiangshan Bay. *J. Shanghai Ocean Univ.* 24, 894–905. doi: 10.12024/jsou.20150701500

Liu, Y. L., Wang, Q., Zhan, C., Yi, H. P., Tian, Q., and Zhang, M. M. (2011). Response of drowned river valley estuary - tidal inlet bay towards human activities in the past 50 years: a case study on the Dingzi Bay, Jiaodong Peninsula, China. *J. Coast. Res.* 64, 676–680. https://www.jstor.org/stable/26482257

Ma, P. C., Shi, H. Y., Xue, H. Y., Li, P. P., and Sun, Y. K. (2024). Analysis of tidal current energy potential in the major channels of the Bohai Strait based on Delft3D. *Periodical Ocean Univ. China* 23, 12. doi: 10.1007/s11802-024-5721-y

Malcangio, D., and Petrillo, A. F. (2010). Modeling of brine outfall at the planning stage of desalination plants. *Desalination* 254, 114–125. doi: 10.1016/j.desal.2009.12.005

Malfeito, J., Díaz-Caneja, J., Fariñas, M., Fernandez-Torrequemada, Y., Gonzalez-Correa, J. M., Carratala-Gimenez, A., et al. (2005). Brine discharge from the Javea desalination plant. *Desalination* 185, 87–94. doi: 10.1016/j.desal.2005.05.010

Minh, N. Q., Huong, N. T. T., Khanh, P. Q., Hien, L. P., and Bui, D. T. (2024). Impacts of resampling and downscaling digital elevation model and its morphometric factors: A comparison of hopfield neural network, bilinear, bicubic, and kriging interpolations. *Remote Sens.* 16, 20. doi: 10.3390/rs16050819

Paparella, F., D'agostino, D., and Burt, J. A. (2022). Long-term, basin-scale salinity impacts from desalination in the Arabian/Persian Gulf. *Sci. Rep.* 12, 12. doi: 10.1038/s41598-022-25167-5

Pérez-Díaz, B., Castanedo, S., Palomar, P., Henno, F., and Wood, M. (2019). Modeling nonconfined density currents using 3D hydrodynamic models. *J. Hydraulic Eng.* 145, 19. doi: 10.1061/(asce)hy.1943-7900.0001563

Purnalna, A., Al-Barwani, H., and Al-Lawatia, M. (2003). Modeling dispersion of brine waste discharges from a coastal desalination plant. *Desalination* 155, 41–47. doi: 10.1016/S0011-9164(03)00237-6

Purnama, A., and Al-Barwani, H. (2006). Spreading of brine waste discharges into the Gulf of Oman. *Desalination* 195, 26–31. doi: 10.1016/j.desal.2005.09.036

Ruso, Y. D. P., De La Ossa Carretero, J. A., Casalduero, F. G., and Lizaso, J. S. (2007). Spatial and temporal changes in infaunal communities inhabiting soft-bottoms affected by brine discharge. *Mar. Environ. Res.* 64, 492–503. doi: 10.1016/j.marenvres.2007.04.003

Sun, X. Y., Bian, H. X., Yin, C. F., Chen, J. S., and Wang, L. J. (2012). "Study on numerical simulation of concentrated brine discharged from desalination plant," *World Automation Congress 2012*, Puerto Vallarta, Mexico, pp. 1–4. doi: 10.1007/s11814-011-0201-7

Tian, R. (2019). Factors controlling saltwater intrusion across multi-time scales in estuaries, Chester River, Chesapeake Bay. *Estuar. Coast. Shelf Sci.* 223, 61–73. doi: 10.1016/j.ecss.2019.04.041

Tian, Q., Wang, Q., and Liu, Y. L. (2017). Geomorphic change in Dingzi Bay, East China since the 1950s: impacts of human activity and fluvial input. *Front. Earth Sci.* 11, 385–396. doi: 10.1007/s11707-016-0586-z

Tsiourtis, N. X. (2001). Desalination and the environment. *Desalination* 141, 223–236. doi: 10.1016/S0011-9164(01)85001-3

Uncles, R. J., and Stephens, J. A. (2011). The effects of wind, runoff and tides on salinity in a strongly tidal sub-estuary. *Estuaries Coasts* 34, 758–774. doi: 10.1007/s12237-010-9365-3

Voutchkov, N. (2009). Salinity tolerance evaluation methodology for desalination plant discharge. *Desalination Water Treat* 1, 68–74. doi: 10.5004/dwt.2009.126

Wang, G., Han, B., Wang, Y. B., Liu, J., Zheng, Y. C., Zheng, L., et al. (2023). Distribution, source, and risk assessment of polycyclic aromatic hydrocarbons (PAHs) in surface sediments from Dingzi Bay, China. *J. Sea Res.* 193, 6. doi: 10.1016/j.seares.2023.102387

Wang, X., Liu, X., Liang, S., and Shi, X. (2009). The effect of brine discharged from desalination plant on the distribution of the salinity in the Jiaozhou Bay. *Acta Oceanologica Sin.* 31, 44–51. doi: 10.3321/j.issn:0253-4193.2009.01.006

Ye, Y. Y., Chen, K. B., Zhou, Q. Q., Xiang, P., Huo, Y. L., and Lin, M. (2018). Impacts of thermal discharge on phytoplankton in daya bay. *J. Coast. Res.* 83, 135–147. doi: 10.2112/si83-022.1

Zhan, C., Liu, C. K., Shi, H. Y., Zhu, J., and Wang, H. Y. (2024). Prediction of Diffusion of Concentrated Seawater into the Sea and Evaluation of Ecological and Environmental Impacts of Seawater Desalination Project in Estuary ——A Case Study of Shandong Peninsula Dingzi Bay. Available online at: https://link.cnki.net/urlid/12.1076.p.20240523.1143.002.

Zhan, C., Yu, J. B., Wang, Q., Li, Y. Z., Zhou, D., Xing, Q. H., et al. (2017). The evolutionary process of the geomorphology of tidal embayments in southern Jiaodong Peninsula, China. *Estuar. Coast. Shelf Sci.* 194, 182–191. doi: 10.1016/j.ecss.2017.06.016

Zhang, L. L., Shi, H. Y., Xing, H., Li, P. P., and Ma, P. C. (2023). Analysis of the evolution of the Yellow River Delta coastline and the response of the tidal current field. *Front. Mar. Sci.* 10. doi: 10.3389/fmars.2023.1232060

Zhang, X. R., Shi, H. Y., Zhan, C., Zhu, J., Wang, Q., and Li, G. Q. (2023). Numerical simulation calculation of thermal discharge water diffusion in coastal nuclear power plants. *Atmosphere* 14, 19. doi: 10.3390/atmos14091371

Zheng, X., Chen, D., Wang, Q., and Zhang, Z. X. (2014). Seawater desalination in China: Retrospect and prospect. *Chem. Eng. J.* 242, 404–413. doi: 10.1016/j.cej.2013.12.104

Zhi-Guo, L., Cheng, H., and Dong-Ming, W. (2018). Empirical research on the relationship between natural gas consumption and economic growth in the Northeast Asia. *Energy Environ.* 29, 216–231. doi: 10.1177/0958305x17745273

frontiers | Frontiers in Marine Science

TYPE Original Research
PUBLISHED 21 March 2025
DOI 10.3389/fmars.2025.1564173

OPEN ACCESS

EDITED BY
Qin Zhu,
Southern Marine Science and Engineering Guangdong Laboratory, China

REVIEWED BY
Liwei Zhang,
East China Normal University, China
Wei Zhang,
Zhengzhou University, China

*CORRESPONDENCE
Qingqing Zhao
qingqingzhao@qlu.edu.cn
Jia Jia
jiajiast@126.com

RECEIVED 21 January 2025
ACCEPTED 03 March 2025
PUBLISHED 21 March 2025

CITATION
Zhao Q, Jia J, Song F, Li T, Zhang W and Huang Y (2025) Variations in the archaeal community in wetlands soils under various hydrologic conditions in the Yellow River Estuary.
Front. Mar. Sci. 12:1564173.
doi: 10.3389/fmars.2025.1564173

Variations in the archaeal community in wetlands soils under various hydrologic conditions in the Yellow River Estuary

Qingqing Zhao[1*], Jia Jia[2*], Fanyong Song[1], Tianyuan Li[1], Wen Zhang[1] and Yujie Huang[1]

[1]Shandong Provincial Key Laboratory of Applied Microbiology, Ecology Institute, Qilu University of Technology (Shandong Academy of Sciences), Ji'nan, China, [2]Henan Key Laboratory of Ecological Environment Protection and Restoration of Yellow River Basin, Yellow River Institute of Hydraulic Research, Zhengzhou, China

Unraveling the relationships between archaea and factors influencing their diversity and distribution is a critical issue in marine ecosystems. Here, the archaeal diversity and community structure in 0 - 20 cm soils from freshwater influenced wetlands (FIW), flooding freshwater and underground seawater influenced wetlands (MIW) and seawater influenced wetlands (SIW) in the Yellow River Nature Reserve were examined utilizing high-throughput sequencing of 16S rRNA gene sequencing. Based on the comparison of the alpha diversity indices, the abundance and diversity of the archaeal community in wetlands with varying hydrologic conditions did not significantly change ($p > 0.05$), with Thaumarchaeota and Marine_Group_I as the predominant archaeal phylum and class in all the three sampled sites, respectively. Thaumarchaeota, Woesearchaeota and Euryarchaeota constituted more than 90% of the total soil archaeal community in all wetlands. However, beta diversity indices revealed that significantly different distribution patterns of archaea were found among the three wetlands ($p < 0.05$). And the archaeal community structure in different wetlands varied as the hydrologic conditions changed. Less discriminated archaeal taxa were found in MIW (1 taxon) than in FIW (24 taxa) and SIW (18 taxa). Furthermore, statistical analysis confirmed that the difference in soil salinity caused by different hydrologic conditions was the major driver of archaeal community structure. Overall, this study highlights the role of hydrologic conditions in structuring the soil archaeal community in coastal wetlands.

KEYWORDS

archaea, diversity and community structure, soil salinity, hydrologic conditions, coastal wetlands

1 Introduction

As an abundant, ubiquitous and diverse community, archaea on the earth widely inhabit not only the terrestrial and marine ecosystems, but also the gut systems of insects or termites (Pfeifer et al., 2021). The archaeal lineages featured with thermophility and/or halophilism can survive in extreme environments with harsh salinity, acidity, alkalinity, and temperature conditions (Naitam et al., 2023; Saavedra-Bouza et al., 2023). Because they can withstand harsh conditions, archaea make up the third domain of life, different from bacteria and eukaryotes (Meng et al., 2022). Archaea are ecologically important and essentially involve in various biogeochemical processes, playing a vital role in global elements (i.e. carbon, nitrogen, sulfur, iron) cycles and energy flow (Baker et al., 2020). For instance, archaea in the phylum Thaumarchaeota are representatives of ammonium oxidizers, while methanogenic archaea (methanogens) are renowned for producing methane after energy metabolism and their influence on global climate changes. Both Thaumarchaeota and methanogens constitute important links of food webs in anaerobic and marine environments (Pfeifer et al., 2021). Besides, archaea hold great promise for a wide range of biotechnological uses, since thy can produce active enzymes those can that withstand challenging industrial settings and additional bioproducts such as lipids (Saavedra-Bouza et al., 2023). Moreover, archaea are also reported to potentially degrade hydrocarbons and dissolved proteins, remediate metals, perform dehalogenation reaction, drain acid mine (Lazar et al., 2016; Krzmarzick et al., 2018). And some archaea can be used as bioremediators for appropriate waste treatment, as well as a feed supplement for growth promotion and disease control (Jifiriya et al., 2023). Thus, the community composition of archaea profoundly affects biogeochemical processes. Moreover, information pertaining to the composition of the archaeal community structure and its dynamic diversity holds significant importance. This information not only contributes substantially to the in - depth understanding of the microbial ecology of wetlands and the refinement of global climate change modeling, but also serves as an indicator of environmental stress and ecosystem changes occurring within wetland soils (Chambers et al., 2016; Cheung et al., 2018). Considering the role of wetlands in the global carbon cycling and the microbial control of wetlands' functions and services (Wu et al., 2021), understanding both the community structure and diversity of archaea and associated influencing factors in wetlands is imperative.

As an essential element of the sedimentary ecosystems, archaea have a high diverse population in estuaries (Zou et al., 2020a). The ecological functions of estuaries largely depend on the composition of microbes (Xie et al., 2014). And the biogeochemical processes in marine sediments are profoundly affected by the structure and metabolic activities of microbes (Wang et al., 2020a). For example, wetland microbial communities act as key determinants in controlling both the production and release of greenhouse gases (Maietta et al., 2020). The composition and dynamics of microbial populations also serve as critical biomarkers for assessing ecosystem health in estuarine environments (Wang et al., 2025). Thus the investigation of potential drivers of archaeal community is necessary to understand the possible changes in ecological services provided by estuaries. Besides, estuaries connect the land and ocean, exhibiting distinct gradient changes of soil physiochemical properties due to the variations in freshwater inputs, tidal heights and geomorphologic changes along the mouth of the estuaries (Webster et al., 2015; Zou et al., 2020b). The hydrology in estuarine wetlands not only determines basic structures and ecological functions, but also controls physicochemical conditions such as soil salinity due to interactions among tidal flooding, precipitation induced runoff, groundwater flow, and evapotranspiration processes (Zedler, 2000; White and Madsen, 2016; Zhao et al., 2023). The variability of hydrologic conditions affects the community structure of soil and methane cycling microbes and the gene abundances of both ammonia-oxidizing archaea and ammonia-oxidizing bacteria (Liu et al., 2021; Maietta et al., 2020). However, the impact of hydrologic variability on microbial community composition was differently presented by several researches (Peralta et al., 2014; Maietta et al., 2020). Moreover, how archaeal communities respond to salinization caused by salt water intrusion, especially how the shifts of methanogenic archaea affect the global greenhouse gas budget, still exists as uncertainty (Wen et al., 2017). Despite the fact that salinity has been documented as a primary determinant of the archaeal community composition, there remains a lack of consensus regarding the impacts of salinity on archaea. Some researchers found that rising salinity could increase the abundance and diversity of archaeal community (Liu et al., 2016; Wei et al., 2020), while Webster et al. (2015) reported that the diversity of archaea decreased as salinity increased. Furthermore, Chambers et al. (2016) found that the increased inundation frequency played a more decisive role than salinity in determining microbial community structure of brackish soil more strongly. The sea level rise and the intensified global climate warming could introduce seawater high up to the estuaries, which inevitably causes changes of wetland hydrology (i.e. water table and flooding duration) and soil salinity (Chambers et al., 2016). Thus, the response of estuarine archaea to various hydrologic conditions needs further investigation.

Here, to clarify variations in the diversity and community structure of soil archaea in wetlands under various hydrologic conditions, we collected soil samples of 0 - 20 cm depth in wetlands affected by freshwater influenced wetlands (FIW), flooding freshwater and underground seawater influenced wetlands (MIW) and seawater influenced wetlands (SIW). The inundation frequency in the three sampling sites ranked in the order SIW > FIW > MIW. The study aims at: (1) identifying the distribution pattern of soil archaea in wetlands under various hydrologic conditions and (2) clarifying the effects of hydrologic conditions on the archaeal community composition and diversity of archaea in coastal wetlands. Overall, this study will provide information for the management of coastal wetlands.

2 Materials and methods

2.1 Study area, soil collection and soil physicochemical analysis

The study area is located in the Yellow River Nature Reserve, and the selected sampling sites (FIW, MIW and SIW), soil collection (0 - 20 cm depth) for the measurements of soil physicochemical properties and the corresponding analysis have been previous described in the previous researches (Zhao et al., 2020a, b). Soil EC, Na^+, K^+, Mg^{2+}, Cl^- and SO_4^{2-} increased and soil moisture decreased as the influence of tides intensified and reached the highest level in SIW along the sampling belt (FIW-MIW-SIW) (Zhao et al., 2020b). Thus, FIW, MIW and SIW were also defined as low salinity wetlands, medium salinity wetlands and high salinity wetlands, respectively. Their dominant plants are *Phragmites australis*, *P. australis* and *Suaeda salsa*. And the comparison of other soil properties among three wetlands can also be found in the previous research (Zhao et al., 2020b). Soil samples designated for 16S rRNA sequencing were initially positioned in an ice - cooled box. Subsequently, they were dispatched to Majorbio Bio - pharm Technology Co., Ltd. (Shanghai, China) to undergo further sequencing procedures. In addition, Majorbio was also responsible for conducting the data processing.

2.2 DNA extraction, 16S rRNA gene amplification, and sequencing

Genomic DNA was extracted from about 0.5 g of each sample's soil using the soil DNA kit (Omega Bio-tek, Norcross, GA, U.S.). PCR amplification (ABI GeneAmp® 9700) of the V4-V5 region of the 16S rRNA gene was conducted using TransGen AP221-02 (TransStart Fastpfu DNA Polymerase) to analyze archeal community. The forward primer 515F (5′-GTGCCAGCM GCCGCGG-3′) and the reverse primer 915R (5′-GTGCTCCCC CGCCAATTCCT-3′) was used with the following protocol: 95°C for 2 min, 25 cycles of denaturation (95°C; 30 s), annealing (55°C; 30 s), and extension (72°C; 60 s) and a final elongation (72°C; 10 min). The amplified DNA was quantified with a TBS-380 fluorometer (Promega Corporation, CA, USA) after purification using the AxyPrep DNA Gel Extraction Kit (Axygen Biosciences, Union City, CA, USA). Then barcoded pyrosequencing of the 16S rRNA gene was performed on an Illumina MiSeq PE250 system. The sequencing data was deposited in the NCBI database under the accession number SRP099022.

2.3 Analysis of sequencing-derived data

The primers were excluded after alignment and sequences with a length shorter than 200 bp or low quality were removed. Valid sequences were defined as seeds with complete sequence barcodes, and were further classified using Mothur software (http://www.mothur.org) and aligned via the Silva bacterial reference database (http://www.arb-silva.de). The number of operational taxonomic units (OTUs) in all samples was defined at Usearch (version 7.1, http://drive5.com/uparse/) with sequence similarity of 97%. Species classification information represented by each OTU was obtained by RDP Classifier Bayes algorithm (version 2.2 http://sourceforge.net/projects/rdp-classifier/) on the Qiime platform (version 2.2 http://sourceforge.net/projects/rdp-classifier/). The alpha diversity indices determined in this study included the Coverage index, the observed species (Sobs), the richness indices (the abundance-based coverage estimator (ACE) and bias-corrected Chao1 richness estimator), the Shannon diversity index, the community evenness index (Shannoneveness) and Faith's phylogenetic diversity (PD) index. Within Mothur, they were calculated to examine the sequencing depth, richness and diversity of the archaeal community, respectively. The beta diversity indices, such as principal coordinate analysis (PCoA) and Non-MetricMulti-Dimensional Scaling (NMDS), were determined to evaluate the difference in distribution pattern of archaeal community among the three wetlands. PCoA identifies potential principal components affecting archaeal community through reducing dimensions and was drawn based on the selected distance matrix. NMDS spatially exhibits the dissimilarities among different species and are often used when the accurate similarities or dissimilarities among research objects are hardly obtained.

2.4 Statistical analysis

One-way ANOVA analysis was used to identify the significant differences in archeal community richness and diversity, and in soil properties among three wetlands. Differences were considered to be significant if $p < 0.05$. Both one-way ANOVA and Pearson correlation analysis between soil properties and the alpha-diversity indices were performed using SPSS v22.0 (SPSS Inc.). The analysis of similarity (ANOSIM) and Adonis test were conducted based on the Bray-Curtis dissimilarity matrix to test significant differences in archaeal community among three wetlands. Additionally, Spearman correlation analysis and Mantel test between archaeal community and environmental factors were performed to identify environmental variables those influenced archaeal community composition. The ANOSIM, Adonis test, Spearman correlation analysis and Mantel test were conducted on the cloud platform of Majorbio Group.

3 Results

3.1 Alpha and beta diversity metrics of soil archaea in three wetlands

The number of OTUs generated from high-quality sequences was the least in the MIW (1100), and higher in the FIW (2014) and SIW (1902) (Supplementary Figure S1). The number of specific OTUs in FIW, MIW and SIW were 1498, 313 and 1120, respectively. And the

shared OTUs' number of three wetlands was 169. The comparison of alpha diversity indices of archaea is shown in Table 1. The values of Coverage index for soil archaeal community were higher than 99% in all sampling sites, implying the sequencing depth could reflect the archaeal community in the three wetlands. More than 400 archaeal species were found in each of the three wetlands, but the number of archaeal species did no significantly differ among the three wetlands ($p > 0.05$), as revealed by the Sobs vales. Additionally, the richness indices (ACE and Chao1), the diversity index (Shannon), the Shannoneveness index and PD index showed no significant differences among FIW, MIW and SIW ($p > 0.05$). In sum, no significant difference in alpha diversity was observed among three types of wetlands ($p > 0.05$). Statistically, the values of Sobs, ACE, Chao1, Shannon and PD indices were generally lower in MIW than in FIW and SIW.

PCoA and NMDS based on Bray-Curtis distance matrices were performed to identify the relationships among the samples with respect to archaeal community composition, as shown in Figures 1a, b, respectively. In the PCoA and NMDS plots, samples in the FIW, MIW and SIW can be clearly separated, indicating that the distribution patterns of archaea community in the three wetlands were significantly different ($p < 0.05$). The ANOSIM and Adonis test further verified that archaeal community among FIW, MIW and SIW was significantly dissimilar ($p < 0.01$) (Supplementary Tables S1, S2).

3.2 Community structure of soil archaea in three wetlands

Community structure of archaea at the phylum and class level in the three wetlands is shown in the Circos plots of Figures 2a, b, respectively. The left half circle (small semicircle) indicates the taxonomic composition of soil fungal communities of each group. The outer green, blue and red ribbon represents SIW, MIW and FIW, respectively. Different colors of the inner ribbon characterize different archaeal species at phylum or class level, and the length of the inner ribbon reflects the relative abundance of corresponding archaeal phyla or class. The right half circle (large semicircle) indicates the proportions of the archaea at phylum or class level in different wetlands. Specifically, the outer ribbon shows archaea taxa and the different colors of the inner ribbon represent different wetlands. And length of the inner colored ribbon represents the relative abundance of the certain archea in different wetlands. Symbols p1 - p7 and c1 - c13 represents archeal phyla and class as below: p1: Thaumarchaeota, p2: Woesearchaeota, p3: Euryarchaeota, p4: Bathyarchaeota, p5: others, p6: Aenigmaarchaeota, p7: Miscellaneous_Euryarchaeotic_Group_MEG. C1: Marine_Group_I, c2: norank_p:Woesearchaeota, c3: Thermoplasmata, c4: Halobacteria, c5: Soil_Crenarchaeotic_Group_SCG_incetae_sedis, c6: unclutured_p_Thaumarchaeota, c7: norank_p_Bathyarchaeota, c8: others, c9: Deep_Sea_Euryarchaeotic_Group_DSEG_norank, c10: Methanomicrobia, c11: South_African_Gold_Mine_Gp_1_SAGMCG_1, c12: norank_p_Miscellaneous_Euryarchaeotic_Group_MEG_, c13: Group_C3. The sequencing of 16S rRNA gene amplicons from the soils in the FIW averagely generated 56732 ± 9832 high-quality reads per sample (Supplementary Table S3). These sequences were categorized into 6 archaeal phyla. The archaeal sequences in the FIW were mainly composed of Thaumarchaeota (58.83%), Woesearchaeota (19.76%), Euryarchaeota (11.54%), Bathyarchaeota (5.72%), Aenigmaarchaeota (0.55%) and Miscellaneous_Euryarchaeotic_Group_MEG (1.21%) (Figure 2a). At the class level, a total of 6 archaeal classes were recognized (Figure 3b). Marine_Group_I represented 38.63% of the total archaeal community and was the most abundant archaeal class in the FIW, followed by Soil_Crenarchaeotic_Group_SCG_incetae_sedis (11.80%). The rest identified archaeal classes were Thermoplasmata (8.65%), Methanomicrobia (2.50%), South_African_Gold_Mine_Gp_1_SAGMCG_1 (2.27%) and Group_C3 (1.07%) (Figure 2b).

An average of 53683 ± 11291 sequences per sample was yielded through 16S rRNA sequencing in the MIW (Supplementary Table S3). Among the 6 archaeal phyla, the relative abundance of Thaumarchaeota ranked the highest with the percentage of 62.19%, and the relative abundance of Woesearchaeota (20.62%) and Euryarchaeota (14.74%) followed by as the second and the third, respectively. However, the relative abundance of Bathyarchaeota (0.10%), Aenigmaarchaeota (1.93%) and Miscellaneous_Euryarchaeotic_Group_MEG (0.01%) was quite lower (Figure 2a). At the class level, archaeal community in the MIW was mostly represented by Marine_Group_I (56.49%), Thermoplasmata (14.61%) and Soil_Crenarchaeotic_Group_SCG_incetae_sedis (3.54%) (Figure 2b).

TABLE 1 Alpha diversity metrics of archaea obtained at 97% sequence similarity.

	FIW	MIW	SIW
Coverage (%)	99.42 ± 0.53	99.79 ± 0.10	99.76 ± 0.11
Sobs	486.83 ± 230.37[a]	441.33 ± 155.02[a]	530.25 ± 131.72[a]
ACE	574.84 ± 266.41[a]	490.96 ± 179.88[a]	606.78 ± 170.45[a]
Chao1	569.32 ± 264.77[a]	492.58 ± 179.08[a]	610.38 ± 170.83[a]
Shannon	3.57 ± 0.89[a]	3.56 ± 0.20[a]	3.68 ± 0.64[a]
Shannoneveness	0.58 ± 0.13[a]	0.60 ± 0.05[a]	0.59 ± 0.10[a]
Phylogenetic diversity	42.81 ± 14.68[a]	38.29 ± 9.97[a]	40.68 ± 6.90[a]

[ab]Different letters represent significant differences ($p < 0.05$) between sampling sites.

10.3389/fmars.2025.1564173

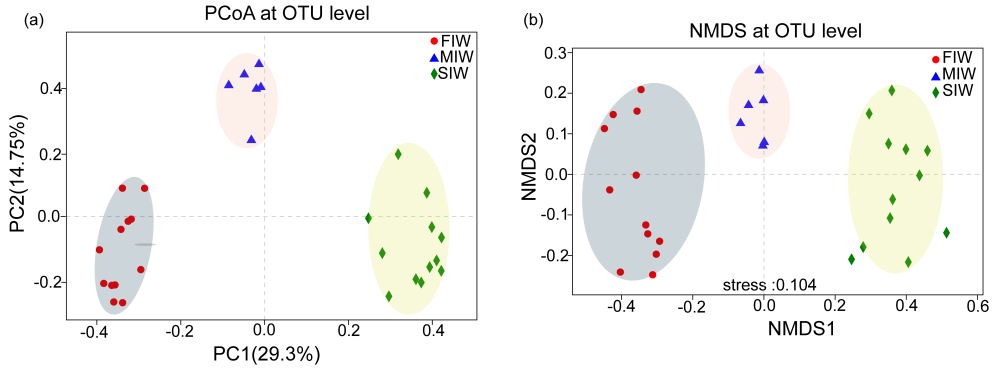

FIGURE 1
PCoA **(a)** and NMDS **(b)** plots of the archaeal communities in wetlands under various hydrologic conditions.

Sequencing of the soils in the SIW averagely yielded 57307 ± 9826 sequences per sample (Supplementary Table S3). Similar to FIW and MIW, Thaumarchaeota (42.92%), Woesearchaeota (30.64%) and Euryarchaeota (24.30%) occupied much higher proportions than Bathyarchaeota (0.35%), Aenigmaarchaeota (0.58%) and Miscellaneous_Euryarchaeotic_Group_MEG (0.04%) (Figure 2a). At the class level, Marine_Group_I (41.09%), Thermoplasmata (6.83%), Halobacteria (17.35%) and Soil_Crenarchaeotic_Group_SCG_incetae_sedis (1.79%) largely represented the archaeal community in the SIW (Figure 2b).

Generally, Thaumarchaeota, Woesearchaeota and Euryarchaeota represented higher than 90% of the total archaeal community in the soils of all three wetlands. An obviously increasing trend was observed in the relative abundance of Woesearchaeota and Euryarchaeota as soil salinity increased, while the relative abundance of Bathyarchaeota and Miscellaneous_Euryarchaeotic_Group_MEG decreased with increasing soil salinity. Thaumarchaeota and Aenigmaarchaeota are more abundant in MIW than in FIW and SIW. Marine_Group_I absolutely dominated the archaeal community in all three wetlands, showing a general increasing trend as salinity increased. The relative abundance of Thermoplasmata is highest in MIW than in FIW and SIW, showing an initial increasing then decreasing tend. The relative abundance of Halobacteria increased with increasing salinity, while Methanomicrobia, South_African_Gold_Mine_Gp_1_SAGMCG_1, Group_C3 and Soil_Crenarchaeotic_Group_SCG_incetae_sedis showed an absolutely decreasing tend as salinity increased. As for Thermoplasmata, the peak value of its relative abundance was observed in MIW, showing an initial increasing then decreasing tend.

The community composition of archaea at the order, family, genus and species level are shown in Figures 3a–d, respectively. As shown in Figure 3, three order (Thermoplasmatales, Halobacteriales and Methanosarcinales), three family (Halobacteriaceae, Marine_Group_II and ASC21), five genus (Candidatus_Nitrosopumilus, Candidatus_Nitrosoarchaeum, Candidatus_Nitrosopelagicus, Halogranum and Candidatus_Nitrososphaera), and two species (Halogranum_gelatinilyticum and Thaumarchaeota_archaeon_MY2) were recognized. All the recognized archaeal taxa only occupied a small proportion. Generally, the relative abundance of

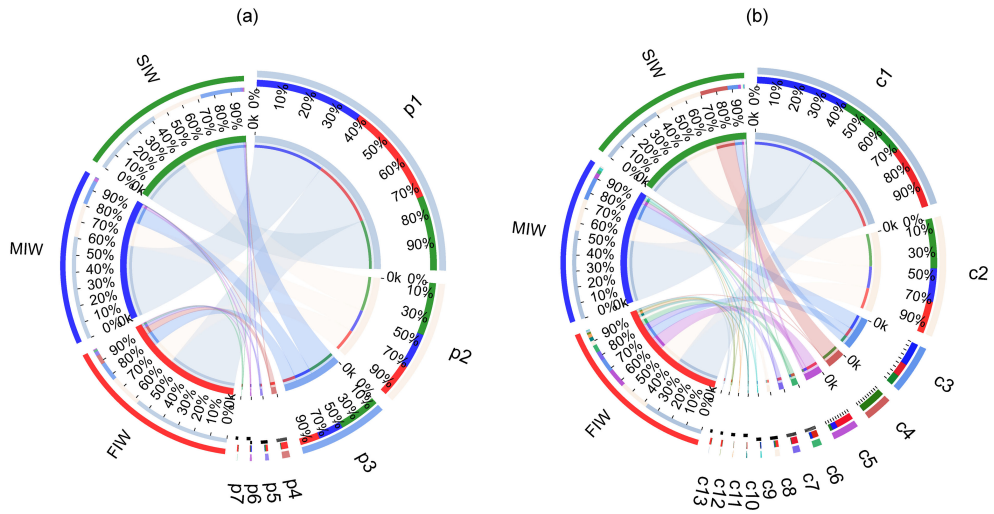

FIGURE 2
Circos plots for the community composition at the phylum **(a)** and class **(b)** levels in wetlands under various hydrologic conditions.

10.3389/fmars.2025.1564173

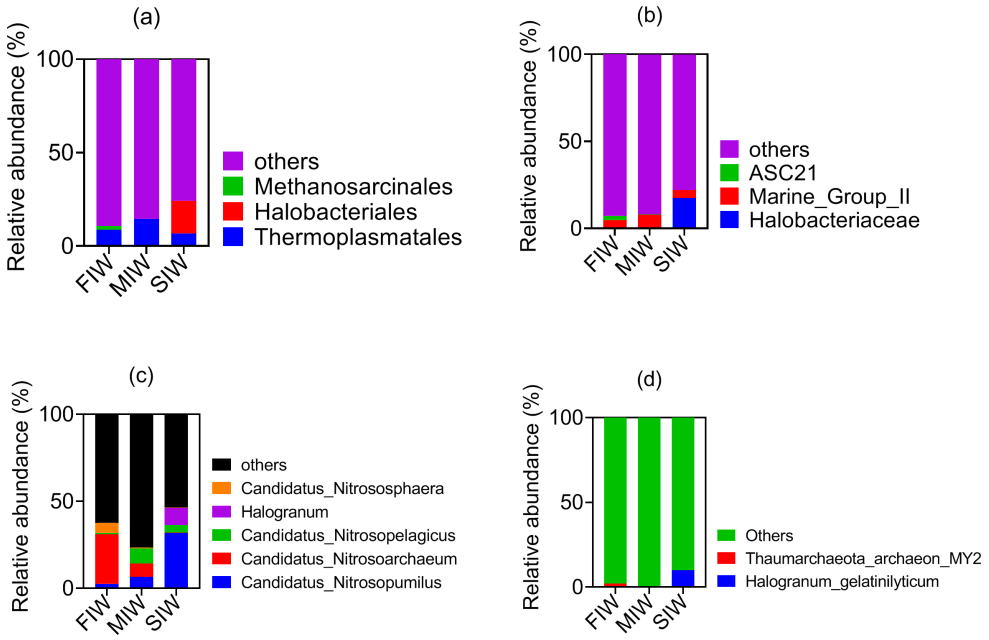

FIGURE 3
Community structure of archaea at the order **(a)**, family **(b)**, genus **(c)**, and species **(d)** levels in wetlands under various hydrologic conditions.

Halobacteriales, Halobacteriaceae, Candidatus_Nitrosopumilus, *Halogranum* and *Halogranum_gelatinilyticum* increased as salinity increased, while the relative abundance of Methanosarcinales, ASC21, *Candidatus_Nitrosoarchaeum*, *Candidatus_Nitrososphaera* and *Thaumarchaeota_archaeon_MY2* decreased with increasing salinity. As for Thermoplasmatales, Marine_Group_II and *Candidatus_Nitrosopelagicus*, the peak value of their relative abundance occurred in MIW.

3.3 Discriminated archaeal taxa among the wetlands under various hydrologic conditions

Discriminated archaeal taxa significantly affected the difference between groups are revealed by Linear Discriminant Analysis (LDA) effect size (LEfSe) in Figure 4 (norank, unclassified archaeal taxa and those with relative abundance < 1% were not shown in Figure 4). The all-against-all strategy was adopted in the recognition of discriminated archaeal taxa, which is more strict than one-against-all strategy. Totally, FIW, MIW and SIW had 14, 1 and 18 significantly enriched archaeal taxa, respectively ($p < 0.05$). Notably, Thaumarchaeota was the only taxa that had significantly higher relative abundance of in the soils of MIW than in FIW and SIW ($p < 0.05$). At the phylum level, Miscellaneous_Euryarchaeotic_Group_MEG_, Bathyarchaeota, Marine_Benthic_Group_E, Aenigmarchaeota_Incertae_Sedis, Methanomicrobia and the order (Methanomicrobiales), the families (Methanoregulaceae, Methanocorpusculaceae, GOM_Arc_I, Methanosarcinaceae, and Methanosaetaceae), the genra (Methanosaeta, Methanosarcina, Candidatus_Methanoperedens, Methanoregula, Methanobacterium, Methanocorpusculum, Methanosphaerula) belonging to this class, Soil_Crenarchaeotic_Group_SCG_, South_African_Gold_Mine_Gp_1_SAGMCG_1_, Terrestrial_Miscellaneous_Gp_TMEG_, ASC21 and CCA47 were significantly enriched in FIW ($p < 0.05$), while Halobacteria, the order (Halobacteriales), the family (Halobacteriaceae) and the genra (Halogranum, Halorussus, Natronomonas, Halomicroarcula, Halorubellus, Halomarina, Haloarcula, Halorientalis, Haloplanus, Halarchaeum, Haloferax, Salinigranum, Haloarchaeobius, Halolamina, Halogeometricum) belonging to this class were significantly enriched in the soils of SIW ($p < 0.05$).

3.4 Environmental variables that structure the archaeal community

The mantel test between soil archaea and soil physiochemical properties at the OTU, phylum and class level is shown in Table 2. At the OTU level, DOC, pH and BD significantly influences soil archaeal community structure ($p < 0.05$). DOC, TN, BD, clay and Ca^{2+} positively affected the relative abundance of archaeal phyla ($p < 0.05$), but silt negatively affected the archaeal community structure at the phylum level ($p < 0.05$). DOC, TN and pH showed a positively significant relationship with archaeal community structure at the class level ($p < 0.05$), and SOC and silt showed a negatively significant relationship with archaeal community structure ($p < 0.05$).

As shown in Figure 5, soil properties except for pH and BD affected the archaeal community structure at both phylum (Figure 5a) and class (Figure 5b) levels. Specifically, soil salinity parameters including EC, Na^+, K^+, Mg^{2+}, Ca^{2+}, Cl^- and SO_4^{2-} significantly and positively influenced the relative abundance of Diapherotrites,

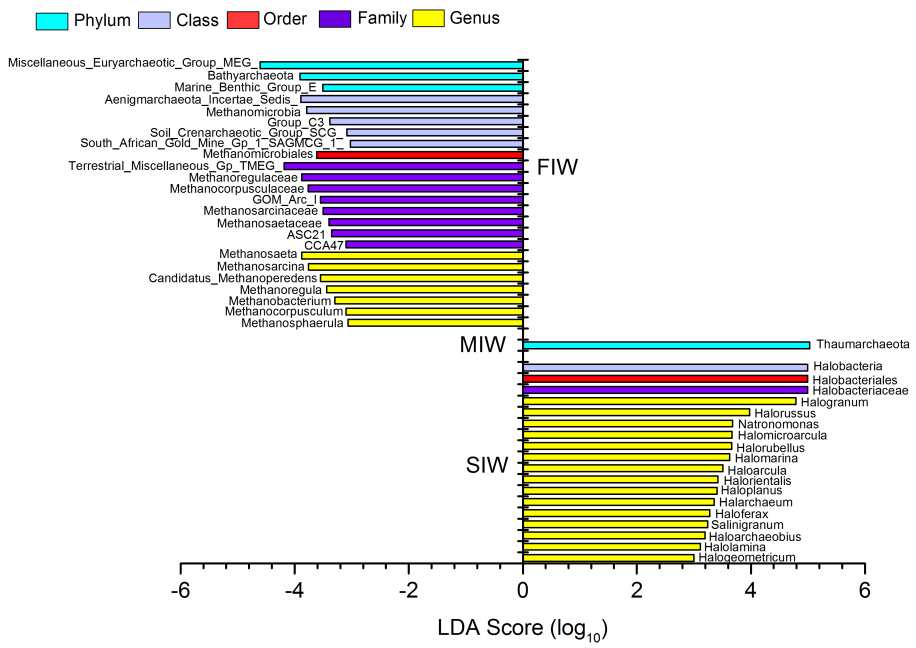

FIGURE 4
Archaeal taxa with Linear discriminant analysis (LDA) score greater than 3 present in wetlands under various hydrologic conditions.

Euryarchaeota, Nanohaloarchaeota, Woesearchaeota, Deep_Sea_Euryarchaeotic_Group_DSEG_, Diapherotrites_Incertae_Sedis_ and Halobacteria ($p < 0.05$), but negatively and significantly influenced the relative abundance of Altiarchaeales, Bathyarchaeota, Candidate_division_YNPFFA, Hadesarchaea, Lokiarchaeota, Marine_Benthic_Group_E, Miscellaneous_Euryarchaeotic_Group_MEG_, Parvarchaeota, Group_C3, Methanobacteria, Methanomicrobia, Soil_Crenarchaeotic_Group_SCG_, South_African_Gold_Mine_Gp_1_SAGMCG-1_ and WCHA1-57 ($p < 0.05$). Moreover, Supplementary Table S4 shows the correlation relationships between alpha diversity indices and soil properties, which indicates that the alpha diversity indices of archaeal community were not significantly affected by soil properties ($p > 0.05$).

4 Discussion

4.1 The effects of hydrologic conditions on richness and diversity of archaeal community

The redox gradients caused by hydrologic variations result in the difference in the abundance and composition of archaeal community (Maietta et al., 2020; Wang et al., 2020a). It has been reported that the members of Marine Group I were more enriched in aerobic environments, while Woesearchaeota and Bathyarchaeota were generally found in the oxygen depleted zones (Wang et al., 2020a). The different hydrologic conditions created the significant difference in some soil properties besides soil salinity in 0 - 20 cm soils of the three wetlands, as presented in our previous work (Zhao et al., 2020a; Zhao et al., 2020b). Specifically, soil SOC was significantly higher in FIW than in MIW, while pH showed a significantly higher value in SIW than in MIW. Soil silt content was significantly lower in MIW than in FIW and SIW, while soil sand content showed an opposite trend. Previous researches showed that salinity differently affected the diversity of archaea in various environments. For example, Webster et al. (2015) found that the abundance of archaeal community was higher in brackish sediments with low salinity than in the high-salinity marine sediments. Liu et al. (2016) found that the archaeal diversity increased with salinity in Tibetan Plateau lake sediments. Wei et al. (2020) reported that archaeal diversity increased with rising salinity in soils covered with wheat, cotton, paddy, wild plant *Suaeda salsa* and barren fields without any plants. In this study, both the abundance and diversity of archaea showed no significant differences among soils with low, medium and high salinity ($p > 0.05$) and also were not significantly affected by soil properties ($p > 0.05$). Similar results were found by Zou et al. (2020b) in surface sediments of the Pearl River, which showed that no significant differences of archeal diversity index were found in sample groups with different salinity, and no strong correlations between the 16S rRNA gene abundance of archaea and the parameters investigated were observed.

4.2 The effects of hydrologic conditions on archaeal community structure in three wetlands

Maietta et al. (2020) presented that soil microbial composition in inundated or saturated soils (more than 50% of the year) were quitely different from soils that were rarely flooded, which is consistent with this current study. Chen et al. (2022) found that

10.3389/fmars.2025.1564173

TABLE 2 The mantel test between archaeal community and soil properties (at the OTU, phylum and class level).

	R (OTU)	R (phylum)	R (class)
SOC	0.17	-0.08	-0.02*
MBC	0.09	0.10	0.08
ROOC	0.105	-0.03	-0.05
DOC	0.04*	0.00**	0.00**
TN	0.07	0.04*	0.03*
C/N ratio	0.12	0.09	0.03*
pH	-0.01*	0.05	0.03*
BD	0.00**	0.01*	0.12
moisture	0.22	0.08	0.14
clay	0.24	0.02*	0.05
silt	0.08	-0.03*	-0.02*
sand	0.12	0.11	0.13
EC	0.78	0.16	0.30
Na^+	0.78	0.16	0.28
K^+	0.59	0.18	0.29
Mg^{2+}	0.62	0.14	0.23
Ca^{2+}	0.37	0.00**	0.08
Cl^-	0.76	0.19	0.32
SO_4^{2-}	0.55	0.09	0.20

*and **represent the significant difference at $p < 0.05$ and $p < 0.01$ level, respectively.

tide-driven hydrodynamic disturbance control the composition of microbial community. It was concluded that the different hydrologic conditions in three wetlands resulted in the varying archaeal community structure in this study. Furthermore, the variations in plant species caused by different hydrologic conditions can lead to differences in the archaeal community (Gao et al., 2024). Except for the direct influence of hydrologic conditions on soil archeal community, the indirect effects of hydrologic conditions which are mainly fulfilled though influencing soil properties should also be highlighted. Numerous researches have reported that soil physiochemical properties largely determined the community structure of archaea, especially soil salinity, which played a dominant role in shaping the composition of archaea (Xie et al., 2014; Zhang et al., 2015; Liu et al., 2017; Wei et al., 2020; Zou et al., 2020a, b). Although no apparent effects of salinity on the abundance and diversity of archaea, the community structure of archaea was significantly affected by salinity as revealed by spearman correlation analysis (Figure 5). LEfSe analysis showed that archaea distributed in the phyla including Aenigmarchaeota, Bathyarchaeota, Euryarchaeota, Halobacterota, Marine_Benthic_Group_E, Miscellaneous_Euryarchaeotic_Group_MEG_ and Thaumarchaeota showed significant differences among FIW, MIW and SIW ($p < 0.05$).

Bathyarchaeota essentially involve in the global carbon cycle due to their utilization of various organic substrates, capacity of methane metabolism and carbon fixation (Zou et al., 2020a; Liang et al., 2023). Additionally, some members of Bathyarchaeota were reported to potentially participate in nitrogen and sulfur metabolism (Chen et al., 2020).The relative abundance of Bathyarchaeota was positively and significantly correlated with SOC (Figure 5), which is also reported by Ma et al. (2016) and Zou et al. (2020a). Besides, consistent with other studies (Chen et al., 2020; Zou et al., 2020a), salinity posed significantly negative effects on the relative abundance of Bathyarchaeota in the current study ($p < 0.05$, Figure 5). Soil texture has been proved to affect the distribution of microbes (Maier and Pepper, 2009), and modulate the influence of response biochemical quality of organic inputs on ammonia-oxidizing bacterial and archaeal communities (Muema et al., 2016). The relative abundance of Bathyarchaeota was significantly and positively related with clay and silt contents and soil moisture (WC) ($p < 0.01$), but showed significantly negative relationship with sand content ($p < 0.01$). Thus, the significantly higher SOC content and silt content, and lower salinity and sand content in soils of FIW than in MIW and SIW ($p < 0.05$, Zhao et al., 2020b) contributed to the significantly higher relative abundance of Bathyarchaeota in FIW. Similar to Bathyarchaeota, members of Miscellaneous_Euryarchaeotic_Group_MEG_ and Marine Benthic_Group_E (recently named Candidatus Hydrothermarchaeota) were more enriched in soils of FIW due to the positive effects of higher SOC content and lower salinity in FIW than in MIW and SIW ($p < 0.05$, Figure 5).

Euryarchaeota not only essentially involve in the global carbon cycling through methane production, anaerobic methane oxidation, the transformation of hydrocarbons, but also involve in the sulfur, nitrogen and iron cycling (Baker et al., 2020). 17 species of Euryarchaeota identified by LEfSe analysis were more enriched in soils of FIW than in soils of MIW and SIW in this study, distributing in three classes: Thermoplasmata (3 families), Methanomicrobia (14 taxa) and Methanobacteria (1 family). Thermoplasmata, Methanomicrobia and Methanobacteria comprise methanogens and essentially involve in methane production. The relative abundance of Euryarchaeota, Methanomicrobia and Methanobacteria were significantly and negatively affected by salinity ($p < 0.05$, Figure 5), thereby showing significantly higher values in FIW than in MIW and SIW ($p < 0.05$).

As a ubiquitous archaeal phylum in water and soil/sediment environments, Thaumarchaeota represent a large prokaryotic biomass involved in nitrification process (Webster et al., 2015) and have been reported to obviously predominate in the freshwater wetlands in the Yangtze estuary (Liu et al., 2017), in sediments of the Pearl River Estuary (Wang et al., 2020a) and estuary water of Chesapeake Bay, United States (Wang et al., 2020b). Webster et al. (2015) found that salinity importantly impacted distribution and composition of Thaumarchaeota. Yang et al. (2018) reported that the Thaumarchaeota populations in lake sediments were not significantly influenced by salinity. Kuznetsova et al. (2020) revealed that the occurrence of Thaumarchaeota in the saline

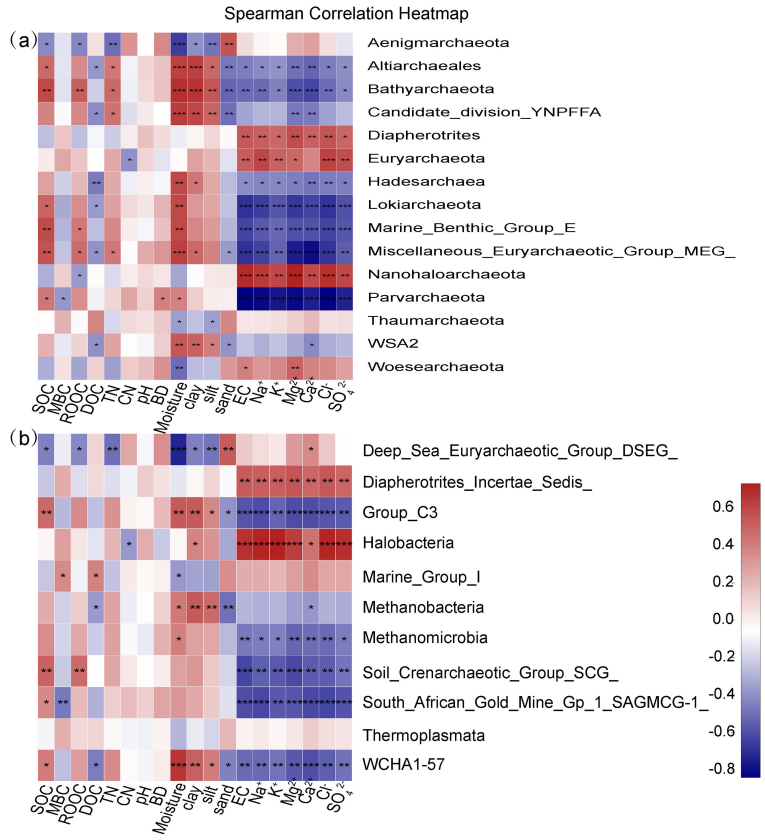

FIGURE 5
Heatmap for Spearman correlation coefficients between archaeal phyla **(a)**, class **(b)** and soil properties.

soils in the Lake Elton area was driven by both salinity and pH. In this current study, Thaumarchaeota was also found to be the dominant archaea in all the three wetlands. However, the relative abundance of Thaumarchaeota was only negatively and significantly correlated with soil WC and silt content instead of soil salinity ($p < 0.05$, Figure 5a). The significantly lower soil moisture in soils of MIW than in FIW and lower slit content in MIW than in FIW and SIW explained why Thaumarchaeota was significantly enriched in MIW. Consistently, an estuarine sediment-seawater microcosm experiment confirmed that AOA showed the most abundant and the highest transcriptional activity under moderate salinity (Zhang et al., 2015). The differences in salinity range of such different environments might contribute to the different effects of salinity on the relative abundance of Thaumarchaeota. Besides, three classes (Group_C3, Soil_Crenarchaeotic_Group_SCG_ and South_African_Gold_Mine_Gp_1_SAGMCG-1_) belonging to Thaumarchaeota showed significantly higher relative abundance in soils of FIW than MIW and SIW. Thus, the methane emissions in FIW and ammonia oxidation in MIW would be affected in the scenario of seawater intrusion caused by sea level rise.

The class Halobacteria and 17 archaeal species belonging to Halobacteria were significantly enriched in the soils of SIW and all belong to the phylum Halobacterota. Members in the phylum Halobacterota can survive in environments with high salinity due to their high tolerance to salt (Xiao et al., 2021), showing a positively significant relationship with salinity ($p < 0.05$, Figure 5). Haloarchaea naturally inhabit and thrive under saline and hypersaline conditions (Torregrosa-Crespo et al., 2018; Naitam et al., 2023) and the high salinity in soils of SIW provided suitable habitats for archaea belonging to Halobacteria. Some members of *Haloarcula* and *Haloferax* were recognized as denitrifiers, contributing significantly to NO and N_2O emissions and consequently contributing to ozone depletion and climate change (Torregrosa-Crespo et al., 2018). Therefore, the possible increased area of salt marshes might affect the emission of greenhouse gases.

5 Conclusions

This study highlighted the changes of archaeal community in wetlands under various hydrologic conditions. The different hydrologic conditions created differences in SOC, salinity, pH, WC and silt and sand contents in coastal wetlands, which consequently affected the archaeal community. Although the abundance and diversity of archaea were not affected by hydrologic conditions, the community structure of archaea differed among coastal wetlands with various hydrologic conditions. The relative abundance of Bathyarchaeota,

Marine_Benthic_Group_E, Miscellaneous_Euryarchaeotic_Group_MEG_ and methanogens in the phylum Euryarchaeota decreased as the influence of saltwater intrusion enhanced. As representatives of ammonium oxidizers, Thaumarchaeota showed preference for soils of wetland with medium salinity, although they were detected as the dominant archaea in all sampling sites. The halophilic archaea in the class Halobacteria showed preference for high-salinity soils affected by tides. In the scenario saltwater intrusion due to sea level rise or climate change, the nitrification process and methanogenesis would be changed in coastal wetlands.

Data availability statement

The datasets presented in this study can be found in online repositories. The names of the repository/repositories and accession number(s) can be found below: https://www.ncbi.nlm.nih.gov/sra/?term=SRP099022.

Author contributions

QZ: Writing – original draft, Writing – review & editing, Formal Analysis, Investigation. JJ: Funding acquisition, Investigation, Writing – original draft, Writing – review & editing. FS: Funding acquisition, Visualization, Writing – review & editing. TL: Methodology, Software, Writing – original draft. WZ: Supervision, Validation, Writing – review & editing. YH: Project administration, Supervision, Writing – review & editing.

Funding

The author(s) declare that financial support was received for the research and/or publication of this article. This study was financially supported by National Natural Science Foundation (42207527), Major Innovative Projects in the Pilot Program for the Integration of Science, Education, and Industry of Qilu University of Technology (2024ZDZX10), and National Natural Science Foundation (U22A20615).

Conflict of interest

The authors declare that the research was conducted in the absence of any commercial or financial relationships that could be construed as a potential conflict of interest.

Generative AI statement

The author(s) declare that no Generative AI was used in the creation of this manuscript.

Publisher's note

Supplementary material

The Supplementary Material for this article can be found online at: https://www.frontiersin.org/articles/10.3389/fmars.2025.1564173/full#supplementary-material

References

Baker, B. J., De Anda, V., Seitz, K. W., Dombrowski, N., Santoro, A. E., and Lloyd, K. G. (2020). Diversity, ecology and evolution of Archaea. *Nat. Microbiol.* 5, 887–900. doi: 10.1038/s41564-020-0715-z

Chambers, L. G., Guevara, R., Boyer, J. N., Troxler, T. G., and Davis, S. E. (2016). Effects of salinity and inundation on microbial community structure and function in a mangrove peat soil. *Wetlands* 36, 361–371. doi: 10.1007/s13157-016-0745-8

Chen, Y. J., Leung, P. M., Cook, P. L. M., Wong, W. W., Hutchinson, T., Eate, V., et al. (2022). Hydrodynamic disturbance controls microbial community assembly and biogeochemical processes in coastal sediments. *ISME J.* 16, 750–763. doi: 10.1038/s41396-021-01111-9

Chen, Y., Li, S., Yu, Z., Chen, Y., Mi, T., and Zhen, Y. (2020). Characteristics of the Bathyarchaeota community in surface sediments from the southern Yellow Sea and northern East China sea. *Estuarine Coast. Shelf Sci.* 235, 106595. doi: 10.1016/j.ecss.2020.106595

Cheung, M. K., Wong, C. K., Chu, K. H., and Kwan, H. S. (2018). Community structure, dynamics and interactions of bacteria, archaea and fungi in subtropical coastal wetland sediments. *Sci. Rep.* 8, 14397. doi: 10.1038/s41598-018-32529-5

Gao, X., Wang, S., Kong, W., Li, G., Zhang, L., and Yin, X. (2024). Floristic changes and environmental drivers of soil fungi and archaea in different salt-tolerant plant communities in the intertidal habitat of coastal wetlands. *Environ. Geochem. Health* 46, 167. doi: 10.1007/s10653-024-01951-2

Jifiriya, M. J., Preena, P. G., Rejish Kumar, V. J., Nair, A. J., and Joseph, V. (2023). Role of archaea in aquaculture: prospects and challenges. *Aquacult. Int.* 32, 3169–3194. doi: 10.1007/s10499-023-01317-y

Krzmarzick, M. J., Taylor, D. K., Fu, X., and McCutchan, A. L. (2018). Diversity and niche of archaea in bioremediation. *Archaea-An Int. Microbiol. J.* 2018, 1–17. doi: 10.1155/2018/3194108

Kuznetsova, A. I., Ivanova, E. A., Samylina, O. S., Kurbanova, F. G., Gruzdev, D. S., Kanapatskiy, T. A., et al. (2020). Prokaryotic communities in saline soils of the lake Elton area in a soil catena along the Khara river. *Microbiology* 89, 670–684. doi: 10.1134/S0026261720060119

Lazar, C. S., Baker, B. J., Seitz, K., Hyde, A. S., Dick, G. J., Hinrichs, K., et al. (2016). Genomic evidence for distinct carbon substrate preferences and ecological niches of Bathyarchaeota in estuarine sediments. *Environ. Microbial.* 18, 1200–1211. doi: 10.1111/emi.2016.18.issue-4

Liang, W., Tiantian, Y. U., Dong, L., Jia, Z., and Wang, F. (2023). Determination of carbon-fixing potential of Bathyarchaeota in marine sediment by DNA stable isotope probing analysis. *Sci. CHINA: Earth Sci.* 66, 8. doi: 10.1007/s11430-022-1002-4

Liu, K., Luo, X., Jimmy Jiao, J., Gu, J.-D., and Aravena, R. (2021). Gene abundances of AOA, AOB, and anammox controlled by groundwater chemistry of the Pearl River Delta, China. *China Geol.* 4, 1–14. doi: 10.31035/cg2021081

Liu, Y., Priscu, J. C., Xiong, J., Conrad, R., Vick-Majors, T., Chu, H., et al. (2016). Salinity drives archaeal distribution patterns in high altitude lake sediments on the Tibetan Plateau. *FEMS Microbiol. Ecol.* 92. doi: 10.1093/femsec/fiw033

Liu, X. Y., Tao, K. Y., Sun, J., He, C. Q., Cui, J., and Chen, X. P. (2017). The introduction of woody plants for freshwater wetland restoration alters the archaeal community structure in soil. *Land Degrad. Dev.* 28, 1933–1942. doi: 10.1002/ldr.v28.7

Ma, Y., Liu, F., Kong, Z., Yin, J., Kou, W., Wu, L., et al. (2016). The Distribution Pattern of Sediment Archaea Community of the Poyang Lake, the Largest Freshwater Lake in China. *Archaea* 2016, 9278929.

Maier, R. M., and Pepper, I. L. (2009). Chapter 4 - Earth Environments. in R. M. Maier, I. L. Pepper and C. P. Gerba, editors. *Environmental Microbiology* (*Second* Edition). (San Diego: Academic Press), 57–82. doi: 10.1016/B978-0-12-370519-8.00004-3

Maietta, C. E., Hondula, K. L., Jones, C. N., and Palmer, M. A. (2020). Hydrological conditions influence soil and methane-cycling microbial populations in seasonally saturated wetlands. *Front. Environ. Sci.* 8. doi: 10.3389/fenvs.2020.593942

Meng, K., Chung, C. Z., Soll, D., and Krahn, N. (2022). Unconventional genetic code systems in archaea. *Front. Microbiol.* 13, 1007832. doi: 10.3389/fmicb.2022.1007832

Muema, E. K., Cadisch, G., and Rasche, F. (2016). Soil texture modulates the response of ammonia-oxidizing prokaryotes to biochemical quality of organic inputs in tropical agricultural soils. *Soil Biol. Biochem.* 100, 218–228. doi: 10.1016/j.soilbio.2016.06.027

Naitam, M. G., Ramakrishnan, B., Grover, M., and Kaushik, R. (2023). Rhizosphere-dwelling halophilic archaea: a potential candidate for alleviating salinity-associated stress in agriculture. *Front. Microbiol.* 14, 1212349. doi: 10.3389/fmicb.2023.1212349

Peralta, A. L., Ludmer, S., Matthews, J. W., and Kent, A. D. (2014). Bacterial community response to changes in soil redox potential along a moisture gradient in restored wetlands. *Ecol. Eng.* 73, 246–253. doi: 10.1016/j.ecoleng.2014.09.047

Pfeifer, K., Ergal, İ., Koller, M., Basen, M., Schuster, B., and Rittmann, S. K. M. R. (2021). Archaea biotechnology. *Biotechnol. Adv.* 47, 107668. doi: 10.1016/j.biotechadv.2020.107668

Saavedra-Bouza, A., Escuder–Rodríguez, J.-J., deCastro, M.-E., Becerra, M., and González-Siso, M.-I. (2023). Xylanases from thermophilic archaea: A hidden treasure. *Curr. Res. Biotechnol.* 5, 100116. doi: 10.1016/j.crbiot.2022.11.003

Torregrosa-Crespo, J., Bergaust, L., Pire, C., and Martinez-Espinosa, R. M. (2018). Denitrifying haloarchaea: sources and sinks of nitrogenous gases. *FEMS Microbiol. Lett.* 365. doi: 10.1093/femsle/fnx270

Wang, H., Bier, R., Zgleszewski, L., Peipoch, M., Omondi, E., Mukherjee, A., et al. (2020b). Distinct distribution of archaea from soil to freshwater to estuary: implications of archaeal composition and function in different environments. *Front. Microbiol.* 11, 576661. doi: 10.3389/fmicb.2020.576661

Wang, Z., Fuad, M. T. I., Liu, J., Lin, K., Liu, L., Gao, C., et al. (2025). Spatial patterns of microbial communities in intertidal sediments of the yellow river estuary, China. *Microb. Ecol.* 87, 173. doi: 10.1007/s00248-025-02494-4

Wang, W., Tao, J., Liu, H., Li, P., Chen, S., Wang, P., et al. (2020a). Contrasting bacterial and archaeal distributions reflecting different geochemical processes in a sediment core from the Pearl River Estuary. *AMB Express* 10, 16. doi: 10.1186/s13568-020-0950-y

Webster, G., O'Sullivan, L. A., Meng, Y., Williams, A. S., Sass, A. M., Watkins, A. J., et al. (2015). Archaeal community diversity and abundance changes along a natural salinity gradient in estuarine sediments. *FEMS Microbiol. Ecol.* 91, 1–18. doi: 10.1093/femsec/fiu025

Wei, G., Li, M., Shi, W., Tian, R., Chang, C., Wang, Z., et al. (2020). Similar drivers but different effects lead to distinct ecological patterns of soil bacterial and archaeal communities. *Soil Biol. Biochem.* 144, 107759. doi: 10.1016/j.soilbio.2020.107759

Wen, X., Yang, S., Horn, F., Winkel, M., Wagner, D., and Liebner, S. (2017). Global biogeographic analysis of methanogenic archaea identifies community-shaping environmental factors of natural environments. *Front. Microbiol.* 8, 1339. doi: 10.3389/fmicb.2017.01339

White, S. M., and Madsen, E. A. (2016). Tracking tidal inundation in a coastal salt marsh with Helikite airphotos: influence of hydrology on ecological zonation at Crab Haul Creek, South Carolina. *Remote Sens. Environ.* 184, 605–614. doi: 10.1016/j.rse.2016.08.005

Wu, D., Zhao, C., Bai, H., Feng, F., Sui, X., and Sun, G. (2021). Characteristics and metabolic patterns of soil methanogenic archaea communities in the high-latitude natural forested wetlands of China. *Ecol. Evol.* 11, 10396–10408. doi: 10.1002/ece3.v11.15

Xiao, F., Li, Y., Li, G., He, Y., Lv, X., Zhuang, L., et al. (2021). High throughput sequencing-based analysis of the soil bacterial community structure and functions of Tamarix shrubs in the lower reaches of the Tarim River. *PeerJ* 9, e12105. doi: 10.7717/peerj.12105

Xie, W., Zhang, C., Zhou, X., and Wang, P. (2014). Salinity-dominated change in community structure and ecological function of Archaea from the lower Pearl River to coastal South China Sea. *Appl. Microbiol. Biotechnol.* 98, 7971–7982. doi: 10.1007/s00253-014-5838-9

Yang, J., Jiang, H., Wu, G., and Liu, W. (2018). Phylum-level archaeal distributions in the sediments of Chinese lakes with a large range of salinity. *Geomicrobiol. J.* 35, 404–410. doi: 10.1080/01490451.2017.1382611

Zedler, J. B. (2000). Progress in wetland restoration ecology. *Trends Ecol. Evol. (Amst.)* 15, 402–407. doi: 10.1016/S0169-5347(00)01959-5

Zhang, Y., Chen, L., Dai, T., Tian, J., and Wen, D. (2015). The influence of salinity on the abundance, transcriptional activity, and diversity of AOA and AOB in an estuarine sediment: a microcosm study. *Appl. Microbiol. Biotechnol.* 99, 9825–9833. doi: 10.1007/s00253-015-6804-x

Zhao, Q., Bai, J., Gao, Y., Zhao, H., Zhang, G., and Cui, B. (2020b). Shifts in the soil bacterial community along a salinity gradient in the Yellow River Delta. *Land Degrad. Dev.* 31, 2255–2267. doi: 10.1002/ldr.v31.16

Zhao, Q., Bai, J., Wang, X., Zhang, W., Huang, Y., Wang, L., et al. (2020a). Soil organic carbon content and stock in wetlands with different hydrologic conditions in the Yellow River Delta, China. *Ecohydrol. Hydrobiol.* 20, 537–547. doi: 10.1016/j.ecohyd.2019.10.008

Zhao, Z., Zhang, L., Zhang, G., Gao, H., Chen, X., Li, L., et al. (2023). Hydrodynamic and anthropogenic disturbances co-shape microbiota rhythmicity and community assembly within intertidal groundwater-surface water continuum. *Water Res.* 242, 120236. doi: 10.1016/j.watres.2023.120236

Zou, D., Liu, H., and Li, M. (2020b). Community, distribution, and ecological roles of estuarine archaea. *Front. Microbiol.* 11, 2060. doi: 10.3389/fmicb.2020.02060

Zou, D., Pan, J., Liu, Z., Zhang, C., Liu, H., and Li, M. (2020a). The distribution of bathyarchaeota in surface sediments of the Pearl river estuary along salinity gradient. *Front. Microbiol.* 11, 285. doi: 10.3389/fmicb.2020.00285

Frontiers in Marine Science

Explores ocean-based solutions for emerging global challenges

The third most-cited marine and freshwater biology journal, advancing our understanding of marine systems and addressing global challenges including overfishing, pollution, and climate change.

Discover the latest Research Topics

See more →

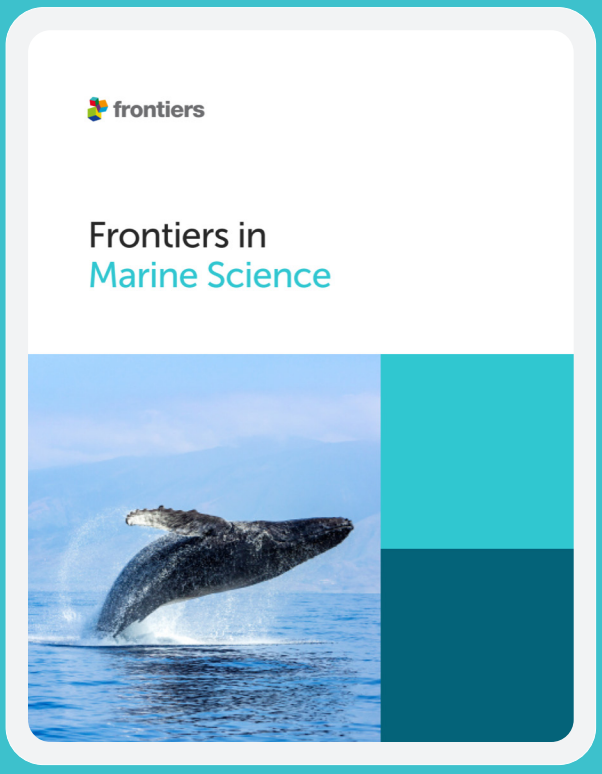

Frontiers

Avenue du Tribunal-Fédéral 34
1005 Lausanne, Switzerland
frontiersin.org

Contact us

+41 (0)21 510 17 00
frontiersin.org/about/contact